Vol. 134, Nos. 1–6

Sept.-Oct., 1960

PROCEEDINGS OF THE ACADEMY OF SCIENCES

OF THE USSR

(DOKLADY AKADEMII NAUK SSSR)

Physical Chemistry Section

A publication of the Academy of Sciences of the USSR

IN ENGLISH TRANSLATION

Year and issue of first translation:
Vol. 112, Nos. 1-6 Jan.-Feb. 1957

Annual subscription	*$160.00*
Single issue	*35.00*

Printed in the United States of America

PROCEEDINGS OF THE ACADEMY OF SCIENCES OF THE USSR

Physical Chemistry Section

Volume 134, Numbers 1-6 September-October, 1960

CONTENTS

CONTENTS (continued)

CONTENTS (continued)

THIN OXIDE FILMS ON TITANIUM, ZIRCONIUM, MOLYBDENUM, AND TITANIUM ALLOYS

V. V. Andreeva and E. A. Alekseeva

Institute of Physical Chemistry, Academy of Sciences of the USSR
(Presented by Academician A. N. Frumkin, April 28, 1960)
Translated from Doklady Akademii Nauk SSSR, Vol. 134, No. 1, pp. 106-109, September, 1960
Original article submitted April 28, 1960

Much work has been devoted to the oxidation of titanium, zirconium, and molybdenum at temperatures above 300° [1-3]. There is, however, very little information on the oxidation of these metals in the temperature interval from 20 to 300°. The present work has involved a study of the kinetics of oxidation of Ti, Zr, Mo, an alloy of Ti with 10% Mo, and an alloy of Ti with 3% Al and 5% Cr, over the temperature range from 50 to 400°.

This study has employed an optical method for measuring the depth of the thin invisible films which are formed on metallic surfaces; this has been described earlier in [1, 4, 5] and involves determination of the ellipticity of the polarized light which is reflected from the surface in question. The initial state of the surface was that obtained by polishing the metal specimen and then carefully degreasing in a Soxhlet extractor. Subsequent oxidation at various elevated temperatures resulted in an increase in the depth of the "natural" oxide film carried by this metallic surface, the depth of which was not included in the calculations. Oxidation was carried out in a tubular furnace in a current of oxygen and was continued for six hours at each temperature. The specimens were removed from the furnace every 60 min, cooled rapidly, and measurement then made of the increase in the film depth. The specimens were returned to the furnace after completion of the measurements. Each specimen was subjected to the entire oxidation cycle at each temperature in the 50-400° interval.

Mean results from several series of measurements of the growth of the oxide films on the various metals and alloys are presented in Figs. 1 and 2. Depths of the oxide films on the investigated specimens at the end of the six-hour oxidation cycle are compiled in Table 1.

The results indicate that oxidation becomes appreciable at 50° with Zr, at 100° with Ti and the Ti + 10% Mo alloy, and at 150° with Mo and the Ti + 5% Cr + 3% Al alloy. An examination of the various curves shows that although the initial rate of oxidation of each metal and alloy is high at each temperature; this rate falls off to practically zero when the layer of reaction product reaches a certain limiting value under which oxidation ceases. Here, the increase in depth of the oxide film with time can be expressed through the logarithmic equation:

$$L = k \lg (k_1 t + k_2). \tag{1}$$

A plot of the depth of the oxide film as a function of the logarithm of the time is a straight line.

The slope of the curve showing the film depth as a function of time begins to change on passing to higher temperatures and the rate of oxidation then follows a parabolic equation

$$L^2 = k_3 t. \tag{2}$$

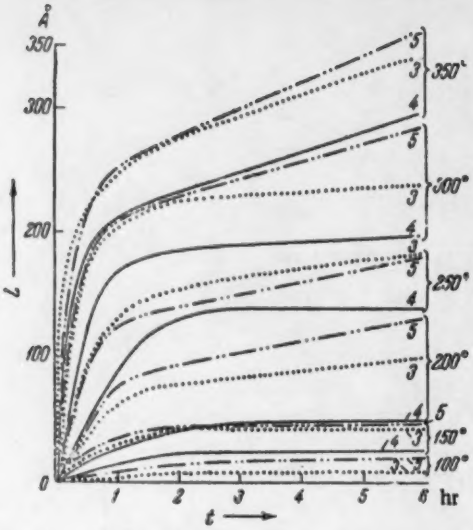

Fig. 1. Film depth as a function of temperature and duration of oxidation: 3) alloy of Ti with 10% Mo; 4) alloy of Ti with 5% Cr and 3% Al; 5) Ti.

The stability of the surface oxide diminishes with rising temperature so that the rate of oxidation is fixed by the diffusion of ions into the oxide crystal lattice. Here, a plot of film depth versus square root of time yields a linear relation. L designates the depth of the film of the oxide and t, the time, in Eqs. (1) and (2).

Table 1 shows for the various investigated metals and alloys those temperature intervals within which each rate of growth law is valid for the oxide film.

The rate of oxidation of each metal rises rapidly on reaching a definite characteristic temperature (Fig. 3). With Zr and Mo, a rapid growth of the film is noted beyond 200°; while with Ti and the Ti alloys containing 10% Mo, or 5% Cr and 3% Al, this rapid growth begins beyond 350°.* It is noteworthy that the rate of oxidation in the interval 200-400° is lower for the alloy of Ti with 10% Mo than for Ti, although the oxidation of Mo is sharply accelerated in this range.

The oxide film formed on titanium at temperatures below 800°, either in pure oxygen or in air, has the composition TiO_2 and shows the rutile structure [6, 11, 12]. This film has a laminated structure at oxidation temperatures in excess of 800°, consisting of a layer of TiO at the metal–oxide interface, an intermediate layer of Ti_2O_3, and an outer layer of TiO_2 at the gas–oxide interface. Oxidation of zirconium in oxygen at temperatures below 250-300° yields an oxide film of ZrO_2 with cubic structure, while at 250° and above, this film is a grain-oriented monoclinic modification [7]. The increase in the rate of oxidation which is observed at 250-300° is related to this passage to the monoclinic modification of ZrO_2. Up to 300°, the film on molybdenum has the composition $MoO_3 \cdot MoO_2$, appears along with the MoO_3 in the temperature interval from 300-700°, obviously as the result of dissociation of MoO_3 according to the equation:

$$2MoO_3 \rightarrow 2MoO_2 + O_2,$$

with subsequent oxidation proceeding essentially to MoO_2 alone. This effect explains the presence of the minimum on curve 2 of Fig. 2 for the oxidation of molybdenum at 350°.

The films which are formed on chromium and aluminum in air at the various temperatures consist exclusively of Cr_2O_3 and Al_2O_3, respectively [8, 10].

A plot of log k as a function of 1/T has the form of a straight line. The energy of activation for the oxidation process on each of the metals and alloys was obtained from the slope of the respective line (see Table 1). The resultant values of the activation energy show the mechanism of interaction with oxygen to be the same for Zr and for Mo, while a somewhat different common mechanism is involved in the interaction with Ti and with its 10% Mo alloy. This can obviously be explained by the formation of a mixed oxide, or solid solution of TiO_2 and $xMoO_3$ on the Ti + 10% Mo alloy. The formation of such a mixed oxide could be beneficial, to a certain degree, since its relatively high heat of formation would result in a diminution in the vapor pressure of the MoO_3. If this is indeed a mixed oxide, there should be a replacement of the Ti^{4+} ions of the TiO_2 lattice by Mo^{6+} ions. On the other hand, lattice replacement by an ion of higher valency but identical radius (ionic radii: Ti^{4+} = 0.64 A; Mo^{6+} = 0.68 A) should result in an increase in the number of free electrons and a diminution in the number of oxygen ion vacancies, since titanium dioxide is an electronic semiconductor. Thus the alloying of molybdenum with titanium would not necessarily reduce the thermal stability but could, on the contrary, improve it somewhat, just as is actually observed to be the case. The formation of a mixed oxide (TiO_2, Al_2O_3, Cr_2O_3) of the spinel type could explain the fact that the resistance to oxidation of the alloy of Ti with 5% Cr and 3% Al is considerably greater than that of titanium itself. A lattice of this kind is known to be highly resistant to oxidation.

* For comparison, Fig. 3 contains curves for the oxidation of chromium and aluminum based on the data of T. N. Krylova [9].

Metal, alloy	Kinetic law for film growth in the given temperature interval								Composition of the oxide film in the temperature interval 50-400°	Energy of activation of oxidation, kcal/mole
	at 50°	at 100°	at 150°	at 200°	at 250°	at 300°	at 350°	at 400°		
Titanium (iodide)	unchanged	logarithmic		Parabolic					TiO_2 (Rutile) [6]	250-300° 10,000
Zirconium (iodide)	logarithmic			Parabolic					ZrO_2 cubic lattice up to 250°, with transition to monoclinic form with further elevation of temperature [7]	200-250° 21,200
Molybdenum (iodide)	unchanged			Parabolic					MoO_3 up to 300°, MoO_3 and MoO_2 above 300° [8]	150-300° 20,000
Titanium + 10% molybdenum	unchanged	logarithmic		Parabolic					obviously, a solid solution of TiO_2 and $xMnO_3$	200-350° 12,000
Titanium + 3% aluminum + + 5% chromium	unchanged			logarithmic		Parabolic			obviously, a solid solution of TiO_2, xCr_2O_3 and yAl_2O_3	

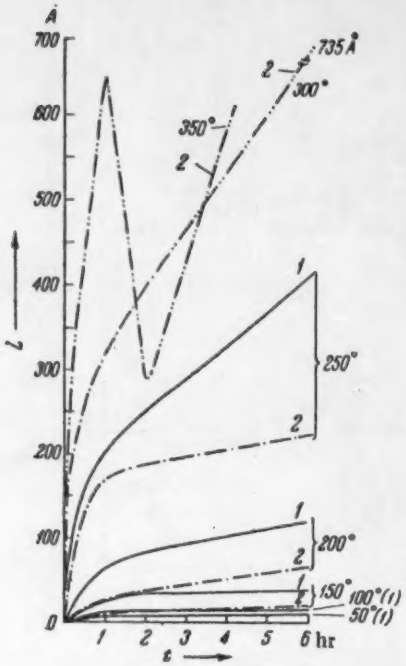

Fig. 2. Film depth as a function of temperature and duration of oxidation: 1) Zr; 2) Mo.

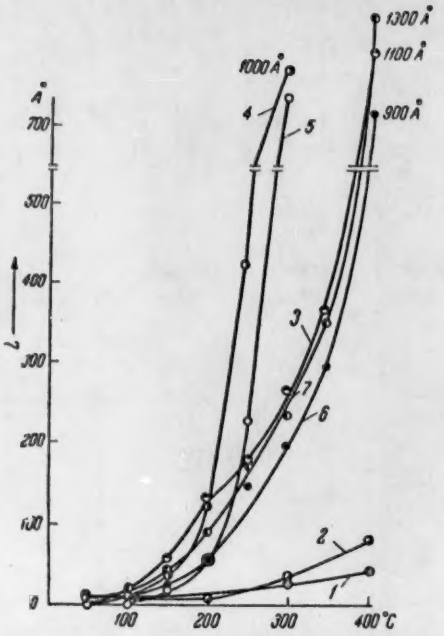

Fig. 3. Rate of oxidation as a function of temperature: 1) Al; 2) Cr; 3) Ti; 4) Zr; 5) Mo; 6) alloy of Ti with 5% Cr and 3% Al; 7) alloy of Ti with 10% Mo.

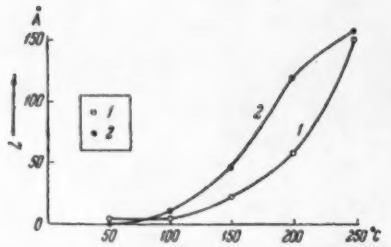

Fig. 4. Film depth as a function of the temperature of oxidation of titanium: 1) in air, saturated with water vapor; 2) in dry air.

The curves of Fig. 4 cover the oxidation of titanium in dry air, and in air saturated with water vapor, over the temperature interval from 50 to 250°. This figure indicates that up to 200°, the film formed on titanium in dry air is twice as thick as that formed in moist air. The depth of film formed in moist air becomes the same as the depth of film formed in dry air when the temperature reaches 250° and the water bonding becomes unstable. The hydrated film is clearly more compact and more nearly free of defects than is the film which is formed in dry air.

LITERATURE CITED

[1] V. V. Andreeva, Tr. Inst. Fiz. Khim. Akad. Nauk SSSR 2, No. 6 (1957).

[2] V. V. Andreeva and N. A. Shishakov, Zhur. Fiz. Khim. 32, No. 7 (1958).

[3] N. A. Shishakov, V. V. Andreeva, and N. K. Andryushenko, The Structure and Mechanism of Formation of Oxide Films on Metals [in Russian] (Izd. AN SSSR, 1959).

[4] V. V. Andreeva, Institute of Technical-Economic Information, Academy of Sciences, USSR Project 9, No. PS-55-503 (1955).

[5] V. V. Andreeva and V. I. Gavrilov, Tr. Inst. Fiz. Khim. 3, Studies on the Corrosion of Metals (1951) Vol. 2.

[6] P. Kofstad and K. Hauffe, Z. Werkstoffe u. Korrosion 2, 642 (1956).

[7] É. S. Sarkisov, N. T. Chebotarev, A. A. Nevzorova, and A. I. Zver'kov, Atomnaya Energ. 5, No. 5 (1958).*

[8] J. Hickmann and E. Gulbransen, Trans. Am. Inst. of Mining and Metallurg. Eng. 171, 344 (1947).

[9] T. N. Krylova, Izvest. Akad. Nauk SSSR, Otdel. Tekh. Nauk, 89 (1938).

[10] E. A. Gulbransen, J. Phys. and Coll. Chem. 51, 5, 1087 (1947).

[11] D. I. Lainer and M. I. Tsypin, Zavod. Lab. 10 (1959).

[12] D. I. Lainer and M. I. Tsypin, Izvest. Akad. Nauk SSSR, Otdel. Tekh. Nauk, 5 (1959).

*Original Russian pagination. See C. B. Translation.

THE EFFECTS OF SPECIFIC GASEOUS TREATMENT ON THE CATALYTIC AND MAGNETIC PROPERTIES OF CHROMIC OXIDE

Academician A. A. Balandin, I. D. Rozhdestvenskaya, and A. A. Slinkin

N. D. Zelinskii Organic Chemistry Institute, Academy of Sciences of the USSR
Translated from Doklady Akademii Nauk SSSR, Vol. 134, No. 1, pp. 110-113, September, 1960
Original article submitted May 17, 1960

It is a well-known fact that the catalytic and semiconducting properties of chromic oxide depend on the specific gas used in the preliminary thermal treatment [1-3].

It is interesting to compare the changes produced in the magnetic and catalytic properties of chromic oxide by various forms of thermal treatment. Turkevich [4] investigated the magnetic and catalytic properties of amorphous and crystalline chromic oxide (treated with hydrogen) in the dehydrocyclization of heptane. He showed that though the amorphous and crystalline samples of chromic oxide differ greatly in their catalytic activity they have identical magnetic properties – both are antiferromagnetic. Most of the papers dealing with variously prepared chromic oxide samples report magnetic susceptibilities (χ) in the range from $18\text{-}26 \cdot 10^{-6}$ [4-6]. For chromic oxide treated with hydrogen at 1000° the value of $\chi = 59{,}0 \cdot 0^{-6}$ is reported [5]. As we will show later on, this high value is probably caused by the presence of ferromagnetic impurities in the sample. At least two ferromagnetic chromium oxides are known [7]: crystalline chromium dioxide with $\chi = 6{,}0 \cdot 10^{-1}$ and chromium monochromate with $\chi = 3{,}5 \cdot 10^{-1}$.

It was also interesting to see how treatment with atomic hydrogen would affect the catalytic properties of chromic oxide. There is as yet very little information with regard to the effects produced by atomic hydrogen on the activity of catalysts. A paper appeared in 1952 [8] in which the activation of tungsten (used as catalyst in the synthesis of ammonia) by atomic hydrogen was studied. A catalyst thus treated proved to be considerably more active than one reduced in the usual manner, though the activity exhibited great variations.

The starting materials, the preparation of chromic hydroxide, and the apparatus used for the kinetic measurements have been described elsewhere [9]. We prepared our catalyst from analytically pure chromic nitrate. The various conditions used in our thermal treatment of chromic hydroxide are represented schematically in diagram I, while the experimentally determined χ in Table 1 (Numbers Ia and IIa designate samples prepared from lower-purity-grade chromic nitrate).

The apparatus shown in Fig. 1 was used for the treatment of catalysts with atomic hydrogen. The hydrogen, which was prepared by electrolyzing aqueous potassium hydroxide, was freed from oxygen by passing over Pd-asbestos at 180° and from water vapor by passing through a column filled with anhydrous silica gel. Pure hydrogen was introduced into discharge tube 1, which was made of molybdenum glass. The aluminum electrodes 2 were supported on tungsten wires which were sealed into the glass. A 10,000-12,000 v potential was applied to the electrodes.

Schematic Diagram 1

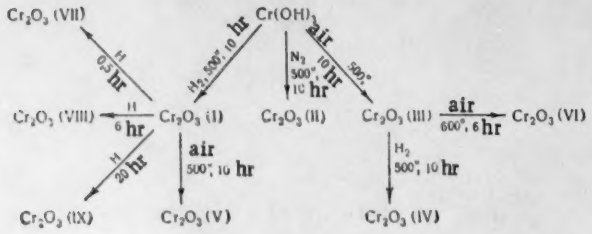

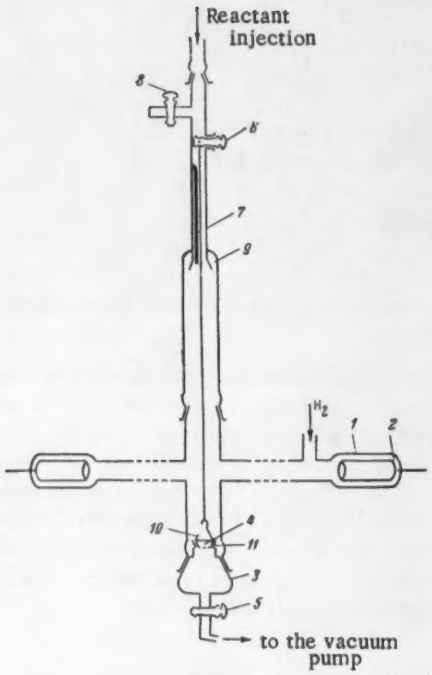

Fig. 1.

A glass receiver 3, inserted into a ground joint at the bottom of the discharge tube, was topped by another ground joint 11 into which a small cup 4 containing a weighed sample of the catalyst was inserted. The cup had a perforated bottom. The inserted receiver had thermocouple leads and was connected through stopcock 5 to a vacuum pump and a pressure gauge. The cup with the catalyst was located 15 cm from the line of discharge. A 0.7 g sample of the catalyst was used. The catalyst was reduced as follows. The discharge tube was evacuated to a 10^{-3} mm pressure, checked for leaks, and filled with pure hydrogen. Subsequently the hydrogen was pumped continously through the cup containing the catalyst so as to maintain a 1-2 mm pressure in the system while a potential was applied to the electrodes. After the atomic hydrogen generated in the discharge tube was sucked through the cup for a fixed length of time, the discharge was stopped, the system filled with hydrogen, and the cup together with the catalyst was raised by means of a string and pulley (attached to a stopcock) into the catalytic tube 7 until the upper joint of the cup 10 fit into the ground joint of tube 9. At the same time the thermocouple socket came into contact with the upper layer of the catalyst. While maintaining a steady stream of hydrogen (introduced through stopcock 8) we disconnected the discharge tube and connected the catalytic tube directly to the receiver bulb; after this the oven was turned on and the experiment carried out at a fixed temperature. Prior to every experiment the catalyst was regenerated for 2 hours at 500°C in a stream of molecular hydrogen in order to remove any reaction products that might have remained on its surface.

Table 1 shows that catalysts I and II, which were prepared by treating the hydroxide with hydrogen and nitrogen respectively, are both antiferromagnetic and have a Néel temperature of about 50°C. Sample IX, prepared by treating sample I with atomic hydrogen, is also antiferromagnetic. On the other hand, when the hydroxide is treated with air under similar conditions (at 500°C) one detects a considerable amount of ferromagnetism (sample III). The appearance of ferromagnetism has two unusual features. 1) It is not connected with the presence of any ferromagnetic impurities in the sample, since the treatment of the original hydroxide with hydrogen or even atomic hydrogen fails to produce any ferromagnetism, while $Cr(OH)_3$ prepared from incompletely purified $Cr(NO_3)_3$ when treated with hydrogen (sample Ia) exhibits ferromagnetism which can be attributed to impurities present in the original salt. 2) The ferromagnetism appears only if the hydroxide is heated in air at a definite temperature and declines rapidly when the ferromagnetic sample III is heated in air at 600°C (sample IV). Heating the ferromagnetic sample II in a stream of H_2 converts it into the paramagnetic sample IV. In our opinion the ferromagnetism indicates that some chromium dioxide might be formed when the original

TABLE 1

Variation of χ with Temperature for Various Cr_2O_3 Samples

Catalyst No.	$\chi \cdot 10^6$ at: 20°C	50°C	80°C	160°C	Δ°, K	μ_B	Catalyst No.	$\chi \cdot 10^6$ at: 20°C	50°C	80°C	160°C
I	24,0	25,3	24,4	23,3			VI	24,4	25,2	23,4	23,0
II	23,8	25,0	23,6	22,9			VII	92,0	—	—	—
III	340,0	—	—	—			Ia	96,0	—	—	—
IV	28,0	—	25,8	24,0	500	3,7	IIa	21,8	—	22,1	20,8
V	22,8	24,3	23,3	22,8							

hydroxide is subjected to a specific thermal treatment. The catalytic properties of the resulting samples were tested in relation to the dehydration of isopropyl alcohol and dehydrogenation of cyclohexane. The results presented in Table 2 show that chromic oxide samples prepared from the same hydroxide but subjected to different gaseous treatment exhibit different catalytic properties; they differ in their activities V_0, selectivities, activation energies ϵ (kcal/mole), and in the bond energies Q (kcal) between the catalyst surface and the active atoms of the reacting molecules. Antiferromagnetic catalysts I and II have the same catalytic action in the decomposition of isopropyl alcohol as in the dehydrogenation of cyclohexane. (The difference between the catalytic properties of samples Ia and IIa is related to the fact that the former contains ferromagnetic impurities.) An examination of Table 2 reveals one striking fact – that the ferromagnetic catalyst III and the antiferromagnetic catalyst IX, though prepared from the hydroxide under entirely different conditions, still have identical catalytic action on the investigated reactions. In fact both catalysts strongly suppress the dehydrogenation of cyclohexane and greatly enhance the dehydration of isopropyl alcohol. On the basis of this one would conclude that the surfaces of catalysts III and IX have the same chemical structure. The enhanced dehydration of isopropyl alcohol seems to be connected with the formation of $\geq Cr - OH$ centers on the surface in analogy with the $\geq Al - OH$ centers formed on Al_2O_3 [10].

The formation of hydroxyl groups in catalyst IX can be attributed to the chemisorption of atomic hydrogen [12], whereas in catalyst III they result from a reaction between CrO_2 and the hydrogen formed in the initial stages of the reaction. As indirect evidence for such a reaction we might mention the fact that the adsorption of isopropyl alcohol or cyclohexane on the surface of catalyst III is a highly exothermic process. In catalyst IV the hydroxyl groups, which promote dehydration of alcohols, arise from the reduction of CrO_2 by hydrogen.

The strong influence of OH groups on the dehydrogenation of cyclohexane has also been demonstrated by treating chromic oxide (sample I) with water vapor and then regenerating it in a stream of H_2 at 500°. A catalyst thus treated became completely inactive toward dehydrogenation of cyclohexane. Water is known to deactivate chromic oxide with respect to deuterium – hydrogen exchange [13].

With regards to the relationship between the magnetic and catalytic properties of the various chromic oxide catalysts studied by us we can state the following. By varying the gaseous treatment of chromic oxide we can produce samples of different magnetic properties. However, both the magnetic as well as electric data describe bulk properties, and in several cases do not reflect the changes produced in the chemical structure of the surface. In the work reported here it is the variations in surface properties which ultimately determine the course of chemical reactions, and hence it was impossible to establish a simple relationship between the magnetic and catalytic properties of chromium oxide catalysts.

The measurement of magnetic susceptibilities turned out to be extremely useful in this work, since we were able to detect a new phase of chromium dioxide in the oxidized samples of chromic oxide. X-ray and electron-diffraction measurements showed that all of the investigated samples contain the crystalline α-Cr_2O_3. These measurements, however, due to their low sensitivity, failed to detect any CrO_2. Experiments in which chromic oxide was treated with atomic hydrogen showed that such a treatment radically deactivates the catalyst with respect to the dehydrogenation of cyclohexane. On the other hand, as we have already mentioned, a similar treatment with atomic hydrogen promotes the catalytic dehydration of isopropyl alcohol. These hydroxyl groups seem to be formed very rapidly at first (as the difference between the properties of catalysts I and VII would indicate) and then upon further treatment the reaction between atomic hydrogen and the catalyst surface abruptly

TABLE 2

Catalyst No.	Dehydration of iso-C_3H_7OH						Dehydrogenation of C_6H_{12}						S, m^2/g
	reaction temp., °C	V_{0H_2}, ml/min	V_{0H_2O}, ml/min	% olefin	Δ, °C	ϵ H_2, kcal/m	ϵ H_2O, kcal/m	reaction temp., °C	V_{0H_2}, ml/min	Δ, °C	ϵ H_2	O_{HK}	O_{CK}	O_{OK}	
I	241—295	4.0—10.7	0.3—2.6	6.4—19.3	22	9.5	23.1	335—395	11.1—32.8	0	14.5	66.3	22.8	41.5	55
II	250—295	4.3—10.5	0.3—2.0	5.7—15.6	22	10.3	24.3	331—403	6.0—25.8	0	15.8	66.1	22.1	41.5	28
III	289—328	3.1—8.8	2.2—8.6	41.0—49.4	107	18.4	25.7	394—444	7.1—36.5	49	31.8	56.4	21.3	51.2	35
IV	280—326	3.8—9.6	1.9—8.0	33.0—45.5	6	11.8	19.2	348—419	10.4—35.4	0	14.4	62.2	26.9	42.7	19
V	246—286	4.6—11.3	0.6—2.7	11.6—19.5	36	14.3	23.8	378—450	5.0—10.6	22	26.5	60.1	21.1	39.8	25
Ia	265—304	5.2—13.1	0.8—3.0	12.4—18.7	22	14.5	20.3	362—416	6.5—34.2	0	26.7	57.0	23.9	52.1	56
IIa	252—291	3.7—11.0	0.50—3.5	12.0—27.0	10	21.3	27.1	339—381	10.3—25.5	0	17.6	60.0	27.0	33.9	
VII	299—356	4.1—8.6	1.1—3.1	20.7—26.7		9.0	13.1	433—476	8.9—23.3	0	22.3	57.4	26.6	56.3	
VIII	300—367	3.8—11.5	1.2—4.5	23.3—27.0		10.6	13.8	436—463	8.0—23.0	0	25.4	55.7	26.1	57.9	
IX	305—364	4.5—9.1	1.4—4.1	24.0—30.6		8.6	12.7	438—486	4.3—17.1	0	30.8	54.5	23.7	65.3	35

slows down. One should also note that the samples treated with atomic hydrogen retain their full activity during each experiment and even when we switch from one experiment to another.

LITERATURE CITED

[1] S. E. Voltz and S. Weller, J. Am. Chem. Soc. 75, 5227 (1953).

[2] S. Weller and S. E. Voltz, J. Am. Chem. Soc. 76, 4695 (1954).

[3] P. B. Weisz, C. D. Prater, and K. D. Rittenhouse, J. Chem. Phys. 21, 2236 (1953); R. Chaplin, P. R. Chapman, and R. H. Griffith, Nature 172, 77 (1953); P. R. Chapman, R. H. Griffith, and J. D. F. Marsh, Proc. Roy. Soc. A224, 419 (1954).

[4] J. Turkevich, J. Chem. Phys. 12, 345 (1944).

[5] W. H. Albrecht and E. Wedekind, Z. anorg. u. allgem. Chem. 210, 105 (1933).

[6] S. S. Bhatnagar and A. Cameron, et al., J. Chem. Soc. 1433 (1939).

[7] T. V. Rode, Doctoral Thesis [in Russian] (IONKh, AN SSSR, Moscow, 1957).

[8] S. L. Kiperman, N. A. Rybakova, and M. I. Temkin, Zhur. Fiz. Khim. 26, 621 (1952).

[9] A. A. Balandin and I. D. Rozhdestvenskaya, Zhur. Fiz. Khim. 34, 6 (1960).

[10] K. V. Topchieva, K. Yung-p'ing, and I. V. Smirnova, Coll.: Chemical Surface Compounds and Their Role in Adsorption and Catalysis [in Russian] (Moscow, 1957).

[11] A. M. Rubinshtein and A. A. Slinkin, Izvest. Akad. Nauk SSSR, Otdel Khim. Nauk 9, 1054 (1958).*

[12] O. Glemser, U. Hauschild and G. Lutz, Z. anorg. Chem. 269, 93 (1952).

[13] S. E. Voltz and S. Weller, J. Am. Chem. Soc. 75, 5231 (1953).

*Original Russian pagination. See C. B. Translation.

THE NATURE OF THE MOSAIC STRUCTURE OF GERMANIUM AND SILICON SINGLE CRYSTALS

O. V. Bogorodskii, Ya. S. Umanskii, and S. Sh. Shil'shtein

I. V. Stalin Moscow Steel Institute

(Presented by Academician P. A. Rebinder, April 26, 1960)
Translated from Doklady Akad. Nauk SSSR, Vol. 134, No. 1, pp. 114-116, September, 1960
Original article submitted March 2, 1960

At present, it is a generally accepted opinion that mosaic structure originates from dislocations. The simplest model of a dislocational boundary between blocks is shown in Fig. 1. In this case, the boundary is a wall of edge dislocations, each with Burgers vector $\underline{b}$, and the angle of misfit θ is determined by the distance between the dislocations $\underline{h}$:

$$\theta = \frac{b}{h}. \qquad (1)$$

To reveal dislocations in germanium and silicon single crystals (generally, dislocation density is not higher than 10^6 cm^{-2}) etch patterns are mostly used. On Ge and Si etch patterns are developed to the best advantage on the (111) plain. As investigations [1, 2] have shown, nearly all dislocations in crystals, grown by pulling in the melt, along the (111) axis, are edge dislocations with Burgers vector a/2 (110). In particular cases the etch patterns on the polished section form straight lines called low-angle boundaries.

It has been shown [3] that for such boundaries the misfit between the blocks, as determined by the x-ray method, agrees well with that calculated from relation (1) (the distance between the dislocations in the boundary has been determined metallographically).

We have investigated Ge and Si single crystals, which had been prepared by pulling in the melt along the (111) axis. The samples were 2-3 mm thick slices cut from the ingots perpendicularly to the growth direction in such a way that the plain of the section did not deviate more than a few degrees from the crystallographic (111) plain.

For the x-ray investigation were chosen Ge samples with dislocation densities in the range $10^2 - 10^6$ cm^{-2} and Si samples with dislocation densities $10^2 - 10^3$ cm^{-2}. The sample with the lowest dislocation density was used as monochromator. The x-ray investigation was executed by means of a two-crystal spectrometer [4] with the crystals parallel (Fig. 2).

The principle of the method consists in holding the counter fixed and turning the sample II, on which falls a previously monochromatized beam of x rays, over small angles. At each position of the sample the intensity of the twice-diffracted beam is measured and thus, point for point, the so-called rocking curve (the curve giving the relation between the intensity I and the angle β over which the sample has been turned) is constructed. Since the beam of x rays diffracted by an ideal crystal is very narrow (of the order of a few seconds), the sample has to be turned over angles of the order of 1°. We have developed a special goniometric head [5], by which turning over small angles (with an accuracy up to 0.5°) can be realized. The study was carried out using the equipment URS-50I provided with a Geiger counter. Slits 3, 4 with a height of 0.7 mm were inserted to diminish the vertical divergence of the beam (Fig. 2).

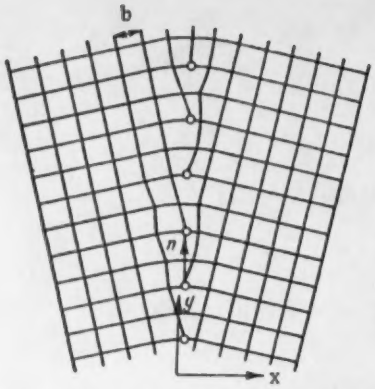

Fig. 1. Grain boundary model according to Burgers.

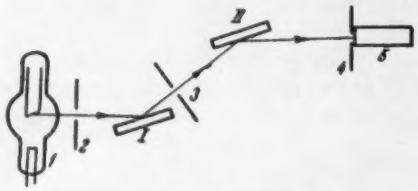

Fig. 2. Scheme of the set-up.

For an ideal crystal the width of the twice-diffracted beam may be calculated [4], and for the (111) reflex of Cu-Kα radiation on Ge and Si it is about 20" and 7", respectively. Since the accuracy of the experiment is 5", one can expect to obtain on Si only qualitative results. For this reason the basic experiments were done on Ge samples. Particular Ge samples gave rocking curves with a width of about 20", which indicates that geometrical broadening is practically completely absent.

Consequently, the broadening of the rocking curve may be connected with the mosaic structure of the crystal. The curve will be broadened noticeably above 20", when the angle of misfit between the blocks surpasses 10".

The main types of experimental rocking curves are shown in Fig. 3. If it is assumed, as a first approximation, that the scattering of x rays by the various blocks is completely incoherent, then the rocking curve for the mosaic structure is the simple superposition of the curves for the separate blocks (see Fig. 3c). The distances between the maxima of the elementary curves are equal to the angles of misfit between the blocks, and from the number of these curves the block size may be determined.

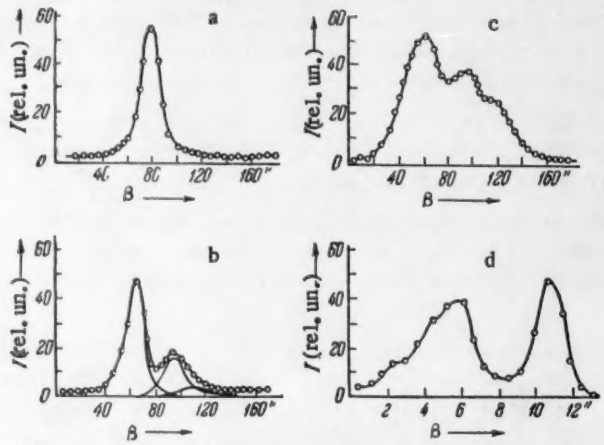

Fig. 3. Typical rocking curves: a) for an ideal crystal; b) for a mosaic crystal; d) for a sample with small-angle boundaries; c) way in which rocking curves are analyzed.

In our experiments we used Ge samples in which the dislocations were irregularly distributed. In a crystal with a dislocation density of the order of 10^2 cm^{-2} it is difficult to assume a mosaic structure, as given by the Burgers model, since the dislocations, which are arranged at distances of the order of 1 mm, cannot cause a noticeable misfit between the blocks. In general, it is difficult to expect that an irregular distribution of dislocations will produce mosaic structure. Nevertheless, the results of the x-ray investigation show that at all

TABLE 1

Sample No.	Dislocation density, cm^{-2}	Block size, cm	Tilt between blocks	Sample No.	Dislocation density cm^{-2}	Block size, cm	Tilt between blocks
2	$6 \cdot 10^3$	$8 \cdot 10^{-2}$	13″	10	$2 \cdot 10^6$	$7 \cdot 10^{-2}$	22″
6	$2 \cdot 10^4$	$6 \cdot 10^{-2}$	22″	11	$3 \cdot 10^6$	$8 \cdot 10^{-2}$	23″
9	$7 \cdot 10^4$	$9 \cdot 10^{-2}$	14″				

dislocation densities the Ge single crystals have a mosaic structure; meanwhile the angles of misfit and the block sizes change little, when the dislocation density is varied over four orders of magnitude. This fact does not fit to the model of Burgers. The results of the experiments are given in Table 1.

An investigation of Si samples with low dislocation densities of the order of $10^2 - 10^3$ cm^{-2} showed that in silicon the block size is much smaller than in germanium. This fact also does not fit to the model of Burgers, since the lattice period of Ge and Si differ little.

It might be supposed that the disagreement between the metallographic and the x-ray data is caused by experimental errors. To check the latter method Ge samples with low-angle boundaries were investigated. The rocking curves of these samples have a shape as shown in Fig. 3d. They indicate that, when low-angle boundaries are present, Ge crystals have a grain structure and also that the tilts between the grains, as to order of magnitude, agree with the values calculated from the distances between the dislocations in the boundaries.

The results of the experiments point out that, if the block boundaries in Ge and Si are connected with dislocations, it is not by the way of low-angle boundaries. Here, possibly, some other defect structures play a role, and not dislocations. The boundaries between grains are built up from dislocations in complete agreement with the model of Burgers. Consequently, the boundaries between the blocks and those between the grains are of different natures.

LITERATURE CITED

[1] F. L. Vogel and W. G. Pfann, Acta metallurgica 7, 377 (1957).

[2] V. Gerold and F. Meier, Z. Phys. 155, No. 4 (1959).

[3] F. L. Vogel and W. G. Pfann, et al., Phys. Rev. 90, 489 (1953).

[4] R. W. James, Optical Principles of the Diffraction of X rays [in Russian] (IL, Moscow, 1950).

[5] O. V. Bogorodskii and M. Sh. Shil'shtein, Zavodskaya Lab. (1960) [in press].

CHARACTERISTICS OF THE MECHANISM LIMITING MOLECULAR CHAINS DURING POLYMERIZATION WITH COMPLEX CATALYSTS

S. E. Bresler, M. I. Mosevitskii, I. Ya. Poddubnyi,

and Shih Kuang-ui

S. V. Lebedev All-Union Scientific Research Institute of Synthetic Rubber
Institute of High Molecular Compounds, Academy of Sciences of the USSR
(Presented by Academician V. G. Kargin, April 20, 1960)
Translated from Doklady Akademii Nauk SSSR, Vol. 134, No. 1, pp. 117-120, September, 1960
Original article submitted March 21, 1960

Complex catalysts of the Ziegler type are now widely used for preparing polymers with molecular chains with a highly regular structure. In this connection it is fundamentally important to establish the mechanism of separate stages in polymerization with these catalysts. In the present report we give some results of investigating the mechanism of isoprene polymerization under the action of a complex catalyst, formed by the reaction of $Al(iso\text{-}C_4H_9)_3$ and $TiCl_4$, and these results were obtained from data on the sedimentation of polymers in an ultracentrifuge combined with data on the polymerization kinetics.

We previously showed [1] that macromolecules grew very rapidly in the polymerization of isoprene with this catalyst and that small fractions of a minute were required from the moment of initiation of an active chain to its deactivation. Due to this a stationary state was established almost immediately in the system. However, the polymer molecular weight distributions obtained experimentally with an ultracentrifuge differ radically from the equilibrium distributions corresponding to the kinetic schemes of polymerization known up to now. They are characterized by a relatively low dispersion and, mainly, by a strong displacement in the high-molecular region; in most cases, macromolecules with a molecular weight of less than 200-300 thousand are practically absent from the polymer.

These characteristics of the polymers we studied may be interpreted only by new hypotheses, as no known mechanism results in a narrow molecular weight distribution with a chain limiting reaction. We need to find a limiting mechanism which would be extremely sensitive to the molecular weight (length) of a chain and this would result in chain termination only within a definite, quite narrow range of molecular weights. We consider that this mechanism is due to the heterogeneity of the polymerization, i.e., to the fact that during its growth the polymer chain is attached by one end to a catalytic complex on the catalyst surface. The attachment of the macromolecule end to the surface limits the possible configurations of the polymer chain as the space on the other side of the limiting surface is forbidden to its segments. Consequently, the breakaway of the macromolecule from the surface would be accompanied by an increase in the configuration entropy by the value ΔS, which equals the difference in the logarithms of the statistical sums for a chain remote from the wall (in solution) and for a chain close to the wall with its end attached to the wall.

To calculate the number of possible configurations for a polymer chain, we used the method of quasi-lattices with a coordination number γ for segments in the volume and $\gamma/2$ for segments on the surface, and we determined that the "defect" in the configuration entropy (ΔS) grows with an increase in the number of kinetic segments in a polymer chain (z) according to the equation

$$\Delta S = k\sqrt{z} \qquad (1)$$

(k is Boltzmann's constant).

In order to have a concrete basis for further discussion, we will start with the model for the growth of a polymer chain during heterogeneous, catalytic polymerization which is most reliable at present. According to this model the growing polymer chain has at its active end an alkyl- or haloalkylaluminum. The latter forms a catalytic complex with the titanium halide on the catalyst surface by a bridge ("semi") bond. This bond has an energy of 10-15 kcal/mole and is, evidently, the weakest unit connecting a polymer molecule to the surface. Consequently, the break away of such a molecule from the catalyst surface would most probably occur at this very bond, i.e., would be accompanied by dissociation of the catalytic complex. Natta et al. [2] were the first to report the possibility of reversible dissociation of catalytic complexes.

Let us examine separately the dissociation and the regeneration of a catalytic complex. The rate constant of the chemical reaction (K) is determined by the relation

$$K = \frac{kT}{h} e^{-\frac{\Delta U^* - T\Delta S^*}{kT}}, \qquad (2)$$

where k is Boltzmann's constant, h is the Planck's constant, ΔU^* is the activation energy and ΔS^* is the activation entropy.

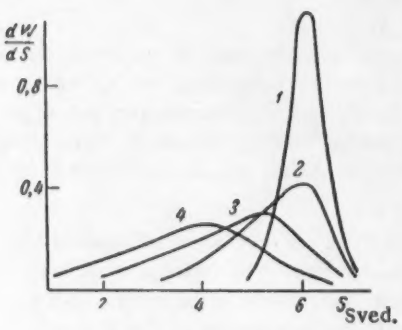

Fig. 1. Molecular weight distribution of polyisoprenes. 1) $Al(iso\text{-}C_4H_9)_3 : TiCl_4 = 1:1$. The catalyst was kept for 24 hours. Polymerization temperature 0°; 2) fresh catalyst $Al(iso\text{-}C_4H_9)_3 : TiCl_4 = 1:1$; 3) $Al(isoC_4H_9)_3 : TiCl_4 = 1:1 + 0.5$ $Al(iso\text{-}C_4H_9)_3$ (with monomer); 4) $Al(iso\text{-}C_4H_9)_3 : TiCl_4 = 1:1 + 1$ $Al(iso\text{-}C_4H_9)_3$. 2-4) Polymerization temperature 30°.

The structure of the initial complex is retained in the activated state during monomolecular dissociation, i.e., a macromolecule is connected to the surface as in the initial state. Therefore, in this case, as in other monomolecular reactions, the activation entropy is low and $T\Delta S^* << \Delta U^*$. Consequently, the rate constant for the breakaway of the polymer chain from the catalyst surface $K_1 \simeq 10^2 - 10^4$ sec^{-1}. Such a high value for K_1 indicates that the growth of the polymeric chain must be interrupted many times due to dissociation of the active center at the bridge bond. The aluminum remains at the end of the chain and its growth may be renewed after regeneration of the catalytic complex. The rate of the reversible regeneration of the catalytic complex when one of the reagents is a polymer molecule is determined then,not by the activation energy, which is low in this case, but by the activation entropy, whose value depends on the size of the polymer chain. Actually, in this reaction the activated state differs little structurally from the final one, i.e., the transition to an activated state is related to the connection of the end of the polymer chain to the surface. However, as follows from Eq. (1), the configuration entropy of the chain thereupon decreases by the value $\Delta S = k\sqrt{z}$. At a sufficiently large value of z the latter will form the main part of the activation entropy for the regeneration of the catalytic complex.

It follows from the above that the probability of a macromolecule being in the solution (x) or connected to the surface (1 − x) is determined by the following equation:

$$\frac{x}{1-x} = e^{-\frac{\Delta U - T\Delta S}{kT}}, \qquad (3)$$

where ΔU is the energy required for the breakaway of the polymer molecule from the catalyst surface.

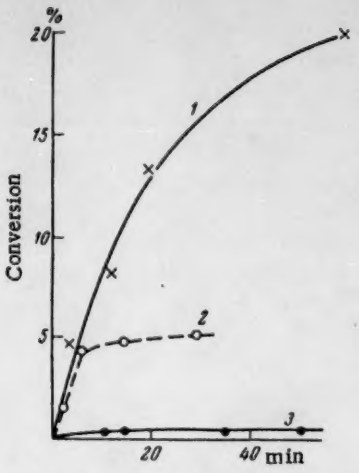

Fig. 2. Kinetic curves for isoprene polymerization at 30°C. 1) Al(iso-$C_4H_9)_3$: $TiCl_4$ = 1 : 1; 2) Al(iso-$C_4H_9)_3$: $TiCl_4$ = 1 : 1 + 0.5 Al(iso-$C_4H_9)_3$ (with monomer); 3) Al(iso-$C_4H_9)_3$: $TiCl_4$ = 1.5 : 1.

From relations (1) and (3) we obtained the following equation for the molecular weight distribution of the polymer:

$$\frac{dw}{dM} = \frac{\sqrt{\frac{M}{rM_0}}\, e^{-\frac{\Delta U}{kT}+\sqrt{\frac{M}{rM_0}}}}{2\left(1+e^{-\frac{\Delta U}{kT}+\sqrt{\frac{M}{rM_0}}}\right)^2}, \qquad (4)$$

where w is a weight fraction, r is the number of monomer links in a kinetic segment, and M_0 is the molecular weight of the monomer.

This distribution is characterized by a curve whose dispersion coefficient ($\delta M/M$) is determined by the equation

$$\frac{\delta M}{M} \simeq \frac{3kT}{\Delta U}. \qquad (5)$$

Thus, the disperion of the distribution curve is determined by the energy of the bond between the growing polymer molecule and the catalyst surface. At $\Delta U \simeq 10-15$ kcal/mole the dispersion coefficient of the molecular weight distribution equals approximately 0.1, i.e., is extremely small. Consequently, the proposed mechanism for the limiting of molecular chains during polymerization under the action of heterogeneous complex catalysts envisages the possibility of obtaining polymers with a very narrow molecular weight distribution. We actually prepared such a polymer by polymerizing isoprene as the pure monomer at a low temperature (0°) with a catalyst that was kept for 24 hours and had a component ratio of 1 : 1. Figure 1, 1 gives the distribution curve of this polymer in coordinates dw/ds (s is the sedimentation constant in octane at a polymer concentration of 2 mg/ml) and this curve is characterized by a dispersion coefficient equal to 0.1, which corresponds to a dispersion coefficient for the molecular weight distribution curve of ≃0.15.

Thus, complex catalysts are outstanding not only in stereospecificity but also in that they ensure the formation of highly homogeneous polymers under certain conditions. However, the mechanism for limitation of chains given above comes into effect only if the growth of macromolecules does not cease before then. One of the factors producing the "premature" termination of molecular chains is the presence of free triisobutylaluminum in the catalyst [3]. We checked this factor in special experiments in which a previously prepared catalyst (1 : 1 component ratio) was introduced into the monomer containing a measured amount of Al(iso-$C_4H_9)_3$. Under these conditions, at the beginning of polymerization, when the excess Al(iso-$C_4H_9)_3$ was still in the free state, the polymerization rate was approximately the same as it would have been without the addition of the free organoaluminum compound (Fig. 2), but the molecular weight distributions of the polymers were sharply displaced toward low molecular weights (Fig. 1, 3, 4). These facts indicate that the mechanism for limiting chains is similar to the transference mechanism when the former is affected by the chemically free organoaluminum compound, i.e., the mechanism proceeds with regeneration of active centers. Apparently, for the same reason when the polymerization is carried out with a freshly prepared catalyst (1 : 1 component ratio) which still contains a certain amount of free Al(iso-$C_4H_9)_3$, the polymer formed contains low-molecular fractions that are absent in the case of polymerization with the same catalyst that has been kept for 24 hours (Fig. 1, 1, 2).

The results given indicate that in catalytic polymerization, termination of molecular chains by the transference mechanism occurs only in the particular case when free organoaluminum compound or other components capable of transference reactions are present in the system. When these components are absent, the molecular chains are terminated by the mechanism presented above that is specific for heterogeneous polymerization.

LITERATURE CITED

[1] S. E. Bresler, M. I. Mosevitskii, I. Ya. Poddubnyi, and N. N. Chesnokova, Zhur. Tekhn. Fiz. 28, 2487 (1958).

[2] G. Natta and I. Pasquon, Atti Accad. Naz. Lincei, Rendi Sci. Fix. 26, 45, 617 (1959).

[3] G. Natta, I. Pasquon, and E. Giachetti, Chim. et Ind. 40, 97 (1958).

THE EFFECTS OF THE SEMICONDUCTOR PROPERTIES OF OXIDE FILMS ON THE ELECTROCHEMICAL BEHAVIOR OF METALS IN ELECTROLYTES UNDER THE ACTION OF ULTRAVIOLET LIGHT

A. V. Byalobzheskii and V. D. Val'kov

Institute of Physical Chemistry, Academy of Sciences of the USSR
(Presented by Academician A. N. Frumkin, April 28, 1960)
Translated from Doklady Akademii Nauk SSSR, Vol. 134, No. 1, pp. 121-124, September, 1960
Original article submitted April 8, 1960

It has been established by V. I. Veselovskii that oxide films have a considerable influence upon the electrochemical behavior of metals at irradiation with ultraviolet light [1]. However, this author observed and studied the photoelectrochemical effects only in anodic processes.

We have discovered that for several metals photoelectrochemical phenomena are observed exclusively in the region of cathodic polarization. Further investigations have shown that the character of the photoelectrochemical processes is intimately connected with the conductivity type of the oxide films which are present on the surface of the metals investigated. In Table 1 the results of our experimental investigation into the influence of ultraviolet light upon the potential of a series of metals, placed in diluted electrolytes and having an oxide film on their surface, are given. The data of Table 1 show: 1) the direction into which the metal potential is shifted by irradiation with uv depends upon the conductivity type of the oxide film on its surface. For n-type semiconductors the potential tends to shift in the negative direction, for p-semiconductors, on the contrary, in the positive direction; 2) reinforcement of the oxide film results in amplifying the effect mentioned. The Cd/CdO electrode is an exception. According to data in literature cadmium oxide belongs to the n-semiconductors, yet irradiation with uv shifts its potential not in the negative, but in the positive direction. At the same time reinforcement of the film thickness results in a decreased positive value of the photoeffect instead of an increased one, as should be found, according to the data given, in the case of p-semiconductors. Preliminary experiments have shown that a variation of the oxygen concentration in the solution has a considerable influence upon the magnitude and the character of the photoeffect. This gives reason to suppose that the potential shift under the action of uv light is connected with a change in the adsorptive properties of the oxide film with respect to oxygen and, possibly, to water molecules.

By means of a potentiostatic method we have investigated the influence of uv light upon the cathodic and anodic polarization of the metals, listed in Table 1. It was discovered that, for metals having on their surface an oxide film of the n-type, irradiation with uv facilitates the course of the anodic process and has no influence on the cathodic one. When a p-type oxide film is present, the picture is reversed. In Fig. 1 the magnitude of the photoeffect and the regions where it manifests itself in the metals examined are indicated. We see that cadmium, in which an effect is found in the cathodic as well as in the anodic region, again is an exception to the rule stated above. A further investigation is required to elucidate why Cd behaves in this way.

The behavior of copper is very peculiar. As may be seen in Fig. 1 its photoeffect has two waves. The origin of each wave (when the sequence of polarization goes from more negative to more positive potentials) corresponds with a reaction potential: for the first wave, that of cuprous oxide formation:

$$2Cu + 2OH^- \rightleftarrows Cu_2O + H_2O + 2\bar{e},$$

for the second wave, that of the formation of hydrated cupric oxide:

$$Cu_2O + 2OH^- + H_2O \rightleftarrows Cu(OH)_2 + 2\bar{e}.$$

The data given testify with certainty that even the very thin oxide films, which are formed on metals in electrolytes, have an influence on the electrochemical behavior of the metals; in this not only the presence of the film but also the type of its conductivity plays a role. Consequently, metal oxides manifest their semiconductor properties even in very thin layers. Obviously, this factor should be taken into account in corrosional and electrochemical investigations. A similar conclusion has been drawn in the study [2].

TABLE 1

The Influence of Ultraviolet Light upon the Change in Metal/Oxide-Film Electrode Potential in Aqueous Electrolyte Solutions

Metal/oxide	Conductivity type of the oxide according to literature	Electrolyte	Electrode with a natural oxide film: stationary electrode potential,* v			Electrode with reinforced** oxide film, v			
			without uv, V_{dark}	under illumination, V_{light}	potential change, v $\Delta V = V_{light} - V_{dark}$		V_{dark}	V_{light}	$\Delta V = V_{light} - V_{dark}$
Zn/ZnO	n	0,1*N*NaOH	−1,360	−1,360	0	+2,00	−0,710	−0,712	−0,002
							−0,100***	−0,712	−0,612
Zr/ZrO_2	n	0,1*N*NaOH	−0,592	−0,710	−0,118	+10,00	−0,430	−1,230	−0,800
Ta/Ta_2O_5	n	0,5*N*Na_2SO_4	−0,145	−0,370	−0,125	+12,00	−0,105	−0,500	−0,395
Ti/TiO_2	n	0,1*N*NaOH	−0,461	−0,735	−0,274	+3,00	+0,238	−0,865	−1,103
		0,5*N*Na_2SO_4	−0,138	−0,345	−0,207	+6,00	+0,210	−0,275	−0,485
Ni/NiO	p	0,1*N*NaOH	−0,135	+0,076	+0,211	+0,80	−0,131	+0,108	+0,239
Cu/Cu_2O	p	0,1*N*NaOH	−0,253	−0,240	−0,013	−0,45	−0,250	−0,022	+0,228
Cd/CdO	n	0,1*N*NaOH	−1,240	−0,388	+0,852	+2,00	−0,980	−0,950	+0,030

* Potential values referred to a saturated calomel electrode.

** The oxide film was reinforced by polarizing the samples at the potential indicated in the same solution as was used for the measurements; the duration of the polarization was fixed by the time required to establish a constant current density.

*** The potential given is not the stationary value, but the one measured immediately after terminating the anodic treatment.

The analysis of the data obtained permits us to confirm that the photoelectrical effects observed are connected not only with an increased conductivity of the semiconducting oxide layer but, chiefly, with the facilitation of the electrochemical reaction at the electrolyte-oxide boundary. This follows already from the fact that for most films irradiation effects are only found either in the cathodic or in the anodic region of polarization (see Fig. 1), while an increase in conductivity should operate identically without being dependent upon the current direction.

A similar conclusion also follows from an inspection of the curve describing the photoelectric current on a tantalum electrode (see Fig. 2).

It has been established [3] that the film thickness (d) on a tantalum electrode in 0.5 N Na_2SO_4 increases proportionally to the applied voltage (V) and, consequently, V/d = constant. The simplest calculation gives here I_{ph} = constant, but this is not in accordance with the experimental curve, which shows that the photocurrent I_{ph} changes when the film thickness increases. The curve shown consists of three parts. Part I is left out of consideration, because the formation of the film at its very start takes place under certain peculiar conditions and requires a special discussion, which would go beyond the scope of this paper. In part II we have a raised photocurrent at increasing film thickness. This raise may be explained, if one starts with the assumption that the electrode reaction at the surface is facilitated by the incoming current carriers.

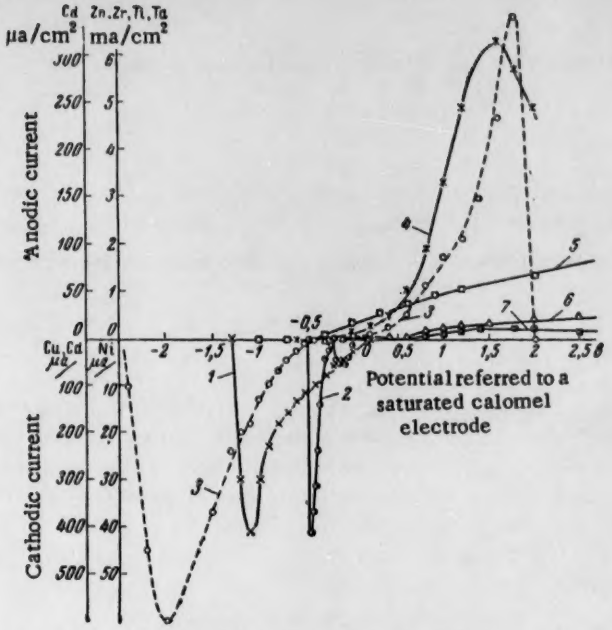

Fig. 1. Magnitude of the photoeffect as a function of the potential for various metals at their polarization in electrolytes: for Ta in 0.5 N Na_2SO_4, for the other metals in 0.1 N NaOH. 1) Ni; 2) Cu; 3) Cd; 4) Zn; 5) Ti; 6) Ta; 7) Zr.

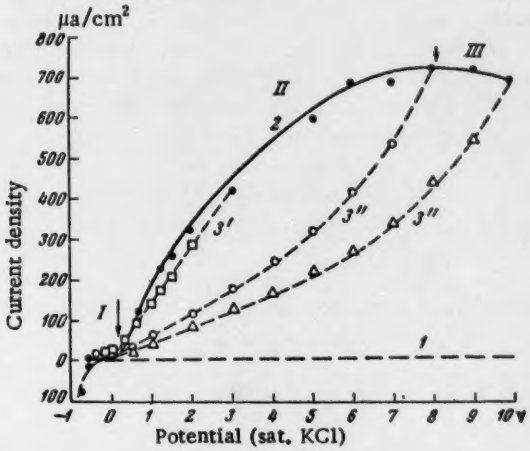

Fig. 2. Influence of uv irradiation upon the polarization of Ta/Ta_2O_5 in 0.5 N Na_2SO_4. 1) Dark current; 2) photocurrent; 3', 3", 3"') photocurrent curves for reversed polarization.

Then

$$I_{ph} = en_d^{\equiv}\alpha, \tag{1}$$

where e is the electron charge in coulomb; n_d the total number of current carriers, generated in a film of a

given thickness under the action of irradiation with given intensity; α the fraction of these carriers utilized at the surface.

From the general laws for the absorption of radiation energy it follows that

$$n_d = n(1 - e^{-\mu d}), \tag{2}$$

where d represents the film thickness; n the total number of carriers, generated at complete absorption of the radiation energy; μ the absorption coefficient.

Assuming that for very thin films $\alpha \approx$ constant and substituting voltage for film thickness, instead of relation (1) we may write:

$$I_{ph} = An(1 - e^{-BV}), \tag{3}$$

where A and B are constants for a given radiation intensity. Relation (3) is similar to the one cited by Young[4]. However, in contrast with Young, who obtained very scattered data for thicker films and assumed that in this region I_{ph} is constant, we always observed a decrease in I_{ph} as part III of curve 2 in Fig. 2 shows. We explain this by the fact that relation (3) is only valid as long as the film thickness does not exceed the layer of primary uv absorption (d_{max}). Upon further increasing the oxide thickness a d_1 layer with a higher ohmic resistance makes its appearance, which results in a decreased voltage in the layer d_{max} and, consequently, in a diminished I_{ph}. This may be expressed by the relation

$$I_{ph} = k\eta V, \tag{4}$$

where η is a coefficient which indicates the fractional voltage drop in the layer d_{max}. It is easy to show that $\eta \to 0$ and that it decreases faster than V increases. This makes the curve descend in part III. We have not determined as yet the exact way in which η varies at increasing film thickness.

The difference between the curves 3', 3", 3"' and curve 2 has its origin in the fact that for each of the former curves we have d = constant where d"' > d" > d', The path of these curves proves graphically that the photocurrent is connected with the voltage of the field in the film. The difference in shape between curve 3', which is substantially a straight line, and curves 3" and 3"' should also be noticed. Obviously this is connected with the fact that the curves 3', 3", 3"' come from different parts of the curve 2 and, consequently, the film 3' does not contain the layer d_1, which is present in films 3"' and 3".

LITERATURE CITED

[1] V. I. Veselovskii, Zhur. Fiz. Khim. 15, 145 (1941); 20, 269 (1946); 22, 1427 (1948); 23, 1095 (1949); 24, 366 (1950).

[2] I. L. Rozenfel'd and E. K. Oshe, Doklady Akad. Nauk SSSR 125, 139 (1959).*

[3] H. E. Haring, J. Electrochem. Soc. 99, 30 (1952).

[4] L. Young, Trans. Farad. Soc. 50, No. 2 (1954).

* Original Russian pagination. See C. B. Translation.

INVESTIGATION OF COMPRESSION WAVES DURING THE COMBUSTION OF GASEOUS MIXTURES

S. M. Kogarko and A. S. Novikov

Institute of Chemical Physics, Academy of Sciences of the USSR
(Presented by Academician V. N. Kondrat'ev, April 28, 1960)
Translated from Doklady Akademii Nauk SSSR, Vol. 134, No. 1, pp. 125-127, September, 1960
Original article submitted April 22, 1960

The formation and amplification of compression waves [1, 2] is observed in the combustion process during the propagation of flames in explosive gas mixtures with practically constant velocity under certain conditions of test. The mechanism of the phenomenon of the amplification of compression waves during combustion consists of an increase in the rate of the chemical reaction in the region of the flame, with an interaction of the flame with the compression wave, and a temporary retention of the additional energy released in the reaction zone.

In the absence of external disturbances and acceleration of the flame, all processes which occur in the reaction zone of the flame and the space surrounding it are steady. There exists, on the one hand, a diffusion flow of the initial mixture into the reaction zone of the flame and a thermal flow out of the reaction zone into the initial mixture, and, on the other hand, an efflux of reaction products from the region of the flame.

If there is imposed in the region of the chemical reaction a disturbance in the form of a compression wave, which increases somewhat the temperature and density of the reacting mixture, then there will consequently be an increase in the rate of the chemical reactions in the burning region. Since the establishment of a new temperature in the reaction zone, corresponding to the compression of the reacting mixture by the wave, takes place significantly faster than the removal from the reaction zone of the additional energy released into the surrounding space, part of the excess energy is temporarily entrapped in the reaction zone. This leads to an increase of pressure in the reaction zone and the formation at its boundaries of additional waves, which also amplify the compression waves.

The formation of the initial compression wave occurs, as a rule, as a result of the combustion of a small volume of the mixture at the moment of its ignition by an electric spark or other ignition source. Its formation is possible also as a result of the accidental combustion of a small volume of mixture already in the process of burning. It is obvious that the amplitude of the initial compression wave and the degree of its amplification in the subsequent burning process will depend on the physicochemical properties of the mixture. During the combustion of a mixture in closed or semiclosed spaces, the compression wave, as a rule, will cross the flame front many times during the entire combustion process. Therefore, it is necessary to examine the repeated interaction of the compression wave with the reaction zone of the flame.

Since the amplification of a compression wave is associated with a disturbance of the steady nature of the processes in the flame, then if a repeated act of interaction of the compression wave with the reaction zone occurs after steady conditions have been reestablished, all phenomena examined earlier will be repeated. In the contrary case, i.e., when a new interaction of the compression wave with the reaction zone occurs before the reestablishment of the steady nature of all processes, the rate of the release of the additional energy in the reaction zone may prove to be sufficient only to compensate its nonstationary resorption into the surrounding

Fig. 1. Record of compression waves during the combustion process in a tube of length L = = 170 mm. Mixture: a) $CH_4 + 2O_2 + 8O_2$; b) $CH_4 + 2O_2 + 8N_2$.

TABLE 1

Composition of mixture	Length of tube, mm	Maximum amplitude of compression wave, mm
$CH_4+2O_2+10O_2$	170	19
	75	0
$CH_4+2O_2+8O_2$	170	64
	75	38
$CH_4+2O_2+6O_2$	42	0
	42	66
	32	7
9.5%CH_4+90.5 air	170	13.0
	75	0

flame space. In this case, there will not be amplification of the compression wave. In experiment, all of the intermediate cases can also be realized.

Appropriate tests were carried out for the purpose of investigating further the amplification of compression waves in the process of combustion, and to check experimentally certain conclusions of the theory.

The tests were carried out in glass tubes of diameter 10 mm. Registration of the compression waves in the combustion process was carried out on a rotating photographic film with the help of a piezoelectric quartz transducer and a cathode-ray oscillograph. The transducer was situated at one end of the tube. The other end of the tube, at which ignition of the mixture was carried out by means of an electric spark, was open to the atmosphere.

As a result of the investigations, it was established that the formation and amplification of compression waves occur in the process of burning methane-oxygen in tubes, open at one end, for the methane in the mixture ranging from 7.5 to 53%. With a reduction of the methane content in the mixture from 9.1 to 6.7%, there is observed at first a rapid decrease in the maximum amplitude of the compression wave, and with a further reduction in the methane content amplification of the initial compression wave during the combustion process ceases completely.

In mixtures with insufficient combustible gas, replacement of the excess oxygen by nitrogen leads to a sharp change of the amplification of the compression waves during the combustion process. Since the thermal conductivity, the diffusion coefficient, the heat capacity, and also, in the regime of insufficient fuel, the maximum temperature of the flame all remain practically constant, then a certain reduction in the value of the normal flame velocity upon replacing the excess oxygen by nitrogen should be ascribed to a reduction in the chemical reaction rate in the flame [3]. Figure 1 shows photographic records of compression waves in the following mixtures: a) $CH_4 + 2O_2 + 8O_2$ and b) $CH_4 + 2O_2 + 8N_2$. In the second case, in the combustion process, there is recorded a very weak compression wave in comparison with the compression waves recorded during the combustion of the first mixture. The results of these experiments confirm our ideas that the amplification of a compression wave depends on the chemical reaction rate in the flame region and its changes under the influence of disturbances imposed on the flame.

A series of tests using tubes of different lengths was carried out for the purpose of studying the effect of the frequency of encounters of the compression waves with the reaction zone of the flame on the development of compression waves during the combustion process. The results of these tests showed that for a number of the methane-oxygen and methane-air mixtures of stochiometric composition investigated by us there are critical tube lengths, for less than which the combustion process proceeds without compression waves.

Table 1 shows the experimental data, and Fig. 2, for illustration, the corresponding photographic records.

An analysis of the photographs of Fig. 2 and the data of Table 1 leads to the conclusion that in the combustion of a mixture of composition $CH_4 + 2O_2 + 8O_2$, the maximum amplitude of the compression wave decreases upon shortening the tube, i.e., with an increase in the frequency of encounters of the flame with the compression wave, and in a tube of length L = 42 mm, becomes equal to zero. In the latter case, there is not observed any compression wave during the entire combustion process. Thus, tube length of 42 mm is the critical length for the given mixture. In a mixture of composition $CH_4 + 2O_2 + 6O_2$, with a large value of the normal velocity, and consequently a smaller width of the reaction zone, the development of a compression wave during

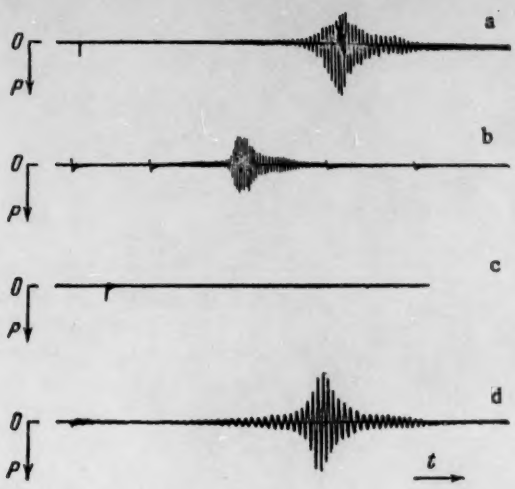

Fig. 2. Records of compression waves during the combustion process in tubes of various lengths. Mixture $CH_4 + 2O_2 + 8O_2$: a) 170 mm; b) 75 mm; c) 42 mm; mixture $CH_4 + 2O_2 + 6O_2$: d) 42 mm.

the combustion process in a tube of the indicated length (Fig. 2d) proceeds approximately the same as for the mixture $CH_4 + 2O_2 + 8O_2$ in a tube of length 170 mm (Fig. 2a).

The experimental data obtained on the critical lengths of tubes is in agreement with our theoretical concepts regarding the mechanism of the amplification of compression waves during the combustion process. As the methane content in methane-oxygen mixtures in which there is an excess of oxygen is reduced, the value of the normal flame velocity is reduced, and, consequently, the width of the reaction zone increases. This is associated with an increase in the time interval necessary for complete resorption of a previous disturbance. Therefore, for normal amplification, the frequency of encounters of the compression wave with the flame should be reduced, and the critical tube length will be increased.

LITERATURE CITED

[1] S. M. Kogarko and V. I. Skobelkin, Doklady Akad. Nauk SSSR 120, No. 6 (1958).*

[2] S. M. Kogarko, Zhur. Tekh. Fiz. 30, 110 (1960).

[3] W. Jost, Explosions- u. Verbrennungsvorgänge in Gasen (1939).

*Original Russian pagination. See C. B. Translation.

THE PROBLEM OF HYDROGEN OVERPOTENTIAL ON PLATINUM

Ya. M. Kolotyrkin and A. N. Chemodanov

The L. Ya. Karpov Physicochemical Institute
(Presented by Academician A. N. Frumkin, April 26, 1960)
Translated from Doklady Akademii Nauk SSSR, Vol. 134, No. 1, pp. 128-131, September, 1960
Original article submitted April 11, 1960

It is known from the literature [1] that for low overpotentials the rate of electrochemical evolution of hydrogen in acid solutions at active electrodes made of noble metals, particularly platinum, is determined by the Tafel equation:

$$\eta_{H_2} = a + b \cdot \lg i \qquad (1)$$

in which the slope b has a value close to 20 mv at room temperature. Such a value for the slope may be connected with a retardation of the recombination stage, in which the atoms of hydrogen discharged at the electrode surface are combined into molecular hydrogen [2]. An alternative point of view, first formulated for the case of a palladium cathode, postulates that in this range of potentials the process is in the main regulated by the rate of diffusion of molecular hydrogen away from the cathode surface into the body of the liquid [3]. In the course of this, the surface concentration of hydrogen is increased in comparison with that in the bulk, and, in accordance with the Nernst equation,

$$\varphi = \varphi_0 + \frac{RT}{nF} \cdot \ln \frac{C^2_{H^+}}{P_{H_2}}, \qquad (2)$$

the cathode potential is shifted towards the negative. With increase in the current density, the diffusion component of the total overpotential, η_d, reaches a limiting value of the order of 30 to 60 mv, which corresponds to an increase of the surface hydrogen concentration by a factor between 10 and 100.

We have carried out experiments to test this suggestion by means of a direct experimental determination of the hydrogen concentration in the neighborhood of a functioning platinum microcathode by the method of oscillographic polarography. If hydrogen accumulates during cathodic polarization in the preelectrode region of the solution, then a sufficiently rapid positive shift in the electrode potential should lead to the observation of a peak in the anodic oxidation of this hydrogen, the height of which should be proportional to its concentration. The coefficient of proportionality may be determined experimentally in experiments in which the pressure of hydrogen is increased.

Two series of experiments have been performed. In one of these anodic polarograms were recorded (with a rate of potential increase at the electrode, $\alpha \leq 10$ v/sec), using a platinum electrode in 1 N sulfuric, perchloric or hydrochloric acid saturated with hydrogen at pressures of hydrogen, P_{H_2}, up to 440 atm, commencing at potentials, φ_{init}, equal to zero against the hydrogen electrode in the same solution. In the other series the $i - \varphi$ curves were recorded for atmospheric pressure of the hydrogen, commencing at various potentials, in which φ_{init} was ≤ 0 against the normal hydrogen electrode. The work was carried out using two electrode cells in which the cathodic and anodic areas were not separated. The surface area of the electrodes under test varied from

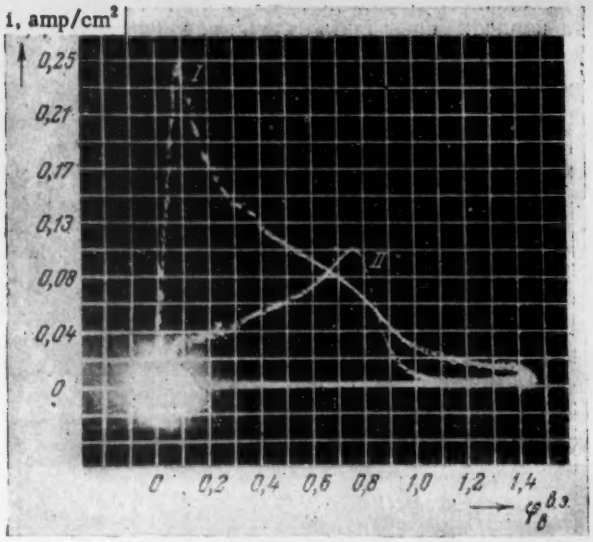

Fig. 1. The anodic oxidation of hydrogen on platinum in 1 N sulfuric acid at a hydrogen pressure of 65 atm. The rate of change of potential, α = 10 v/sec. I) Forward direction, φ_{init} = 0 (against the hydrogen electrode); II) reverse direction. Area of electrode = 0.0156 cm².

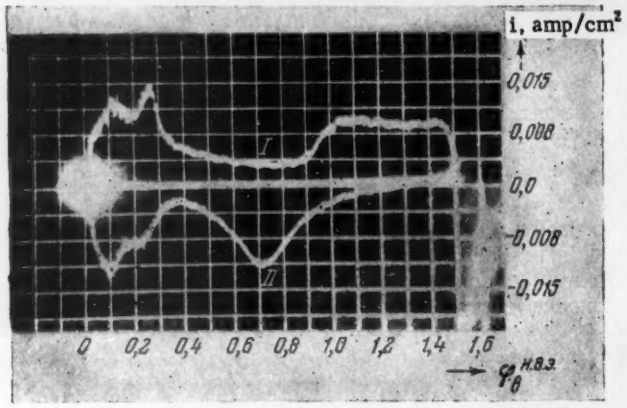

Fig. 2. Anodic polarization of platinum in 1 N sulfuric acid. Hydrogen pressure = 1 atm. I) Forward direction, φ_{init} = 0 (against normal hydrogen electrode); II) reverse direction. Area of electrode = 0.0156 cm².

0.01 to 0.08 cm².* A large platinized platinum electrode was used as the auxiliary electrode. The design of the experiments required anodic activation of the electrode, and its polarization for a given value of φ_{init} for a period of 1 sec (which was believed to be sufficient for the attainment of stationary concentration in the neighborhood of the electrode), followed by the recording of the anodic and cathode-anodic polarograms up to the potential at which oxygen (chlorine when hydrogen chloride solutions were used) was liberated. Curves obtained in the reverse direction were also recorded.

* The surface area of the electrode was determined from the magnitude of the limiting diffusion current for the ionization of hydrogen [4].

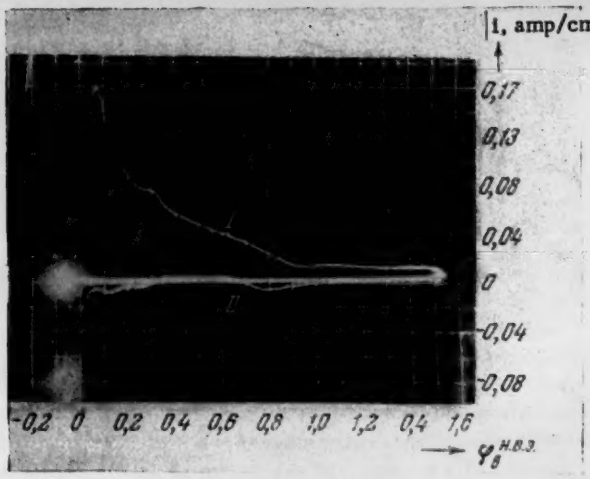

Fig. 3. Anodic polarization of platinum in 1 N sulfuric acid. Hydrogen pressure = 1 atm. I) Forward direction, φ_{init} = = − 77.7 mv (against normal hydrogen electrode); II) reverse direction. Area of electrode = 0.0156 cm².

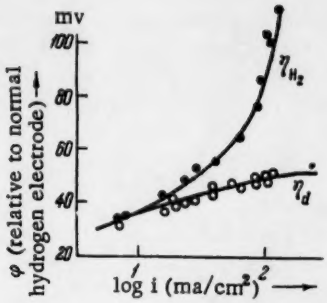

Fig. 4. Relationship between the overpotential of hydrogen on platinum in 1 N sulfuric acid on the logarithm of the initial current density, $i_{init} \cdot \eta_{H_2}$ = total overpotential; η_d = diffusion component of the total overpotential, calculated on the basis of Eqs. (3) and (2).

Figure 1 gives an example of the procedure in the form of a polarogram (in both forward and reverse directions), with α = = 10 v/sec, delayed at φ = 1450 mv for 0.075 sec before returning, and recorded using 1 N sulfuric acid and P_{H_2} = 65 atm. It may be shown that the maximum obtained on the forward curve (and also on the reverse curve), is connected with the ionization of the hydrogen dissolved in the preelectrode layers of the solution, and not of that adsorbed on the surface or penetrated into the surface layers of the metal. The quantity of electricity needed to shift the potential of the electrode to the potential maximum is at least ten times that corresponding to a monolayer of hydrogen on the surface (it seems that the adsorption of hydrogen on platinum does not exceed this value [5]) and, in addition, is dependent on the value of α. The height of the maximum current (i_{max}) on the polarogram is proportional to $\alpha^{\frac{1}{2}}$ and to the bulk hydrogen concentration (C), and therefore also to the pressure of hydrogen P_{H_2}. When α = 10 v/sec,

$$i_{max} = 3{,}8 \cdot P_{H_2} \text{ ma/cm}^2, \tag{3}$$

when the pressure is expressed in atmospheres. Calculation of i_{max} by means of the Shevchik-Rendels equation [6] gives:

$$i_{max} = K \cdot n^{3/2} \cdot \alpha^{1/2} \cdot D^{1/2} \cdot C, \tag{4}$$

where K is a constant,* and n is the number of electrons taking part in the reaction. D is the diffusion coefficient for various values of α and P_{H_2}. This equation gives values within an order of magnitude of those obtained experimentally. The decrease in current after the maximum has been reached proceeds according to the diffusion law:

$$i = \frac{A}{\sqrt{\tau}} + B, \tag{5}$$

*The value of K used is the numerical value calculated for a solid electrode in [7].

TABLE 1

η_{H_2}, mv	33,7	35,4	44,4	56,4	65,4	77,7	87,9	104,4	152,7	179,7
η_d, mv	32,0	35,9	42,1	46,6	47,2	48,6	50,2	51,3	51,4	49,9
P_{H_2}, atm	12	16	26	37	39	44	49	53	54	48

where A and B are constants, and τ is the time. The value of B calculated from the polarogram is close to the value of the limiting diffusion current for the ionization of hydrogen.

The shape of the $i - \varphi$ curves obtained in the second series of experiments depends greatly on the value of φ_{init}. It can be seen from Fig. 2 that when $\varphi_{init} \geq 0$ (and, correspondingly, $i_{init} \geq 0$) the oscillogram is a somewhat distorted curve showing the relationship of the capacity of the platinum electrode to the potential, with the characteristic separation between the areas corresponding to adsorption of hydrogen and of oxygen, and maxima of the pseudocapacity in the hydrogen adsorption area [5, 8]. For sufficiently large values of α, the value of the current at all the potentials studied is practically independent of the rate of rotation of the electrode or the rate of stirring of the electrolyte. If the value of φ_{init} is shifted in a negative direction, however, corresponding to $i_{init} < 0$, there arises a maximum in the current similar to that obtained by increasing the hydrogen pressure (Fig. 3). The height of the maximum depends on the values of φ_{init}, pH, α and the duration of the preliminary cathode polarization, though it is independent of the nature of the acid used. The height of the maximum and the rate of reduction of the current after the maximum are greatly reduced by vigorous stirring of the electrolyte or rotation of the electrode.

The data obtained, taken as a whole, justify the view that the oscillographic polarography method, using a platinum microelectrode in an acidic solution, is capable of being used for the determination of hydrogen concentrations both in the bulk of the solution, and close to the surface of the working platinum electrode, providing these are not excessively small. Table 1 gives the values for the overpotential ($\eta_{H_2} = \varphi_{init}$) measured in one of the experiments together with the values of P_{H_2} and η_d calculated from Eqs. (3) and (2). The relationship between η_{H_2} and η_d, on the one hand, and the density of the cathodic current, is given in semilogarithmic coordinates in Fig. 4.

Figure 4 and Table 1 show that the overpotential of hydrogen on the platinum electrode which has been studied, to potentials of the order of $\eta_{H_2} \sim 40$ mv, is of a purely diffusional nature ($\eta_{H_2} = \eta_d$). Further shift of the potential in the negative direction causes η_d to approach a limiting value [3], and then, according to our data, to diminish somewhat. It is possible that the explanation of this lies in the more intense agitation of the solution in the neighborhood of the electrode surface owing to the evolution of hydrogen.

We wish to offer our thanks to I. E. Bryksin for developing and preparing the oscillographic polarograph which we have used in this work.

LITERATURE CITED

[1] J. O. M. Bockris, J. A. Ammar, and A. K. M. S. Hug, J. Phys. Chem. 61, 879 (1957).

[2] J. O. M. Bockris, Some Problems of Contemporary Electrochemistry [Russian translation] (IL, 1958) p. 244; S. Schuldiner, J. Electrochem. Soc. 106, 10, 891 (1959).

[3] L. Kandler, C. A. Knorr, and M. Schwitzer, Z. Phys. Chem. A180, 281 (1937); R. Clamroth and C. A. Knorr, Z. Elektrochem. 57, 6, 399 (1953); A. N. Frumkin and N. A. Aladzhalova, Zhur. Fiz. Khim. 18, 11-12, 493 (1944).

[4] E. V. Nikolaeva and A. I. Krasil'shchikov, Zhur. Fiz. Khim. 32, 7, 1545 (1958).

[5] B. Ershler, Acta physicochem. URSS 7, 327 (1937).

[6] P. Delahay, New Apparatus and Methods in Electrochemistry [Russian translation] (IL, 1957) p. 145.

[7] R. Sh. Nigmatullin, Candidate's Dissertation: Oscillographic Method in Its Application to Polarography at Solid Electrodes) (Kazan', 1953).

[8] E. Wicke and B. Weblus, Z. Elektrochem. 56, 3, 169 (1952).

THE TEMPERATURE DEPENDENCE OF THE SURFACE TENSION OF GERMANIUM

V. B. Lazarev and P. P. Pugachevich

N. S. Kurnakov Institute of General and Inorganic Chemistry, Academy of Sciences of the USSR

(Presented by Academician I. I. Chernyaev, April 13, 1960)
Translated from Doklady Akademii Nauk SSSR, Vol. 134, No. 1, pp. 132-133, September, 1960
Original article submitted April 11, 1960

Technological developments have given rise to the problem of alloying semiconducting substances of exceptionally high purity with infinitesimally small amounts of various additives and relating the compositions and properties of the resulting materials [1]. A study of the surface tensions of such alloys in the molten state would contribute directly to the solution of this problem. An investigation of the surface tensions of molten semiconductors would also have practical bearing on the problem of zone melting, the formation of monocrystals [2], and the wetting of the semiconductors by metals [3], for example, to say nothing of the value of the results which it might furnish for the theory of intermolecular forces and the energy of molecular interaction.

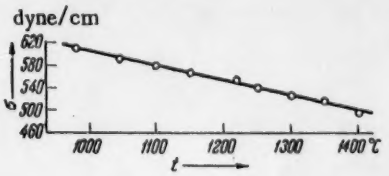

Fig. 1. Temperature dependence of the surface tension of germanium.

The surface tension (σ) of germanium was first measured by Keck and Van Horn [2] using the drop-weight method, a procedure of doubtful theoretical validity [4, 5]. These authors found a value of 600 dyne/cm for the surface tension of germanium at the melting point.

By observing the form of the solidified droplet, Sengster and Carman concluded [6] that the σ value of germanium in the neighborhood of the melting point was 632 dyne/cm. On the other hand, application of this same method to other metals led to σ values which were in error by 20-30% [7]. Moreover, neither of these methods permits the surface tension of the melt to be measured as a function of temperature. It was for this reason that our own measurements were carried out by determining the maximum gas bubble pressure, a technique which is well-grounded theoretically and yields results which are scarcely open to question. The theory of this method as developed by Cantor [8] calls for the use of infinitesimally thin-walled capillaries. Capillaries of this kind were prepared from spectrally-pure graphite. In each case, the end of the capillary which was introduced into the melt was ground so as to eliminate the effect of the wetting angle on the measured value of σ and, at the same time, fix the radius which appears in the working equation [9-11]. Measurements were performed on specimens of monocrystalline germanium with a specific resistance of 20 ohm·cm. These were heated in a graphite crucible inserted in a special vacuum furnace which was heated by passing current at high potential through a cylinder of sheet tantalum. Argon was employed for producing the bubbles, the gas being first purified by passage through molten lithium at 300°. The apparatus was so designed that the measurements could be carried out by the Sugden procedure [12], using two capillaries introduced into the melt at the same level so as to avoid the necessity of a correction for hydrostatic pressure in the calculation of σ. Maximum gas bubble pressures were measured with a membrane manometer. The capillary diameters ranged up to 4 mm, and the effective capillary radii

TABLE 1

Temperature Dependence of the Surface Tension of Germanium

Temp.,°C	Surface tension, dyne/cm		$\Delta\sigma = \sigma_{exp} - \sigma_{calc}$, dyne/cm	Temp., °C	Surface tension, dyne/cm		$\Delta\sigma = \sigma_{exp} - \sigma_{calc}$, dyne/cm
	σ_{exp}	σ_{calc} from (1)			σ_{exp}	σ_{calc} from (1)	
980	609,5	609,9	−0,4	1250	539,8	539,5	+0,3
1045	589,9	593,0	−3,1	1300	526,8	526,5	+0,3
1100	579,9	578,6	+1,3	1355	515,7	512,1	+3,6
1150	564,1	565,6	−1,5	1400	494,2	500,4	−6,2
1225	553,3	547,3	+6,0				

$\overline{\Delta\sigma}_{mean} = \pm 2.5$

employed in the calculation of the surface tension were determined by a method of successive approximations, using the Sugden tables [12]. The densities of molten germanium at various temperatures were also required in the calculations; these were taken from [13] and extrapolated to 1400°. The accuracy of determination of the surface tension under these conditions was 1%, the error being no more than 7 dyne/cm.

The results of our measurements on the temperature dependence of the surface tension of germanium are presented in Table 1 and in Fig. 1. The relation between these factors can be expressed through the equation

$$\sigma = 621{,}4 - 0{,}261\,(t^\circ - 936^\circ), \qquad (1)$$

in which t° is the temperature in centigrade degrees and 936° is the melting point of germanium according to the data of Grejner [14]. The constants of this equation were evaluated by the method of least squares. The equation shows the surface tension of germanium at the melting point to be 621.4 dyne/cm. This result is in good agreement with the theoretical value of 617 dyne/cm obtained by Zadumkin for a certain electron-ion polar model of the crystal lattice [15]. On the other hand, the temperature coefficient of the surface tension of germanium calculated by Zadumkin ($d\sigma/dT = -0{,}054$) is markedly different from that obtained experimentally ($d\sigma/dT = -0{,}21$). It is possible that this difference results from temperature-dependent structural alterations in the melt which were not considered in the Zadumkin theory.

LITERATURE CITED

[1] Germanium, First Collection [in Russian] (Moscow, 1955).

[2] P. H. Keck and W. Van Horn, Phys. Rev. 91, 512 (1953).

[3] A. P. Vyatkin, Zhur. Tekh. Fiz. 27, No. 6 (1957); Izvest. Vyssh. Uch. Zav. Fizika. 2, 48 (1959).

[4] V. K. Semenchenko, Surface Effects in Metals and Alloys [in Russian] (Moscow, 1957).

[5] P. P. Pugachevich, Collection, Nauch. Tr. No. 30, Nauchno-tekhnich. Obshch. Tsvetnoi Metallurgii i Mosk. Inst. Tsvet. Met. i Zolota im. M. I. Kalinina 1, 73 (1957).

[6] R. C. Sengster and I. N. Carman, J. Chem. Phys. 23, 1142 (1955).

[7] O. A. Esin, P. V. Gel'd, and S. I. Popel', Doklady Akad. Nauk SSSR 74, 1087 (1950).

[8] M. Cantor, Ann. Phys. 47, 399 (1892).

[9] A. M. Levin, Elektrometallurgiya, Nauchn. Tr. Dnepropetrovsk. Metallurgich. Inst. 28, 105 (1952).

[10] V. V. Fesenko and V. A. Eremenko, Transactions of a Seminar on Heat-Resistant Materials, Bull. [in Russian] No. 4, 52 (1959).

[11] K. I. Vashchenko and A. P. Rudoi, Izvest. Vyssh. Uch. Zav. Chernaya Metallurgiya 9, 133 (1959).

[12] S. Sugden, J. Chem. Soc. 125, 32, 1167 (1924).

[13] W. Klemm, H. Spitzer, et al., Monatsh. Chem. 83, 629 (1952).

[14] E. S. Grejner, J. Metals 4, 10, 1044 (1952).

[15] S. N. Zadumkin, Doklady Akad. Nauk SSSR, 101, 507 (1955); 112, 453 (1955); Fiz. Tverd. Tela 1, 572 (1959).

RADIATION-INDUCED THERMOLUMINESCENCE OF ORGANIC COMPOUNDS

V. G. Nikol'skii and N. Ya. Buben

Chemical Physics Institute, Academy of Sciences of the USSR
(Presented by Academician V. N. Kondrat'ev, April 28, 1960)
Translated from Doklady Akademii Nauk SSSR, Vol. 134, No. 1, pp. 134-136, September, 1960
Original article submitted April 22, 1960

It is a known fact [1] that many compounds after being exposed to γ-radiation or fast electrons at low temperatures exhibit luminescence upon subsequent warming. In this work we examined such emission (radiation-induced thermoluminescence) from several organic compounds.

The compounds were kept under nitrogen and exposed to a heavy dosage ($5 \cdot 10^5$ rad/sec) of 1.5 Mev electrons. The temperature during the exposure was maintained at about 100°K. We usually used samples in the form of thin films or slices weighing from 1 to 100 mg; the liquids were frozen in silvered brass capsules and the slices were always much thinner than the range of the electrons. The irradiated samples, which were stored in liquid nitrogen, were allowed to warm up at a steady rate of 15 deg/min and the intensity of the light emitted was recorded (we plotted the intensity as a function of temperature). The photometer used for this purpose consisted of a FÉU-19 photoelectric multiplier, a direct current amplifier, and an ÉPP-09 self-recording potentiometer. The recorded integral photocurrent depended on the sensitivity of the FÉU-19 instrument and we did not bother to investigate the spectral composition of the emitted light. The sample temperature was measured with a thin copper–"constantan" thermocouple.

The emission curves exhibit a single or several characteristic maxima at certain fixed temperatures. Thus the high-pressure polyethylene samples exhibited two outbursts of thermoluminescence, with the maximum intensities being at temperatures $T_{M_1} = -120$°C and $T_{M_2} = -40$°C (see Fig. 1, 1). In Figure 1 we have also plotted the emission curve for one of the low-pressure polyethylene samples (curve 2) which had a strong maximum at −119°C and a weak, poorly resolved maximum at −59°C. Some of our experiments were done on samples prepared from ten different cuts of the same compound and the results for various cuts were quite consistent. For example, in high-pressure polyethylene T_{M_1} varied from −124 to 116°C and T_{M_2} from −43 to −31°C. We should point out that when working with various samples prepared from the same cut the results were reproducible to within one or two degrees.

As is well known, high-pressure polyethylene is more highly branched than the low-pressure variety [2] and consequently there is a certain difference between the physical properties of the two types. A study of the temperature dependence of the Young's modulus and of the mechanical and dielectric losses in the range from −150 to 0°C showed that the high-pressure polyethylene undergoes two structural transitions in this temperature range [3-6]. The one which occurs between −125 and −105°C has been observed in many polymers and seems to be connected with the fact that segments of the principal chain and the side chains begin to vibrate [7, 8]. The second transition, between −70 and −20°C, is specific for branched polyethylenes [6]. The temperature at which this transition occurs is usually called the glass point of polyethylene. In the case of the low-pressure polyethylene and polymethylene, things are somewhat different. The mechanical and dielectric losses still exhibit a maximum between −115 and −105°C, but the other maximum, which is supposed to appear between −70 and

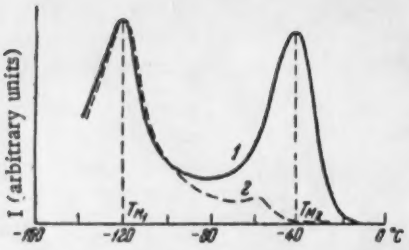

Fig. 1. Polyethylene emission curves: 1) high-pressure polyethylene; 2) low-pressure polyethylene; the radiation dosage was 10^6 rad.

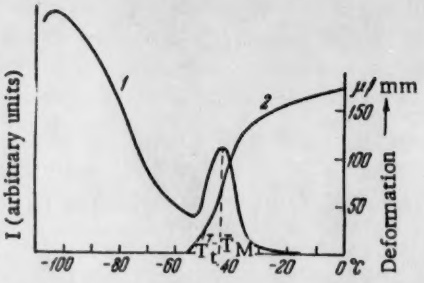

Fig. 2. Emission curve after a dosage of 10^6 rad (1) and the thermomechanical curve (2) for the same polyisobutylene sample.

TABLE 1

Compound	T_M, °C	T_{Md}, °C	Compound	T_M, °C	T_t, °C	T_{Md}, °C
High-pressure polyethylene	−124 −116	−120(4), −108(4)	Polyisobutylene	−118		
	−43 −31	−45(11); −24(11)		−45	−52[3]	
			Teflon	−125		−96(11); −105(15)[3]
Low-pressure polyethylene	−119					+20(14);
	−59			+22		+23(15);
Paraffin, n-$C_{25}H_{52}$	−121					+21(16)
	−50[1]	M.p. +60	Natural rubber	−137		
Plasticized paraffin (1% CCl_4)	+50 − +55		(Synthetic isoprene rubber)	−58	−57[3]	−61(17)
	−134			−126		
	−71			−58	−56[3]	
Octadecane, n-$C_{18}H_{38}$	−111	+24 (13);		+63	+80[3]	
	+20	M.p. +28	SKB-rubber	−49	−46[3]	
Nonane, n-C_9H_{20}	−112			+60	+50 ÷ +70	
	−57		(Synthetic butadiene rubber)	−148		
Polydimethylsiloxane	−54			−115		−120 ÷ −90(11);
	−119			−87		−87,1(11)[4];
			Cyclohexane	−72		−50(18)[5]

(1) N.m.r. data indicate [2] that the methyl groups begin to rotate at − 45° in n-$C_{28}H_{58}$ and at − 40°C in n-$C_{32}H_{66}$; (2) transition to an elasticoviscous state; (3) transition to a viscous state; (4) change in the crystal lattice; (5) beginning of self-diffusion.

−20°C, is either completely absent or shows up very faintly [4, 9]; this difference has been attributed to the smaller number of side groups in the latter polymers. Thus, in the case of polyethylene there is a definite similarity between the maxima on the emission curves and the mechanical and dielectric loss maxima.

In the present work we also established the fact that the positions of the emission maxima, especially the position of T_{M_2}, depend on the preliminary radiation dosage (extent of polymeric crosslinking), the thermal past history of the sample, and on the rate of warming; the shift of T_{M_2} corresponds to the accompanying shift in the glass point of the polymer. Taking all of these facts into consideration we can conclude that the outbursts in thermoluminescence result from the freeing of the frozen molecular vibrations and other forms of motion in polyethylene.

We have also carried out some preliminary measurements of the radiation-induced thermoluminescence of several types of rubber and certain linear and cyclic hydrocarbons, all of which had been exposed to a dosage of 10^6 rad. The temperatures at which the emission curves have a maximum are listed in the T_M column of Table 1. Some of the rubber and polyisobutylene samples used in this work were heated at a rate of 1 deg/min and the thermomechanical curves were recorded for a stress of 0.7 kg/cm^2. The results of these measurements

are shown in the T_t column of Table 1. And, finally, in the T_{Md} column we have compiled the structural transition data found in the literature; these had been obtained from the measurements of: temperature dependence of Young's modulus, dielectric and mechanical losses, specific heats, specific volumes, film stretching, and nuclear magnetic resonance. One cannot fail to notice that the maxima on the emission curves occur very close to the transition points which had been determined for these compounds by other methods.

On the basis of these data one can safely conclude that the emission curves of many irradiated organic compounds provide a means of detecting the beginning of molecular motion and changes in the crystal lattice. Hence radiation-induced thermoluminescence can become a very sensitive method for the investigation of structural changes in solids. Besides being quite accurate and simple the method also has the advantage of being applicable to very small amounts of material (in some cases as little as 10^{-4} g will do).

Later on, we intend to study the emission curves of several compounds as a function of radiation dosage and also examine the spectroscopic composition of the emitted light.

We wish to thank L. I. Golubenkova at the Plastics Institute for the determination of the thermomechanical properties of polyisobutylene and the various rubbers.

LITERATURE CITED

[1] W. S. Alger, T. H. Anderson, and L. A. Webb, J. Chem. Phys. 30, 695 (1959).

[2] J. A. Neuman and E. I. Bockoff, Mod. Plast. 32, 12, 117 (1955).

[3] G. P. Mikhailov, S. P. Kabin, and B. I. Sazhin, Zhur. Tekh. Fiz. 25, 590 (1955).

[4] A. H. Willbourn, Trans. Farad. Soc. 54, 717 (1958).

[5] C. W. Deely, J. A. Sauer, and A. E. Woodward, J. Appl. Phys. 29, 1415 (1958).

[6] D. E. Kline, J. A. Sauer, and A. E. Woodward, J. Polymer Sci. 22, 455 (1956).

[7] E. A. Hoff, D. W. Robinson, and A. H. Willbourn, J. Polymer Sci. 18, 161 (1955).

[8] A. E. Woodward, J. A. Sauer, and R. A. Wall, J. Chem. Phys. 30, 854 (1959).

[9] G. P. Mikhailov, S. P. Kabin, and T. A. Krylova, Zhur. Tekh. Fiz. 27, 2050 (1957).

[10] P. W. Jensen, J. Polymer Sci. 28, 635 (1953).

[11] M. Baccaredda and E. Butta, J. Polymer Sci. 22, 217 (1956).

[12] E. R. Andrew, J. Chem. Phys. 18, 607 (1950).

[13] R. F. Boyer, J. Appl. Phys. 25, 825 (1955).

[14] N. G. McCrum, J. Polymer Sci. 34, 355 (1959).

[15] K. Schulz, J. Chim. Phys. 53, 933 (1956).

[16] D. E. Robers, R. N. Work, et al., J. Appl. Phys. 22, 1085 (1951).

[17] J. Schort, C. Kraus, and R. Zelinsky, Rubber. Chem. Technology 32, 614 (1959).

[18] E. R. Andrew and R. G. Eades, Proc. Roy. Soc. 216A, 398 (1953).

[19] J. G. Aston, J. George, et al., J. Am. Chem. Soc. 65, 1135 (1943).

STATIONARY COMBUSTION IN SOLIDS

B. I. Plyukhin

Chemical Physics Institute, Academy of Sciences of the USSR
(Presented by Academician V. N. Kondrat'ev, April 7, 1960)
Translated from Doklady Akademii Nauk SSSR, Vol. 134, pp. 137-140, September, 1960
Original article submitted April 5, 1960

We are going to analyze the problems involving: 1) the effect of experimental conditions on the combustion rate of a solid (s-phase); 2) the temperature and concentration gradients in the s-phase; 3) the effect of the gaseous smoke (g-phase) and the vapor phase (v-phase) on the thermal processes in the s-phase; 4) the thermal and mass equilibria in the s-phase [1]; 5) the critical conditions for stationary combustion in the s-phase. We will start with the equations:

$$\lambda T'' - cmT' + Q_1\Phi + k\rho q_r e^{k\rho x} = 0, \quad mN_1' + \Phi = 0, \quad N_1 + N_2 = 1,$$
$$1/\rho = N_1/\rho_0 + N_2 RT/PM, \quad \rho_1 = N_1\rho, \quad \rho_2 = N_2\rho, \qquad (1)$$
$$\text{for} \quad T(-\infty) = T_0, \quad N_1(-\infty) = 1, \quad T(0) = T_s, \quad N_1(0) = \mu,$$

where λ is the thermal conductivity coefficient, T is the temperature (T_0 is the initial temperature, T_s is the temperature at the surface of the s-phase, T_1 in the g-phase, and T_2 in the v-phase), c is the specific heat, m is the combustion velocity by weight, Q_1 is the heat of vaporization of the material constituting the s-phase (cal/g), Φ is the reaction rate by weight of the solid compound ($g/cm^3 \cdot sec$), N_1 and N_2 are the relative concentrations of the s-compound and vapor, respectively.

$Q_r(P) = 2\epsilon^* \sigma T_2^4 [E_3(k_1 P M_1 x_1 / RT_1) - E_3(k_2 P M_2 \Delta x / RT_2)]$ is the radiation heat transfer from the flame in the v-phase [2, 3], ϵ^* is the extinction coefficient of the powder along the line of flow [3], σ is the Stefan constant $E_3(x) = \int_1^\infty e^{-xy} \frac{dy}{y^3}$; k, k_1 and k_2 are the absorption coefficients in the s-, g-, and v-phases, respectively,

R is the gas constant, x is a coordinate, x_1 is the width of the g-phase, Δx the width of the flame zone, μ is the relative concentration of the s-compound at the surface of the s-phase (for colloidal powders this corresponds to the dispersion depth [1]),* ρ is the density of the s-phase (ρ_0 being the initial density), ρ_1 and ρ_2 are the concentrations by weight of the s-compound and the vapor, respectively.

We now have to determine m, T(x), $N_1(x)$, $N_2(x)$, $\rho_1(x)$, $\rho_2(x)$, and $\rho(x)$. A solution (a unique solution) is only possible if the sources of heat in the s-phase become scattered by the detonation [4, 5]: we will take $\Phi \equiv 0$ in the region where $T_0 \leq T < T^* < T_s$, otherwise it is impossible to satisfy the boundary condition for $x = -\infty$.

From Eq. (1) we can now derive the equation for the conservation of the energy flux and equations for the

* P. F. Pokhil was the first to fully examine the dispersion effect, which he then used as a basis for his proposed combustion mechanism of ballistic powders and dispersed explosives. Dispersion phenomena have previously been reported by A. V. Belyaev [6], K. K. Andreev [7], et al.

thermal and mass equilibrium in the s-phase:

$$-\lambda T' - q_r e^{\lambda \rho x} + mH = \text{const} = H_0 = -q_h - q_r + mH_s,$$
$$q = cm(T_s - T_0) = q_{chem} + q_h + q_r \qquad m(1-\mu) = \int_{-\infty}^{0} \Phi\, dx, \tag{2}$$

where $H = cT + Q_1N_1 + Q_2$ is the enthalpy in cal/g, Q_2 is the heat of combustion of the vapor formed from the decomposition of the s-compound, φ_s is the temperature gradient on the burning surface, q is the rate of heat absorption in the s-phase (cal/cm^2 · sec), $q_{chem} = mQ_s$ is the chemical heat evolved (cal/cm^2 · sec), $Q_s = Q_1(1-\mu)$ is the heat of reaction in the s-phase (cal/g), $q_h = \lambda\varphi_s = m(cT_s - cT_0 - Q_1 + \mu Q_1) = m(Q_2 + \mu Q_1 - cT_2 + cT_s)$ is the conduction heat transfer (cal/cm^2 · sec).

The surface of the s-phase will be defined by the condition $\mu = \text{const}(P)$, i.e., μ is independent of P. To simplify the problem we will assume that $\Phi = \rho_0 Z_s e^{-E_s/RT_s}$. Equation (1) can now be solved by using the excellent method developed by D. A. Frank-Kamenetskii for the stationary theory of thermally induced detonation [8]:

$$v'' - v' + \delta e^v + \delta_r \psi e^{\psi\xi} = 0, \quad u' + \delta e^v = 0,$$
$$v(-\infty) = v_0, \quad u(-\infty) = u_0, \quad v(0) = 0, \quad u(0) = 0, \tag{3}$$

where

$$v = (T - T_s)E_s/RT_s^2, \quad u = (N_1 - \mu)Q_1E_s/cRT_s^2, \quad \xi = cmx/\lambda,$$
$$\delta_r = \frac{q_r E_s}{cmRT_s^2}, \quad \psi = \frac{k\rho\lambda}{cm}, \quad \delta = \frac{\lambda\rho_0 E_s Q_1 Z_s}{c^2m^2RT_s^2} e^{-E_s/RT_s}. \tag{4}$$

Equations (2) are now transformed into:

$$-v' - \delta_r e^{\psi\xi} + h = \text{const},$$
$$-v_0 = u_0 + \omega_s + \delta_r \qquad u_0 = \delta \int_{-\infty}^{0} e^v d\xi,$$

where

$$h = (H - H_s)E_s/cRT_s = u + v, \quad \omega_s = \lambda\varphi_s E_s/cmRT_s^2.$$

Since the parameter δ does not include T_0 we will also use another, sometimes more convenient, parameter:

$$\delta^0 = \delta(\min v_0)^{-2} = \delta(4RT_0/E_s)^2.$$

Using a special method described by Zel'dovich [5] we can obtain an approximate solution of Eq. (3) (for the case $q_r \approx 0$):

$$\xi = \int_0^v \frac{dv}{v + \sqrt{\omega_s^2 + 2\delta(1 - e^v)}}, \quad u = -\omega_s + \sqrt{\omega_s^2 + 2\delta(1 - e^v)},$$
$$\delta = {}^1/_2(v_0^2 - \omega_s^2) = -u_0(v_0 + {}^1/_2 u_0) =$$
$$= E_s^2 Q_1^2(1-\mu)(\mu - \mu_0)/2c^2R^2T_s^4, \tag{5}$$

$$m^2(T_s, T_0, \mu) = \frac{2\lambda\rho_0 R T_s^2 Z_s}{E_s Q_1 (1-\mu)(\mu-\mu_0)} e^{-E_s/RT_s},$$

where $\omega_s = -v_0 - u_0$, $\mu > \mu_0 = 1 - 2c(T_s - T_0)/Q_1$.

In order to determine $v(\xi)$ we have to resort to numerical integration. The temperature T_s is one of the most important characteristics of the s-phase, since the combustion (decomposition) rate of the s-phase depends primarily on T_s. The combustion rate increases with increasing T_s and T_0. If T_s and T_0 are constant an increase in μ is at first accompanied by a decrease in the combustion rate, which after passing through a minimum then begins to increase too.

An approximate analytic solution of Eq. (3) is also possible. If the kinetics follow the Arrhenius rate law the temperature inside the chemical layer will not fluctuate by more than 3-5% [3]. Hence in the vicinity of the surface we can approximate the function $v(\xi)$ by a parabolic expression: $v^0 = \omega_s \xi - \frac{1}{2}(\delta - \omega_s)\xi^2$. Substituting v^0 in e^v and solving Eq. (3) we will get another approximation (in regions where the parabola accumulates a large error the evolution of heat declines so much that it will cease to have any effect on the temperature and concentration gradients):

$$v = -(\omega_s + \delta_r)(1 - e^{\xi}) - \delta_r (e^{\psi\xi} - e^{\xi})/(\psi - 1) -$$
$$- (\sqrt{\pi}_s \delta\beta/\omega_s)[e^{\beta^2}(\operatorname{erf}(\beta - \gamma\xi) - \operatorname{erf}\beta) - e^{\xi + \beta_0^2}(\operatorname{erf}(\beta_0 - \gamma\xi) - \operatorname{erf}\beta_0)],$$
$$u = (\sqrt{\pi}\,\delta\beta/\omega_s) e^{\beta^2}(\operatorname{erf}(\beta - \gamma\xi) - \operatorname{erf}\beta),$$
$$\sqrt{\pi}\delta\beta(1 - \operatorname{erf}\beta) e^{\beta^2} = -\omega_s(v_0 + \omega_s), \tag{6}$$

where $\beta^2 = \frac{\omega_s^2}{2(\delta - \omega_s)}$, $\beta_0^2 = \frac{(\omega_s - 1)^2}{2(\delta - \omega_s)}$, $\gamma^2 = \frac{\delta - \omega_s}{2}$, $\operatorname{erf}\beta = \frac{2}{\sqrt{\pi}}\int_0^{\beta} e^{-y^2} dy$.

The parameter $\underline{m}$ and all the necessary functions we can get analytically from Eq. (6). The law of enthalpy conservation, which is valid for gases if the Lewis–Landau number $L = 1$, never holds for an s-phase. If $\Psi \to \infty$ (a perfect black body) q_r is absorbed at the surface so that q_h and q_r are additive. For $\Psi \to 0$ (a transparent powder) the initial temperature shows an apparent increase, $T_0^* = T_0 + q_r/cm$.

The g-phase influences the thermal processes in the s-phase through T_s and φ_s, while the v-phase through T_s and q_r [3]:

$$T_s = T_0 + Q_s/c + \lambda\varphi_s/cm + q_r/cm, \quad T_1 = T_2 - Q_2/c + \lambda\varphi_1/cm + q_r/cm,$$
$$\lambda\varphi_s = (Q_2 + \mu Q_1 - cT_2 + cT_s) B_2 P^{n_2/2} e^{-E_s/2RT_s},$$
$$\lambda\varphi_1 = (Q_2 - cT_2 + cT_1) B_2 P^{n_2/2} e^{-E_2/2RT_1}, \tag{7}$$
$$T_s \simeq C_1 (C_2 - \ln P)^{-1}, \quad T_1 \simeq C_1^* (C_2^* - \ln P)^{-1},$$

where φ_1 is the temperature gradient at the boundary between the v-phase and the g-phase, B_2 is the Zel'dovich coefficient for the v-phase [3], $C_1 = E_s/n_2 R$; $C_2 = E_s/n_2 R T_s^0$, $T_s^0 = T_s$ (1 atm); $C_1^* = E_1/R(n_2 - n_1)$; $C_2^* = E_1/RT_1^0 \cdot (n_2 - n_1)$; $T_1^0 = T_1$ (1 atm); n_1 and n_2 are the reaction orders in the g-phase and v-phase, respectively.

The formula for $T_s(P)$ gives good agreement with experimental data [1], and $\varphi_s(P)$ has also been experimentally verified [9], while $T_1(P)$ and $\varphi_1(P)$ are purely theoretical.

Let us introduce the parameters for the thermal equilibrium in the s-phase: $\alpha_{chem} = q_{chem}/q$; $\alpha_h = q_h/q$; $\alpha_r = q_r/q$; $\alpha_{chem} + \alpha_h + \alpha_r = 1$. Using Eqs. (2) and (7) we can get the thermal equilibrium in the s-phase as a function of pressure

$$\alpha_{\text{chem}}(P) = \frac{Q_1(1-\mu)}{c[T_s(P)-T_0]}, \quad \alpha_r(P) = \frac{q_r(P)\,P^{-n_1/2}}{cB_2[T_s(P)-T_0]}\,e^{E_s/2RT_s}, \tag{8}$$

$$\alpha_h(P) = \frac{\mu Q_1 + Q_2 - cT_2 + cT_s(P)}{c[T_s(P)-T_0]} - \alpha_r(P).$$

The validity of Eqs. (8) has been experimentally verified by P. F. Pokhil, V. M. Maltzev, and G. V. Lukashev. To ensure stable fuel combustion inside rocket chambers the thermal equilibrium regime in the s-phase has to be adapted so as to suit the conditions demanded by Eq. (8).

According to Eq. (5), if the solution is to satisfy the boundary conditions, δ cannot exceed a certain critical value:

$$\delta \leqslant \delta_{cr}(T_0) = E^2/32R^2T_0^2, \quad \delta^0 \leqslant \delta_{cr}^0 = 0{,}5. \tag{9}$$

If we vary only T_s then:

$$\delta^0 \leqslant \delta_{cr}^0(T_0, \mu) = c^2T_0^2Q_s/2\,(^2/_3\,cT_0 + {}^1/_3\,Q_s)^3. \tag{10}$$

When the width of the thermal layer $x_t = \lambda/cm$ exceeds the critical dimensions then according to Eqs. (9) and (10) the stationary regime breaks down. Parameter δ gives the ratio between two very important dimensions: the width of the thermal layer and the chemical layer x_{chem} [3]. Stationary combustion is only possible for certain values of this ratio: $x_t/x_{chem} \leq E_s/4RT_0$. For a rigorous determination of what will actually happen, whether the combustion will change into detonation or whether it will be extinguished, one has to solve a nonstationary problem. However, in the case of flameless combustion we get extinction when $\delta^0 > 0{,}5$; this is attributed to the dispersion of heat, which is at first concentrated in a thin layer of the burning surface, throughout the s-phase [10].

The Frank-Kamenetskii treatment of problems involving the combustion of cylindrical charges of a diameter D, with heat losses into the surrounding medium, yields another criterion of stationary combustion:

$$D \geqslant D_{cr} = \frac{2\lambda r_{cr}(T_0, \text{Bi}, \delta_{cr})}{cm_{cr}} = \sqrt{\frac{4\lambda r_{cr}^2(T_0, \text{Bi}, \delta_{cr})\,\delta_{cr}RT_{scr}^2}{\rho Q_1 E_s Z_s}}\,e^{E_s/2RT_{scr}}\,P^{-n_1/2}, \tag{11}$$

$r = cmD/2\lambda$, $\text{Bi} = \eta/cm$ is the Biot number, η is the coefficient of heat exchange. Stationary combustion is only possible for certain combinations of D, x_t, and x_{chem}. On the basis of dimensional considerations A. D. Margolin* had previously arrived at the result $D_{cr}M_{cr} = \text{const}$. Equation (11) yields results in good agreement with experimental data [1, 11].

LITERATURE CITED

[1] P. F. Pokhil, Doctoral Dissertation [in Russian] (Moscow, 1954).

[2] B. I. Plyukhin, Doklady Akad. Nauk SSSR 131, No. 1 (1960).**

[3] B. I. Plyukhin, Doklady Akad. Nauk SSSR 129, No. 5 (1959).**

[4] A. N. Kolmogorov, I. G. Petrovskii, and N. S. Piskunov, Byulletin MGU, Section A1, No. 5 (1937).

[5] Ya. B. Zel'dovich, Zhur. Fiz. Khim. 22, 27 (1948).

[6] A. F. Belyaev and A. E. Belyaeva, Doklady Akad. Nauk SSSR 33, No. 1 (1941).

* Unpublished results.

** See C. B. Translation.

[7] K. K. Andreev, Doklady Akad. Nauk SSSR 53, No. 3 (1946).

[8] D. A. Frank-Kamenetskii, Zhur. Fiz. Khim. 13, 738 (1939).

[9] P. F. Pokhil, V. M. Mal'tsev, and G. B. Lukashenya, Doklady Akad. Nauk SSSR (in press).

[10] K. K. Andreev, Coll. Papers on the Theory of Explosives, edited by K. K. Andreev and Yu. B. Kharitonova [in Russian] (1940).

[11] K. K. Andreev, Zhur. Fiz. Khim. 20, No. 6 (1946).

THE ADSORPTION OF IODIDE IONS ON PLATINUM AND ITS EFFECT ON THE IONIZATION OF HYDROGEN

L. T. Shanina

M. V. Lomonosov Moscow State University
(Presented by Academician A. N. Frumkin, April 15, 1960)
Translated from Doklady Akademii Nauk SSSR, Vol. 134, No. 1, pp. 141-144, September, 1960
Original article submitted April 5, 1960

Anions adsorbed on an electrode surface exert a pronounced effect on the rates of electrode processes, their action being especially marked in the case of the ionization and evolution of hydrogen. The adsorption of Cl^-, Br^-, or I^- ions can either increase or diminish the overvoltage, since the structure of the resulting adsorbed layer varies from metal to metal [1-4]. In the latter case, the process can be retarded still further by increasing the length of time during which the electrode is held in the Br^- or I^- solution [3]. It has been shown in [5-8] that the strength of bonding between the anion and the metallic surface increases with the passage of time, the energy of bonding of hydrogen with this surface being diminished thereby.

The present work has involved a study of the effect of anion adsorption on smooth platinum surfaces. Here, in distinction to [3], the rate of ionization was measured with an electrode upon which Br^- or I^- ions had been adsorbed previously, the electrode being immersed in a 1 N H_2SO_4 solution which was free of these ions. This method is based on the high stability of the adsorption of Br^- and I^- ions by platinum. Among the advantages which it offers is that the adsorption can be carried out at a potential, φ, which is independent of the overvoltage, η, under which the reaction rate is to be measured.

The apparatus and technique employed in this study were the same as described earlier in [9], but the preliminary treatment of the electrodes was somewhat different. The electrode was carried to a certain standard activity prior to each experiment. The activated electrode was then immersed in a 1 N HBr or a 1 N KI + 0.1 N H_2SO_4 solution which had been previously purified by adsorption on a large platinum screen and saturated with hydrogen, and was held there at a definite potential. The poisoning solution was then poured out, the cell and the electrode washed with doubly distilled water (in the case of KI poisoning, this washing was continued until the wash water gave a negative reaction with starch), and hydrogen blown through the system. Finally, the cell was filled with 1 N H_2SO_4 which had been purified and saturated with hydrogen and the anodic polarization curve developed in an atmosphere of hydrogen with the electrode rotating at 5000 rev/min.

Study was made of the effect of the length of time of poisoning of the electrode by the iodide, or bromide ions on the rate of ionization of molecular hydrogen. The electrode was held for 2, or 4, or 8, or 16, or 24 hours in a 1 N KI + 0.1 N H_2SO_4 solution under an atmosphere of hydrogen, and polarization curves then developed. The results obtained are represented in Fig. 1. This figure shows a diminution of the maximum on the polarization curve representing the rate of hydrogen ionization, $\underline{i}$, as a function of the overvoltage, η, with an increase in the length of time of poisoning of the electrode. The maximum disappears after poisoning the electrode for 24 hours and the current is then essentially equal to zero up to potentials of 0.6-0.7 v, the indication being that the ionization of hydrogen is fully suppressed here. The potential at which the electrode is poisoned has a definite effect on the rate of hydrogen ionization. The electrodes were held in a 1 N KI + 0.1 N H_2SO_4 solution under an atmosphere of hydrogen for two hours at a potential of 0.27, 0.17, 0.07, −0.09, −0.13, or −0.23 v with

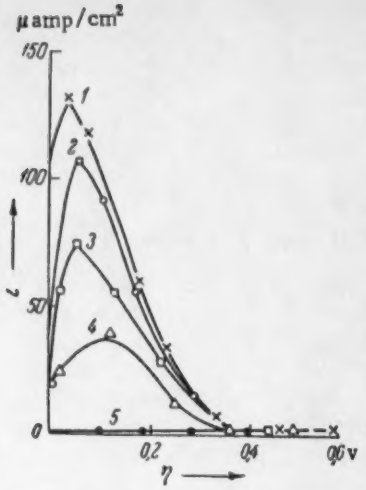

Fig. 1. The electrode activity with respect to hydrogen ionization as a function of the time of poisoning in a 1 N KI + 0.1 N H_2SO_4 solution under an atmosphere of H_2: 1) 2 hours; 2) 4 hours; 3) 8 hours; 4) 16 hours; 5) 24 hours.

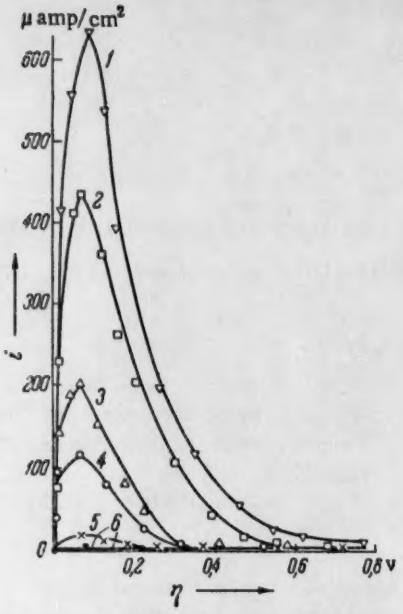

Fig. 2. The electrode activity as a function of the potential at which it was poisoned for two hours in a 1 N KI + 0.1 N H_2SO_4 solution under an atmosphere of H_2. Electrode poisoned at: 1) $\varphi = +0.27$ v; 2) $\varphi = +0.17$ v; 3) $\varphi = +0.07$ v; 4) $\varphi = -0.09$ v; 5) $\varphi = -0.13$ v; 6) $\varphi = -0.23$ v.

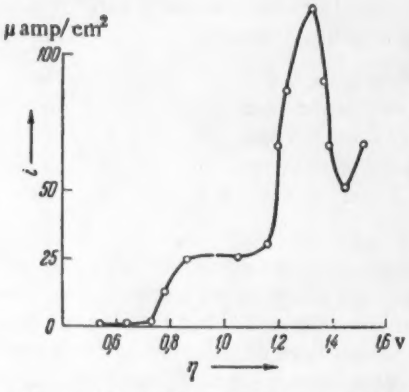

Fig. 3. Polarization curve for an electrode held for four hours in a 1 N KI + 0.1 N H_2SO_4 solution under an atmosphere of H_2.

respect to a saturated calomel electrode in an atmosphere of hydrogen. The experimental results are presented in Fig. 2. It is to be seen from this figure that an electrode poisoned at −0.23 v is quite inactive with respect to the hydrogen ionization. A certain amount of activity is retained by the electrode when the negative potential of poisoning is lowered to −0.09 v. The activity of the electrode with respect to hydrogen ionization rises with an increase in the positive potential of poisoning.

Similar data were obtained with electrodes which had been poisoned with bromide ions. The marked diminution of the rate of ionization of molecular hydrogen with an increase in the length of time during which the electrode was held in the poisoning solution and the almost complete suppression of the process after a 24 hour treatment point to a decrease with time of the number of active centers for the H_2 ionization on the electrode surface.

The relation between the rate of hydrogen ionization and the potential of poisoning of the electrode was not of the expected type. The activity of the poisoned electrode with respect to the hydrogen ionization increased with increasing anodic potential despite the fact that the data of N. A. Balashova [10] point to a rise in the number of adsorbed anions. The low activity of an electrode poisoned at negative potentials can be explained by supposing anion adsorption to be the only surface process occurring under these conditions, the small amount of material taken up being sufficient to render the electrode passive. There is not only an increase in

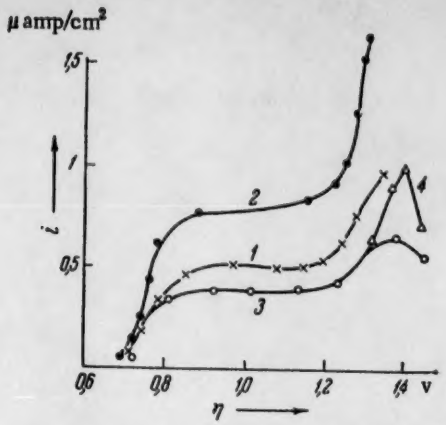

Fig. 4. Polarization curves for an electrode held for four hours in a 1 N KI + 0.1 N H_2SO_4 solution under an atmosphere of H_2: 1,3) in an atmosphere of N_2; 2,4) in an atmosphere of H_2.

the anion adsorption but a certain rejuvenation of the electrode surface as a result of a slight solubility of platinum in the presence of the halide ions when poisoning is carried out at more positive potentials. The comparatively high activity of the electrode with respect to the hydrogen ionization after poisoning at higher positive potentials can be explained on this basis.

Polarization curves obtained with electrodes which had been held for a definite period of time in a KI solution at 0.6-0.7 v (Fig. 3) show a marked rise up to 0.9-1.0 v, following which the current falls slightly and then begins to rise again at 1.2 v. This second increase in the current is greater than the first. The current undergoes a diminution at the higher anodic potentials and then begins to rise once more at 1.6 v. The rise in the current at 0.6-0.7 v is not related to a dissolution of platinum in H_2SO_4 in the presence of the I^-, as was supposed originally, since analysis for platinum by the method of [12] did not give positive results, even though it is quite likely, as has been pointed out above, that traces of the element did pass into solution.

Direct experiments prove that the first wave corresponds to the oxidation of I^- to free iodine, a process for which the normal potential is 0.53 v, while the second wave is associated with the oxidation of I_2 to IO_3^- at 1.19 v. Analysis disclosed the presence of free iodine (or IO_3^- ions) in a solution in which the electrode had been held at 0.95 v (or 1.2 v).

On the other hand, the height of the wave on the polarization curve is not fixed by the oxidation of iodine alone but is also affected by the participation of hydrogen in the electrode process. A series of curves was developed in an atmosphere of nitrogen in order to fix this point. The electrode was given the customary four-hour treatment in the 1 N KI + 0.1 N H_2SO_4 solution, washed free of KI, and then transferred to a nitrogen-saturated 1 N H_2SO_4 solution, following which polarization curves were developed with nitrogen passing through the cell continuously. Hydrogen could be introduced into the cell at will and further development of the curve carried out in an atmosphere of this gas. Figure 4 indicates the current read from curve 1 developed in nitrogen to be only half as large as that read from curve 2 developed in hydrogen. There was a marked rise in the current when hydrogen was passed into the cell while a curve was being developed at 1.2 v (see Fig. 4, curves 3, 4). The quantity of electricity required for separating a given amount of iodine from the electrode in an atmosphere of hydrogen is almost twice as great as that required in an atmosphere of nitrogen.

The electrode gradually became freed of iodine and acquired its original activity with respect to the hydrogen ionization under an extended treatment with an anodic current. These results were obtained not only with a disk electrode, but also with electrodes prepared from massive sheets and screens.

I wish to express my deep thanks to Academician A. N. Frumkin for his interest in this work.

LITERATURE CITED

[1] Z. A. Iofa, B. N. Kabanov, E. M. Kuchinskii, and F. Chistyakov, Zhur. Fiz. Khim. 13, 1105 (1939).

[2] Z. A. Iofa and L. A. Medvedeva, Doklady Akad. Nauk SSSR 69, 213 (1949).

[3] A. N. Frumkin and É. Aikazyan, Doklady Akad. Nauk SSSR 100, 315 (1955).

[4] Ya. M. Kolotyrkin and L. A. Medvedeva, Zhur. Fiz. Khim. 31, 2668 (1957).

[5] É. A. Aikazyan, Zhur. Fiz. Khim. 33, 1016 (1959).

[6] Ya. M. Kolotyrkin and E. Ya. Bunė, Zhur. Fiz. Khim. 21, 581 (1957).

[7] Ya. M. Kolotyrkin and L. A. Medvedeva, Zhur. Fiz. Khim. 25, 1355 (1955).

[8] A. D. Obrucheva, Zhur. Fiz. Khim. 32, 2155 (1958).

[9] A. N. Frumkin and É. A. Aikazyan, Izvest. Akad. Nauk SSSR, Otdel. Khim. Nauk, 202 (1959).*

[10] N. A. Balashova, Zhur. Fiz. Khim. 32, 2266 (1958).

[11] E. Ya. Gailis and G. Goryushina, Zavod. Lab. 20, 14 (1954).

*Original Russian pagination. See C. B. Translation.

DETECTION OF HYDROGEN ATOMS IN REACTIONS INVOLVING THE PHOTOTRANSFER OF AN ELECTRON

B. N. Shelimov, N. N. Bubnov, N. V. Fok, and V. V. Voevodskii, Corresponding Member, Academy of Sciences of the USSR

M. V. Lomonosov Moscow State University
Institute of Chemical Kinetics and Combustion, Siberian Branch, Academy of Sciences of the USSR
Translated from Doklady Akademii Nauk SSSR, Vol. 134, No. 1, pp. 145-148, September, 1960
Original article submitted April 27, 1960

During the previous 15-20 years it has been proposed in a series of studies [1-4] that free hydrogen atoms are formed in photochemical reactions in water, that is, in reactions of the type:

$$M + H_2O + h\nu \rightarrow M^+ + OH^- + H\cdot \qquad (I)$$

Particles M may be ions of metals with a variable valence (V^{2+}, Cr^{2+}, Mn^{2+}, Fe^{2+}, Co^{2+}, U^{3+}, etc.) and even various anions (I^-, N_3^-, SH^-, SO_3^{2-}, etc.).

In all these cases, the conclusion on the course of reaction (I) has been based on an analysis of the chemical reaction products and an investigation of the kinetic characteristics of the process. In a paper of Dainton and James [2] it has been shown that the long-wave limit of the spectral region, in which the process (I) takes place, changes symbatically with the ionization potential of particle M. In the same study it has been shown that, when the polymerization of acrylonitrile or methylmethacrylate is initiated by irradiation, a D atom is found in the terminal group of the polymer as a result of the photoionization of metal ions in D_2O. This result is an important argument to the advantage of the supposition that in the primary act of the photochemical reaction a hydrogen atom is formed, which later on is added to the double bond. In a more recent study, however, these same authors [4] record a series of troubles, which arise when the polymerization is used as a method to investigate the phototransfer of an electron in the course of process (I).

Since the electron paramagnetic resonance (EPR) method has been developed, at present the question may be raised whether reaction (I) can be investigated by directly detecting the hydrogen atoms formed during its course. The identification of hydrogen atoms by EPR is facilitated by the fact that its spectrum in the absence of strong interactions is a doublet with a splitting of ~500 oe between the components. No other radical or free atom has such a spectrum.

Because of the great mobility and the high reactivity of hydrogen atoms, reaction (I) should be carried out under conditions which secure a stabilization of these particles. For this reason we decided to do the measurements in solid phase and at low temperatures. From radiation data in literature it follows that in most frozen solids, ice included, hydrogen atoms diffuse easily even at the temperature of 77°K and that, in order to detect them, it is necessary to work at liquid hydrogen or helium temperatures [5]. The only known exceptions to this rule are frozen solutions of acids in water, in which at 77°K a noticeable concentration of hydrogen atoms can be detected when irradiated by the γ-rays of Co^{60} [6].

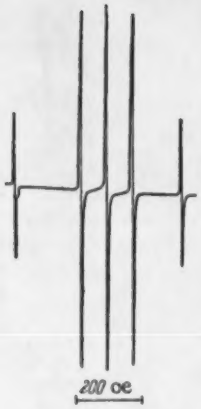

Fig. 1. EPR spectrum of the hydrogen and deuterium atoms, formed when irradiating the system $FeSO_4$-$-D_2O$-H_2SO_4.

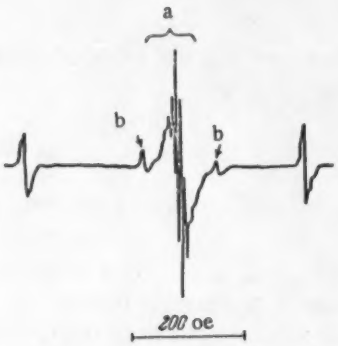

Fig. 2. EPR spectrum of the hydrogen atoms and free radicals, formed when irradiating the system C_6H_6-H_2O-H_2SO_4.

For this reason, we chose frozen solutions of acids in water, which also contained a small amount of $FeSO_4$ or KI, as the medium for our experiments. The samples were irradiated by ultraviolet light during one hour. As radiation source we used a PRK-7 Hg-lamp The electron paramagnetic resonance signals were recorded by means of the EPR-spectrometer described previously [7].

When the frozen solutions of $FeSO_4$ in diluted or concentrated H_2SO_4 or H_3PO_4 (the acid concentration was varied between ~40 and 96%) were irradiated at 77°K, a doublet with a splitting of ~500 oe was detected in the spectrum. This result proves unequivocally the rightness of the proposition that free hydrogen atoms are formed during reactions involving the phototransfer of an electron. A similar spectrum consisting of two components with the same splitting was also observed when frozen solutions of KI in diluted H_2SO_4 or H_3PO_4 were irradiated. In this case the I^- anion, obviously, played the role of particle M, which fact is in agreement with conclusions of the paper [2].

As a final check to the conclusion on the course of reaction (I) we did experiments in solutions containing heavy water. As may be seen in Fig. 1, here the spectrum has a triplet due to deuterium atoms (i = 1) together with the hydrogen atom doublet. The components in the hyperfine structure of deuterium atom EPR spectrum, according to theory, are separated by ~ 78 oe.

It is also of interest to investigate whether hydrogen atoms can be formed by irradiating frozen aromatic systems with ultraviolet light. It is known that condensed aromatic molecules with many rings (anthracene, perylene, naphthacene and others) in concentrated sulfuric acid are ionized easily in the form of positive ions which are radicals [8, 9]. Because the ionization potential of benzene is higher than that of these compounds, its ion (the radical $C_6H_6^+$) is not formed in sulfuric acid. However, if additional energy in the form of a light quantum is supplied to the reacting system, then it may be expected that, in the case of benzene, ionization with simultaneous formation of a hydrogen atom by a process of type (I) will occur:

$$C_6H_6 + H_2O + h\nu \rightarrow C_6H_6^+ + OH^- + H\cdot \qquad (I')$$

$$C_6H_6 + H_3O^+ + h\nu \rightarrow C_6H_6^+ + H_2O + H\cdot \qquad (II)$$

Experiments which we did in the system C_6H_6-H_2O-H_2SO_4 showed that upon irradiating benzene in diluted or concentrated acid hydrogen atoms are actually formed (Fig. 2). An unequivocal interpretation of the central part of the spectrum (Fig. 2a and Fig. 3) cannot be given when using only the data obtained. The four central components (indicated by arrows in Fig. 3) have relative intensities nearly proportional to 1 : 3 : 3 : 1 and they are not saturated at the hf-powers applied by us, while the components farther away undergo a quite noticeable saturation. This fact gives reason to ascribe the two parts of the spectrum to two different radicals. The sharp multiplet in the hyperfine structure of the central line and also the fact that the total width of the central part of the spectrum (quadruplet) $\Delta H \simeq 22$ oe is close to the value characteristic for the anion $C_6H_6^-$ [10] permits us to conclude that this spectrum originates from paramagnetic particles the free valence of which is localized on an aromatic ring.* However, it can be said that this particle cannot be an isolated positive radical ion, since the spectrum of the latter should have an uneven number of components.

* It is known from literature [9] that the EPR spectra of positive and negative radical ions are very similar.

Fig. 3. Central part of the EPR spectrum of the free radicals formed when irradiating the system C_6H_6-H_2O-H_2SO_4.

Fig. 4. Hyperfine structure components in the EPR spectrum of H atoms formed when irradiating: a) C_6H_6-H_2SO_4-H_2O; b) $FeSO_4$-H_2SO_4-H_2O.

The doublet (Fig. 2b) is interesting because of the very high splitting (~ 130 oe). In the study [11] a doublet with a similar splitting is ascribed to the radical HCO. However, it is difficult to assume that such a radical is formed under our conditions.

Attention should also be paid to an interesting feature in the EPR spectrum of the hydrogen atoms. As may be seen in Fig. 4, on both sides of the main components in the hyperfine sturcture of the spectrum for the hydrogen atoms, formed when irradiating the systems C_6H_6-H_2O-H_2SO_4 and $FeSO_4$-H_2O-H_2SO_4, weaker components are observed. These additional components may be ascribed to proton spin reversal in the molecules surrounding the hydrogen atom [6, 12]. As a confirmation of this interpretation note the fact that the splitting between the additional components (5 oe) is close to the value corresponding to the proton resonance frequency at the magnetic field strength H = 3300 oe used by us.

The saturation of the hydrogen atom signal should also be mentioned. In our experiments with benzene the lines for the H atoms are strongly saturated, but in the experiments with Fe^{++} this is not observed, which fact is obviously connected with the high concentrations of the paramagnetic ions having a short relaxation time.

An investigation of the saturation phenomenon and the character of the intensity distribution between the main and the secondary lines in the EPR spectrum of the H atoms may enable us to explain the special features of the weak interaction with the surrounding molecules and gives an approach to the problem of the distance between the H atoms and the original particle, which has given off an electron under the action of light.

LITERATURE CITED

[1] N. Uri, Chem. Rev. 50, 375 (1952).

[2] F. S. Dainton and D. James, J. Chim. Phys. 48, 18 (1951).

[3] B. Ya. Dain and É. A. Liberzon, Doklady Akad. Nauk SSSR 28, 228 (1940); Acta Physicochim. URSS 19, 410 (1944).

[4] F. S. Dainton and D. James, Trans. Farad. Soc. 54, 649 (1957).

[5] M. S. Matheson and B. Smaller, J. Chem. Phys. 28, 1169 (1958); Science 128, 623 (1958).

[6] R. Livingston, H. Zeldes, and E. Taylor, Disc. Farad. Soc. 19, 166 (1955).

[7] A. B. Semenov and N. N. Bubnov, Pribor. i Tekh. Éksp. 1, 92 (1959).

[8] S. I. Weissman, E. de Boer, and J. J. Conradi, J. Chem. Phys. 26, 963 (1957).

[9] A. Carrington, F. Dravnieks, and M. Symons, J. Chem. Soc. 947 (1959).

[10] T. R. Tuttle and S. J. Weissman, J. Chem. Phys. 25, 189 (1956); V. V. Voevodskii, S. P. Solodovnikov, and V. M. Chibrikin, Doklady Akad. Nauk SSSR 129, 1082 (1959).*

[11] W. Gordy, W. B. Ard, and H. Shields, Proc. Nat. Acad. Sci. USA 41, 996 (1955).

[12] G. T. Trammell, H. Zeldes, and R. Livingston, Phys. Rev. 110, 630 (1958).

* The term "dehydration" has been retained as the translation of degidratatsiya to avoid circumlocution, but in fact the process discussed is the removal of the elements of water from alcohols which must be presumed to be already anhydrous – Publisher.

THE COMBINED DEHYDRATION OF ALCOHOLS IN AN ADSORBED LAYER ON ALUMINUM OXIDE CATALYSTS

V. É. Vasserberg, Academician A. A. Balandin, and

T. V. Georgievskaya

The N. D. Zelinskii Organic Chemical Institute, Academy of Sciences of the USSR
Translated from Doklady Akademii Nauk SSSR, Vol. 134, No. 2, pp. 371-373, September, 1960
Original article submitted May 17, 1960

In our investigations of the mechanism of the dehydration of alcohols on alumina in which we have studied the kinetics of the reaction taking place in an adsorbed layer on the catalyst [1, 2], we have shown that the reaction rates for various alcohols on a series of catalysts from different sources are very different [3]. In the present work, which has been carried out on other samples of alumina catalysts, this difference in the rates of dehydration for ethanol and iso-propanol has been confirmed. Sample 1 was precipitated from aluminum nitrate by means of sodium hydroxide solution at the constant pH of 6.3; sample 2 was obtained by hydrolysis of aluminum triisopropyl; and sample 3 was prepared by precipitation from an aluminate solution by means of gaseous carbon dioxide at 0°.

By adsorbing small quantities of the vapor of these substances on a sample of alumina which had been conditioned under high vacuum, and measuring the kinetics of the increase of pressure of olefin over the catalyst, we have found that comparable values of the times of half decomposition, τ, (and also, therefore, of the rate constants of the reactions) for ethanol and isopropanol are only attained when the reactions are carried out in the temperature ranges 180-240° and 120-150°, respectively.

Extrapolation of the Arrhenius straight lines for the dehydration of ethanol in the adsorbed layer to a temperature of 150° leads to a value of τ of 1000-1300 min, which is 2-3 orders of magnitude greater than the experimentally obtained values for isopropanol. On the basis of the fact that at temperatures from 120° to 150° the dehydration of isopropanol in the adsorption layer proceeds with appreciable velocity (τ from 1 to 20 min), while ethanol under these conditions is practically stable, we determined to use ethanol as a well-adsorbed but practically chemically inert substance for investigating the nature of the surface heterogeneity of catalysts by the method of successive blocking which has been described in [3].

This method consists in studying the decomposition of standard small quantities (2 to 4% of a complete monolayer) of a substance on the catalyst, upon which there has been previously adsorbed a quantity of some inert substance. This latter amount is increased from experiment to experiment, and has the effect of blocking the surface against the catalytic reaction. Under these conditions, owing to the fact that the reacting substance is forced to occupy those parts of the surface with less active adsorptive properties, the rate constant of the reaction may be decreased or increased, depending on the relative catalytic activity of the various parts of the surface. It is thus possible to determine the differential (but not the integral, see [1, 2]) curve showing the distribution of the various parts of the surface according to their catalytic activity.

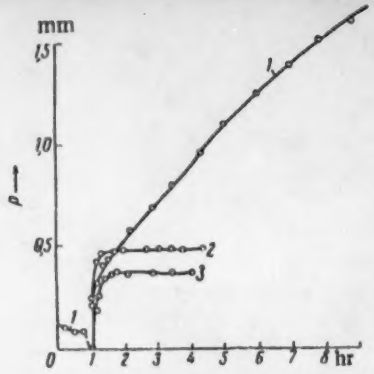

Fig. 1. Combined dehydration of ethanol + isopropanol on catalyst 1 at 150°. 1) Ethanol + isopropanol; 2) water + isopropanol; 3) isopropanol alone (control experiment). The vertical dotted line shows the moment at which the isopropanol is introduced for curve 1 , and the commencement of the experiment for curves 2 and 3 .

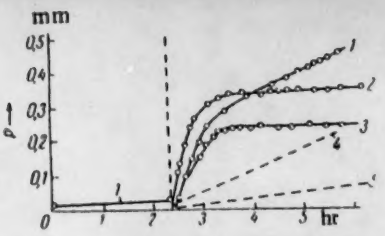

Fig. 2. Combined dehydration of ethanol and isopropanol on catalyst 1 at 120°. 1) Ethanol + isopropanol; 2) isopropanol (control experiment). Period of half-change, τ = 18 min; 3) kinetic curve for the decomposition of isopropanol when this is mixed with ethanol, taking into account the rate of decomposition of the ethanol, and assuming this to have a constant value corresponding to the last rectilinear part of curve 1 . Time of half change: τ = 30 min; 4) rate of decomposition of ethanol when mixed with isopropanol, calculated from the last rectilinear part of curve 1 ; 5) rate of decomposition of ethanol, extrapolated from the initial part of curve 1 .

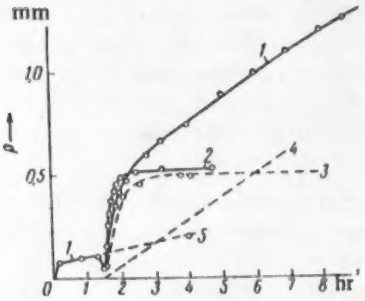

Fig. 3. Combined dehydration of C_2H_5OH + iso-C_3H_7OH on catalyst No.3 at 150°: 1) C_2H_5OH + iso-C_3H_7OH; 2) iso-C_3H_7OH (control experiment); 3) iso-C_3H_7OH mixed with C_2H_5OH; 4) C_2H_5OH mixed with iso-C_3H_7OH; 5) C_2H_5OH before addition of isopropanol. 3-5, calculated curves.

In the course of the investigations, an unexpected difference in effectiveness was observed between water, methanol, and ethanol. When these were adsorbed in the same quantities, they reduced the rate of dehydration of isopropanol to different extents, which also varied with the different origins of the samples of alumina. Water had the lowest effect: even up to very high adsorption densities it had no effect in reducing the rate of decomposition of the alcohol. Ethanol and methanol, however, had very marked effects in retarding the reaction rate: on some samples it was the methanol, and on the others the ethanol, which had the greater inhibiting effect. It is obvious that these facts fall outside the framework of a simple explanation in terms of blocking alone, and for this reason we have in addition studied the kinetics of the decomposition of isopropanol and ethanol in an adsorbed layer on certain samples of alumina in the presence of each other. The former was present to the extent of 0.3 cm^3/g at normal temperature and pressure – that is, to about 2-4% of saturation, and the latter to the extent of 5.3 cm^3/g at normal temperature and pressure.

The experiments were performed in the following way. The adsorption of the ethanol was carried out first at a temperature of 120-150°, and the pressure change was measured in the gas phase for some time (from 40 minutes to 2.5 hours). Since the quantity of ethanol is also relatively low, during the first few minutes the alcohol is practically completely adsorbed by the catalyst without leaving any appreciable pressure in the gas phase. Later the pressure over the catalyst remains constant, or in certain experiments increases slowly on account of the dehydration (see, for example, Figs. 1-3). After the adsorption of the ethanol, the adsorption of the isopropanol is carried out, and the kinetics of the rise of olefin pressure are measured.

In these experiments it was observed that the reaction in all cases proceeded more slowly than in the control experiments in which pure isopropanol was used, or in those in which mixtures of isopropanol and water were employed. Moreover, in a number of cases it was found that the pressure in the apparatus was considerably higher than a value calculated on the assumption of 100% decomposition of the entire adsorbed amount of isopropanol. (In those cases where the decomposition of the ethanol at the commencement of the experiment proceeded at an appreciable rate, the pressure was greater than that calculated from the assumption that the rates for the ethanol and the isopropanol could be regarded as additive.)

This quantity, $p_{\infty\,th}$ should be equal to 0.6 to 0.7 mm Hg, while in practice the value of $p_{\infty\,ex}$ for the decomposition of pure isopropanol was somewhat lower. For catalysts numbers 1, 2 and 3 its average value was 0.50, 0.40 and 0.35 mm Hg, respectively. For the simultaneous presence of ethanol and isopropanol in the adsorption layer, $P_{\infty\,th}$ amounted to some 1.1-1.6 mm and continued to increase. The rate of this pressure increase during a reaction time of 4-6 hours was constant, and 3-7 times greater than the rate of pressure increase caused by the dehydration of pure ethanol during the first period of the experiment (in those cases where this dehydration did in fact proceed with an appreciable velocity).

The results of these experiments show unequivocally that, when ethanol and isopropanol are present together in the adsorption layer on the catalyst, their simultaneous dehydration proceeds at a rate in which the slower reaction (the dehydration of ethanol) is greatly enhanced, and the more rapid reaction (the dehydration of isopropanol) is retarded.

It follows from this that the multiplet complex (that is, the molecule of the reacting substance adsorbed on the active part of the catalyst) in the dehydration of alcohols on alumina, does not consist of an isolated structure, the nature of whose change in the direction in which the reaction is proceeding is independent of the properties of the molecules which are adsorbed on neighboring centers.

Such a multiplet complex should rather be considered as a radical which may react with neighboring molecules, giving more or less stable intermediate products. Thus, the molecules of isopropanol adsorbed on the catalyst (in the case of the dehydration of pure isopropanol) apparently form intermediate complexes which decompose relatively rapidly into the olefin and water, while the mixed ethanol-isopropanol (or methanol-isopropanol) complexes decompose more slowly.

The formation of such less reactive mixed complexes provides a basis for explaining the difference between the effectiveness of previously adsorbed molecules of water, methanol and ethanol. It is evident that the water simply blocks the surface, while the methanol and ethanol, in addition to this, bind relatively more active radical-like multiplet complexes of the isopropyl alcohol, which leads to an additional reduction in the rate of the dehydration reaction.

The data are hardly sufficient to justify a judgment as to the nature of the surface radicals which are formed; but in no case is it possible to attribute the phenomenon which we have observed simply to the formation of intermediate mixed ethers, since this would not explain either the reduction of the rate of the decomposition of isopropyl alcohol or the nature of the kinetic curves which have been obtained. As to the former, we have shown [3] that the rate of dehydration of ethers in a monolayer is about twice as great as that of the corresponding alcohols. As to the latter, the constancy of the rate during the period when the whole of the isopropanol introduced should already be completely decomposed is incompatible with the proposed explanation.

Moreover, it is seen from the facts which we have obtained that combined dehydration, and therefore also the surface radical reaction mechanism, appears most clearly on catalyst no. 3, and then on numbers 1 and 2, while, with respect to their catalytic activity in the decomposition of pure isopropanol in a monolayer at 150°, these catalysts must be placed in the order: $1 < 3 < 2$. This shows that the surface radical mechanism is apparently not the only possible way in which the dehydration of the alcohols can take place in a monolayer, and that side by side with this the reaction may also occur according to the ordinary mechanism, the ratio between the two reactions being different on different catalysts.

In conclusion, we would point out that the proposed radical mechanism for the dehydration reaction is presumably the fundamental basis of the intermolecular dehydration.

LITERATURE CITED

[1] H. Dohse, Z. Phys. Chem. (B) 5, 131 (1929); 6, 343 (1930).

[2] A. A. Balandin and V. É. Vasserberg, Izvest. Akad. Nauk SSSR, Otdel. Khim. Nauk 5, 456 (1945).

[3] V. É. Vasserberg and A. A. Balandin, Symposium on Problems of Kinetics and Analysis [in Russian] (1960) Vol. 10, p. 356.

THE EFFECT OF THE STRUCTURE OF HYDROCARBONS ON THEIR SOLUBILIZATION IN SOLUTIONS OF SODIUM SALTS OF SATURATED ALIPHATIC ACIDS

P. A. Demchenko and Corresponding Member of the Academy of Sciences of the USSR A. V. Dumanskii

Institute of General and Inorganic Chemistry, Academy of Sciences of the USSR
Translated from Doklady Akademii Nauk SSSR, Vol. 134, No. 2, pp. 374-375, September, 1960
Original article submitted May 17, 1960

During the study of the solubilizing powers of various detergent substances, a special kind of colloidal solution of hydrocarbons in the solutions of these substances has been observed [1, 2]. In the current work, results are given of the systematic study of the solubilizing of hydrocarbons of different structures in aqueous solutions of the sodium soaps of saturated aliphatic acids. The specimens of soap used in the investigation were prepared by the neutralization of the pure aliphatic acids by the equivalent quantity of alkali, according to the method described earlier [3]. The comparative solubilizations of the various hydrocarbons were studied by a direct method [4], which gives excellent reproducibility from experiment to experiment. The experimental data on the limiting solubilization of certain aliphatic and aromatic hydrocarbons, in 0.1 M solutions of sodium caprylate, caprate, laurate, myristate, palmitate, and stearate are given in Fig. 1.

From a consideration of the curve showing the relationship between the solubilizing effect and the length of the hydrocarbon radical of the soap, it can be seen that the solubilizations of octane, isooctane, heptane, ethylbenzene, o-xylene, styrene, toluene, and benzene change in a regular manner. Sodium enanthate, which contains seven carbon atoms, and solutions of the still lower homologs of the sodium soaps of saturated aliphatic acids have practically no solubilizing effect on the hydrocarbons under discussion. With increase in the length of the hydrocarbon radical of the soap above seven carbon atoms, the solubilization of hydrocarbons in the aqueous soap solutions becomes considerable. For the homologous soaps of caprylate (C_8) and up to laurate (C_{12}), a nonuniform increase in the solubilization is found: this is denoted by the portion AB of curves in Fig. 1. For further increase in the length of the soap radical from laurate to stearate (C_{12} to C_{18}), a more rapid increase in the solubilization of the hydrocarbons occurs: this is denoted by the practically linear section BC of the curves. Similar regularity was found earlier in a study of the solubilization of chlorinated hydrocarbons [5, 6]. The structure and length of the hydrocarbon chain (of the hydrocarbon being solubilized) exerts a powerful effect on their solubilization in the soaps which have been studied. Aromatic hydrocarbons are solubilized considerably more than aliphatic hydrocarbons of similar molecular weights, while ethylbenzene, which has a mixed structure, is situated between the two groups with respect to the magnitude of its solubilization (Fig. 1, curve 5). By comparison of the solubilization of styrene with that of ethylbenzene, we see that the presence of the double bond in the aliphatic part of the hydrocarbon molecule is responsible for a sharp increase in its solubilization by soap solutions, apparently because of the hydrophilic character of the double bond, which has been investigated earlier in the hydrocarbon radicals of the soaps of oleic and ricinoleic acids [7].

Consideration of the curves giving the relationship between the solubilization of the hydrocarbons and the structure of the radicals of the fatty acid soaps leads to the conclusion that the solubilization of a monomer (styrene) obeys the general regularity which has been established from the study of the solubilization of aromatic

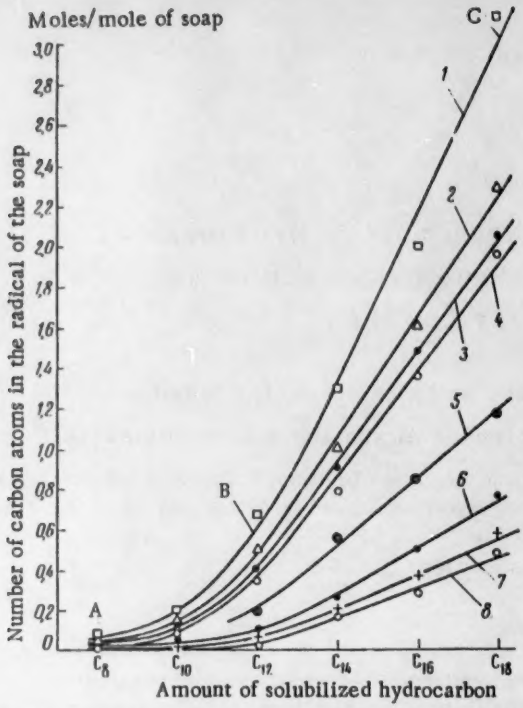

Fig. 1. Solubilization of hydrocarbons of various structures in 0.1 M solutions of the sodium salts of saturated aliphatic acids: 1) benzene; 2) toluene; 3) styrene; 4) o-xylene; 5) ethylbenzene; 6) heptane; 7) isooctane; 8) octane.

hydrocarbons. The presence of ethyl groups in the benzene ring (as in ethylbenzene), or of one of two methyl groups (as in toluene and o-xylene) causes an abrupt reduction of the solubilization of the hydrocarbon in the various solutions of the soaps which have been investigated. Isooctane and heptane are solubilized to a greater extent than normal octane (Fig. 1, curve 8), which reveals the increase in the solubilization of homologous hydrocarbons with shortening of the molecule by a CH_2 group, and by the presence of branching in the hydrocarbon chain.

The hydrocarbons which have been studied can be arranged in the following order with respect to the ease with which they may be solubilized in solutions of the sodium soaps of saturated aliphatic acids: benzene > > toluene > styrene > o-xylene > ethylbenzene > heptane > isooctane > octane.

The regularities which are observed may be explained by supposing that increasing hydrocarbon chain length in the homologous soaps develop a progressively increasing oleophilic micellar structure, which is capable of combining with increasing quantities of the hydrocarbon in the aqueous solution. This assumption is confirmed by the relative position of the solubilization curves for the various hydrocarbons. The quantitative difference in the solubilization depends on the structure and on the energy of the bond between the hydrocarbons and the soaps [3]. The soap micelles have a lower effective volume for the solubilization of aliphatic hydrocarbons than they have for aromatic hydrocarbons.

The partial pressure of the solubilized hydrocarbons is considerably lower than for those which have been emulsified in an aqueous medium [2]. This points to the establishment of a firm bond between the oleophilic portion of the soap micelle and the solubilized hydrocarbons. The determining factor in the colloidal dissolution of the hydrocarbons is apparently the energy of the bond which they form with the soap [3]. The higher value for the solubilization of aromatic hydrocarbons and the styrene monomer is explained by the greater energy of the bond which these substances form with the micellar structure of the soaps in the solution. In the course of

solubilization the hydrocarbons are apparently located not only between the terminal groups of the hydrocarbon chains of the soap (which has been associated into a micellar form), but also in the space between the lines of their side chains.

LITERATURE CITED

[1] Z. N. Markina and P. A. Rebinder, Doklady Akad. Nauk SSSR 109, 1156 (1956).*

[2] M. E. L. McBain and E. Hutchinson, Solubilization and Related Phenomena (New York, 1955).

[3] P. A. Demchenko, A. V. Dumanskii, and L. G. Demchenko, Kolloid. Zhur. 14, 164 (1952).*

[4] P. A. Demchenko, Masloboino-Zhirovaya Promyshlennost' 10, 22 (1959).

[5] P. A. Demchenko, Ukr. Khim. Zhur. 24, 746 (1958).

[6] P. A. Demchenko, Podov. Akad. Nauk Ukr. SSR 5, 494 (1959).

[7] A. V. Dumanskii, V. N. Solnyshkin, and P. A. Demchenko, Ukr. Khim. Zhur. 20, 635 (1954).

* Original Russian pagination. See C. B. Translation.

THE RELATIONSHIP BETWEEN THE FLOATABILITY OF ANTIMONITE AND THE MAGNITUDE OF THE ZETA POTENTIAL

Corresponding Member, Acad. Sci. USSR B. V. Deryagin, and N. D. Shukakidze

Physical Chemistry Institute, Academy of Sciences of the USSR
Translated from Doklady Akademii Nauk SSSR, Vol. 134, No. 2, pp. 376-379, September, 1960
Original article submitted May 25, 1960

The "elementary act" of flotation – the attachment of the mineral particle to the air bubble – can be regarded as a process consisting of three stages: 1) the approach of the mineral particle to the bubble, which is accompanied by the formation of a wetting film subject to the action of surface forces; 2) the decrease in the thickness of the wetting film until it reaches an unstable state; and 3) the rupture of the wetting film and the formation of a wetting perimeter and contact angle which makes possible the firm attachment of the particle to the bubble surface.

The relationship between the wetting contact angle and the floatability has been studied by workers in the Soviet Union [1, 2] and in other countries [3]. The part played by the stage preceding the formation of the contact angle in the flotation process was first noted by A. N. Frumkin [4], who pointed out the importance of studying the process by which the thickness of the wetting film is decreased.

The most significant stage is the third stage, since cases are possible where the wetting film cannot be ruptured, so that flotation is impossible. We shall restrict ourselves to an examination of the criterion of possible ready rupture of the wetting film as the chief criterion for effective floatability.

As a result of the studies carried out in this field, it has been established that the stability of the wetting film is determined chiefly by forces of two different types – Van der Waals forces and electrostatic forces [5-8]. These forces formed the basis of the physical theory of particle interaction and the coagulation of hydrophobic sols and suspensions, including both weakly charged [9] and strongly charged [10] types, and also of the theory of heterocoagulation, the interaction and agglutination of particles of different kinds in electrolyte solutions [11]. The basic hypotheses and conclusions from the theory of heterocoagulation can also be applied to the explanation of the attachment of mineral particles to air bubbles during flotation.

Differences in the nature of the particles undergoing agglutination can lead to a significant change in the nature of the Van der Waals forces and the electrostatic interaction, compared with the case of uniform particles. Thus, when particles of the same type approach, the over-all result of the Van der Waals interactions, taking account of the fact that the molecules of the dispersion medium take part in the interactions, always corresponds to a resultant attraction, while for the case of particles of different kinds in a given medium, on the other hand, a resultant repulsion may be produced. Such repulsion may, for example, be produced when a bulk-hydrophilic particle approaches a bubble.

It follows from the theory of heterocoagulation that the repulsion of particles which have charges of the same sign but not of the same magnitude, when their ionic atmospheres overlap, can be observed only at fairly large distances. When such particles approach, the magnitude of the repulsive forces should pass through a maximum and then decrease, eventually changing to attractive forces at sufficiently small distances. In the

case where the potentials of the two surfaces are of opposite sign, or where the potential of one of them is equal to zero, an attraction should be observed at all distances. This feature of the interaction of surfaces of different types leads to a quantitative modification of the stability criteria, compared with systems with particles of the same type. In the general case, the modified criterion contains the potentials of both surfaces and is fairly complex.

The form of the criterion is greatly simplified in the case where, as a result of the low degree of adsorption of ions on the solution – air interface, the charge of this surface can be taken as equal to zero, while the potential is not given strictly. This case has been examined by Frumkin and Langmuir in the calculation of the repulsive forces in the thin wetting film between a solid surface, charged to a definite potential Ψ_1, and the surface of a bubble, whose charge in solutions containing no capillary-active electrolytes is so small that it may be taken as equal to zero without loss of accuracy. It was shown [12] that the repulsive force preventing the decrease in thickness of the film will be the same as in the case of a film, with double the thickness, between two surfaces charged to the same potential Ψ_1.

This force, which equals the electrostatic component of the pressure forming the wedge, was previously derived by B. V. Deryagin [7], and for the case of low potential Ψ_1 it is equal to

$$P = \frac{\varepsilon}{8\pi} \frac{\psi_1^2}{d^2 \operatorname{ch}^2 (x_0 / d)} = \frac{\varepsilon}{8\pi} \frac{\psi_1^2}{d^2 [1/2 (e^{x_0/d} + e^{-x_0/d})]^2}, \tag{1}$$

where ϵ is the dielectric constant of water, $\underline{d}$ the thickness of the ionic atmosphere, and x_0 is half the thickness of the liquid layer.

By adding the Van der Waals component of the wedge-forming pressure of the wetting film, we obtain for the resultant wedge-forming pressure the value

$$P = \frac{\varepsilon}{8\pi} \frac{\psi_1^2}{d^2 \operatorname{ch}^2 (h_0/d)} + \frac{(A_{12} - A_{11})}{6\pi h^3}, \tag{2}$$

where now h_0 is the thickness of the wetting film, and A_{12} and A_{11} are the Van der Waals constants for the attraction between water and the mineral particle and the attraction within water, respectively.

For bulk-hydrophobic minerals

$$A_{12} < A_{11}, \tag{3}$$

and their difference is equal to a certain positive constant

$$A = A_{11} - A_{12}. \tag{4}$$

According to fairly rough calculations [15], A_{11} for water = $6 \cdot 10^{-13}$ erg. For bulk-hydrophobic minerals, according to Eq. (3), $0 < A_{12}/A_{11} \leq 1$. Without knowing the true value of A_{12}, it is reasonable to assume the value $A_{12} = 3 \cdot 10^{-13}$ erg, corresponding to the "average" value $A_{12}/A_{11} = 0.5$.

The condition for the disappearance of the force barrier, which is dependent on the wedge-forming pressure P(h), will be (see [10, 11])

$$P = \frac{\varepsilon}{8\pi} \frac{\Psi_1^2}{d^2 \operatorname{ch}^2 (h_0/d)} - \frac{A}{6\pi h^3} = 0, \quad \frac{\partial P}{\partial h} = 0. \tag{5}$$

Eliminating A from Eq. (5), we obtain, for the determination of the relationship

$$z \equiv 2h_c/d, \tag{6}$$

where h_c is the film thickness corresponding to disappearance of the force barrier, the equation

$$\frac{z(e^z - e^{-z})}{e^z + 2 + e^{-z}} = 3. \tag{7}$$

The root of this equation is $z \approx 3,2...$ Substituting this value of $\underline{z}$ in place of 2 h/d in the first Eq. (5), we find the condition for the disappearance of the force barrier preventing rupture of the wetting film, i.e., the condition for unhindered flotation:

$$m \equiv dD\psi_1^2/A < 3, \ldots \tag{8}$$

In the case of sufficiently dilute electrolyte solutions and low values of the surface potential, it is possible to equate the surface potential ψ_1 to the ζ-potential. The floatability criterion will then have the form

$$m \cong dD\zeta^2/A < C, \tag{9}$$

where C is a constant approximately equal to 3.

This criterion makes it possible to determine the value of the ζ-potential of a given mineral at which the most complete extraction into the foam product will be obtained. The present study was carried out in order to establish, from the theory, the relationship between the magnitude of the ζ-potential and the floatability of antimonite, and also to examine the possibility of floating the mineral from antimony and antimony – arsenic ores with a single flotation agent.

The studies were carried out with antimonite from the Zopkhito deposits in the Georgian SSR, the Marguzor deposits in the Tajik SSR, and the Kadam-Dzhai deposits in the Kirghiz SSR, with particle size 0.15-0.043 mm, in media with pH values of 3, 4, 5, 6 and 9 established by adding sulfuric acid and caustic soda. The electrokinetic potential was determined by the electroosmosis method, using the apparatus described by V. M. Gortikov [14]. The electrical conductivity of the solutions was measured with a bridge constructed from a 10 m rheostat and KMS-6 resistance box. The bridge was supplied from a signal generator with a current of frequency 1000 cps. A telephone was used as null indicator. The constant of the vessel was determined using KCl solution.

The electrokinetic potential was calculated from the formula $\zeta = 2.4 \cdot 10^6 (V/I)\chi$ mv, where $2.4 \cdot 10^6$ is a constant combining several constant quantities and coefficients used for conversion from absolute quantities to those indicated above, χ is the specific conductance in $ohm^{-1} \cdot cm^{-1}$, V is the quantity of liquid transferred along the capillary, in ml/min, and I is the current strength in ma.

In the calculation of the constant $\underline{c}$ from formula (9), we assumed the values: $A = 0.3 \cdot 10^{-13}$ erg (only the order of magnitude of this quantity is known); D = 80; ζ in CGSE units; and $\underline{d}$ – the reciprocal of the Debye-Huckel parameter $\underline{x}$: $d = 1/x = 4.31 \cdot 10^{-8}/\sqrt{C}$ cm, where C is the concentration in mole/liter of a uni-univalent electrolyte, was determined arbitrarily by calculation for NaCl from the specific conductance measured in the experiment; $C = 1000\chi/\lambda$ g-eq/liter; when $\lambda = 100$ (from the mobility of Na and Cl at 18°), $C = 10\chi$ g-eq/liter.

The experiments on the flotation of antimonite with particle size 0.15-0.043 mm was carried out in a flotation machine constructed by G. A. Khan, with capacity 70 ml, at a solid: liquid ratio = 1: 7 and initial solution pH values of 3, 4, 5, 6 and 9. The foaming agent used was n-hexyl alcohol, the quantity taken being 5 mg/liter for the flotation of antimonite from the Zopkhito deposits and 125 mg/liter for the flotation of antimonite from the Marguzor and Kadam-Dzhai deposits. The duration of the mixing process in all experiments was equal to 2 min, and the duration of the flotation process was 2 min. The degree of extraction was calculated from the weight of foam product and original material.

The results, which are given in Table 1, show that the hydrogen ion concentration has a considerable influence on the value of the electrokinetic potential and floatability of antimonite from the deposits studied.

To determine the influence of the foaming agent on the ζ-potential, measurements were carried out in the presence of n-hexyl alcohol (in quantities corresponding to the amounts used in flotation). The results of

TABLE 1

Mineral	pH	Specific conductance $\chi \cdot 10^5$, $ohm^{-1} \cdot cm^{-1}$	Electrolyte concentration $C \cdot 10^2$, mole/M	Debye thickness of ionic atmosphere $d \cdot 10^6$ cm	Electrokinetic potential ζ, mV	$\frac{dD\zeta^2}{A} \equiv m$	Percentage extraction of antimonite into foam product
Antimonite from Zopkhito deposits	3	0,92	0,92	0,45	—13,2	0,21	93
	4	0,63	0,63	0,54	—36,3	1,9	92
	5	0,42	0,42	0,66	—40,3	2,8	91
	6	0,25	0,25	0,86	—42,0	4,1	64
	9	0,37	0,37	0,71	—53,3	5,3	38
Antimonite from Marguzor deposits	3	1,7	1,7	0,33	—16,3	0,23	93
	4	1,14	1,14	0,36	—32,8	1,1	92
	5	0,63	0,63	0,54	—42,2	2,6	90
	6	0,36	0,36	0,72	—46,6	4,2	72
	9	0,44	0,44	0,65	—52,9	4,9	25
Antimonite from Kadam-Dzhai deposits	3	1,67	1,67	0,33	—17,2	0,27	92
	4	1,35	1,35	0,37	—38,9	1,47	92
	5	0,57	0,57	0,57	—41,0	2,6	88
	6	0,26	0,26	0,85	—48,4	5,2	70
	9	0,33	0,33	0,75	—51,5	5,4	20

the measurements showed that the foaming agent has almost no influence on the value of the ζ-potential of antimonite. At the same time it is clear that at values of the criterion $m \equiv dD\zeta^2/A$ less than 3,0, the degree of extraction is greater than 90%, in accordance with theory. At values of the criterion greater than 3-4, the degree of extraction falls to extremely low values.

LITERATURE CITED

[1] P. A. Rebinder, The Physical Chemistry of Flotation Processes [in Russian] (Moscow, 1933); Studies in the Field of Surface Phenomena [in Russian] (Moscow, 1936).

[2] A. N. Frumkin, A. Gorodetskaya, B. Kabanov, and N. Nekrasov, Zhur. Fiz. Khim. 3, 351 (1932); A. N. Frumkin and A. Gorodetskaya, Zhur. Fiz. Khim. 12, 511 (1938); B. Kabanov and N. Ivanishchenko, Izvest. Akad. Nauk SSSR, Otdel. Khim. Nauk, 755 (1936); E. Cherneva and A. Gorodetskaya, Zhur. Fiz. Khim. 13, 1117 (1939).

[3] W. Luyken and E. Bierbrauer, Theory and Practice of Flotation [Russian translation] (1933).

[4] A. N. Frumkin, Proceedings of the Session of the USSR Academy of Sciences Devoted to the Problems of the Uralo-Kuznets Combine [in Russian] (Leningrad, 1932); Usp. Khim. 2, No. 1 (1933).

[5] B. V. Deryagin and I. I. Abrikosova, Zhur. Éks. i Teoret. Fiz. 21, 245 (1951); 30, 993 (1956); 31, 3 (1956); Doklady Akad. Nauk SSSR 90, 1055 (1953).

[6] B. V. Deryagin and A. S. Titievskaya, Doklady Akad. Nauk SSSR 89, 1041 (1953); Kolloid. Zhur. 15, 416 (1953).*

[7] B. V. Deryagin, Izvest. Akad. Nauk SSSR, OMEN, Ser. Khim. 5, 1153 (1937); Acta Phys. Chim. 10, 333 (1939); Trans. Farad. Soc. 36, 203, 730 (1940).

[8] B. V. Deryagin, Kolloid. Zhur. 6, 291 (1940).

[9] B. V. Deryagin, Kolloid. Zhur. 7, 285 (1941); Trans. Farad. Soc. 36, 730 (1940).

[10] B. V. Deryagin and L. D. Landau, Zhur. Éks. i Teoret. Fiz. 2, 802 (1941); reprinted in Zhur. Éks. i Teoret. Fiz. 15, 11, 662 (1945); Acta Physicochim. URSS 14, 633 (1941).

[11] B. V. Deryagin, Kolloid. Zhur. 16, No. 5 (1954).**

* Original Russian pagination. See C. B. Translation.

** See C. B. Translation.

[12] A. N. Frumkin and A. Gorodetskaya, Acta Physicochim. URSS 9, 327 (1938); Zhur. Fiz. Khim. 12, Nos. 5-6 (1938).

[13] A. N. Brodskii, Physical Chemistry [in Russian] (1948) Vol. 1.

[14] V. M. Gortikov, Kolloid. Zhur. 1, No. 3 (1931).

[15] I. C. Slater and I. G. Kirkwood, Phys. Rev. 37, 682 (1931) (cited in H. Kruyt, Colloid Science [Russian translation] (IL, 1955) Vol. 1, p. 375.

CONVECTIVE INSTABILITY IN AN ELECTROCHEMICAL SYSTEM

Corresponding Member, Acad. Sci. USSR. V. G. Levich

and Yu. A. Chizmadzhev

Electrochemistry Institute, Academy of Sciences of the USSR

Translated from Doklady Akademii Nauk SSSR, Vol. 134, No. 2, pp. 380-383, September, 1960

Original article submitted June 25, 1960

In the study of the electrolytic reduction of persulfate anions at a dropping-mercury electrode, A. Ya. Gokhshtein and A. N. Frumkin [1] detected nondamped spontaneous oscillations of the drop potential and of the current flowing through the drop. Experiments showed that these oscillations are produced in the region of the falling branch of the polarization characteristic with tangential movements of the mercury surface. Retardation of these movements leads to stabilization of the steady-state passage of current. The dropping-mercury electrode, considered as a dynamic system, has an infinite number of degrees of freedom, since the potential and concentration of the ions are not constant over the surface. It follows from experiment [1], however, that the amplitude of the oscillations of potential over the surface, produced by mechanical oscillation of the mercury drop, is small compared with the amplitude of the oscillations of the average potential (Fig. 1). This makes it possible to consider the problem of the oscillations of the average quantities using a model with a finite number of degrees of freedom. It has previously been shown [2], that a model of the 1st order does not describe the spontaneous oscillation phenomena for a single-valued polarization characteristic. We shall therefore consider the dropping-mercury electrode with tangential movements as a system of the 2nd order. The choice of dynamic variables has a certain degree of arbitrariness and requires explanation.

We introduce a spherical system of coordinates with origin at the center of a drop of radius a. The distributions of ion concentrations and potential, which are invariant with respect to rotation about the z axis (see Fig. 2) will depend on the radius r and the angle θ cut off on the z axis in the plane of the diagram. The total solution volume is divided into three regions: the outer face of the diffuse double layer covered by the range $a < r < a + \delta$, the electrically neutral region of variable concentration $a + \delta < r < a + d$, and the main volume of the solution with constant concentration $r > a + d$. It is known [3] that in the steady state, the current of the electrochemical reduction of persulfate anions can be expressed in terms of the reagent concentration by means of the formula

$$j = c_s f(\varphi_{met} - \varphi_s). \tag{1}$$

The period of the observed oscillations is $\tau \sim 10^{-2}$ sec, which is much greater than the relaxation time of the double layer $\tau_\delta \sim 10^{-6}$ sec. This ratio between the times shows that the processes in the double layer region do not play a significant part in the production of the oscillations. We shall therefore use Eq. (1), assuming that the double layer is without inertia. Thus we shall take as one dynamic variable the anion concentration c_s at $r = a + \delta$. It will subsequently be convenient, by making use of the fact that δ is very small compared with d, to consider the double-layer region as a surface and to introduce the effective surface anion concentration Γ, which is related to the bulk concentration c by the relationship $\Gamma = \int_a^{a+\delta} c(r)dr$.

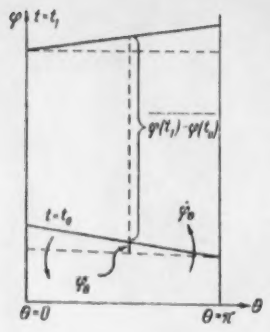

Fig. 1.

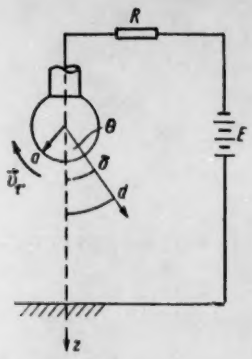

Fig. 2.

It can readily be seen that Γ satisfies the condition $\Gamma \leq c_s \delta$. It is convenient to choose as second dynamic variable the jump in the potential $\varphi = \varphi_{met} - \varphi_s$, where φ_{met} is the potential of the metallic face of the double layer and φ_s is the potential on a sphere of radius $a + \delta$, dependent on the angle θ.

We can write equations describing the behavior of the quantities φ and Γ with time. The law of conservation of charge for the circuit represented in Fig. 2 is of the form:

$$\frac{E - \varphi_{met}}{R} = C_0 \int \frac{\partial (\varphi_{met} - \varphi_s)}{\partial t} ds + \int j \, ds, \tag{2}$$

where R is the resistance of the external circuit, E is the applied voltage, and C_0 the capacity of the double layer per 1 cm^2. The left-hand side of the equation contains the total current passing through the circuit, which is equal to the sum of the integral capacity current and the integral current of the electrochemical reaction. We shall assume that the area of the drop surface remains unchanged with time. We also assume that $\varphi_s \ll \varphi_{met}$. Equation (2) can be then be written in the differential form

$$\frac{\partial \varphi}{\partial t} = \frac{E - \varphi}{RC} - \frac{K}{C} [\varphi_0 - \varphi] \Gamma, \tag{3}$$

if we make the approximation that the polarization characteristic in the region of the falling branch is a linear decreasing function $j = K_0[\varphi_0 - \varphi]\Gamma$ and introduce the drop capacity C.

We can write the conservation law for the number of anions, taking account of the tangential electrocapillary movement of the surface [4], in the form

$$\frac{\partial \Gamma}{\partial t} = I_{diff} - \frac{1}{nF} j(\varphi, \Gamma) - \operatorname{div}_s (\Gamma v_\tau). \tag{4}$$

According to this equation, the surface concentration of anions increases as a result of diffusion from the bulk, decreases as a result of the reaction current, and also changes under the influence of tangential transfer, which is described by the surface divergency $\operatorname{div}_s[\Gamma \mathbf{V}_\tau]$. If the change in concentration along the drop surface is small,

$$\operatorname{div}_s (\Gamma v_\tau) \simeq \Gamma \operatorname{div}_s (v_\tau),$$

and Eq. (4) can be rewritten in the form

$$\frac{\partial \Gamma}{\partial t} = I_{diff} - \frac{1}{nF} j(\varphi, \Gamma) - \Gamma \operatorname{div}_s (v_\tau). \tag{5}$$

We can examine the case where the steady state φ^0, Γ^0 is unique. If it is unstable, then according to deductions from the theory of oscillations [5], we can expect the production of a periodic process. Thus the problem of the possibility of oscillations becomes the problem of the stability of the steady state. The stability of the steady state is determined by the sign of the expression [5]

$$\sigma = \left[-\frac{1}{RC} - \frac{1}{C}\frac{\partial j}{\partial \varphi}\right]_{\varphi^0, \Gamma^0} + \left[\frac{\partial I_{\text{diff}}}{\partial \Gamma} - \frac{1}{nF}\frac{\partial j}{\partial \Gamma} - \operatorname{div}_s(\mathbf{v}_\tau)\right]_{\varphi^0, \Gamma^0}. \tag{6}$$

It should be noted particularly that all the quantities in Eq. (6) should be calculated for the steady state.

Using the familiar expression [4] for the surface divergency $\operatorname{div}_s(\mathbf{V}_\tau) = (2v_0(\varphi)/a)\cos\theta$, where $v_0(\varphi)$ is the velocity at the equator, we obtain an expression for σ:

$$\sigma = \frac{1}{C}\left(-\frac{1}{R} + K\Gamma^0\right) + \left[\frac{\partial I_{\text{diff}}}{\partial \Gamma} - \frac{K}{nF}(\varphi_0 - \varphi^0) - \frac{2v_0}{a}\cos\theta\right]. \tag{7}$$

The plus sign for $v_0(\varphi)$ corresponds to movement from below upwards.

The steady state is unique only when $|1/R| > K\Gamma^0$. The first term in formula (7) is negative. Consequently, the steady state can be unstable only when the expression in square brackets is positive. The first term in the square brackets, corresponding to diffusion from the bulk, is negative. In fact

$$\frac{\partial I_{\text{diff}}}{\partial \Gamma} = \frac{\partial I_{\text{diff}}}{\partial c_s}\frac{\partial c_s}{\partial \Gamma} \sim \frac{\partial}{\partial c_s}\left[D\,\frac{c_0 - c_s}{d}\right]\frac{1}{\delta} = -\frac{D}{d\delta} < 0.$$

The second term, corresponding to the reaction, is also negative. The last term, the convective term, becomes positive, however, when $\theta > \pi/2$.

The following conclusions can thus be drawn from formula (7):

1. Instability can appear only in the region of the decreasing characteristic.

2. In addition, the appearance of instability requires the existence of a sufficiently intense tangential movement.

3. In the absence of tangential movement, the steady state on the decreasing characteristic in the unique range is stable, and spontaneous oscillations are impossible.

4. Diffusion, unlike convection, facilitates stabilization of the steady state. It is possible to estimate roughly the order of magnitude of the tangential velocity which can produce instability. From formula (7) we have:

$$v_0 > v_{\text{init}} = \frac{aD}{d\delta} \sim 10^{-1}\,\text{cm/sec}. \tag{8}$$

5. It follows from formula (8) that with increase in the drop diameter the production of instability is made more difficult, which is in accordance with experimental results [1].

6. From the formulas obtained it is clear that the critical velocity v_{crit} and the critical radius a_{crit} depend on the applied voltage, which is again in accordance with experimental data [1].

7. Experiment has shown [1] that the surface oscillations are more marked in the screened parts of the electrode. This is in accordance with theory, from which it follows that instability is produced when $\theta > \pi/2$.

8. The period of the oscillations in this system should be of the order of $T \sim RC$. The error in this estimate is large, but the calculated value $T \sim 100$ cps is in good agreement with experiment: 60 cps $< T <$ 175 cps.

The physical mechanism of the oscillation process can be represented as follows. We can derive the system from the steady state φ^0, Γ^0 by introducing a small increment $+\Delta\varphi$. This leads to a decrease in the

reaction current $\underline{j}$ and in the current in the external circuit $(E-\varphi)/R$. In the unique range, however, the reaction current decreases to a greater extent than the current in the external circuit. This leads to a decrease in the potential. The concentration, as a result of this process, increases, which leads also to an increase in the reaction current $\underline{j}$. The existence of two degrees of freedom in the system means that the reaction current and the potential jump beyond the steady state by a quantity $-\Delta\varphi$ and then start to decrease. When the convective movement is sufficiently intense, the amplitude of these oscillations starts to increase, and the system moves into the region of increasing characteristic, which restricts the amplitude of the oscillations. The form of the oscillations may be extremely complex and differ considerably from sinusoidal ones.

Finally, it is possible to make certain suggestions regarding the nature of the potential distribution over the drop in the oscillation process. If we use the symbols φ_θ and Γ_θ to denote the small deviation from the average, calculated over the surface, we can write Eqs. (4) and (5) in the form

$$C\frac{\partial\varphi_\theta}{\partial t}=\left(-\frac{1}{R}-\frac{\partial j}{\partial\varphi}\right)\varphi_\theta-\frac{\partial j}{\partial\Gamma}\Gamma_\theta,$$

$$\frac{\partial\Gamma_\theta}{\partial t}=-\frac{\partial j}{\partial\varphi}\varphi_\theta-\frac{\partial j}{\partial\Gamma}\Gamma_\theta+\frac{\partial I^{\text{diff}}}{\partial\Gamma}\Gamma_\theta-\frac{\partial\,\mathrm{div}_s(\Gamma v_\tau)}{\partial v}dv-\frac{\partial\,\mathrm{div}_s(\Gamma v_\tau)}{\partial\Gamma}\Gamma_\theta \tag{9}$$

and examine them for stability. It can readily be seen that the "local" stability is determined by the same expression, σ, as the average stability, from which it follows that the macroscopic oscillations should be accompanied by a redistribution of potential over the surface. From Eq. (9) it follows that the sign of the rate of change in the local potential is different for positive and negative values of φ_θ.

The theory developed here is based on the semiquantitative theory of polarographic maxima, and cannot be expected to show numerical agreement with experiment. The chief result of the work is to show that the most important part in the production of instability in the electrochemical system is played by the tangential movements.

We wish to thank Academician A. N. Frumkin for discussion of the results of this work.

LITERATURE CITED

[1] A. Ya. Gokhshtein and A. N. Frumkin, Doklady Akad. Nauk SSSR 132, No. 2 (1960).*

[2] Yu. A. Chizmadzhev, Doklady Akad. Nauk SSSR 133, No. 5 (1960).*

[3] A. N. Frumkin, V. S. Bagotskii, Z. A. Iofa, and B. N. Kabanov, The Kinetics of Electrode Processes [in Russian] (1952).

[4] V. G. Levich, Physicochemical Hydrodynamics [in Russian] (1959).

[5] A. A. Andronov, A. A. Vitt, and S. É. Khaikin, The Theory of Oscillations [in Russian] (1959).

* See C. B. Translation.

THE STRUCTURE OF GRAPHITIZED THERMAL CARBON BLACK PARTICLES AND OF THEIR FISSION PRODUCTS

E. A. Leont'ev and V. M. Luk'yanovich

Institute of Physical Chemistry, Academy of Sciences of the USSR
(Presented by Academician M. M. Dubinin, April 27, 1960)
Translated from Doklady Akademii Nauk SSSR, Vol. 134, No. 2, pp. 384-386, September, 1960
Original article submitted April 22, 1960

An electron-microscope study of some carbon blacks has shown that in some cases, for example the thermal blacks, the images obtained (with a dark background) are characterized by an increased brightness at the particle edges [1-3]. An analysis of this phenomenon leads to the following conclusion: in these blacks, the structural elements (parallel layers of groups which consist of 2-4 layers of hexagonally packed carbon atoms) are orientated parallel to the particle surface. The particles of a heat-treated thermal black, initially spherical, are converted to polyhedra. On the basis of electron microscope and x-ray data, it was assumed that each polyhedron was built up from a few pyramid-shaped graphite crystals, with their apices orientated towards the center of the polyhedron and their bases forming the basic (001) graphite plane [4, 3].

Direct evidence concerning this assumption of the structure of thermal and heat-treated thermal-black particles was obtained as a result of a microdiffraction investigation, carried out in a high-voltage electron microscope – an "electronograph" [5]. Also, it showed for the first time that the graphite crystals of a particle of heat-treated black are separated by layers of amorphous carbon about 100 A thick.

In this present paper, another approach to the structure of graphitized carbon-black particles has been used an electron-microscope investigation of the oxidized and "exploded" particles. When graphite is treated with strong oxidizing agents in a liquid medium, oxygen atoms penetrate the interplanar lattice spaces and become chemically bonded to carbon atoms [6]. On heating the dried products at 180-200°, explosive formation of CO and CO_2 occurs, resulting in fission of the crystal along the c axis into blocks with a relatively small number of basic planes. Polycrystalline graphitic solids subjected to this treatment will be exploded, i.e., split up into individual crystals, which are deformed (elongated) along the c axis but are unchanged along the a and b axes. This procedure was used to obtain the crystals which form spherical particles of graphite in cast iron [7].

The thermal black used for this investigation was heat treated at 3200° in an inert atmosphere for 20 min (the same sample as that used in [5]). After heat treatment, the particles assumed the form of polyhedra (Fig. 1a,b). An oxidized sample was obtained by mixing 1 g black with a mixture of concentrated acids: 30 ml H_2SO_4 (d = 1.84) + 10 ml HNO_3 (d = 1.40). Then 10 g powdered $KClO_3$ were added and mixed in during 15-20 min, and the mixture allowed to stand for 1.5 to 2 hr. The black was washed with water until free from Cl'. The oxidized black was well wetted with water so that a sample for observation in the electron microscope could easily be prepared from its aqueous suspension. Figure 1c shows that the particles swell as a result of oxidation, the polyhedron form is smoothed out, and there is a noticeable aligning of the surface planes of some particles. The coarse particles become swollen preferentially, most of the fine ones being unchanged.

To obtain exploded particles, small quantities of dried, oxidized black are heated in air, and the products dispersed by the explosion are collected on sieves covered with a film or lining. In a few cases they were prepared from particles of oxidized black already deposited on a quartz layer by breaking them up on a red-hot spiral in vacuo.

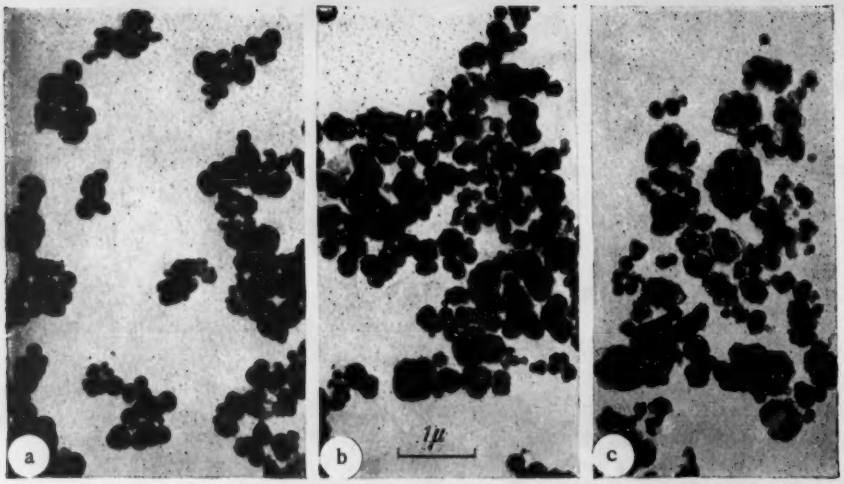

Fig. 1. Particles of a thermal black: a) originally; b) heat treated at 3200°; c) heat treated and oxidized in the liquid phase.

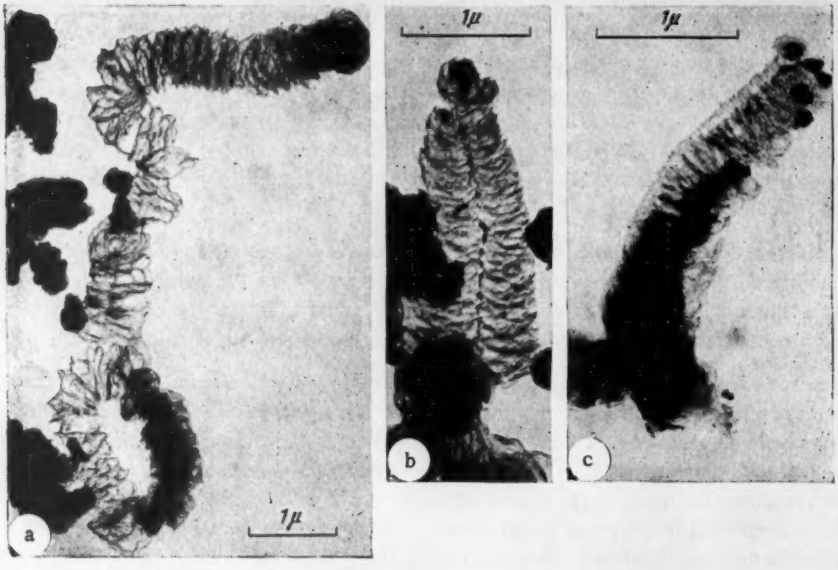

Fig. 2. Exploded particles of a thermal black.

Typical photomicrographs of exploded particles are shown in Fig. 2, where their elongated formations can be seen. A study of the stereophotomicrographs shows that they are three-dimensional formations and not just flat strips. From what was said earlier, these formations can only consist of graphite layers which have been cleaved and deformed by the strong explosion, but are linked up together.

A noticeable feature of the exploded particles is their width, which is quite considerable. Their lateral cross section often corresponds to Fig. 2a, or even exceeds Fig. 2b, the diameter of oxidized carbon-black particles. It is possible that the graphite crystals are preserved in the carbon during heat treatment, their dimensions along the a and b axes corresponding to the width of the exploded particles (e.g., those shown in Fig. 2a). However, it seemed more likely to us that in most cases the exploded particles consisted of a few deformed graphite crystals linked together. Amorphous carbon would serve as the bonding material, since it is known not to

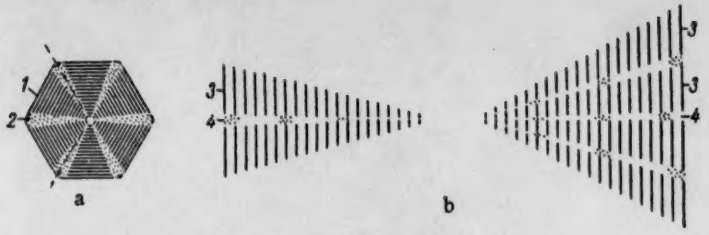

Fig. 3. Schematic representation of the structure of particles of a heat-treated thermal black (a) and of its cleaved exploded particles (b). 1) Graphite crystal; 2) band of amorphous carbon; 3) deformed graphite crystal; 4) "seam" in an exploded particle. The dotted lines show the cleavage planes of the original particles.

swell up or be broken down. On many photomicrographs, exploded particles joined together by a seam can actually be seen (e.g., Fig. 2b).

For this seam to appear, one must obviously assume that amorphous layers are present in the particles of heat-treated blacks. From Fig. 2c, the wide exploded particles are seen to be built up of some narrower formations.

The schematic structures of heat-treated and exploded thermal-black particles are in Fig. 3. Fission of the particles along the planes, which are shown in Fig. 3 by dotted lines, would give rise to two formations (Fig. 3b). The length of the fission products has been considerably reduced in the illustration; the length is actually of the order of, or greater than, the diameter of the original carbon-black particles. The schematic drawing shows how the exploded particles have been expanded to their final form, and why their lateral cross sections can be greater than the diameter of the original carbon-black particle. The dark portions on the narrower tips of exploded particles (Fig. 2b) represent residues of material still intact from the central carbon-black particle.

Thus, allowing for the presence of amorphous layers between the graphite crystals in particles of heat-treated blacks enables the specific morphology of exploded particles to be explained. The coatings, separated from oxidized particles (Fig. 1c), evidently occur as the surface coatings of graphite crystals, joined by layers of amorphous carbon.

This present work confirms that the shape and dimensions of the fission products of a graphitic material are a function of the structure of the material, and in our opinion a study of them can give additional information about this structure. This method of fission is particularly useful in an investigation of polycrystalline graphitic materials consisting of rather large crystals, where x-ray analysis is difficult.

LITERATURE CITED

[1] U. Hofmann, A. Ragoss, et al., Z. anorg. Chem. 255, 195 (1947).

[2] C. E. Hall, J. Appl. Phys. 19, 271 (1948).

[3] H. P. Boehm, Z. anorg. Chem. 297, 315 (1958).

[4] E. A. Kmetko, Proceedings of the First and Second Conferences of Carbon (Buffalo, New York, 1956) p. 21.

[5]. N. M. Popov, V. I. Kasatochkin, and V. M. Luk'yanovich, Doklady Akad. Nauk SSSR 31, 609 (1960).*

[6] U. Hofmann, Ergebn. exakt. Naturwiss. 18, 229 (1939).

[7] E. A. Leont'ev, V. M. Luk'yanovich, and B. S. Mil'man, Doklady Akad. Nauk SSSR 112, 461 (1957).*

*Original Russian pagination. See C. B. Translation.

A POLAROGRAPHIC STUDY OF IODOMETHYLTRIALKYLSILANES

AN UNUSUAL POLAROGRAPHIC MAXIMUM ON THE IODOMETHYLPHENYLDIMETHYLSILANE

S. G. Mairanovskii, V. A. Ponomarenko, N. V. Barashkova, and A. D. Snegova

N. D. Zelinskii Institute of Organic Chemistry, Academy of Sciences of the USSR
(Presented by Academician A. A. Balandin, April 29, 1960
Translated from Doklady Akademii Nauk SSSR, Vol. 134, No. 2, pp. 387-390, September, 1960
Original article submitted April 28, 1960

Nothing appears to have been published in the literature up to now on the polarographic behavior of silicoorganic compounds. In a solitary published article [1], which was devoted to the polarography of the chlorosilanes, the waves which were observed were attributed, apparently, not to the silanes but to the discharge of pyridinium ions formed by the hydrolysis of the chlorosilanes in aqueous pyridine.

In the current work, we report for the first time the investigation of the polarographic behavior of organic molecules containing silicon. We have studied the effect of the presence of the trialkylsilyl group on the electrochemical discharge of compounds in which a range of such groups is linked with a C—I bond. In the course of this we have studied the polarographic behavior of iodomethyltrimethylsilane (I), iodomethyldiethylmethylsilane (II), iodomethyldi-n-propylmethylsilane (III), iodomethyldi-n-butylmethylsilane (IV), and iodomethyldimethylphenylsilane (V). For comparison, we have also obtained polarograms for n-butyl primary iodide, $CH_3 \cdot CH_2 \cdot CH_2 \cdot CH_2I$ (VI), and isobutyl primary iodide, $(CH_3)_2 \cdot CH \cdot CH_2I$ (VII).

The polarograms were obtained in 57%-by-volume ethanol solution at 25° in a thermostatted cell of the construction described earlier [2]. The dropping electrode was provided with a spatula to secure forced removal of the drop. Its characteristics were: m = 1.52 mg/sec, t = 0.23 sec, $m^{2/3}t^{1/6} = 1.032\ mg^{2/3}sec^{-1/2}$. A saturated calomel electrode was introduced to serve as anode. The curves were obtained on the recording polarograph TsLA [3], with potentiometric control of potentials in relation to an auxiliary saturated aqueous calomel electrode, as described earlier [4].

The silanes which were investigated in this work were prepared in the following way. The method developed earlier by one of us [5] was used for the synthesis of compounds I to IV. This consisted in causing chloromethylmethyldichlorosilane to react with an alkyl magnesium iodide:

$$(CH_3)\,Cl_2SiCH_2Cl + 2RMg\,I \rightarrow (CH_3)\,(R)_2\,SiCH_2Cl + 2MgClI \rightarrow$$
$$\rightarrow (CH_3)\,(R)_2\,SiCH_2I + MgCl_2 + MgClI,$$

where R = CH_3, C_2H_5, C_3H_7, or C_4H_9.

Of the chloromethylmethyldichlorosilane 0.25 mole were taken, with the equational amount of the alkyl magnesium iodide in 150-200 ml of absolute ether. After the completion of the addition of the chloromethylmethyldichlorosilane to the Grignard reagent, the ether was distilled off, and the residue heated on a water bath

TABLE 1

No. of compound	Substance	Temp., °C	$n^{20}D$	d^{20}_4	$E_{\frac{1}{2}}$ relative to saturated calomel electrode	Gradient, mv^{-1}
I	$(CH_3)_3SiCH_2I$	140,5(743,5)	1,4891	1,4301	−1,580	136
II	$(C_2H_5)_2(CH_3)SiCH_2I$	102,5(50)	1,5000	1,3690	−1,603	140
III	$(C_3H_7)_2(CH_3)SiCH_2I$	82(6)	1,4920	1,2694	−1,630	200
IV	$(C_4H_9)_2(CH_3)SiCH_2I$	99,5(12)	1,4877	1,2116	−1,652	230
V	$(C_6H_5)(CH_3)_2SiCH_2$	97,2(3)	1,5730	1,4496	−1,470	150
VI	$n\text{-}C_4H_9I$	–	–	–	−1,782	100
VII	$\begin{matrix}CH_3\\CH_3\end{matrix}\!\!>\!CH\!-\!CH_2I$	–	–	–	−1,795	95

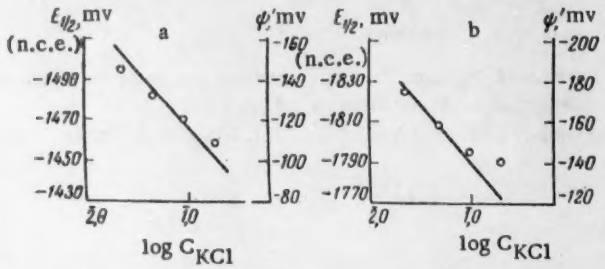

Fig. 1. Relationship between $E_{\frac{1}{2}}$ (circles) and the concentration of potassium chloride for substance V (A) and VII (B); and also between the Ψ^1-potential and the concentration.

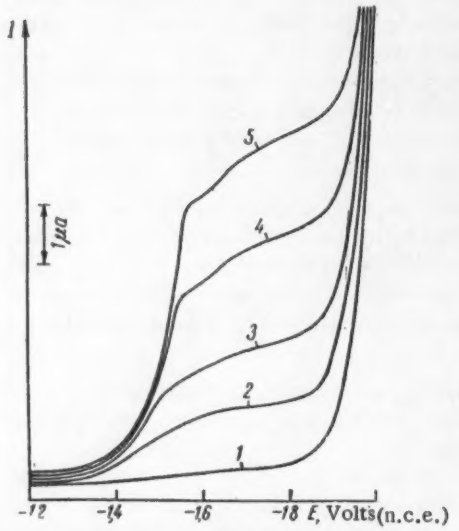

Fig. 2. Polarograms for substance (V) at various concentrations. 1) 0; 2) $0.573 \cdot 10^{-3}$M; 3) $1.093 \cdot 10^{-3}$M; 4) $2.00 \cdot 10^{-3}$M; 5) $2.78 \cdot 10^{-3}$M.

at 80-85° for 15-16 hr. The ether which had been distilled off was then added to the reaction products, the mixture was decomposed in water, and the ether layer dried over anhydrous sodium sulfate. The ether was then distilled off again, and the product distilled through a column under vacuum. The yield of the iodide in passing from $(CH_3)_3SiCH_2I$ to $(C_4H_9)_2(CH_3)Si_6H_2I$ diminished from 61% to 8%. In connection with this, the synthesis of compound (V) was carried out by the interaction of $(C_6H_5)(CH_3)_2SiCH_2Cl$ (13.2 g) with potassium iodide (17 g) in 170 ml of absolute acetone at the boiling point for 57 hours. The yield of (V) was 43% of the theoretical. All the iodides were redistilled several times under vacuum before their polarograms were obtained. The properties of the iodomethylsilanes are given in Table 1.

At low concentrations, all the substances investigated give clear, single-stage reduction waves, whose limiting currents (as is shown by experiments using different heights of the mercury column) are determined by the diffusion of the depolarizer. The values of the constant for the diffusion current, $i_{diff} = Cm^{2/3}t^{1/6}$, for the substances studied varies between the limits of 1.9 and 2.2 $\mu a/mmole \cdot mg^{2/3} \cdot sec^{-1/2}$. Calculation of the number of electrons taking part in the electrode process on the basis of the Il'kovich equation (on the assumption that the diffusion coefficient is of the order of $3 \cdot 10^{-6}$ cm^2/sec) gave the value 2. The half-wave potentials, $E_{\frac{1}{2}}$, of the substances studied do not depend on the pH of the solution. Hence, the reduction of the compounds which we have studied evidently takes place

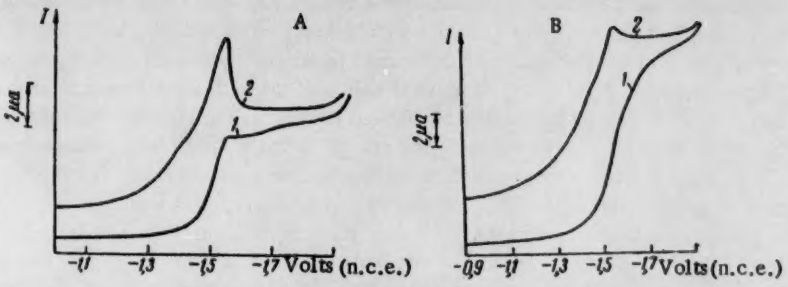

Fig. 3. Polarograms for substance (V) for mercury column height of 30 cm (A) and 110 cm (B). 1) C_V = 2.99 mM in the absence of BSTEA; 2) C_V = = 2.64 mM in the presence of 0.083 M BSTEA in a base solution of 0.09 N KCl in 57% ethanol.

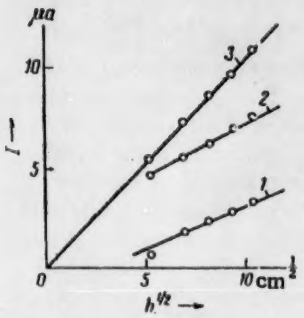

Fig. 4. Relation between the heights of the apparent steps in the wave from substance (V), and the height of the mercury column. 1) Upper step; 2) lower step; 3) total (diffusion) current. C_V = = 2.64 mM.

according to the same mechanism as that of other alkyl halides – that is, with the transfer of two electrons and the exchange of the halogen atom of the organic molecule for a hydrogen atom. Logarithmic graphs of the waves of all the substances investigated, using the relationship $\log [i/(i_{lim}-i)] = f(E)$, give straight lines; the larger values, which are in the inverse order of their slopes, follow from the irreversible character of the waves. The magnitudes of the half-wave potentials of the waves, $E_{\frac{1}{2}}$, which are obtained from the logarithmic graphs, are independent, within the limits of experimental error, of the concentration of the depolarizer.

In Table 1, the values of $E_{\frac{1}{2}}$ for the substances investigated are given for 0.09 N solutions of potassium chloride as base solution. Comparison of these $E_{\frac{1}{2}}$ values for the compounds studied shows that compounds I to IV (that is, the substituted alkylsilanes) have values for $E_{\frac{1}{2}}$ which lie very close to each other, while compound V, which has a phenyl group attached to the silicon atom, is reduced considerably more easily. This behavior of the compounds studied is quite natural: the size of the alkyl radicals exerts practically no influence on the electronegativity of the trialkylsilane radical, and, therefore, also exerts practically no influence on the splitting of the C–I bond occurring throughout the series. The slight shift of the half-wave potential to the negative side with increase in the length of the alkyl radicals is apparently connected with a steric factor [6]. The effect of introducing a phenyl radical into the silyl group is to increase its electronegativity, and, in addition, it increases the polarizability; hence, the nucleophilic rupture of the C–I bond in compound (V) occurs considerably more easily than with the alkylsilyl derivatives.

Comparison of the magnitudes of the half-wave potentials of the iodoalkylsilanes with the iodoalkyls (Table 1) shows that the introduction of alkylsilyl groups into the molecule of an iodoalkyl diminishes the value of $E_{\frac{1}{2}}$; that is, it appears to facilitate the nucleophilic rupture of the C–I bond. Thus, the alkylsilyl group seems to behave in a more electronegative manner than the alkyl group itself. This conclusion, however, is not in accord with observations which have been made previously [7], according to which the substitution of the hydrocarbon residue in carboxylic acids by the same group (containing the silicon atom in the α-position with respect to the carboxyl) has the effect of reducing the dissociation constant of the acid. Hence, the alkylsilyl group possesses greater electron-donor properties than the corresponding hydrocarbon group. The lowering of the half-wave potential for the reduction of the C–I bond, in moving from the alkyl halide to the corresponding silicon derivative, is apparently [8] connected with the large difference in adsorption energy and solvation energy between the substances concerned and those formed at the electrode at the potential-determining stage, between the silicoorganic compounds and those containing no silicon.

The nature and concentration of the indifferent electrolyte exerts a considerable influence on the value of the half-wave potential for the waves of the substances studied. As we have already remarked, the waves have irreversible nature, and according to A. N. Frumkin's theory of delayed discharge [9] the effect of the indifferent electrolyte on the value of this potential should be determined in the main by the change in the ψ'-potential. Figure 1A and B, gives the experimental values of the half-wave potential for waves given by substances (V) and (VII) in 57% ethanol solution for various concentrations of potassium chloride in the base solution. The curves in the same figures represent the change in the ψ'-potential, calculated according to Stern's method [10]. For these calculations, the dielectric constant has been taken as 50, and the capacity of the double layer as 16 and 18 $\mu F/cm^2$ for Figs. 1A and 1B, respectively. It is seen from Fig. 1 that the shift in the half-wave potential with increase in the potassium chloride concentration is in fact closely connected with the reduction of the ψ'-potential. As would have been expected, a considerably greater negative shift of the half-wave potential is observed when surface-active cations are added to the solution. Thus, the introduction into 0.1 N potassium chloride base solution of 0.08 N tetraethylammonium benzensulfonate (BSTEA) causes the half-wave potential of compound (V) to undergo a positive shift of about 110 mV. A small shift of the half-wave potential of substance (V) is also observed when gelatin is added to the solution.

Because of the irreversible character of the electrode process, the values of the half-wave potential depend on the height of the mercury column, h_{Hg}. Thus, when h_{Hg} is doubled, the value of the half-wave potential is changed by ~25 mV, which is in excellent agreement with theoretical deductions [11].

There are very interesting phenomena observed in the waves given by substance (V), iodomethylphenyldimethylsilane. When the concentration of this in the solution is raised higher than 1.0 mM, a small maximum appears at the mean portion of the wave, which creates an impression of the separation of the wave into two steps (Fig. 2). Addition to the solution of tetraethylammonium benzenesulfonate causes a shift of the curves towards a more positive potential, and the maximum on them is shifted to its "usual place" at the upper part of the wave (Fig. 3). It is interesting to note that the potential corresponding to the maximum remains practically unchanged when this occurs. When the height of the mercury column is increased the maximum on the wave of substance (V), in the presence of tetraethylammonium benzenesulfonate diminishes; it diminishes in almost the same way in the absence of this, but then the division of the wave into two steps is less apparent. Figure 3 gives the polarograms of substance (V) for two values of the height of the mercury column: (A) 30 cm, and (B) 110 cm, both in the absence of tetraethylammonium benzenesulfonate (1) and in its presence (2). Figure 4 shows the relationship between the heights of these apparent steps for waves from substance (V), and the height of the mercury column.

Addition of gelatin in concentration 0.05% to the solution causes the complete elimination of the maximum in the waves of substance (V): in these circumstances the waves of substance (V) are more extended.

LITERATURE CITED

[1] E. A. Abrahamson and C. A. Reynolds, Anal. Chem. 24, 1827 (1952).

[2] S. G. Mairanovskii and F. S. Titov, Zhur. Anal. Khim. 15, 121 (1960).*

[3] S. B. Tsfasman, Zavodskaya Lab. 22, 131 (1956).

[4] S. G. Mairanovskii, A. A. Fainzil'berg, et al., Doklady Akad. Nauk SSSR 125, 2, 351 (1959).*

[5] V. A. Ponomarenko and V. F. Mironov, Doklady Akad. Nauk SSSR 94, 3, 485 (1954).

[6] F. L. Lambert and K. Kobayshi, Chem. and Ind. 30, 949 (1958).

[7] P. D. George, M. Prober, and J. R. Elliott, Chem. Rev. 56, 1161 (1956).

[8] N. S. Hush, Z. Elektrochem. 61, 734 (1957).

[9] A. N. Frumkin, V. S. Bagotskii, et al., Kinetics of Electrode Processes [in Russian] (Moscow, 1952) p. 177.

[10] A. N. Frumkin, V. S. Bagotskii, et al., Kinetics of Electrode Processes [in Russian] (Moscow, 1952) p. 15.

[11] P. Delahay, New Apparatus and Methods in Electrochemistry [Russian translation] (IL, 1957) p. 103.

*Original Russian pagination. See C. B. translation.

A STUDY OF THE MECHANISM OF OXIDATION OF COPPER BY LIQUID SULFUR USING THE S^{35} ISOTOPE

I. I. Pokrovskii and M. M. Pavlyuchenko, Academician,
Academy of Sciences of the Belorussian SSR

V. I. Lenin Belorussian State University
Translated from Doklady Akademii Nauk SSSR, Vol. 134, No. 2, pp. 391-393, September, 1960
Original article submitted May 12, 1960

The oxidation of copper by liquid or gaseous sulfur is accompanied by the formation and growth of various layers of sulfide scale on the metallic surface [1, 2]. The principal compact portions of the scale are the outer and the intermediate layers which are composed of CuS and Cu_2S, respectively, of characteristic acicular structure. The porous portion of the scale is its inner layer which is also composed of Cu_2S.

The available data [3] show the oxidation of copper by liquid sulfur to be described by a parabolic equation and the process must, therefore, be controlled by the diffusion of one, or both, of the reagents through the sulfide scale. The existence of a porous inner layer of Cu_2S whose structure is quite different from that of the principal portion of the sulfide scale is a clear indication that the oxidation involves not only a diffusion of copper through the scale, but a counterdiffusion of sulfur as well. It has also been suggested, however [4], that the reaction is due solely to copper diffusion, with the porous Cu_2S layer at the copper surface resulting from some secondary process such as recrystallization.

It would seem that the problem of the mechanism of the oxidation of copper by liquid sulfur could be settled definitely by using the radioisotope S^{35} to study the process. The technique which was followed here has involved the introduction of S^{35} into the sulfide scale at various stages in the reaction, with subsequent determination of its distribution, either by autoradiography or by radiometric analysis of the individual layers.

The copper specimens were in the form of bars 7 × 8 × 25 mm which had been prepared from metal plates of 99.9% purity. Each specimen was annealed in vacuum at 1000° for six hours. Oxidation of the copper by liquid sulfur was carried out over the temperature interval from 270 to 444°.

Two series of experiments were performed. In the first series, a scale of definite depth was formed on the copper surface and the metal then oxidized by radioactive sulfur. This was accomplished by allowing the reaction to proceed for a fixed period and then introducing the S^{35} into the liquid sulfur.

In the second series, a thin sulfide scale containing S^{35} was first formed on the copper surface and the metal then oxidized by liquid sulfur. This was done by treating the copper specimens, prior to reaction, with a benzene solution of S^{35} at high specific activity and then oxidizing with liquid sulfur. After removal from the melt, the scale-covered specimens were washed free of the adhering sulfur with a ten-percent solution of sodium sulfide, rinsed with water, alcohol, and ether, dried, and then sectioned at right angles to the long axis. The unreacted copper core was extracted from the interior of the specimen and replaced with liquid sulfur so as to strengthen the porous layer of scale. The scale specimens prepared in this manner were ground, polished, and subjected to autoradiography, in order to establish the distribution of the radiosulfur.

Typical results from the two series of experiments are represented in Figs. 1 and 2. Figure 1 is a positive of an autoradiograph of a section of scale which had been formed by oxidizing copper at 444°, first for 17 min

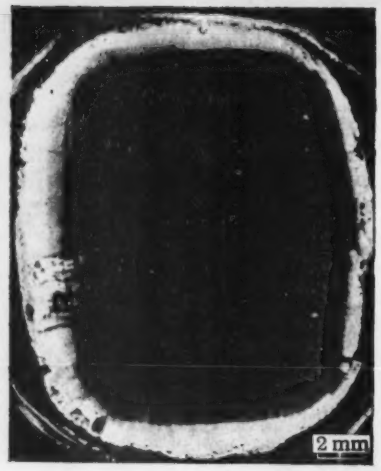

Fig. 1.

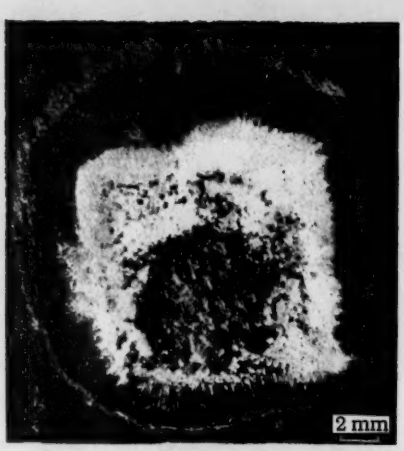

Fig. 2.

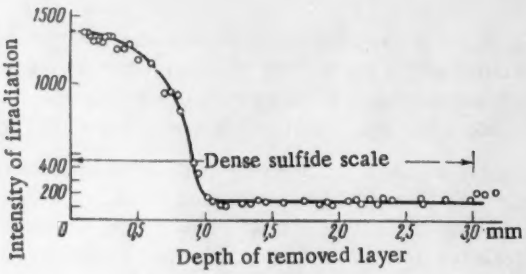

Fig. 3.

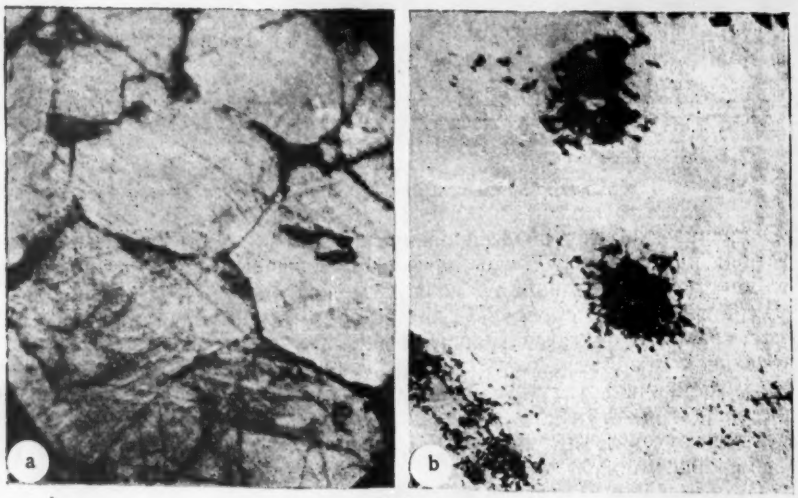

Fig. 4.

with inactive sulfur and then for an additional 43 min in the presence of S^{35}. Figure 2 is a positive of an autoradiograph of a section of scale which had been formed on copper at 400°, the specimen having been first treated with the benzene solution of S^{35} and then oxidized in inactive sulfur for 8 hr.

The observed distribution of S^{35} can be explained by assuming that the dense portion of the scale grows outward through diffusion of metal from the copper core during the reaction.

But if reaction were due solely to the diffusion of copper, it is clear that the inner side of the scale should be inactive in the experiments of the first series.* The experiments of this series showed, however, that the inner side of the scale had an appreciable activity in every case. In addition, radiometric analysis of the individual layers disclosed the presence of S^{35} throughout that part of the scale which was formed during oxidation by the inactive sulfur. A radiometric curve for the scale formed on copper held at 444° for 96 min is represented in Fig. 3. The S^{35} isotope was introduced into the liquid sulfur 24 min after initiating this reaction.

Finally, comparison of microphotographs and microautoradiographs (negatives) of a portion of the section parallel to the surface of the specimen at the level of the initial inactive layer (Fig. 4) show diffusion of sulfur to the copper core to proceed along the grain boundaries and along the joints of various acicular crystals in the compact part of the scale.

On the basis of these results, it can be affirmed that the formation of the sulfide scale on copper is the result of diffusion of both reagents.

LITERATURE CITED

[1] L. Czerski and S. Patzau, Arch. Górn.-Hutn. PAN 2, 353 (1954).

[2] V. I. Arkharov and S. Mardeshev, Fiz. Metal. i Metalloved. 1, 2, 273 (1955).

[3] K. Hauffe, Reaktionen in und an festen Stoffen (Berlin, 1955).

[4] I. Mikulski, S. Mrowec, et al., Roczn. Chem. 33, 1285 (1959).

*Supposing the oxidation of copper in the inactive sulfur to be sufficiently extensive so that the radiation from the S^{35} is totally absorbed by the resulting layer of scale.

THE RELAXATION MECHANISM IN THE CRITICAL REGION OF SEPARATION INTO LAYERS

L. A. Rott

S. M. Kirov Belorussian Forest Technology, Institute
(Presented by Academician A. N. Frumkin, April 27, 1960)
Translated from Doklady Akademii Nauk SSSR, Vol. 134, No. 2, pp. 394-396, September, 1960
Original article submitted April 27, 1960

At the critical point of separation into layers in a binary liquid system, the rate of diffusion falls to zero, and the derivative of the chemical potential with respect to mole fraction becomes equal to zero [1, 2].

In accordance with the Onsager hypothesis in the thermodynamics of irreversible processes, the average rate of damping of the concentration fluctuations should be linearly dependent on the diffusion current. If this assumption is also justifiable for the critical region, the study of the diffusion properties in the neighborhood of the critical point should serve as a means of studying the mechanism of the fluctuations in a many-component system.

Calculations have shown [3] that the change in the mole fraction concentration of a component in comparatively small volumes, of the order of the wavelength of light, for example, takes place extremely slowly (for some systems a significant change in the mole fraction is observed only after 10^3 sec). If follows from the Onsager hypothesis that the concentration equilibrium should be established slowly in the critical region.

If we regard the free energy of the system as a function of the volume V and the mole fraction of a component N_2 at constant temperature, we find the pressure P of the system in the nonequilibrium state:

$$P = -\left(\frac{\partial F}{\partial V}\right)_T = -\frac{\partial}{\partial V} F(V, N_{20} + \varepsilon) = -\frac{\partial F(V, N_{20})}{\partial V} - \varepsilon \frac{\partial^2 F(V, N_{20})}{\partial N_2 \partial V},$$
$$P - P_0 = -\varepsilon \frac{\partial}{\partial V}\left(\frac{\partial F}{\partial N_2}\right)_{N_2 = N_{20}}, \tag{1}$$

where $N_2 = N_{20} + \epsilon$, and N_{20} is the mole fraction of the second component in the state of thermodynamic equilibrium.

Using the relationship

$$\frac{\partial}{\partial N_2} = \left(\frac{\partial}{\partial n_2}\right)_{n_1} - \left(\frac{\partial}{\partial n_1}\right)_{n_2} \tag{2}$$

(n_1 and n_2 are the number of moles of the first and second components in the solution, respectively, and $n_1 + n_2 = 1$), we obtain

$$P - P_0 = -\varepsilon \frac{\partial}{\partial V}(\mu_{20} - \mu_{10}). \tag{3}$$

Since at the critical point in a binary system the following conditions apply

$$\left(\frac{\partial \mu_2}{\partial N_2}\right)_{P,T} = 0, \quad \left(\frac{\partial^2 \mu_2}{\partial N_2^2}\right)_{P,T} = 0, \tag{4}$$

we can, by restricting ourselves to the first two terms in the expansion, write the expression

$$\mu_{20} = \mu_{2,\,\text{crit}} + \beta_2 (N_{20} - N_{2,\,\text{cr}})^3. \tag{5}$$

On the other hand, the difference $P - P_0$ between the true pressure and the equilibrium pressure in the state of the system with density $\rho + \delta\rho$ is equal to [4]

$$P - P_0 = \frac{\tau\rho}{1 - i\omega\tau} (c_0^2 - c_\infty^2) \operatorname{div} \mathbf{v} \tag{6}$$

(c is the velocity of sound, $c_0 = c$ when $\omega\tau \ll 1$, $c_\infty = c$ when $\omega\tau \gg 1$, ω is the frequency, and τ is the relaxation time.

The change in density is related to the movement of the liquid, which also determines the change in the molefraction δN_2. It is then related to the velocity of the liquid $\mathbf{v}$ by the continuity equation

$$\frac{d\delta N_2}{\partial t} + N_2 \operatorname{div} \mathbf{v} = 0. \tag{7}$$

The basic assumption made in earlier work [3], that the speed of the change in concentration of one of the components is determined by its chemical potential gradient, leads to an equation for isothermal diffusion in the critical region of separation into layers

$$\frac{\partial N_2}{\partial t} = -\frac{D_0}{RT} \operatorname{div} (N_2 \operatorname{grad} \mu_2). \tag{8}$$

From the expansion of (5)

$$\operatorname{grad} \mu_2 = 3\beta_2 (N_2 - N_{2,\,\text{cr}})^2 \operatorname{grad} N_2. \tag{9}$$

Making use of Eqs. (7) and (8), we may write

$$\begin{aligned} -N_2 \operatorname{div} \mathbf{v} - \mathbf{v} \operatorname{grad} N_2 = -\frac{3\beta_2 D_0}{RT} (N_2 - N_{2,\,\text{cr}}) [(N_2 - N_{2,\,\text{cr}}) (\operatorname{grad} N_2)^2 + \\ + 2N_2 (\operatorname{grad} N_2)^2 + N_2 (N_2 - N_{2,\,\text{cr}}) \Delta N_2]. \end{aligned} \tag{10}$$

If $N_{20} \to N_{2,\,\text{crit}}$, then it is approximately true that

$$N_2 \operatorname{div} \mathbf{v} + \mathbf{v} \operatorname{grad} N_2 = \frac{6\beta_2 D_0}{RT} N_2 (N_2 - N_{20}) (\operatorname{grad} N_2)^2. \tag{11}$$

Equating the right-hand sides of Eqs. (3) and (6), and making use of div $\mathbf{v}$ from (11), we obtain an expression for the determination of the relaxation time τ:

$$\begin{aligned} (N_2 - N_{20}) \frac{\partial}{\partial V} (\mu_{20} - \mu_{10}) = \\ = \frac{\tau\rho (c_0^2 - c_\infty^2)}{1 + \omega^2\tau^2} \left[\frac{\mathbf{v}}{N_2} \operatorname{grad} N_2 + \frac{6\beta_2 D_0}{RT} (N_2 - N_{20}) (\operatorname{grad} N_2)^2 \right]. \end{aligned} \tag{12}$$

From this

$$\tau = \frac{A}{2B\omega^2} + \sqrt{\frac{A^2}{4B^2\omega^4} - \frac{1}{\omega^2}}, \tag{13}$$

where

$$A = \rho(c_0^2 - c_\infty^2)\frac{v}{N_2}\operatorname{grad} N_2, \qquad B = (N_2 - N_{20})\frac{\partial}{\partial V}(\mu_{20} - \mu_{10}).$$

Direct estimation shows that

$$\frac{6\beta_2 D_0}{RT}(N_2 - N_{20})(\operatorname{grad} N_2)^2 \ll \frac{v}{N_2}\operatorname{grad} N_2, \qquad \frac{A}{B} \gg 1.$$

Let us examine movement in one dimension. In this case

$$\operatorname{grad} N_2 \cong \frac{N_2 - N_{20}}{\lambda/4}$$

(λ is the wavelength):

$$v = c\frac{\Delta\rho}{\rho}; \qquad \left(\frac{\partial\mu_2}{\partial V}\right)_{T,N_2} = \left(\frac{\partial\mu_2}{\partial P}\right)_{T,N_2}\left(\frac{\partial P}{\partial V}\right)_{T,N_2} = \bar{V}_2\left(\frac{\partial P}{\partial V}\right)_{T,N_2}.$$

We can estimate the relaxation time in the critical range of separation into layers. For liquids, $c \sim 10^5$ cm·sec^{-1}, $c_0^2 - c_\infty^2 \sim 10^9$, $N_2 - N_{2,crit} \sim 10^{-2}$ and $\Delta\rho \sim 10^{-2}$ g·cm^{-3}. Since

$$\frac{\partial(\mu_{20} - \mu_{10})}{\partial V} = \bar{V}_2\left(\frac{\partial P}{\partial V}\right)_{T,N_2} - \bar{V}_1\left(\frac{\partial P}{\partial V}\right)_{T,N_1},$$

$\bar{V}_1 - \bar{V}_2 \sim 10$ cm^3, and $\partial P/\partial V \sim 10^2$ atm·cm^{-3}, it follows that $\partial(\mu_{20} - \mu_{10})/\partial V \sim 10^2 - 10^3$ atm. For these data and a frequency of sound $\omega = 10^7$ cps,

$$\tau \sim 10^{-7} - 10^{-8} \text{ sec.},$$

which is much greater than the relaxation time outside the critical region. A value of the order of 10^{-7} has been obtained for τ in the critical region of pure xenon [5].

The expression obtained (13) makes it possible to follow the way in which the relaxation time depends on the properties of the system and the parameters of the sound wave, without making use of models of the system.

LITERATURE CITED

[1] I. P. Krichevskii, N. E. Khazanova, and L. R. Linshits, Doklady Akad. Nauk SSSR 99, 113 (1954).

[2] I. R. Krichevskii and Yu. V. Tsekhanskaya, Zhur. Fiz. Khim. 30, 2315 (1956).

[3] L. A. Rott, Doklady Akad. Nauk SSSR 121, 678 (1958).*

[4] L. D. Landau and E. M. Lifshits, The Mechanics of Continuous Media [in Russian] (1953).

[5] A. G. Chynoweth and W. G. Schneider, J. Chem. Phys. 20, 1776 (1952).

*Original Russian pagination. See C. B. Translation.

MECHANISM OF GAS FORMATION DURING RADIOLYSIS OF ORGANIC SUBSTANCES AND ITS CONNECTION WITH THEIR AGGREGATE STATE

A. B. Taubman, L. P. Yanova, R. S. Maslovskaya, and P. Ya. Glazunov

Institute of Physical Chemistry, Academy of Sciences of the USSR
(Presented by Academician P. A. Rebinder, May 9, 1960)
Translated from Doklady Akademii Nauk SSSR, Vol. 134, No. 2, pp. 397-399, September, 1960
Original article submitted May 4, 1960

In an investigation of the temperature dependence of gas formation during radiation destruction of polymers (polymethylmethacrylate and polytetrafluoroethylene) by electron radiation, we showed [1, 2] that in the region of the transition of the irradiated polymer* from the highly elastic to the viscous-flow state (at temperatures $t \geq T_T$) the rate of gas liberation with a constant dose increases sharply (jump). We interpreted the mechanism of this phenomenon by the hypothesis that high, local supersaturations of gas solutions, arising as a result of radiolysis, are resorbed by diffusion of the gas in the highly elastic "solid" state more slowly than in the "liquid" viscous-flow state so that in the latter case, nuclei of a new gas phase are formed and their growth is considerably facilitated. As a result of the more rapid separation of the radiolysis products from the reaction sphere in the less viscous medium, the equilibrium of the quasireversible process: destruction $\rightleftharpoons$ recombination of free radicals is displaced to the left and the gas-formation rate rises. However, there may be another explanation for the given effect, for example, it may be regarded as the result of a fall in the thermal destruction temperature of the polymer produced by the radiation, which is not connected with any changes in its physical state and the viscosity conditions at the transition point [3].** On the other hand, the more intense gas formation at $t \geq T_T$ may be caused by a change in the actual mechanism of polymer destruction occurring under these conditions by a mode characteristic of thermal destructions, namely, by elimination of monomer units from the ends of the chains, in contrast to normal radiation destruction at lower temperatures, which proceeds by random rupture of the chains [3].

It might be possible to demonstrate the accuracy of our interpretation of the effect more precisely by also observing this effect at quite low temperatures at which the possibility of thermolysis is completely excluded and on substances of a nonpolymeric nature. This requirement is obviously satisfied by normal organic substances of low molecular weight. Thus, the present investigation was intended not as a quantitative study of the temperature dependence of gas formation during radiolysis, but for the detection of: 1) differences in the intensity of this process during the irradiation of organic substances in the liquid and solid state with the same dose and 2) relations between the temperature of the change in gas-formation kinetics and the melting point (m.p.) of the given compound.

* The temperature at which there is a change in the kinetics of gas formation corresponds to the transition point not of the original, but the irradiated sample because the radiolysis of polymers which mainly suffer destruction is accompanied by a fall in their molecular weight and, consequently, in the transition point, as is shown by thermomechanical curves [2].

** Radiation activation of thermal destruction processes has been demonstrated by a number of authors [4, 5], but they have not considered the effect of radiation on gas formation, but the intensification during the combined action of radiation and heat in the formation of condensed (liquid and solid) radiolysis products [4] and the decrease in the energy for breaking macromolecule chains under such conditions [5].

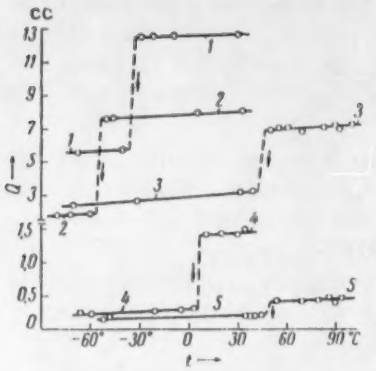

Fig. 1. Temperature dependence of gas formation (the arrows indicate the melting point of each substance): 1) n-decane, $E_0 = 1.2 \cdot 10^{18}$ ev/cc·sec, $E = 4.3 \cdot 10^{21}$ ev/cc; 2) n-octane, $E_0 = 0.6 \cdot 10^{18}$ ev/cc·sec, $E = 2.2 \cdot 10^{21}$ ev/cc; 3) paraffin, $E_0 = 1.1 \cdot 10^{18}$ ev/cc·sec, $E = 4.0 \cdot 10^{21}$ ev/cc; 4) nitrobenzene, $E_0 = 1.9 \cdot 10^{18}$ ev/cc·sec, $E = 6.8 \cdot 10^{21}$ ev/cc; 5) p-dichlorobenzene, $E_0 = 1.5 \cdot 10^{18}$ ev/cc·sec, $E = 5.4 \cdot 10^{21}$ ev/cc.

We irradiated the compounds n-octane, n-decane, paraffin, nitrobenzene, and p-dichlorobenzene (specially purified Kahlbaum preparations, apart from the paraffin) at various temperatures with a beam of fast electrons on an accelerator operating at 680-750 kv with a dose strength varying over the range $E_0 = 0.6\text{-}1.9 \cdot 10^{18}$ ev/cc·sec; with a constant irradiation time of one hour, the dose varied over the range $E = 2.2\text{-}6.8 \cdot 10^{21}$ ev/cc. The ferrous sulfate method was used for dosimetry. The temperature range investigated for each compound covered a region above and below the melting point and the temperature was maintained with an accuracy of ±4° by thermostatting (in a Hepler thermostat) when there was little heating of the samples by the radiation. Therefore, by setting the experimental temperature accurately at the melting point, in two sample irradiation experiments it was possible to have a minimum difference of 8° between the temperatures corresponding to the liquid and solid states (above and below the melting point). The samples were irradiated in a glass cell through a membrane 0.06-0.07 mm thick and the temperature was measured with a thermocouple whose junction was introduced into the center of the sample through a glass pocket in the cell. The amount of gaseous radiolysis products was measured by volume after they had been liberated from the sample in the liquid state.

The results of the measurements are given in Fig. 1 as curves of the relation between gas volume and temperature $Q = f(t)$.

As can be seen, the effect of a change in temperature on the formation of gaseous radiolysis products by the substances investigated when in both the solid and liquid states is very slight (in accordance with the low activation energies of these reactions) and the temperature coefficients are practically the same, while in the transition region, at the melting point (denoted by an arrow for each substance in Fig. 1) the gas-formation process changes suddenly.

The "critical" point, corresponding to the change in the kinetics of the process, accurately coincides with the melting point of the compound, regardless of the nature of the substance, over a wide temperature range right down to very low temperatures (in our experiments, down to −56.5°, which is the melting point of octane). It is interesting to note that water behaves analogously to organic compounds when irradiated as ice and in the liquid state, showing a similar sharp change in gas-formation kinetics at 0°.

The results obtained show that this peculiarity of radiolysis is not specific, but is of a general nature and common to polymers and low-molecular organic and inorganic compounds. It is connected with the gas-formation conditions accompanying radiolysis and cannot be explained by intensification of thermal decomposition under the action of radiation or thermal activation of radiolysis as in both these cases the curves would show a monotonically increasing effect of rising temperature.

It is evident that at the basis of the phenomena illustrated by the curves in Fig. 1 lies the same mechanism as mentioned above for polymers. At the same time, for low-molecular substances there is strict correspondence between the point at which the gas-formation rate increases sharply and the melting point, in contrast to polymeric substances, where this correspondence is observed over the more or less wide temperature range over which the polymer softens and, moreover, this changes during the action of radiation of the polymer [2]. The widespread occurrence of the effect we observed for substances of very different composition and molecular structure in which the mechanism of radiation-chemical reactions undoubtedly differ considerably gives little ground for explaining it by the "cage effect" [6], especially as we are considering differences in the gas-formation process which refer only to condensed systems. It is more probable that these reactions, which are of a reversible nature in the free-radical formation stage (i.e., up to the moment when nuclei of the new gas phase are formed), are retarded to a different extent in irradiated objects in solid and liquid states in accordance with the magnitude of the diffusion coefficients.

There are very few data in the literature for comparing the permeability of the same organic compounds in different states of aggregation but, for example, according to [7] the temperature coefficient of gas permeability (for H_2, N_2, and CO_2) of gutta percha in its softening range (42-50°) increases more than ten times faster than at temperatures above and below this range (this polymer also has a high viscosity in the liquid state). On the other hand, the diffusion and self-diffusion coefficients in metals in the solid and molten states are of the order of 10^{-9} and 10^{-5} cm^2/sec, respectively [8, 9].

Therefore, the differences in the diffusion permeability of the solid and liquid phases of organic substances with respect to the gases formed in them by radiolysis produce a sharp change in the gas-formation rate in the region of the phase transition point.

A study of the chemical composition of the gases formed during the radiolysis of low-molecular organic compounds and polymers under the given conditions may give additional data for elucidating the mechanism of the effect examined.

LITERATURE CITED

[1] A. B. Taubman and L. P. Yanova, Doklady Akad. Nauk SSSR 118, 5, 991 (1958).*

[2] L. P. Yanova and A. B. Taubman, Action of Ionizing Radiations on Inorganic and Organic Systems [in Russian] (Izd. AN SSSR,1958) p. 314.

[3] Proc. of the First All-Union Conference on Radiation Chemistry, Discussion [in Russian] (Izd. AN SSSR, 1958) p. 307.

[4] R. Bolt and J. Carroll, International Conference on the Peaceful Use of Atomic Energy [Russian translation] (1955) Vol. 7, p. 663.

[5] P. Alexander, R. Black, and A. Charlesby, Proc. Roy. Soc. A232, 44 (1955).

[6] J. Franck and E. Rabinowitch, Trans. Farad. Soc. 70, 120 (1934).

[7] G. Amerongen, J. Polym. Sci. 11, No. 4 (1947).

[8] F. Holbrook, Ind. and Eng. Chem. 24, 993 (1932).

[9] R. Eckert and H. Drickamer, J. Chem. Phys. 20, 532 (1952).

* Original Russian pagination. See C. B. translation.

THE THERMODYNAMIC PROPERTIES OF LIQUID INDIUM–BISMUTH ALLOYS

N. V. Alekseev, Corresponding Member Acad. Sci. USSR

Ya. I. Gerasimov, and A. M. Evseev

M. V. Lomonosov Moscow State University

Translated from Doklady Akademii Nauk SSSR, Vol. 134, No. 3, pp. 618-620, September, 1960
Original article submitted May 25, 1960

With the help of emf measurements, we determined the thermodynamic functions of the In–Bi system at temperatures between 240 and 300°C. We used the following type of concentration cell in our study: $In_l \mid In^+$ (in molten KCl, LiCl, $ZnCl_2$) $\mid (N_1In + N_2Bi)_l$. A mixture of salts melting at ~220°C and containing: 11% (by weight) KCl, 10% LiCl, and 79% $ZnCl_2$ served as electrolyte.

The electrolyte was prepared in the following way. Commercial analytically pure $ZnCl_2$ was heated in an oven until it melted. A stream of hydrogen chloride was then bubbled through the red-hot molten salt until the liquid became entirely clear. It was essential that the $ZnCl_2$ used in the electrolyte be completely anhydrous. To the required amount of molten $ZnCl_2$, we added thoroughly dried KCl and LiCl. Hydrogen chloride was again bubbled through the molten mixture until the liquid cleared. Subsequently, a weighed amount of InCl was added to the molten mixture.

We prepared the alloys from pure (99.999%) indium and analytically pure bismuth. We determined the emf of these alloys at 240, 260, 280, and 300°C. Within the range of experimental errors, E can be regarded as a linear function of T. From the experimentally determined emf, we computed the activities by using the equation

$$\lg a_{In} = -\frac{zFE}{4{,}576 \cdot T}.$$

Indium was assumed to be monovalent. The activity of bismuth in the alloy was determined by a graphical integration of the Gibbs-Duhem equation. Smoothed activity values were used to calculate the corresponding partial and integral thermodynamic functions. The activities and thermodynamic functions are compiled in Tables 1 and 2.

The accuracy of the final results can be estimated on the basis of the errors in E. A ~1.5% error in E leads to an ~1.5% error in a, a ~22% error in $\Delta\overline{H}$, and ~35% error in $\Delta\overline{S}$.

The thermodynamic functions of liquid indium-bismuth alloys have been determined by Terpilowsky [1] who measured the emf of the cell:

$$In_l \mid In^+ \text{ (in molten LiBr, KBr, InBr)} \mid (N_1In + N_2Bi)_l$$

in the temperature range from 400-500°C, and by Wittig and Miller [2], who determined calorimetrically the heats of mixing at 350°C. By using the equations for ideal solutions the latter workers computed the partial

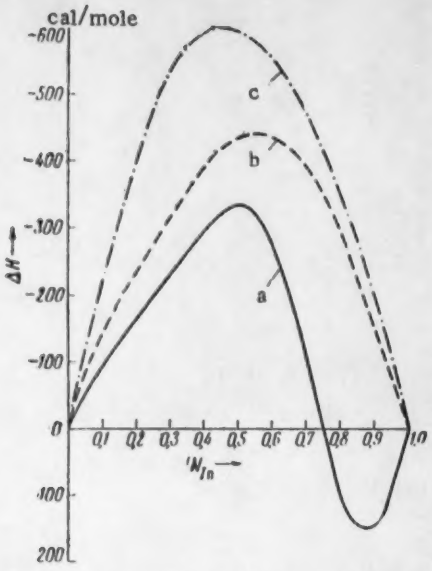

Fig. 1. Integral heats of mixing for the In-Bi system. a) Our results; b) data taken from [2]; c) taken from [1].

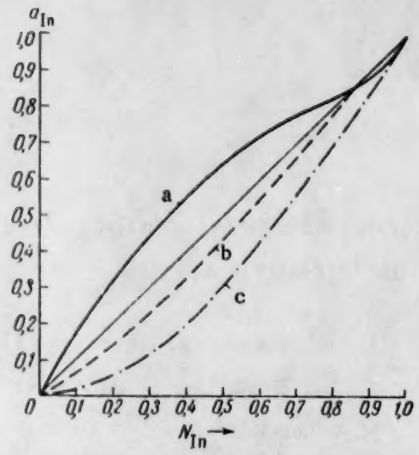

Fig. 2. Activity of indium in the In-Bi system. a) Our results; b) data taken from [2]; c) taken from [1].

heats of mixing of indium and bismuth from the experimental integral heats of mixing. In Fig. 1, the values of ΔH determined by us are compared with the results obtained by earlier workers. The following characteristics should be noted: the integral heat of mixing decreases as expected when the temperature is lowered; it is 597 cal/mole at 450°, 440 cal/mole at 350°, and 340 cal/mole at 270°C. At the same time our data indicate that ΔH has a region of positive as well as negative values. A transition of this type can be very clearly demonstrated by comparing the values of $\Delta\overline{H}_{in}$ obtained at various temperatures.

Another interesting property of the indium-bismuth system involves a transition from a positive to a negative deviation from ideality as the temperature is changed (Fig. 2). The strong negative deviations which are observed at 450° greatly decrease in magnitude when the temperature is lowered by 100° and become positive at 270°. A similar process can be detected in a whole series of liquid alloys which form compounds in the solid state (K-Hg; Cu-Cd, etc.). This phenomenon can be attributed to the fact that the ΔS^{excess} which is very small and positive at high temperatures becomes very large and negative at low temperatures.

TABLE 1

The Activities of Indium and Bismuth in Alloys

N_{In}	573°K		553°K		533°K		513°K	
	a_{In}	a_{Bi}	a_{In}	a_{Bi}	a_{In}	a_{Bi}	a_{In}	a_{Bi}
0,0	0,000	1,000	0,000	1,000	0,000	1,000	0,000	1,000
0,1	0,177	0,987	0,175	0,985	0,172	0,983	0,169	0,980
0,2	0,331	0,956	0,385	0,954	0,318	0,951	0,315	0,948
0,3	0,455	0,850	0,447	0,844	0,439	0,838	0,430	0,833
0,4	0,564	0,753	0,554	0,747	0,548	0,742	0,535	0,738
0,5	0,655	0,636	0,647	0,632	0,636	0,628	0,625	0,624
0,6	0,726	0,508	0,720	0,505	0,715	0,502	0,708	0,498
0,7	0,775	0,369	0,779	0,368	0,783	0,366	0,787	0,366
0,8	0,813	0,225	0,816	0,225	0,819	0,226	0,825	0,226
0,9	0,867	0,102	0,871	0,102	0,875	0,103	0,880	0,103
1,0	1,000	0,000	1,000	0,000	1,000	0,000	1,000	0,000

TABLE 2

The Thermodynamic Functions of Indium–Bismuth Alloys at 543°K

N_{In}	$\Delta\bar{H}_{In}$	$\Delta\bar{H}_{Bi}$	ΔH	$\Delta\bar{S}_{In}$	$\Delta\bar{S}_{Bi}$	ΔS	ΔS^{excess}
	cal/mole			cal/deg·mole			
0,0	(—415)	0,00	0,00	(3,95)	0,00	0,00	0,00
0,1	—457	—37	—96	1,40	0,22	0,34	—0,40
0,2	—495	—76	—167	0,62	0,33	0,36	—0,62
0,3	—525	—113	—237	0,25	0,38	0,34	—0,86
0,4	—530	—153	—298	0,10	0,47	0,32	—1,00
0,5	—452	—230	—336	0,22	0,49	0,37	—0,99
0,6	—245	—457	—334	0,62	0,47	0,52	—0,80
0,7	+132	—516	—212	0,72	0,73	0,72	—0,48
0,8	+190	—437	+65	0,68	2,35	0,91	—0,13
0,9	+147	—173	+115	0,27	4,25	0,66	—0,07
1,0	0,00	(+93)	0,00	0,00	(4,45)	0,00	0,00

*Note. Extrapolated values are given in parentheses.

It seems that the nature of the local order varies in this case with concentration and temperature.

LITERATURE CITED

[1] I. Terpilowsky, Arch. Hutnictwa 3, 227 (1958).

[2] F. Wittig and E. Müller, Z. Phys. Chem. 21, 71 (1959).

THE COMPARATIVE REACTIVITIES OF THE C–H AND C–T BONDS IN η-HEPTANE, BENZENE, TOLUENE, ETHYL BENZENE, AND CYCLOHEXANE IN LIQUID PHASE REACTIONS WITH CH_3. RADICALS

THE EFFECT OF A PHENYL GROUP AND AROMATIC MEDIUM

V. L. Antonovskii, I. V. Berezin, and L. V. Shevel'kova

M. V. Lomonosov Moscow State University
(Presented by Academician N. N. Semenov, April 27, 1960)
Translated from Doklady Akademii Nauk SSSR, Vol. 134, No. 3, pp. 621-624, September, 1960
Original article submitted March 28, 1960

The relative reactivities of individual CH bonds were determined by using the tritium labeling technique. Let us examine a system consisting of two organic compounds one of which (A) has r types of reactive CH bonds and has the hydrogens of type j replaced by tritium, while the other (B) is unlabeled and has p-types of CH bonds.

If methyl free radicals are generated in the system the composition of the methane formed in the reaction: $RH(T) + CH_3\cdot \rightarrow R\cdot + CH_4(CH_3T)$ (where RH = A or B) will be given by the equation:

$$\frac{[CH_4]}{[CH_3T]} = \frac{[A]\sum^{r} n_i k_i^H + [B]\sum^{p} n_i k_i^H}{k_{jA}^T [A-t]}, \qquad (1)$$

where k_{jA}^T is the rate constant for the reaction between CH_3. and the tritium atoms of the j-th bond in compound A; k^H is the rate constant for a similar reaction but involving various carbon–hydrogen bonds in compounds A and B; n gives the number of bonds of a kind, while the square brackets denote concentrations of the respective compounds. Expressing the concentrations of tritium-labeled compounds in terms of their specific activities we get:

$$\frac{I_A}{I_M} = \frac{k_{\sigma A}^H}{k_{jA}^T} + \frac{k_{\sigma B}^H}{k_{jA}^T}\cdot\frac{[B]}{[A]}, \qquad (2)$$

where $k_{\sigma A}^H = \sum^{r} n_i k_i^H$; $k_{\sigma B}^H = \sum^{p} n_i k_i^H$; I_A is the specific activity of compound A, and I_M that of methane.

Using experimental data and Eq. (2) one can determine the ratios between the various rate constants.

a) Determination of $k_{\sigma A}^H / k_{jA}^T$. This is done by generating CH_3. in pure A [then the second term on the right side of Eq. (2) is zero].

b) Determination of $k^H_{\sigma B}/k^H_{\sigma A}$. Methyl radicals are generated in a mixture of A and B. The desired ratio is obtained from the equation $k^H_{\sigma B}/k^H_{\sigma A} = [A]/[B] \times (I^0_M/I_M - 1)$, where I^0_M is the activity of methane determined in a).

It is obvious that I_A does not have to be determined.

c) Determination of $k^H_{\sigma B}/k^H_{jA}$. If the specific activity of A is large, then by taking [A] << [B], determining I_M and I_A, and neglecting the first term on the right side of Eq. (2) we can calculate $k^H_{\sigma B}/k^T_{jA}$.

Using such a scheme we determined the rate constant (k^H) for the stripping of hydrogens (by methyl radicals) from n-heptane (secondary bonds), benzene, and toluene (both unlabeled) relative to the stripping rate from cyclohexane, which was labeled with tritium and used as a standard. In another set of experiments we determined the rates of tritium stripping (by the same radical) from methyl groups of toluene and ethylbenzene relative to the rate of hydrogen stripping from cyclohexane; this enabled us to determine the influences of a phenyl group on the reactivity of the corresponding bonds.

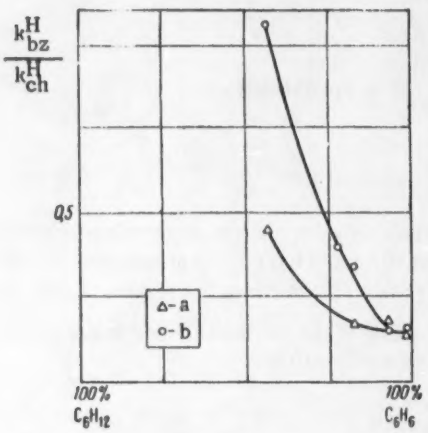

Fig. 1. k^H_{bz}/k^H_{ch} as function of composition (mole %): a) 55°; b) 85°C.

CH_3. radicals were generated by the thermal decomposition (55-85° ± 0.05°) of 0.02-0.03 M acetyl peroxide [1]. The reaction was carried out in evacuated sealed tubes; subsequently methane was separated from the other mixture components and its activity determined in a counter which could be filled with the gas. The same counter was used to determine the activities of the hydrocarbons. Experimental details have been described elsewhere [2, 3]. At 55-85°C methyl radicals strip secondary hydrogens from n-heptane twelve times as fast as they do the primary [2]. Therefore $k^H_{\sigma hp} = 10.5\ k^H_{sec.hp}$, or in other words n = 10.5. In toluene n = 3 since the CH bonds of the methyl group are about 150 times as reactive as the ring CH bonds [4]. All the CH bonds in cyclohexane were considered structurally equivalent and we assumed that n = 12.

Table 1 shows the experimental results obtained on n-heptane. In all the cases only about 50% of acetyl peroxide was decomposed since it has been shown that the extent of decomposition had no effect on the experimental results [5]. Each value in Table 1 is based on at least two measurements.

Experiments at various $[C_6H_{12}]/[C_7H_{16}]$ ratios indicate that within the range of experimental errors the relative rate constants of saturated hydrocarbons are independent of percent composition. The ratio of the rates can be expressed as a function of temperature by the following equation: $k^H_{sec.hp}/k^H_{ch} = 10 \exp[(-1440 \pm 300)/RT]$. It is worth noting that k^H_{ch} has a much smaller frequency factor than does $k^H_{sec.hp}$. This may probably be connected with the high symmetry of cyclohexane. In fact, $A^H_{hp}/A^H_{ch} \sim \sigma_{ch}/\sigma_{hp}$, where A is the frequency factor and σ the corresponding symmetry number. For cyclohexane $\sigma = 6$, while for n-heptane $\sigma = 1$.

Experiments carried out on benzene–cyclohexane and toluene–cyclohexane mixtures (labeled cyclohexane) showed that the respective rate-constant ratios do depend on the compositions of the experimental mixtures (Figs. 1 and 2). The concentration of the aromatic component has the same effect on these ratios whether benzene or toluene is used. In both cases the ratios of constants decrease with increasing concentration of the aromatic hydrocarbon. After certain concentrations are attained the ratios increase much more slowly and approach values which are characteristic of these same reactions in the gas phase (at 85° $k^H_{bz}/k^H_{ch} = 0.07$; $k^H_t/k^H_{ch} = 2.2$ [6]).

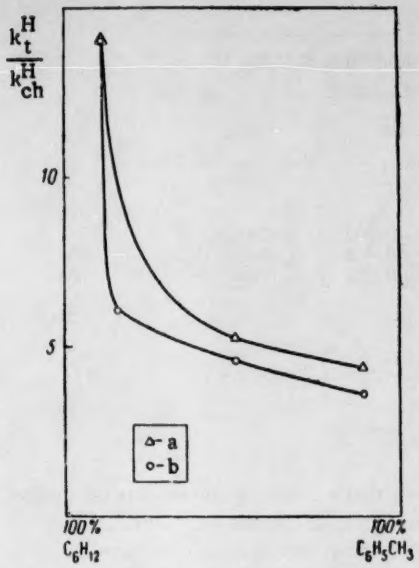

Fig. 2. k_t^H / k_{ch}^H as a function of composition (mole %): a) 55°; b) 85°C.

Russel [7] found that aromatic compounds have similar effects on the reactivity of chlorine atoms in reactions with saturated hydrocarbons. He attributed this behavior to the solvation of chlorine through a π-interaction, which would render the halogen less reactive. In our case things seem to be somewhat more complicated. If we were dealing only with a π-interaction of toluene or benzene with the methyl radical then the reaction would be more selective and the k_t^H / k_{ch}^H ratio would increase with increasing toluene concentration; nothing of the sort, however, is observed.

When we found that the ratios of rate constants for the individual reactions depend on the solvent, we were obliged to alter the sequence of experiments dealing with the effects of a phenyl group on the reactivity of primary bonds. We prepared some very active toluene and ethylbenzene, both of which had the tritium on the methyl group. Experiments were made on dilute solutions of toluene and ethylbenzene in cyclohexane. Calculations, which involve the use of Eq. (2), have already been described in detail elsewhere [8]. The results are presented in Table 2.

The activation-energy differences and the frequency-factor ratios given in Table 3 were calculated from the data in Table 2. An examination of the results obtained with toluene and ethylbenzene reveals that in dilute solutions the relative rate of tritium stripping from the methyl group is practically independent of the aromatic hydrocarbon concentration. Hence, these values can be regarded as representing the "true" ratios, undistorted by the peculiar effects exhibited by aromatic compounds at higher concentrations.

In the case of toluene if we disregard the values of A^T/A_{ch}^H and ΔE for the 0.134% sample (since they clearly do not fit) we get the expression: $k_t^T / k_{ch}^H = 1.4 \exp(-1400/RT)$. Assuming that the isotope effect for toluene [5] can be accounted for by the expression $0.55 \exp(2200/RT)$ we find that at 85°C $k_t^H / k_{ch}^H = 2.3$; this ratio is quite close to the value obtained by Steacie in the vapor phase [6]. However, this ratio is somewhat smaller than one would expect from the Polanyi relationship [8]. The latter fact may be attributed to a conjugation between the unpaired electron contributed to the activated complex by the CH_3. radical and the aromatic π-system of toluene; such an interaction would tend to increase the energy barrier for the reaction.

A comparison between the reactivities of the CH_3 groups of toluene and ethylbenzene can only be done for the CT bonds. On the average $k_t^T / k_{eb}^T = 1.9$ at 85°C, which indicates that the activation induced by the phenyl group declines rather slowly with distance. Using some earlier data [2] on our current results we can make a comparison with the reactivity of a C–T bond in a methyl group of n-heptane. We find that at 85° $k_{hp}^T : k_{eb}^T : k_t^T = 1 : 14.5 : 28$.

TABLE 1

Temp., °C	$k_{sec.hp}^H / k_{ch}^H [C_6H_{12}]/[C_7H_{16}]$ is:		
	1.4	1.097	0.0655
85	1,49±0,15	1,43±0,1	1,32±0,05
55	1,27±0,13	1,05±0,08	—

TABLE 2

Temp., °C	k^T/k^H_{ch} when the wt.% of hydrocarbon in C_6H_{12} is:			
	0,134	0,200	0,466	4,00
		Toluene		
85	0,190±0,002	0,205±0,003	0,166±0,002	0,170±0,002
70	0,180±0,002	—	0,152±0,003	0,154±0,002
55	0,172±0,002	0,174±0,002	0,135±0,005	0,142±0,002
		Ethylbenzene		
	0,140	0,337	0,644	
85	0,083±0,002	0,105±0,002	0,100±0,001	—
55	0,155±0,002	0,158±0,002	—	—

TABLE 3

Wt. % in C_6H_{12}	A^T/A^H_{ch}	$\Delta E = E^T - E^H_{ch}$, kcal/mole
	Toluene	
0,134	0,6	0,8±0,2
0,200	1,3	1,3±0,25
0,466	1,6	1,6±0,4
4,00	1,2	1,4±0,2
	Ethylbenzene	
0,140	10^{-4}	—4,8±0,3
0,337	$1,2 \cdot 10^{-3}$	—3,2±0,3

We can see that a phenyl group renders the hydrogens on the methyl group of toluene very labile. It is surprising, though, that this effect should still remain quite pronounced in the methyl group of ethylbenzene. One should also note the unusual frequency factor and activation energy for the stripping of tritium from ethylbenzene. One cannot exclude the possibility that instead of the electromeric effect of the phenyl ring some other, yet unknown, mechanism may be responsible for the lability of primary hydrogens in ethylbenzene.

LITERATURE CITED

[1] M. Levy and M. Szwarc, J. Am. Chem. Soc. 76, 5981 (1954).

[2] V. L. Antonovskii and I. V. Berezin, Doklady Akad. Nauk SSSR 127, 124 (1959).*

[3] V. L. Antonovskii and I. V. Berezin, Nauch. Dokla. Vyssh. Shkol. Khim. i Khim. Tekh. 320 (1958).

[4] I. V. Berezin, N. F. Kazanskaya, and K. Martinek, Zhur. Obshch. Khim. 30, No. 9 (1960).*

[5] V. L. Antonovskii, Dissertation [in Russian] (MGU, 1959).

[6] A. F. Trotman-Dickenson, and E. W. R. Steacie, J. Chem. Phys. 19, 329 (1951).

[7] G. A. Russel, J. Am. Chem. Soc. 79, 2977 (1957).

[8] N. N. Semenov, Certain Problems in Chemical Kinetics and Reactivity [in Russian] (Izd. AN SSSR, 1958).

* Original Russian pagination. See C. B. Translation.

THE CATALYTIC ACTIVITY OF TUNGSTEN PENTOXIDE

Academician A. A. Balandin, A. A. Tolstopyatova,

and V. Stshizhevskii

M. V. Lomonosov Moscow State University
Translated from Doklady Akademii Nauk SSSR, Vol. 134, No. 3, pp. 625-628,
September, 1960
Original article submitted May 17, 1960

In this work the dehydration of ethyl, isopropyl, n-butyl, tert-butyl, and cyclohexyl alcohols and dehydrogenation of methanol and tetralin on W_2O_5 were investigated under isothermal conditions. The catalyst (blue W_2O_5) was prepared by heating tungstic acid at 350-400°C in a stream of air and reducing the resulting WO_3 to W_2O_5 at the experimental temperature of 200-300°C used during the reaction with alcohols. We used a simple flow apparatus with the liquid reactants injected automatically. An automatic Patrikeev gas meter was used for introducing gases and for collecting gaseous products. The experiments were carried out in the kinetic region without allowing the reaction to go to completion – usually less than 30% conversion was allowed. Gaseous reaction products were analyzed chromatographically as well as in a VTI apparatus. We also made use of the Kaufman-Gal'pern method for the quantitative determination of unsaturated hydrocarbons dissolved in liquid products. The reactants were purified until their physical constants agreed with those given in the literature.

We noted during our experiments with W_2O_5 that the cooling produced by the endothermic dehydration of alcohols interfered with our kinetic measurements. To eliminate this effect we diluted the catalyst (2 g, or 2 ml) with quartz of about the same grain size at the ratio of 2 parts catalyst to 3 parts quartz. The alcohol was also diluted with one of the reaction products (water or the corresponding olefin). Thus, for example, to determine the relative water-adsorption coefficients we prepared 3 aqueous solutions containing 80, 65, and 54 mole % of alcohol respectively. By diluting the catalyst and the alcohols we rendered the reaction conditions, for all practical purposes, isothermal. Using this method we determined the apparent activation energies for the dehydration of ethyl, isopropyl, n-butyl, tert-butyl, and cyclohexyl alcohols under isothermal conditions (see Table 1). There seems to be a correlation between the apparent activation energies and the alcohol structures. Primary alcohols (ethyl and n-butyl) have the same dehydration activation energy of about 30 kcal/mole. The activation energy of the secondary (isopropyl) alcohol is ~6 kcal/mole smaller than that of the primary, while the activation energy of the tert-butyl alcohol is in turn ~6 kcal/mole smaller than that of the secondary. The dehydration activation energies of primary, secondary, and tertiary alcohols on W_2O_5 decrease by approximately 6 kcal/mole in that order. The relationship observed by us resembles the one reported by Adadurov and Krainii [2], who studied the dehydration of alcohols on tungsten blue in a flow system and discovered that the introduction of a methyl group in the α-position lowered the dehydration activation energy of alcohols by 5.5 kcal/mole.

To compute the actual reaction rate constants K we used Eq. (1), which was derived from Balandin's general rate equation for monomolecular heterogeneous catalytic reactions in flow systems [3]. For cases involving binary mixtures of alcohols and dehydration products the equation assumes the form:

$$K = (z_2 N + z_3 A_1) \ln \frac{A_1}{A_1 - m} - (z_2 + z_3 - 1) m, \qquad (1)$$

TABLE 1

Apparent Activation Energies for the Dehydration of Alcohols on Tungsten Pentoxide Under Isothermal Conditions

Alcohol	Mole % alcohol in mixture	Temp. range, °C	ε, kcal/mole	
Ethyl	65	269-303	29.8	29.4
	80	269-301	29.0	
Isopropyl	65	168-199	23.7	23.8
	80	168-200	23.7	
	50	168-200	23.9	
n-Butyl	65	230-262	29.5	29.9
	80	230-262	29.9	
	54	230-262	29.9	
	65	230-262	30.5	
tert-Butyl	65	92-113	17.8	
Cyclohexyl	65*	180-204	21.9	

*A mixture of cyclohexyl alcohol and cyclohexene was used.

TABLE 2

Relative Adsorption Coefficients z_2 and z_3 for the Dehydration Products of Alcohols Under Isothermal Conditions

n-Butyl alcohol			Isopropyl alcohol		
Temp., °C	z_2	z_3	Temp., °C	z_2	z_3
262	0,58	0,58	200	0,48	0,42
255	0,53	0,60	192	0,55	—
245	0,37	0,70	184	0,49	0,39
230	0,76	—	173	—	0,54
235	—	0,70	176	0,50	—
	av 0,56	av 0,65		av 0,50	av 0,45

TABLE 3

A Check of the Applicability of Eq. (1) to the Dehydration of Alcohols

Mole % of iso-C_3H_7OH in aqueous mixture	Temp. °C	m, ml/min	K
80	194	20,1	27,2
65	194	18,1	28,2
50	194	15,0	28,0
80	181,3	9,9	12,1
65	181,3	8,8	12,3
50	181,3	7,3	12,0

where A_1 is the volumetric flow rate of alcohol (in ml/min converted to gas volume at STP), N the combined amount of alcohol and olefin in the initial mixture (in ml/min, converted to gas volume at STP), $\underline{m}$ the amount of unsaturated products formed in experiments with binary mixtures (in ml/min), z_2 and z_3 the relative adsorption coefficients of water and olefins, respectively (i.e., the ratios of the adsorption coefficients of the reaction products to that of the initial alcohol); z_2 and z_3 were calculated from Eq. (2), which was also derived from the general rate expression of A. A. Balandin [3],

$$z = \left(\frac{m_0}{m} - 1\right) \Big/ \left(\frac{100}{P} - 1\right), \qquad (2)$$

where $\underline{m}$ is the quantity of olefins formed per unit time in experiments with binary mixtures (alcohol–water or alcohol–olefin), m_0 the calculated value of $\underline{m}$ for pure alcohol and P the mole percent of alcohol in the binary mixture.

In using Eq. (2) to calculate z_2 and z_3 we used the calculated instead of the experimental value of m_0. Taking advantage of the fact that $\underline{z}$ remains constant at any fixed temperature and is independent of the component ratio in the mixture we first substitute into Eq. (2) an experimentally determined m_1 for a mixture

TABLE 4

Dehydration of Alcohols on Tungsten Pentoxide Under Isothermal Conditions

Alcohol	Temp. range, °C	z_2	z_3	ϵ_{app}, kcal/mole	ϵ_{tr}, kcal/mole	K_0	$\frac{\epsilon}{\log K_0}$
n-Butyl	230-262	0.56	0.65	29.9	33.4	$1.88 \cdot 10^{15}$	2.19
Isopropyl	168-200	0.50	0.45	23.7	26.1	$4.29 \cdot 10^{13}$	1.91

TABLE 5

The Energy Binding the Active Atoms of the Reacting Molecules to the W_2O_5 Catalyst Surface

Alcohol	Alcohol dehydration activation energy	Bond energy		
		Q_{HK}	Q_{CK}	Q_{OK}
n-Butyl	29.9	56.7	15.9	39.2
Ethyl	29.4	56.4	16.3	39.5
Isopropyl	23.7	52.6	19.4	43.3
Cyclohexyl	21.9	51.5	21.3	44.4
tert-Butyl	17.8	48.7	24.0	47.3

of given P_1, then substitute P_2 and a corresponding m_2 for another mixture, and solve the two equations simultaneously for m_0; the resulting equation has the form:

$$m_0 = (1 - a) \Big/ \left(\frac{1}{m_1} - \frac{a}{m_2}\right), \text{ where } a = \left(\frac{100}{P_1} - 1\right) \Big/ \left(\frac{100}{P_2} - 1\right). \qquad (3)$$

Since we only used three mixtures of each reaction product with the corresponding alcohol, three equations of type (3) could be set up for every alcohol, and an average value of m_0 could be determined at each temperature. The experimentally determined relative adsorption coefficients for the dehydration products of isopropyl and n-butyl alcohols under isothermal conditions are presented in Table 2. The relative adsorption coefficients of water, propylene, and butylene are independent of temperature within the investigated temperature range. The applicability of Eq. (1) to the dehydration of alcohols is confirmed by the fact that if we substitute into the equation experimental values of m (obtained at fixed temperatures with mixtures of various percent compositions and using catalysts of the same activity) the calculated dehydration rate constants all come out about the same (Table 3). In Table 4 we have compiled the principal results of our kinetic studies of the dehydration of isopropyl and n-butyl alcohols. The data in Table 4 show that the true activation energy exceeds the apparent value by about 3 kcal/mole.

The relative adsorption coefficient z represents the equilibrium constant for the process involving the displacement of a reactant adsorbed on the catalytically active surface by a reaction product. In the case of alcohol dehydration we have the displacement of alcohol by water and the corresponding unsaturated hydrocarbon. Hence, with the help of ordinary thermodynamic equations one can readily compute the change in free energy ΔF, entropy ΔS, and heat content ΔH (heat of displacement with the sign reversed) for the process.

Since we found that the relative adsorption coefficients of water and olefins are temperature independent, the corresponding ΔH values must be zero. All the alcohols must therefore have the same heat of adsorption, since the heat changes for the replacement of adsorbed alcohols by water are all identical (equal to zero). Hence, it follows that the alcohols, though different in structure, are all similarly oriented (during the dehydration) towards the active surface portions of W_2O_5 in such a way that the group $>\underset{\underset{H}{|}}{C}-\underset{\underset{O-}{|}}{C}<$, common to all the alcohols, is

adsorbed on the catalytically active surface by always having the same atoms bonded to the surface.

Determination of the energies involved in forming bonds between the C, H, and O atoms of the reacting molecules and the catalytically active W_2O_5 surface. The bond energies were determined by the Balandin kinetic method [4]. To do this we determined the dehydrogenation activation energy of tetralin in the 449-491° temperature range (ϵ_1 = 26.8 kcal/mole) and the dehydrogenation activation energy of methyl alcohol in the 380-420°C temperature range (ϵ_2 = 24.4 kcal/mole), both on the surface of W_2O_5. To complete the bond energies Q_{HK}, Q_{OK}, and Q_{CK} [5, 6] by means of Eq. (4) we used the dehydration activation energies ϵ_3 obtained for the primary, secondary, and tertiary alcohols listed in Table 1 as well as the values of ϵ_1 given above and ϵ_2. This enabled us to study the effects of alcohol structure on these bond energies (the bond energies Q_{CH}, Q_{CO}, and Q_{OH} were taken from Cottrell [7]).

$$Q_{HK} = \frac{1}{3}(-\varepsilon_1 - 2\varepsilon_2 + 2\varepsilon_3) + 62;$$
$$Q_{CK} = \frac{1}{3}(-\varepsilon_1 + 2\varepsilon_2 - 2\varepsilon_3) + 28{,}5; \qquad (4)$$
$$Q_{OK} = \frac{1}{3}(3\varepsilon_1 - 2\varepsilon_2 - 2\varepsilon_3) + 48{,}6.$$

It turned out that a stepwise replacement of the carbinol hydrogens by methyl groups increases the values of Q_{OK} and Q_{CK} and decreases Q_{HK} (ethyl, isopropyl, and tert-butyl alcohols, see Table 5). Let us note that neither one of the two hydrogens replaced by methyls nor the methyl groups themselves are directly involved in the reaction; we are dealing in this case with the effects of substituents outside the "frame" [8] on the energies involved in bonding between the catalyst and the C, H, and O atoms.

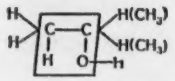

LITERATURE CITED

[1] G. D. Gal'pern, Trudy Instituta Nefti 4, 141 (1954).

[2] I. E. Adadurov and P. Ya. Krainii, Zhur. Fiz. Khim. 5, 1125 (1934).

[3] A. A. Balandin, Zhur. Fiz. Khim. 31, 745 (1957).

[4] A. A. Balandin, Zhur. Obshch. Khim. 16, 793 (1946).

[5] A. A. Balandin and A. A. Tolstopyatova, Zhur. Fiz. Khim. 30, 1367, 1636 (1956).

[6] A. A. Tolstopyatova and A. A. Balandin, Problems in Kinetics and Catalysis, X. The Physics and Physical Chemistry of Catalysis [in Russian] (Izd. AN SSSR, 1960) p. 351.

[7] T. Cottrell, The Strengths of Chemical Bonds [Russian translation] (IL, 1956).

[8] A. A. Balandin, Uchebny. Zapiski MGU, 175, 97 (1956).

THE STATE OF THE CARBON IN LIQUID CAST IRON

A. A. Vertman and Corresponding Member, Acad. Sci. USSR

A. M. Samarin

A. A. Baikov Metallurgical Institute, Academy of Sciences of the USSR
Translated from Doklady Akademii Nauk SSSR, Vol. 134, No. 3, pp. 629-631, September, 1960
Original article submitted May 20, 1960

In spite of its practical importance, the problem of the structure of liquid iron–carbon alloys has been little studied. The following represent some of the works devoted to this question.

K. P. Bunin [1], by spraying white cast iron onto the surface of iced water, showed that at a rate of cooling equal to several thousand degrees per second, it is possible to fix a certain quantity of undissolved graphite in the metal. This led him to suggest that more or less extensive formations, enriched in graphite, are present in the liquid cast iron, as a result of fluctuations.

S. T. Konobeevskii [3] found that even when iron and graphite powder are heated to 2000°, complete breakdown of the planar layers of the graphite lattice does not take place, and the iron cations are merely introduced between these planar layers. An analogous phenomenon appears to take place in liquid iron when graphite is dissolved in it, particularly since the temperature of the metallurgical processes never reaches 2000°.

D. P. Ivanov [2], in a study of the nature of the crystallization of graphite during the cooling of cast iron superheated to 1400°, concluded that the liquid alloy contained individual blocks of graphite packets of different sizes, containing a metallic electronic bond, together with regions occupied by dissolved packets in the form of planar graphite molecules with the ionic bonds of introduced solvents, and finally, isolated carbon ions introduced into the iron lattice sites.

In [4], a study was made of the distribution of carbon in a 2650 mm high column of liquid cast iron, and it was shown that irregular distribution of the carbon, unlike that of other impurities, is possible only if a certain proportion of the carbon is present in the form of undissolved graphite.

Thus, the available data suggest that the carbon in liquid cast iron is present in the form of more or less extensive formations. The problem of the sizes of these formations and the existence of boundaries of separation between the carbon formations (colonies, micelles) is not yet clear, however.

Moreover, with the exception of K. P. Bunin's experiments [1], the available data on the structure of liquid cast iron are indirect, so that it was considered useful to collect direct experimental data on the structure of liquid cast iron. For this purpose we centrifuged the cast iron. The experiments were carried out on a centrifuge assembly for long-term strength testing [5]. The material was heated in a SiIit furnace, which made it possible to obtain a very long isothermal zone. The temperature was kept constant automatically, to within ±5°, by means of a platinum–platinorhodium thermocouple, which also served as recording instrument, and an ÉPP-09 electronic potentiometer.

The centrifuging was carried out in corundum crucibles approximately 60 mm long, with diameter 5-7 mm. The number of revolutions was checked with a tachometer. The crucibles were placed in special holders of heat-resistant steel, which were fixed horizontally at the head of the centrifuge shaft. The head of the shaft with the

TABLE 1

Change in the Carbon Content of Liquid Cast Iron During Centrifuging

Expt. No.	C content, %		Length of specimen, mm	Number of rpm	Temperature, °C	Duration of rotation, min
	upper	lower				
1	4,20	2,76	30	1700	100	1230
2	4,34	2,70	49	1700	100	1230
3	2,71	4,16	32	500	120	1250
4	4,00	2,70	33	1900	120	1275
5	3,90	2,87	29	1900	120	1275
6	3,96	3,60	33	1900	120	1260
7	3,44	2,40	38	1900	120	1260
8	3,32	3,36	25	—	20	—
9	2,68	3,48	40	—	—	1250

crucibles could be removed rapidly from the furnace by means of a telescopic lifting column. The extent of the superheating above the melting point amounted to only 30-50°, so that the crystallization took place almost instantaneously when the shaft was taken from the furnace. The specimens were quenched in water, removed from the crucibles, and turnings were removed from the upper and lower end faces of the specimens and analyzed by the usual chemical methods.

The results of the analysis are given in Table 1. In spite of the slight scatter of the data, it is still possible to detect a distinct tendency towards an irregular distribution of the carbon under the influence of the centrifugal forces. The upper end, which was closer to the axis of rotation, is enriched in carbon to a greater extent than the lower end. It should be noted that the experiments were carried out in air, so that the open end of the specimen surface was oxidized. In spite of the oxidation, however, the effect of the centrifuging process predominates over the effect of oxidation when the rate of rotation is 1700-1900 rpm. The magnitude of the force field during centrifuging is determined by the expression

$$L = \left(\frac{2\pi n}{60}\right)^2 \frac{l}{g}, \qquad (1)$$

where n is the number of revolutions and l the distance from the axis of rotation.

Under our experimental conditions, the force acting on the specimens exceeded the force of gravity by a factor of 320 at 1900 rpm, and by a factor of 20 at 500 rpm. It was found that in the latter case the loss of carbon as a result of oxidation was greater than the effect of centrifuging. It can thus be stated that in a force field 320 times greater than the force of gravity, separation of the liquid cast iron takes place. In this respect, cast iron, as a eutectic alloy, does not differ from readily fusible eutectics previously studied [6, 7]. The only difference is that a much smaller field is necessary for the separation of cast iron, and this is explained by the specific features of the graphite–iron system: the large difference in the densities (2.2 and 7.8 g/cm^3) and the exceptional strength of the planar layers of the graphite lattice.

It is possible to make an approximate estimate of the dimensions of the carbon colonies present in cast iron. We shall restrict ourselves to an examination of the results of the most characteristic experiment (No. 4), since the change in the carbon content in this experiment is close to the average value. The number of particles in a colony is determined by the expression [7]:

$$\nu = \frac{kT}{C_2^0 \delta} \ln \frac{C_1(x_2)}{C_1(x_1)},$$

where $\delta = \dfrac{\omega^2 M_1 M_2 \Delta d (x_2^2 - x_1^2) C_2^0}{2N_a g [M_1 C_1^0 d_2 + M_2 C_2^0 d_1]}$, ω is the peripheral velocity, M_1 and M_2 are the molecular weights of the 1st and 2nd components, respectively, Δd is the difference in the densities, x is the distance from the axis of rotation, C_1^0 and C_2^0 are the initial concentrations of the 1st and 2nd component, respectively, in atomic fractions, $C(x)$ is the concentration of a component at a distance x from the axis of rotation, and T is the temperature (in °K).

It can be seen that in our case $\delta = 3{,}36 \cdot 10^{-21}$. From this, the number of carbon particles in the liquid cast iron is $\nu = 2{,}5 \cdot 10^7$. The number of particles in the colony can be used to determine the volume and

dimensions of the colony. According to [8], the graphite lattice, consisting of 12 atoms, has the parameters: $a = b\sqrt{3} = 4.252 \pm 0.003$ A; $b = 2.455 \pm 0.002$ A; $c = 6.69 \pm 0.010$ A. The volume of this lattice is $23.2 \cdot 10^{-24}$ cm^3.

Thus the volume of the colonies is

$$V = \frac{\nu}{12} 23.2 \cdot 10^{-24}\ \text{cm}^3 \simeq 50 \cdot 10^{-18}\ \text{cm}^3,$$

i.e., the diameter of the particles is of the order of 10^{-6}cm. This particle size is characteristic of colloidal disperse systems, which have a high stability (in particular, their particles do not settle under the influence of gravity).

Thus there are grounds for suggesting that cast iron is a nonequilibrium microheterogeneous system consisting of a dispersion medium, which is a saturated solution of carbon in iron, and colonies or micelles enriched in carbon, with particle diameters of the order of 10^{-6}cm. In the present communication we have not dealt with the problem of the structure of the micelles or their binding with the dispersion medium. It can be emphasized, however, that the experimentally established fact that liquid cast iron undergoes separation during centrifuging can be taken as proof of the colloidal state of carbon in liquid iron.

LITERATURE CITED

[1] K. P. Bunin, Trudy Ural'sk. Industrial'n. Inst. 19 (1944).

[2] D. P. Ivanov, Collection: The Preparation of Castings from High-Strength Cast Iron [in Russian] (Izd. AN SSSR, 1955) p. 36.

[3] S. T. Konobeevskii, Zhur. Fiz. Khim. 3, No. 3 (1930).

[4] A. Ya. Khrapov and V. P. Chernobrovkin, Izvest. Vyssh. Uchebn. Zav. Chernaya Metallurgiya 5, 41 (1958).

[5] V. F. Prokhanov, Zavodskaya Lab. 8, 983 (1957).

[6] K. P. Bunin, Izvest. Akad. Nauk SSSR, Otdel. Tekh. Nauk 2 (1946).

[7] A. A. Vertman, A. M. Samarin, and A. M. Yakobson, Izvest. Akad. Nauk SSSR, Metallurgiya i Topliva, 3 (1960).

[8] L. Ya. Markovskii, D. P. Orshanskii, and V. P. Pryanishnikov, Chemical Electrothermal Processes [in Russian] (1952).

THE DIELECTRIC CONSTANT AND MOLECULAR STRUCTURE OF SOLUTIONS HAVING A CRITICAL REGION OF SEPARATION INTO LAYERS

N. N. Lomova and M. I. Shakhparonov

M. V. Lomonosov Moscow State University

(Presented by Academician V. I. Spitsyn, April 4, 1960)
Translated from Doklady Akademii Nauk SSSR, Vol. 134, No. 3, pp. 632-635, September, 1960
Original article submitted April 2, 1960

If large positive deviations from ideal behavior are observed in the thermodynamic properties of solutions, i.e., if the concentration fluctuations are large, then, as has been shown in [1], the experimentally measured effective dielectric constant of the solution ϵ should be less than the average local dielectric constant $\bar{\epsilon}_l$

$$\varepsilon = \varepsilon_1 - \frac{\left(\partial\bar{\varepsilon}_1 \,/\, \partial\varphi\right)^2 \overline{(\Delta\varphi)^2}}{\left(2 + \dfrac{\partial\bar{\varepsilon}_1 \,/\, \partial\varphi}{\partial\varepsilon \,/\, \partial\varphi}\right)\varepsilon} \tag{1}$$

In order to study the influence of the concentration fluctuations $\overline{(\Delta\varphi)^2}$ (where φ represents the volume fractions) on ϵ, we have carried out measurements of ϵ, the density ρ_4^t, the refractive index n_D of solutions of nitrobenzene, in cyclohexane, n-hexane, n-heptane and n-octane. The critical point of separation into layers for these systems, according to our data, lie at temperatures of 4.0, 20.0, 19.3 and 19.1° and nitrobenzene concentrations (in mole percentages) of 48.0, 43.15, 47.5, and 51.0%, respectively. The measurements of ϵ were carried out at a frequency of 700 kc by the beat method. The condenser, with capacity 10 $\mu\mu$f, was kept at constant temperature in a thermostat with an accuracy of ± 0.005°. The chance error in the measurement of ϵ did not exceed 0.05%. The average relative error in the measurment of ϵ did not exceed 0.5%.

The materials used had the following constants. Nitrobenzene: m. p. 5.75°, $n^{20}D$ 1.5528, ρ^{20}_4 1.2043, b. p. 211.0° at 765 mm. Cyclohexane: $n^{20}D$ 1.4290, ρ^{20}_4 0.7797, b. p. 80.5° at 745 mm. n-Hexane: $n^{20}D$ 1.3755, ρ^{20}_4 0.6597, b. p. 68.7° at 756 mm. n-Heptane: $n^{20}D$ 1.3882, ρ^{20}_4 0.6850, b. p. 98.0° at 758 mm. n-Octane: $n^{20}D$ 1.4003, ρ^{20}_4 0.7060, b. p. 125.5° at 750 mm.

The measurements were carried out over a wide range of concentrations at temperatures from 10 to 45°.

The data obtained were used to construct isotherms for ϵ, some of which are shown in Fig. 1. The solid lines give the values of ϵ and the broken lines the values of $\bar{\epsilon}_l$, calculated from the Onsager equation ([2], Eq. (36))

$$\left(1 - \sum \vartheta_i\right)\left(\bar{\varepsilon}_1 - 1\right) + \left(2\bar{\varepsilon}_1 + 1\right)\sum \vartheta_i \left(\bar{\varepsilon}_1 - n_i^2\right) / \left(2\bar{\varepsilon}_1 + n_i^2\right) = 4\pi N_i \mu_i \mu_i^* / 3kT, \tag{2}$$

which is applicable in those cases where the orientational order of the dipole moment is absent, and is thus applicable to solutions of nitrobenzene in hydrocarbons [1].

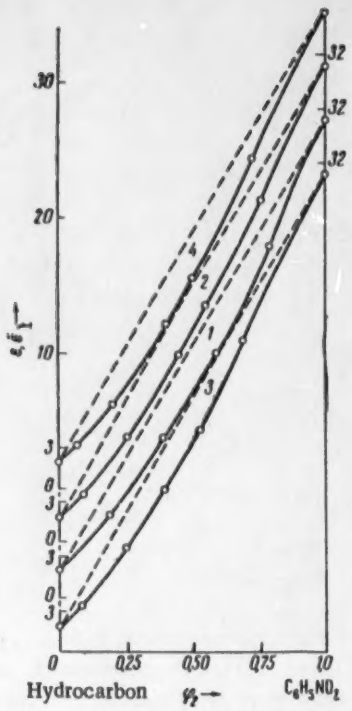

Fig. 1. ϵ and $\overline{\epsilon}_l$ isotherms for nitrobenzene solutions: 1) in cyclohexane; 2) in n-hexane; 3) in n-heptane; 4) in n-octane at 25°. The solid lines give ϵ values, the broken lines $\overline{\epsilon}_l$ values.

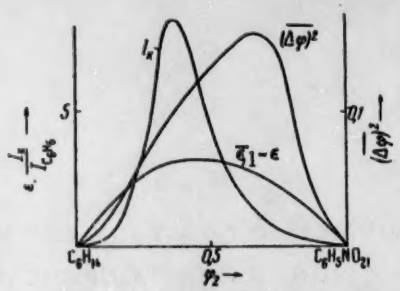

Fig. 2. Dependence of $\overline{\epsilon_l} - \epsilon$, I_k and $(\Delta\varphi)^2$ on the nitrobenzene concentration as a volume fraction φ, in nitrobenzene–n-hexane solutions at 40°.

The data for ϵ, $\overline{\epsilon}_l$, $\partial\overline{\epsilon_l}/\partial\varphi$ and $\partial\epsilon/\partial\varphi$ were used to calculate the values of $\overline{(\Delta\varphi)^2}$. The dependence of $\overline{(\Delta\varphi)^2}$ on t and φ is the same for all four systems. In the range of values of $\varphi \approx 0.6$–0.7, $\overline{(\Delta\varphi)^2}$ passes through a broad maximum. $\overline{(\Delta\varphi)^2}$ changes little with temperature. The values of $\overline{(\Delta\varphi)^2}$ remain almost unchanged when one hydrocarbon is replaced by another.

Figure 2 compares the changes in the values of $\overline{\epsilon}_l - \epsilon$, $\overline{(\Delta\varphi)^2}$, and I_k – the intensity of the Rayleigh scattering of light of $\lambda = 5780$ A – with change in concentration for nitrobenzene–n-hexane solutions at 40° [3]. The figure shows that the $\overline{(\Delta\varphi)^2}$ maximum is much broader than the I_k maximum and is displaced, relative to the latter, into the range of higher $C_6H_5NO_2$ concentrations.

The scattering of light in the optical range is due chiefly to fluctuations whose linear dimensions are greater than $\lambda/20$, i.e., not less than 25–30 A. As far as the quantities $\overline{\epsilon}_l - \epsilon$ and $\overline{(\Delta\varphi)^2}$ are concerned, the major part is here played by fluctuations whose linear dimensions are not more than 2-3 times the diameters of the molecules [1], i.e., less than 20 A for low-molecular solutions. We assume for the sake of simplicity that the molecular volumes of the components of the binary solutions are the same.

Then

$$\overline{N}^4\overline{(\Delta\varphi)^2} = \overline{N}_1^2\overline{(\Delta N_2)^2} - 2\overline{N}_1\overline{N}_2\overline{\Delta N_1\Delta N_2} + \overline{N}_2^2\overline{(\Delta N_1)^2}, \tag{3}$$

where $\overline{N}$ is the average number of molecules 1 and 2 in the volume element dV, $\overline{N}_1$ and $\overline{N}_2$ are the average number of molecules, and ΔN_1 and ΔN_2 are the fluctuations of N_1 and N_2 in dV. Using the expression for $\overline{\Delta N_i \Delta N_j}$ from the statistical theory of fluctuations [4], we obtain

$$\overline{N}\,\overline{(\Delta\varphi)^2} = x_1^2x_2\left\{1 + \frac{4\pi x_2}{v}\int_{dV}[g_{22}(q) - 1]\,dq\right\} - \\ - \frac{8\pi}{v}\,x_1^2x_2^2\int_{dV}[g_{12}(q) - 1]\,dq + x_1x_2^2\left\{1 + \frac{4\pi x_1}{v}\int_{d}[g_{11}(q) - 1]dq\right\}. \tag{4}$$

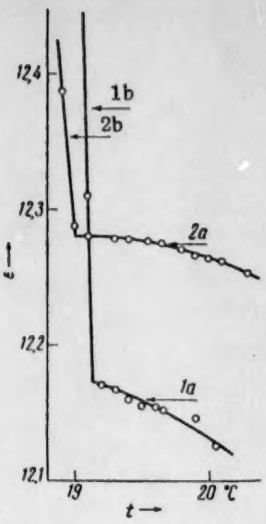

Fig. 3. $\epsilon = f(t)$ graphs close to the critical point of separation into layers. 1) nitrobenzene–n-heptane solution, $x_{C_6H_5NO_2} = 0.489$; 2) nitrobenzene–n-octane solution. $x_{C_6H_5NO_2} = 0.514$. Branches 1a and 2a) before separation into layers; branches 1b and 2b) after separation into layers.

In order to estimate $\overline{(\Delta\varphi)^2}$, in accordance with what has been said above, we restrict ourselves to consideration of the interaction of neighboring molecules.

X-ray structural studies of the structure of liquids shows that the function g(q), within the limits of the first coordination sphere, is only slightly dependent on the temperature. If the potential energy of the j–j interaction is much greater than the energy of the i–i and i–j interactions [as is the case of hydrocarbon (i)–nitrobenzene (j) systems], then the greatest contribution to $\overline{(\Delta\varphi)^2}$ will be made by the term containing $g_{jj}(q)$, and the $\overline{(\Delta\varphi)^2}$ maximum should lie in the concentration range where there is an excess of j molecules. Since at small distances, $g_{ij} - 1$, $g_{ij} - 1$ and $g_{jj} - 1$ are of the same order of magnitude, the $\overline{(\Delta\varphi)^2}$ maximum should be fairly flat and broad. With increase in the size of dV, the $\overline{(\Delta\varphi)^2}$ maximum should be gradually displaced to the range of concentrations corresponding to the minimum value of $\partial P_1/\partial x_1$, and should simultaneously become more sharp.

Differentiating (1) with respect to t, we obtain:

$$\left(\frac{\partial\varepsilon}{\partial t}\right)_\varphi = \frac{\varepsilon\varphi_2 - {}^2/_3\,\overline{(\Delta\varphi)^2}\,(\varepsilon_2 - \varepsilon_1)}{2\varepsilon - \overline{\varepsilon_1}}\,\frac{\partial\varepsilon_2}{\partial t} - \frac{1}{3}\,\frac{(\varepsilon_1 - \varepsilon_1)^2}{2\varepsilon - \overline{\varepsilon_1}}\,\frac{\partial\,\overline{(\Delta\varphi)^2}}{\partial t}, \qquad (5)$$

where ϵ_2 is the dielectric constant of nitrobenzene. Calculations show that $\partial\overline{(\Delta\varphi)^2}/\partial t$ has its highest values close to the critical point of separation into layers in the solutions. If the critical point is an upper point, then $\partial\overline{(\Delta\varphi)^2}/\partial t < 0$ and we should expect a considerable decrease in the values of $(\partial\epsilon/\partial t)_\varphi$ for the solutions as the critical point is approached. If the critical point of separation into layers is a lower point, however, then $\partial\overline{(\Delta\varphi)^2}/\partial t > 0$, and $(\partial\epsilon/\partial t)_\varphi$ should therefore increase.

Figure 3 shows the results of measurements of ϵ in the temperature range near the point of separation into layers for nitrobenzene solutions. In accordance with what has been said above, the derivative $(\partial\epsilon/\partial t)_\varphi$ decreases close to the point of separation into layers, as can be seen particularly clearly at temperatures and concentrations close to the critical state.

Thus, the literature reports [5] that ϵ maxima exist in the critical range are not confirmed.

Thermodynamic analysis of the critical state gives no grounds for the statement that ϵ maxima are present on the $\epsilon = f(t)$ curves in the critical region.

J. W. Gibbs' work ([6], p. 185) shows that there is no rigorous, general thermodynamic proof to justify relationships of the form

$$\left(\frac{\partial X_i}{\partial x_i}\right)_{x_j} = 0, \qquad \left(\frac{\partial^2 X_i}{\partial x_i^2}\right)_{x_j} = 0 \qquad (6)$$

in the critical region. In each specific case, the applicability of these relationships requires experimental verification, or theoretical proof on the basis of molecular models. It should also be pointed out that in a heterogeneous system, the intensities of the magnetic fields **E** and **H** do not have the properties of "generalized forces" in the thermodynamic sense, since at thermodynamic equilibrium between the phases a and b, conditions of the type

$$\mathbf{E}_a = \mathbf{E}_b; \quad \mathbf{H}_a = \mathbf{H}_b, \qquad (7)$$

which are analogous to the conditions $\mu_{ia} = \mu_{ib}$, $p_a = p_b$, and $T_a = T_b$ are not fulfilled. Thus equations of the type $(\partial E/\partial D) = 1/\epsilon = 0$ have no physical significance at the critical point.

LITERATURE CITED

[1] M. I. Shakhparonov, Zhur. Fiz. Khim. 34, No. 7 (1960).

[2] L. Onsager, J. Am. Chem. Soc. 58, 1486 (1936).

[3] D. K. Beridze and M. I. Shakhparonov, Uch. Zap. Moskovsk. Obl. Ped. Inst. im. N. K. Krupskoi 92, 4, 49 (1960).

[4] I. Z. Fisher, "Studies on the theory of liquids," Dissertation [in Russian] (Minsk, 1958).

[5] V. K. Semenchenko and M. Azimov, Zhur. Fiz. Khim. 30, 1821, 2229 (1956).

[6] J. W. Gibbs, Thermodynamic Works [Russian translation] (Moscow-Leningrad, 1950).

EFFECT OF IONIZING GAMMA RADIATION ON THE STRUCTURAL MECHANICAL PROPERTIES OF STARCH GELS

V. F. Oreshko, L. E. Chernenko, and N. G. Shakhova

Moscow Technological Institute of the Food Industry

(Presented by Academician P. A. Rebinder, March 18, 1960)
Translated from Doklady Akademii Nauk SSSR, Vol. 134, No. 3, pp. 636-638, September, 1960
Original article submitted February 4, 1960

Ionizing gamma radiation produces destruction of the polymeric molecules of starch [1, 2], which should lead to a change in the structural mechanical properties of gels prepared from irradiated starches. In the present work we investigated the change in the plastic strength of starch gels in relation to the ionizing radiation dose. The investigation was carried out with potato starch, which had an equilibrium moisture content of 16.6%.

The starch was irradiated in sealed glass ampoules at room temperature with Co^{60} γ-radiation doses varying from $1 \cdot 10^6$ to $18.2 \cdot 10^6$ r at a dose strength of $2 \cdot 10^3$ r/min. Gels containing 12.0% of dry starch were prepared from irradiated and control starch under strictly identical conditions and the ultimate shear stress P_m determined with a conical plastometer [3].

The nature of the change in the plastic strength of gels from starches irradiated with various doses in relation to time are given in Fig. 1. The change in ultimate shear stress of completely formed gel in relation to radiation dose is shown in Fig. 2.

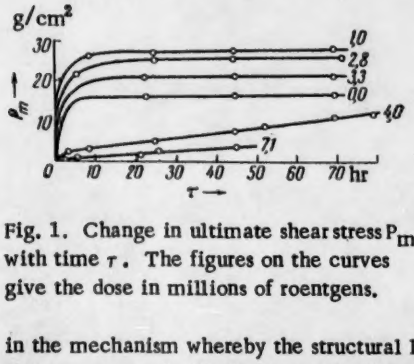

Fig. 1. Change in ultimate shear stress P_m with time τ. The figures on the curves give the dose in millions of roentgens.

The action of ionizing γ-radiation first produced an increase in the plastic strength of the system and then, with an increase in the radiation dose, there was a fall in the ultimate shear stress. At a dose of $7.1 \cdot 10^6$ r the ultimate stress was close to zero (P_m = 3 g/cm²) and at a dose of $18.2 \cdot 10^6$ r, the gel had a semiliquid consistency and it became practically impossible to measure P_m with a conical plastometer.

The nature of the increase in plastic strength with time was different (Fig. 1) for gels prepared from starches irradiated with doses of $4 \cdot 10^6$ and $7.1 \cdot 10^6$ r and for gels from starches irradiated with lower doses. This indicates a change in the mechanism whereby the structural lattice of the gel is formed with an increase in the absorbed dose and this is connected with depolymerization of the polymeric molecules of starch by the action of radiation.

As the formation of the structural lattice in starch gels is caused by hydrogen bonds arising between hydroxyls of the glucopyranose rings of polymeric molecules of starch [2], it may be assumed that the form of the curve of $P_m = f(D)$ with a maximum (Fig. 2) is connected with a change in the number of hydroxyl groups capable of forming hydrogen bonds due to the action of γ-radiation.

In unirradiated native starch, part of the hydroxyl groups are shielded and cannot participate in the formation of the structural lattice. Depolymerization under the action of radiation should promote the uncovering

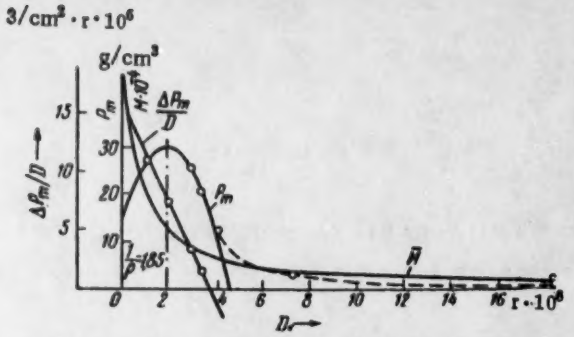

Fig. 2. Dose dependence of ultimate shear stress.

and freeing of the shielded hydroxyls, leading to an increase in the plastic strength of the system. The subsequent fall in P_m with an increase in radiation dose is undoubtedly connected with a decrease in the total number of hydroxyls, caused by their elimination with the formation of gaseous products [1]. As was shown by V. F. Oreshko and K. A. Korotchenko [1], the cleavage of a polymeric molecule of starch at the 1-4 and 1-6 bonds of the main valences by radiation forms n molecules:

$$n = \frac{\overline{M}_0}{\varepsilon_d N_0} D. \tag{1}$$

If each cleavage leads to the uncovering of shielded hydroxyls, then $[H\ldots]_1$ additional hydrogen bonds are formed in the gels where

$$[H\ldots]_1 = \frac{\varkappa}{2} \frac{\overline{M}_0}{N_0 \varepsilon_d} D, \tag{2}$$

where $\overline{M}_0$ is the mean molecular weight of the unirradiated starch, N_0 is Avogadro's number, ϵ_d is the energy required to break one bond in a starch molecule, and D is the radiation dose. The elimination of hydroxyls, which occurs simultaneously with depolymerization [1], follows the equation:

$$[OH]_{11} = kn_0 D + \frac{\rho}{2} \frac{\varkappa \overline{M}_0}{N_0 \varepsilon_d} D^2. \tag{3}$$

By neglecting the first term in Eq. (3), we obtain an expression for the total number of hydrogen bonds in a starch gel:

$$[H\ldots] = [H\ldots]_0 + \frac{\varkappa \overline{M}_0}{2 N_0 \varepsilon_d} D - \frac{\varkappa \rho \overline{M}_0}{4 N_0 \varepsilon_d} D^2. \tag{4}$$

Assuming that $P_m \sim [H\ldots]$, we obtain*

$$P_m = k[H\ldots] = P_m^0 + \frac{k\varkappa}{2} \frac{\overline{M}_0 D}{N_0 \varepsilon_d} - \frac{k\varkappa}{4} \frac{\rho \overline{M}_0}{N_0 \varepsilon_d} D^2, \tag{5}$$

where κ is the number of shielded hydroxyls uncovered by each cleavage of the molecule, k and ρ are coefficients, and P_m^0 and P_m are the ultimate shear stresses of gels from unirradiated and irradiated starches, respectively.

* According to Zuev [5], $P_m \sim n^{2/3}$, where n is the number of contacts per cc of gel, but the experimental data in the case of starch show direct proportionality between these values.

The relation

$$\frac{P_m - P_m^0}{D} = \frac{k\varkappa \bar{M}_0}{2N_0\varepsilon_d} - \frac{k\varkappa\rho\bar{M}_0}{4N_0\varepsilon_d} D, \qquad (6)$$

when constructed from experimental data, was expressed by a straight line over the range from $1 \cdot 10^6$ to $4 \cdot 10^6$ r (Fig. 2) and this confirms the accuracy of the premises used in deriving Eq. (5).

From the experimental data it follows that

$$\frac{k\varkappa}{2}\frac{\bar{M}_0}{N_0\varepsilon_d} = 15{,}1 \cdot 10^6 \frac{g}{cm^2 \cdot g} \; ; \; \frac{k\varkappa\rho\bar{M}_0}{4N_0\varepsilon_d} = 4{,}1 \frac{g}{cm^2},$$

and hence $\rho = 0{,}54 \cdot 10^{-6}\ r^{-1}$.

From the analysis of Eq. (5) it also follows that the maximum of the curve of $P_m = f(D)$ lies at $1/\rho = 1{,}85 \cdot 10^6$ r, while $k\varkappa = 20{,}8$, using the values $\bar{M}_0 = 462{,}000$ and $\epsilon_d = 26$ ev for the given starch, according to the measurements of V. F. Oreshko and K. A. Korotchenko [1].

The solid line in Fig. 2 shows the theoretical curve obtained from Eq. (5) and the circles represent experimental points.

Thus, in the region of integral doses $< 4 \cdot 10^6$ r, the change in plastic strength of gels from irradiated starches is caused by the change in the number of hydroxyls capable of forming hydrogen bonds. The depolymerizing action of ionizing γ-radiation leads to uncovering of shielded hydroxyls and strengthening of the gel lattice, while the destructive action, causing elimination of functional groups, decreases the total number of hydroxyls and leads to a decrease in the number of hydrogen bonds and a fall in the strength of the system.

Apparently, the terminal groups of the macromolecular chains of starch (aldehydic groups, for example) can also participate in the formation of the structural lattice, but in normal, unirradiated starch their role is very small and the strength of the gel is determined by hydrogen bonds arising between hydroxyls of the glucopyranose rings. As a result of the depolymerizing action of radiation, the number of terminal groups increases considerably and the size of the molecules decreases. Figure 2 shows a curve of the decrease in the mean molecular weight with an increase in dose obtained by V. F. Oreshko and K. A. Korotchenko [1]. With $4\text{-}5 \cdot 10^6$ r, the mean molecular weight falls by a factor of 10. The degraded molecules acquire a higher mobility and may participate in the formation of the structural lattice of the gel by reacting through the terminal groups, which should lead to some increase in the plastic strength and a change in the nature of the formation of the gel structure with time, which was observed in our experiments.

In the dose range where the structural lattice is formed by hydrogen bridges (from 0 to $\approx 4 \cdot 10^6$ r), the plastic strength of the gel increases rapidly, reaching the maximum value of P_m. At $4 \cdot 10^6$ r and above (Fig. 1) there is a considerable effect due to another mechanism, namely, the formation of a structure lattice by reaction of the macromolecule terminal groups; the plastic strength increases slowly and apparently does not reach a limiting value. With time there is gradual strengthening of the gel lattice as a result of rearrangement and deformation of the degraded, but still quite large molecules. Further depolymerization by ionizing radiation ($18.2 \cdot 10^6$ r) leads to such a great decrease in the size of the molecules that the latter lose their capacity to form gels.

LITERATURE CITED

[1] V. F. Oreshko and K. A. Korotchenko, Izvest. Vyssh. Uch. Zaved. (Pishchevaya Tekhnologiya) 4, 52 (1959).

[2] M. Samec, Die Stärke, 9, 76 (1958); 10, 285 (1959).

[3] E. E. Segalova and P. A. Rebinder, Kolloid. Zhur. 9, No. 5 (1947).

[4] Yu. S. Zuev, Kolloid. Zhur. 12, 36 (1950); 10, No. 4 (1948).

KINETIC ISOTOPE EFFECTS OF TRITIUM IN THE LIQUID-PHASE REACTION OF HYDROCARBONS WITH FREE METHYL RADICALS

V. L. Antonovskii and I. V. Berezin

M. V. Lomonosov Moscow State University
(Presented by Academician N. N. Semenov, April 27, 1960)
Translated from Doklady Akademii Nauk SSSR, Vol. 134, No. 4, pp. 860-863, September, 1960
Original article submitted March 28, 1960

The study of kinetic isotope effects of tritium and the rules of their change in relation to the structure of the reacting particles, medium, temperature, etc., are problems of great importance. The solution of these problems would not only create bases for quantitative comparisons in investigations of the chemistry and kinetics of elementary processes, but in a number of cases it would make it possible to draw conclusions on the nature of activated states through which reactions proceed [1, 2].

We recently determined the intermolecular kinetic isotope effects of tritium in the reactions of hydrocarbons with free methyl radicals ($i = k^H/k^T$):

$$RH + CH_3\bullet \xrightarrow{k^H} R\bullet + CH_4, \quad (I)$$

$$RT + CH_3\bullet \xrightarrow{k^T} R\bullet + CH_3T. \quad (II)$$

Determination of the magnitude of the kinetic isotope effect during the replacement of a small portion of the hydrogen atoms by tritium is possible in the case where the molecule of the hydrocarbon investigated contains only one sort of reactive bond. Then:

$$\frac{[CH_4]}{[CH_3T]} = \frac{nk^H[RH]}{k^T[RT]}.$$

Here n is the number of reactive C–H bonds in the molecule RH. If $[RT] \ll [RH]$, then $\gamma I_{RH} = [RT]/[RH]$, where I_{RH} is the specific activity of the compound expressed as the count per unit time per mole and γ is the proportionality coefficient which depends only on the design of the counter used. Finally we have:

$$i = \frac{k^H}{k^T} = \frac{I_{RH}}{nI_M}, \quad (1)$$

where I_M is the specific activity of the methane formed in the experiment. Determinations were carried out with benzene and toluene. As the reactivity of the hydrogen atoms in the toluene nucleus is a factor of 150-170 less than that of the hydrogen atoms in the methyl group [3], it may be considered that n = 3 in this case.

The determination of the isotope effect in the case of aromatic and unsaturated compounds requires particular care as together with the main replacement, there may occur parallel reactions which are not considered

TABLE 1

$I_{C_6H_6}$	Initial peroxide conc., mole/liter	I_{CH_4} at the following degrees of decomposition			Mean of 5 experiments	$i=\frac{k^H}{k^T}$
		10%	25%	50%		
5960±100	0,025	165±4	165±1	167±1	166±2	5,98±0,13
5960±100	0,010	163±3	161±2	164±1	163±2	6,09±0,13

TABLE 2

Temp., °C	Benzene			Toluene		
	$I_{C_6H_6}$	I_{CH_4}	k^H/k^T	$I_{C_6H_5CH_3}$	I_{CH_4}	k^H/k^T
85	5960±100	166±1	5,98±0,13			
	5000± 80	136±1	6,19±0,13	35 200± 700	968±7	12,1 ±0,1
	5770± 30	163±1,5	5,90±0,06			
70	5770± 30	145±2	6,63±0,13	35 200±700	829±11	14,14±0,2
55	5770± 30	130,6±2	7,36±0,09	35 200±700	737±6	15,9 ±0,3

TABLE 3

Hydrocarbon	A^H/A^T	$\Delta E = E^T - E^H$, kcal/mole	k^H/k^T at 85°
Benzene	0,66	1570±100	6,0
Toluene	0,55	2200±100	12,1
Cyclohexane	0,38	2700±100	17,2
Cyclopentane	0,16	3500±350	22,8
Cycloheptane	0,19	3430±250	23,5
n-Heptane (secondary bonds)	0,20	3400±130	23,2

in Eq. (1). In connection with this, it is relevant to recall the uncertainty of the results of Willen and Eliel [4] in the determination of the isotope effect for the same reaction with toluene deuterated in the CH_3 group. In the reaction of $CH_3\cdot$ with aromatic compounds, in addition to reactions (I) and (II), a source of methane may be the following process (in the case of benzene):

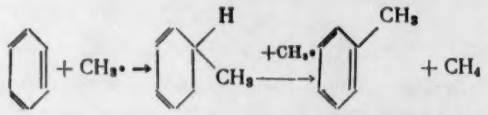

The isotope effect of this reaction should equal 1, as was found by Price and Convery for the phenylation of 2,4-dinitrobenzene [5]. If this reaction plays a substantial role in our case (benzene and toluene with $CH_3\cdot$), then the value of the isotope effect calculated according to Eq. (1) should depend on the concentration of methyl radicals.

The source of methyl radicals we used was acetyl peroxide, which was decomposed in hydrocarbons labelled with tritium [2]. The concentration of methyl radicals depended both on the degree of decomposition of the peroxide and on its initial concentration. Table 1 gives the results of experiments* with T-benzene at 85° and from these it follows that the value of the isotope effect was independent of both the initial concentration and the degree of decomposition of the acetyl peroxide.

From Table 1 it follows that the experimental results were not distorted by the reaction of a methyl radical with the reaction products. Experiments with α-T-toluene led to the same conclusions.

Table 2 gives the results of experiments with benzene and toluene at 55, 70, and 85° (± 0.05°). The values of the methane activity were obtained as a result of 3-6 experiments and the mean square errors are given.

* In Tables 1 and 2, the specific activity is expressed in counts/min per mm pressure of substance in the counter.

The relation between $\log k^H/k^T$ and $1/T$ was linear. The values of the ratio of the preexponents (A^H/A^T) and the difference in the activation energy ($E^T - E^H$), calculated by the method of least squares, are given in Table 3. These values for other hydrocarbons are also given [6, 7].

For the secondary bonds of n-heptane, cycloheptane, and cyclopentane, despite the considerable structural peculiarity of the latter (strain in the ring and the cis position of all the hydrogen atoms), the isotope effects are practically identical with respect to ΔE and the ratio of the preexponents. On these grounds we can draw the conclusion that for all secondary aliphatic, unconjugated carbon–hydrogen bonds, the kinetic isotope effect of tritium in the reaction with a free methyl radical is the same. The expression for the mean isotope effect for secondary bonds, calculated from available data, has the following form:

$$k^H/k^T = 0{,}18\exp(3450/RT).$$

A different picture is observed for other hydrocarbons for which the effect of structural factors appears more clearly. In the case of cyclohexane, the change in the value of the isotope effect is connected mainly with conformational characteristics and the presence of structural difference in the bonds. In this case it is more correct to talk of the isotope effect separately for axial and equatorial bonds. The mean isotope effect $i_m = (k_e^H + k_p^H)/(k_e^T + k_p^T)$(the indices e and p correspond to equatorial and polar bonds)is measured experimentally. By simple rearrangement it is possible to show that

$$1 + \frac{k_e^H}{k_p^H} = \frac{i_m}{i_p}\left(1 + \frac{i_p}{i_e}\frac{k_e^H}{k_p^H}\right), \qquad (2)$$

where i_p and i_e are the isotope effects for the polar and equatorial bonds. From spectroscopic data for $C_6H_{11}D$ [8] it follows that the polar and equatorial bonds are similar energetically. On this basis it may be assumed that $k_e^H/k_p^H \approx 1$, and considering this (2) may be rewritten:

$$\frac{1}{i_e} + \frac{1}{i_p} \approx \frac{2}{i_m}. \qquad (3)$$

Equatorial C–H bonds are structurally similar to normal secondary bonds of alicyclic hydrocarbons. If it is assumed that $i_e = i_{sec} = 0.18\exp(3450/RT)$, then for i_p we obtain the following expression:

$$i_p = 0{,}48\exp(2300/RT).$$

The nature of the change in the values of the isotope effects in the series toluene–n-heptane (see Table 3) indicates a definite relation of them to the energetics of the rupturable C–H bonds. For the abstraction of hydrogen atoms by $CH_3^\bullet$ radicals it is known [6, 9] that $E_{cp}^H - E_{tl}^H = 2.2$ kcal, $E_{hp}^H - E_{tl}^H = 2.0$ kcal, and $E_{ch}^H - E_{tl}^H = 0.6$ kcal (cp – cyclopentane, hp – n-heptane, ch – cyclohexane, and tl – toluene). In other words, the activation energy decreases in the series: secondary CH bonds, cyclohexane, toluene. Both ΔE of the isotope effect and its magnitude decrease in the same direction. The value of A^H/A^T increases. The magnitude of the isotope effect in benzene differs sharply and this is apparently connected with the effect of the aromatic nucleus on the energy levels of the transition state.

The magnitude of the isotope effect depends not only on the nature of the bond broken, but also on the form of the attacking particle. The isotope effect of deuterium increases in the series $Cl^\bullet$, $Br^\bullet$, N-succinimidyl, $(CH_3)_3CO^\bullet$ and $CH_3^\bullet$ [10]. Therefore, the values obtained in the present work may be regarded as the upper limit of the values of the kinetic isotope effects of tritium with other free-radical particles.

LITERATURE CITED

[1] S. Z. Roginskii, Theoretical Bases of Isotopic Methods of Studying Chemical Reactions [in Russian] (Izd. AN SSSR, 1956).

[2] V. L. Antonovskii and I. V. Berezin, Nauchn. Doklady Vyssh. Shkol. Khim. i Khim. Tek. 320 (1958).

[3] I. V. Berezin, N. F. Kazanskaya, and K. Martinek, Zhur. Obshch. Khim. (in press).

[4] H. Wilen and E. L. Eliel, J. Am. Chem. Soc. 80, 3309 (1958).

[5] R. J. Convery and C. C. Price, J. Am. Chem. Soc. 80, 4104 (1958).

[6] V. L. Antonovskii and I. V. Berezin, Nauchn. Doklady Vyssh. Shkol. Khim. i Khim. Tekh. 731 (1958).

[7] V. L. Antonovskii and I. V. Berezin, Doklady Akad. Nauk SSSR 127, 124 (1959).*

[8] M. Lamaudie, Compt. rend. 235, 154 (1952).

[9] V. L. Antonovskii, I. V. Berezin, and L. V. Shevel'kova, Doklady Akad. Nauk SSSR 134, No. 3 (1960).*

[10] K. B. Wiberg, Chem. Rev. 55, 713 (1955).

*Original Russian pagination. See C. B. Translation.

INVESTIGATION INTO THE ADSORPTION OF IODINE ON SMOOTH PLATINUM AND ITS DESORPTION BY A TRACER METHOD

V. E. Kazarinov and N. A. Balashova

Institute of Electrochemistry, Academy of Sciences of the USSR
(Presented by Academician A. N. Frumkin, May 6, 1960)
Translated from Doklady Akademii Nauk SSSR, Vol. 134, No. 4, pp. 864-867, September, 1960
Original article submitted May 6, 1960

Previous work has shown that very stable adsorption of iodine takes place on platinized and smooth platinum [1-3]. However, the nature of this adsorption and the effect of different factors on it are not yet very clear.

This present paper deals with adsorption of iodine from acid, and, in a few cases, alkaline solutions of sodium iodide on smooth platinum, and its relation to concentration and time. Desorption of iodine under different conditions has also been studied. The work was carried out by a tracer method using I^{131} and Pt^{193} isotopes. The smooth platinum electrodes were subjected to a preliminary activation by alternate cathode and anode polarization in 1 N H_2SO_4. The solutions were prepared from recrystallized, chemically pure salts, and sulfuric acid and water, both of which had been distilled twice. The experiments were carried out as follows: the activated electrode was immersed for a given time in a tracer solution* under given conditions, then removed in air, washed with distilled water (2 min) and placed in front of a radioactivity measuring device. The adsorption was calculated from the measured radioactivity. In earlier work, we provisionally termed adsorption, measured in this way, "irreversible" [1, 5]. Experiments on desorption and exchange under differing conditions were also carried out.

It was discovered that commercial radioactive preparations of sodium iodide "with no carrier" containing radiochemically pure I^{131} isotope, in addition to simple I' anions also contained an impurity which consisted of I^{131} in some other chemical form and which possessed considerably greater sorbability than the I' anions. For example, this impurity could be complex ions of heavy metals. In this case the amount of adsorption per unit surface, calculated on the assumption that the stable and radioactive ions are completely identified, is higher than the highest concentration of stable ions [5]. This, however, can be eliminated by a preliminary purification of the commercial sodium iodide tracer, in which iodine (obtaining by oxidizing I' with potassium dichromate) is sublimed and then electrochemically reduced back to I' ion. This purification was used for this present work and gave reproducible results to within ± 15%.

The maximum value for irreversible iodine adsorption on smooth platinum, obtained with the purified iodine isotope, from 1 N H_2SO_4 + 0.01 N KI solution in an atmosphere of nitrogen, is about $1.5 \cdot 10^{-9}$ g·ion/cm^2 for the apparent surface. This is near the value for monolayer formation. The results obtained for smooth platinum under the same conditions in [1], which are considerably higher, are evidently due to the use of impure I^{131} isotope.

The amount of iodine adsorption on smooth platinum in an atmosphere of air or hydrogen from acid solution (concentration > 10^{-3} N), measured immediately after the platinum has been washed with distilled water,

* Solutions in the different experiments contained a maximum amount of isotope of 0.4 mcuries per g dry NaI.

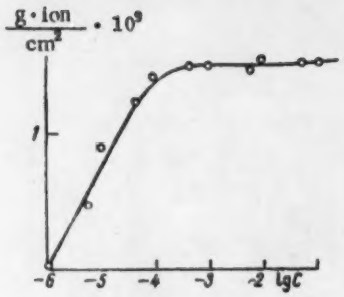

Fig. 1. Relation between irreversible iodine adsorption and concentration of NaI in a 1 N H_2SO_4 base solution in a nitrogen atmosphere. Γ at $1 \cdot 10^{-6}$ N concentration is equal to $8 \cdot 10^{-11}$ g·equiv/cm.

is practically independent of the adsorption time in the interval 10 sec to a few hours. In less concentrated solutions, this relation is observed, and is linked up with diffusion effects.

The isotherm of irreversible iodine adsorption from acid solutions on smooth platinum in an atmosphere of nitrogen, air or hydrogen shows a logarithmic relation in the concentration range 10^{-6} and 10^{-4} N. Saturation is observed at higher concentrations* (Fig. 1).

The amount and rate of desorption from smooth platinum of iodine, which was adsorbed at an air potential from acid solution, depends on its potential in the desorbing solution. In 1 N H_2SO_4 at potentials less positive than 1.25 v (compared to normal hydrogen electrode) desorption proceeds slowly, only 20% of the total sorbed material being desorbed in one hour. With increasing potential the desorption rate increases sharply (Fig. 2). Complete desorption (0.1% remaining) is reached in a few minutes at a potential of 1.7 v.

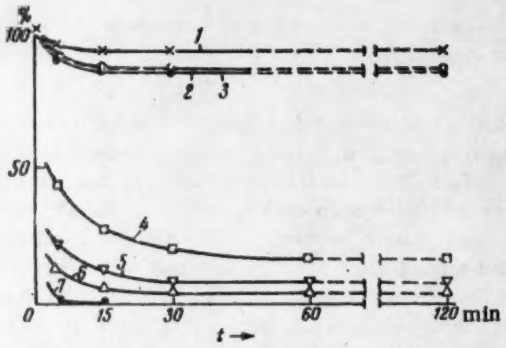

Fig. 2. Desorption of iodine in 1 N H_2SO_4 at different potentials: 1) 0.78 v; 2) 1 v; 3) 1.25 v; 4) 1.35 v; 5) 1.45 v; 6) 1.55 v; 7) 1.75 v; against normal hydrogen electrode.

In 1 N NaOH at potentials more positive than 0.35 v, there is a similar increase in desorption with increasing potential. This effect of potential (for anode desorption) can be explained as the oxidation of the sorbed iodine to IO_3^-, which is evidently not sorbed by the oxidized surface of smooth platinum

Iodine desorption in sulfuric acid at the reversible hydrogen potential increases linearly with the decreasing logarithm of acid concentration. This is due to the increase of negative charge on the surface, which repels iodide anions, on passing to the negative side of potential (Fig. 3). Probably for this reason iodine desorption proceeds more rapidly and completely in water and 1 N NaOH (in a hydrogen atmosphere) than in sulfuric acid. Under these conditions complete desorption takes 30-40 sec.

A similar effect to that observed by decreasing the sulfuric acid concentration is obtained in 1 N H_2SO_4 by increasing the cathode current density from 1.5 to 50 ma/cm². At the highest current density about 90% of the total sorbed material is desorbed in 5 min, i.e., about as much as in 10^{-4} N sulfuric acid without any polarization. The amount of iodine desorbed by cathode or anode polarization in H_2SO_4 and NaOH, or by changing the acid concentration, does not depend logarithmically on time, but obeys a more complex relationship.

* The fact that this measured value is independent of the gaseous atmosphere used is probably connected with the fact that the platinum was kept in air while it was freed from the active solution, with the change in its sorption properties as a result of this, and also with the oxidation of I'.

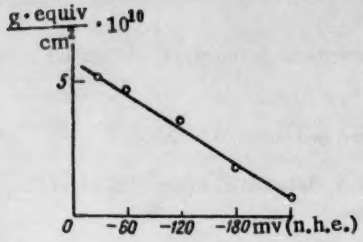

Fig. 3. Relation between iodine desorption and potential in different concentrations of H_2SO_4. (Desorption time 30 min).

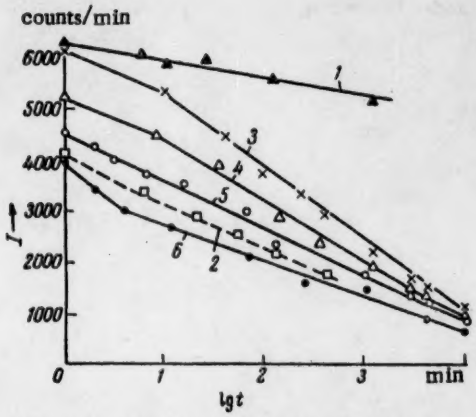

Fig. 4. Relation between iodine desorption and the desorption period. 1) 1 N H_2SO_4; 2) 1 N NaOH; 3) 10^{-3} N NaI; 4) 10^{-2} N NaI; 5) 10^{-1} N NaI; 6) 1 N NaI. At t = 0 the iodine for curves 1 – 6 is equal to 6200 ± 200 counts/min.

Desorption of iodine in water, ethyl alcohol and 1 N NaF, without any polarization and in an atmosphere of air or nitrogen, proceeds very slowly, reaching only 30% after several days. In H_2SO_4, NaOH and NaI solutions under these conditions there is a linear dependence of desorption on the logarithm of time (Fig. 4, curves 1, 2, 6).

The same relation is observed during the exchange process with neutral solutions of sodium iodide at different concentrations, in which exchange increases with increasing concentration. If during 10 min about 20% of the total amount sorbed undergoes exchange at $1 \cdot 10^{-3}$ N concentration, about 40% will undergo exchange during the same length of time at $1 \cdot 10^{-1}$ N concentration, and 60% at 1 N concentration. The gradients of the curves of $\Gamma/\log t$ decrease with increasing NaI concentration (Fig. 4, curves 3-6).

Like A. D. Obrucheva [6], we observed a displacement of potential during iodine adsorption from acid solutions on smooth platinum. At the considerable initial potential in 1 N H_2SO_4 of 0.8 v (compared to normal hydrogen electrode) the potential is displaced to the negative side by 80-100 mv on increasing the concentration of added I' from 10^{-3} N to 1 N in an atmosphere of pure nitrogen, i.e., the relation is analogous to that in [2] on platinized platinum. During iodine adsorption in an atmosphere of air, there is an analogous displacement of the smooth platinum potential to the negative side.

The potential of platinum in sulfuric acid in air, after the KI solution has been washed off with distilled water, is 150-200 mv more negative than its potential prior to adsorption of iodine. From radioactive measurements the amount of iodine adsorbed is only changed a few percent by washing. This change in the air potential of platinum in sulfuric acid is due to the effect of the sorbed iodine in decreasing the exchange current of oxygen, which is responsible for determining the potential.

The results obtained for acid solutions show that most of the iodine is chemisorbed and bonded very stably with the platinum.

A displacement of the potential due to adsorption is not observed during adsorption of iodine from alkaline solutions on smooth platinum, but the amount adsorbed, calculated from the radioactivity, is only a tenth of a monolayer. Hydroxyl ions impede iodine adsorption at all platinum potentials more negative than 1.0 v (normal hydrogen electrode). However, in alkaline solutions, at high anode potentials (oxygen formation potential) there is considerable adsorption of iodine exceeding several monolayers (calculated on the basis of I' anions). This is due to the surface formation of a stable chemical compound between iodine and the oxidized platinum, which is formed under these conditions.

The surface compound obtained dissolves easily in acid, but is stable in alkaline solutions even during cathode polarization. At a cathode current density of 20 ma/cm^2, only about 20% of the measured quantity goes into solution during 10 min, indicating a slow reduction of the compound. Independent experiments with radioactive platinum showed that in a solution of 1 N H_2SO_4 platinum also goes into solution with the sorbed

iodine. If no sorbed iodine is present on the platinum surface, the dissolution of platinum at the same potentials is much less.

We would like to thank Academician A. N. Frumkin for his interest in the work, and for his invalued advice in discussion of it.

LITERATURE CITED

[1] N. A. Balashova, Z. f. phys. Chem. 207, 340 (1957); N. A. Balashova, Zhur. Fiz. Khim. 32, 2266 (1958).

[2] A. D. Obrucheva, Zhur. Fiz. Khim. 32, 2155 (1958).

[3] K. Schwabe, K. Wagner, and Ch. Weissmantel, Z. f. phys. Chem. 206, 309 (1957).

[4] K. Schwabe, Chemische Technik 3, 469 (1958).

[5] N. A. Balashova and N. S. Merkulova, New Methods of Physicochemical Investigation, Tr. Inst. Fiz. Khim. Akad. Nauk SSSR [in Russian] (1957) Vol. 6, p. 12.

[6] A. N. Frumkin, Trans. Symp. Electrode Processes (Philadelphia, 1959).

CHEMICAL DISPLACEMENT OF THE NUCLEAR MAGNETIC RESONANCE OF F^{19} IN FLUOROORGANIC COMPOUNDS

Yu. S. Konstantinov

M. V. Lomonosov Moscow State University
(Presented by Academician I. L. Knunyants, April 12, 1960)
Translated from Doklady Akademii Nauk SSSR, Vol. 134, No. 4, pp. 868-870, October, 1960
Original article submitted April 12, 1960

The discovery and investigation of the chemical displacement of nuclear magnetic resonance (NMR) which is due to the different magnetic screening of the nuclei occupying structurally nonequivalent positions in the molecule, has made it possible to use the nuclear magnetic resonance method with success for the structural and qualitative analysis of organic, and particularly of fluoroorganic, compounds [1-4].

Since it is practically impossible at present to calculate on theoretical grounds the chemical displacements, it is necessary, in order to use the method of nuclear magnetic resonance for the qualitative analysis, to determine by preliminary experiments the breadth of the chemical displacement which is characteristic of each fluorine-containing group which can participate in the structure of organic molecules. The present work is devoted to achieving this object by investigating the nuclear magnetic resonance spectra of F^{19} in approximately 100 fluoroorganic molecules of known structure. This has made it possible to give precise values to the breadths of the chemical displacement for some groups which have been investigated earlier [3, 4], and also to find the values of the displacements for some groups which have been little, if at all, investigated previously. Among the last are CH_2F-, $CHF-$, and CHF_2-. The measurements have been carried out with a synchronized autodyne spectroscope [5], with resolving power $\Delta H/H \cong 10^{-6}$, a detailed description of which is given in [6].

The substances under investigation were sealed into cylindrical glass ampoules of internal diameter 4 mm. The volume of the specimen was about 0.1 cm^3. Diamagnetic correction for the shape of the specimen was not introduced.

As a measure of the chemical displacement the relative magnitude determined by the following equation was taken:

$$\delta = \frac{H_{sp} - H_{st}}{H_{st}} 10^6.$$

In this, H_{sp} and H_{st} are the resonance values of the potential of a constant magnetic field for the sample under investigation and for a standard sample, respectively, for a fixed value of the spectroscope frequency. The standard sample used was freon, CF_2Cl_2. The results obtained are shown in Table 1. Each of the fluorine-containing groups which was investigated gave a minimum and a maximum value for δ which determined the breadth of the chemical displacement which was characteristic of the group in question, and also the mean arithmetical value of the displacement for each displacement width. The values of the displacements were reproducible under repeated measurements to $\pm 1 \cdot 10^{-6}$. If it was desired to transfer the values of the chemical displacement to F_2 or CH_3COOH, which were used as standard samples in [3, 4], then the relationships given in [2] must be employed: $\delta F_2 = \delta CF_2Cl_2 + 434.8$; $\delta CF_3COOH = \delta CF_2Cl_2 - 72.8$.

TABLE 1

Breadth of the Chemical Displacement of Nuclear Magnetic Resonance of F^{19} for Various Fluorine-Containing Groups

$$\left(\delta_{CF_2Cl_2} = \frac{H_{obs} - H_{CF_2Cl_2}}{H_{CF_2Cl_2}} \cdot 10^6\right)$$

Group	Breadth of displacement δ min	Breadth of displacement δ max	No. of groups investigated	Mean value of displacement	Group	Breadth of displacement δ min	Breadth of displacement δ max	No. of groups investigated	Mean value of displacement
$-C(=O)F$	−63	−27	3	−38	d) $C-CF_2-C$	93	105	2	99
					$-CFCl-$	90	119	4	104
					$-CF_2H$	105	133	17	116
					$-CFBr-$	104	136	15	117
					$-CFBrH$	126	136	3	131
$-CF_2Br$	38	55	10	46	$-CFClH$	135		1	135
$-CF_2Cl$	43	59	13	51	a) $C-CFH-S$	168	171 (doublet)	1	169
$-CFCl_2$	57	61	3	56					
$C=(CF_3)_2$	53	67	13	58					
$-CFClBr$	58		1	58	b) $C-CFH-C$	176	203	11	192
$-CFClI$	60		1	60	a) $S-CFH_2$	193	200	2	196
$-CF_3$	53	74	30	66	b) $C-CFH_2$	216	230	3	223
a) $C-CF_2-O$	50	77	9	68					
b) $C-CF_2-N$	78	85	5	81					
c) $C-CF_2-S$	93	97	3	94					

The groups which have been examined are arranged in Table 1 in the order of increasing displacement. The total change in the displacement for all the molecules whose nuclear magnetic resonance spectra have been obtained in the course of the current work was $293 \cdot 10^{-6}$. The smallest value was found for fluorine in the the group $-C(=O)F$, and the greatest in $-CH_2F$. In the groups CHF_2-, $-CHF-$ and $-CH_2F$, the displacement increases with increase in the number of hydrogen atoms attached to the same carbon atom as the single atom of fluorine (n_H/n_F). A similar picture was found in [2] for the series: CF_4, CHF_3, CH_2F_2 and CH_3F. It is interesting to notice that in this series there is a practically linear relationship between the chemical displacement (measured relative to CF_4) and the ratio n_H/n_F.

The large displacement which is characteristic of the groups $-CHF-$ and $-CH_2F$ provides an easy means of detecting the presence of these groups in molecules by the nuclear magnetic resonance method. The identification of $-CHF_2$ is more complicated, since the breadth of the chemical displacement of this group overlaps that of $-CF_2-$, $-CFCl-$, $-CFBr-$, $-CHFBr$ and $-CHFCl$. In the majority of cases, the task is facilitated by the fact that the nuclear magnetic resonance signals from the fluorine in $-CHF_2$ are divided into doublets because of the cross spin-spin interaction of the fluorine and hydrogen nuclei [7]. Multiplet division is also observed with the groups $-CFH-$ and $-CH_2F$.

A change in the chemical displacement has been noted for certain fluorine-containing groups, caused by the influence of neighboring atoms in the aliphatic chain. Thus, for the arrangement $C-CF_2-X$, the magnitude of the displacement in the nuclear magnetic resonance of fluorine in the $-CF_2-$ group depends on the nature of X, and increases in the order O, N, S, C, from 50 for oxygen to 105 for carbon. The same relationship is found in the arrangement $C-CHF-X$, and in CH_2F-X, where X = S or C. In some cases it is possible to observe a small change in δ due to the effect of more remote parts of the molecule. Thus, in the arrangement $C-CF_2-OR$, the magnitude of the displacement for otherwise similar conditions depends on the nature of R.

This provides grounds for hoping that development of experimental data will lead to a link between the values of the chemical displacement of nuclear magnetic resonance of fluorine in any given group, and the constitution of neighboring groups, which will be most important for chemical analysis. Detailed data for the nuclear magnetic resonance spectra of fluorine for all the compounds investigated will be published subsequently.

In conclusion, the author would express his gratitude to S. D. Gbozdover for his interest in the work, and to fellow workers in the Institute of Elementoorganic Compounds of the Academy of Sciences of the USSR, L. S. German and B. L. Dyatkin, for the preparation of specimens and their useful discussion of the results.

LITERATURE CITED

[1] H. S. Gutowsky and C. J. Hoffman, J. Chem. Phys. 19, 1259 (1951).

[2] L. H. Meyer and H. S. Gutowsky, J. Phys. Chem. 57, 481 (1953).

[3] P. M. Borodin and F. I. Skripov, Izvest. Vyssh. Uch. Zaved. Radiofizika 1, 4, 69 (1958).

[4] N. Muller, P. C. Lauterbur, and G. F. Svatos, J. Am. Chem. Soc. 79, 1807 (1957).

[5] Yu. S. Konstantinov, Prib. i Tekh. Éksp. 2, 105 (1958).

[6] Yu. S. Konstantinov, Proceedings of the All-Union Congress on Paramagnetic Resonance [in Russian] (Kazan', 1959) (in press).

[7] H. S. Gutowsky, D. W. McCall, and C. R. Slichter, J. Chem. Phys. 21, 279 (1953).

THE AUTOCATALYTIC NATURE OF THE MARTENSITE TRANSFORMATION

O. P. Maksimova, N. P. Soboleva, and É. I. Éstrin

Metallography and Metal Physics Institute, I. P. Bardin
Central Ferrous Metallurgy Scientific Research Institute
(Presented by Academician G. V. Kurdyumov, May 13, 1960)
Translated from Doklady Akademii Nauk SSSR, Vol. 134, No. 4, pp. 871-874, October, 1960
Original article submitted April 20, 1960

One of the most important problems in the theory of martensite transformations in the present stage of its development is the question of the influence of the structural imperfections of the original phase on the course of the transformation and on the structure and properties of its products. Of particular interest in this connection is the examination of the problem of the part played, not by the imperfections produced in the original austenite phase by external factors (deformation, irradiation, etc.), but by those imperfections which are produced directly in the course of the actual transformation and which influence the further development of the process.

The production of distortions in the austenite during martensite transformation is unavoidable, as a result of the specific features of this type of transformation, which are responsible for the production of marked deformations of the austenite crystal lattice close to the martensite crystals which have been formed: the cooperative mechanism of the transformation and the strictly regular character of the atomic displacements when the elastic properties of the medium are relatively high [1, 2, 16, 17].

The deformations produced in the austenite structure under the influence of the martensite transformation may have opposite effects on its stability [2, 4, 18]. The changes which have a retarding influence on the subsequent course of the martensite transformation (the pressures from all directions, the break-up and reorientation of the blocks, etc. [6, 18-20]) obviously can become significant and play an important part in the transformation only in its later stages [1, 2]. The crystal structure defects in the austenite lattice, which lead to the activation of the transformation (high elastic deformations of local character [22]) influence the subsequent development of the process from its earliest stages [2, 4]. The present paper examines the part played by this type of structural imperfection.

There is a great deal of experimental material which indicates that the martensite transformation is autocatalytic: the phenomenon of "bursting" [7]; the fact that the process is less intense in the powder [7, 22]; the higher intensity of the isothermal transformation in a specimen which contains a small quantity of martensite [9] before treatment; the activation of austenite under the influence of previous deep freezing [23, 24], etc. The production of activating changes during the course of the martensite transformation is also confirmed by the results of theoretical studies [3].

In the present work the autocatalytic effect of the martensite transformation and its part in the transformation were studied: 1) by analysis of the extensive experimental material obtained by earlier workers on the kinetics of martensite transformations, and 2) by carrying out special experimental studies.

We have analyzed the experimental data obtained during the past decade on the kinetics of the martensite transformation with deep freezing and subsequent heating. The data from a large number of experiments for a

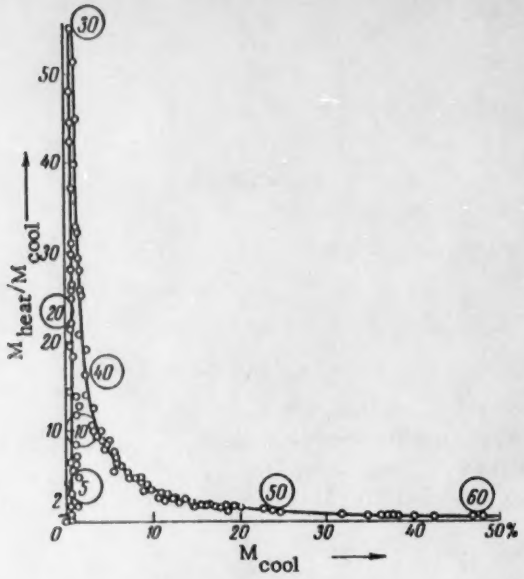

Fig. 1. The activating effect of martensite obtained by cooling on the transformation during subsequent heating. Alloy N24G3 (0.065% C, 23.7% Ni, 2.82% Mn). M_{cool} is the effect of cooling from 20° to −196°, M_{heat} is the effect of subsequent heating from −196° to 20°; the figures in circles represent $M_{\Sigma} = M_{cool} + M_{heat}$.

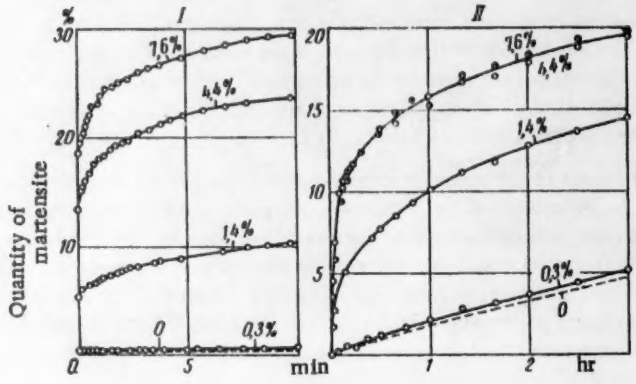

Fig. 2. Activation of the isothermal transformation at −90° under the influence of the martensite previously accumulated at −196° (the quantity of accumulated martensite is indicated on the curves). Alloy N23G4 (0.05% C, 23.0% Ni, 4.00% Mn). I) Total effects; II) isothermal effects.

series of Fe−Ni−Mn and Fe−Cr−Ni alloys were used to calculate 50-150 values of the ratio of the effects of heating (M_{heat}) to the effects of previous cooling (M_{cool}). The relationship between the values of M_{heat}/M_{cool} and the M_{cool} effects was plotted on graphs (Fig. 1).

The fact that the curves obtained have a clearly defined maximum close to the y axis indicates that in all cases the previously formed martensite crystals have a powerful activating effect on the subsequent develop-

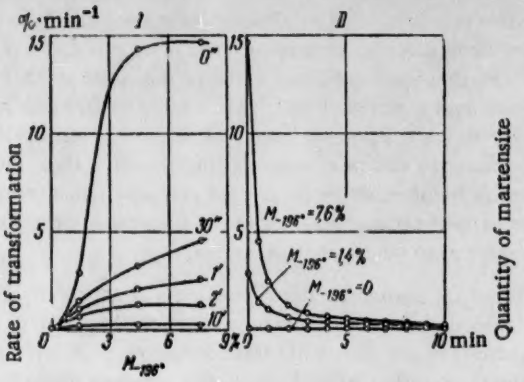

Fig. 3.

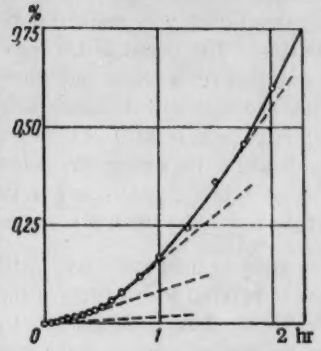

Fig. 4.

Fig. 3. Development and elimination of the activation effect. Alloy N23G4. I) Change in the rate of transformation at −90° with change in $M_{-196°}$; II) decrease in the activation effect during the isothermal treatment.

Fig. 4. Increase in the rate of the isothermal transformation at −196° with time. Alloy N23G4.

ment of the transformation. So long as the development of the process is not limited by a lack of sites capable of undergoing transformation, the relative intensity of the transformation on heating increases sharply with increase in the effect of the preceding deep freezing; of particular interest is the fact that for a given M_{cool} effect, the M_{heat} effect is constant for each alloy and is independent of its previous treatment, i.e., it is independent of the particular features of the austenite (the state of plastic deformation, high annealing, phase cold-working, etc.); in all cases complete exhaustion of all the austenite capable of undergoing transformation (for example, 40-50%) is attained on heating, even in the case where only approximately 1% martensite is formed during the cooling process.

The subsequent experimental study of the autocatalytic character of the martensite transformation was carried out by means of a specially developed apparatus with high sensitivity. A study was made of the change in the course of the isothermal transformation in an Fe−Ni−Mn alloy ($T_M = -30°$) at a definite temperature (−90°) with change in the quantity of martensite ($M_{-196°}$) previously accumulated at −196°.*

The studies yielded direct experimental data showing that the martensite transformation is clearly autocatalytic (Figs. 2 and 3). The presence of the martensite previously accumulated at −196° leads to a considerable increase in the intensity of the subsequent transformation. This is indicated both by the regular rapid increase in the initial rate of the isothermal transformation with increase in $M_{-196°}$ (for example, at $M_{-196°} = 4.4\%$ the initial rate of the transformation increases by a factor of more than 700 − from 0.02 to 14.3% min^{-1}), and also by the regular increase in the effect of the transformation from the storage temperature (−196°) to the control temperature (−90°) as $M_{-196°}$ increases.

The following regular features of the development of the autocatalytic effect were established: there is a very rapid increase in the activation effect when $M_{-196°}$ increases to approximately 5%; with further increase in $M_{-196°}$ to 10%, the autocatalytic effect continues to increase slightly and then gradually decreases (apparently as a result of the exhaustion of sites in the original phase capable of undergoing the transformation at the temperature in question). The initiating action of the previously accumulated martensite on the subsequent course of the transformation is most clearly shown in the initial stages of the isothermal process (Fig. 3b); as the duration of the isothermal process increases, the effect of the activating changes rapidly decreases. This indicates that relaxation processes are taking place even during the transformation itself (at −90°), i.e., it indicates the extremely low temperature stability of the structural defects produced.

* This low temperature of preliminary storage was chosen so that the distortions of the austenite crystal structure should be as high as possible and be preserved as completely as possible.

The autocatalytic nature of the martensite transformation is also clearly shown by the actual course of the isothermal transformation observed in a number of alloys under conditions where the rate of the transformation is extremely small (with very marked or very little supercooling); the process takes place at a rate which increases with time. This course of the transformation was established in the present work at −196° (Fig. 4); the rate of the transformation in this case increases over a period of more than 3 hr. The fact that the isothermal transformation proceeds with an acceleration – which is a normal feature of ordinary phase transformations (when the transformation process involves both the formation of new crystals and the growth of those already formed) – can be explained in the case of the martensite transformations (which are produced almost entirely as a result of the formation of new crystals) only on the basis of the assumption that the transformation products which are formed have an activating influence on the subsequent course of the reaction.

Further study of the autocatalytic effect of the martensite transformation will apparently be most fruitful if carried out in parallel with a study of the directly related phenomenon of the thermal stabilization of austenite, which is one of the most important features of the martensite transformation. The large amount of available data on the regular features of the martensite transformation indicate the accuracy of the view that the thermal stabilization of the austenite involves a gradual relaxation of the distortions activating the austenite, which are produced as a result of partial transformation.

This relaxation process should apparently be regarded as a process involving not only the elimination of the distortions activating the austenite, but also the formation (as a result of the atomic displacements accompanying the relaxation) of a type of structural imperfection which can have a retarding influence on the martensite transformation.

The autocatalytic effect of the martensite transformation and the thermal stabilization of the austenite are directly related to the heterogeneous character of the initiation of the new phase in this type of transformation. This also determines the important part which is played in the martensite transformation by changes in the crystal structure of the initial phase, which take place both during the actual transformation (the production of defects) and also during subsequent treatment (the gradual healing of the defects).

LITERATURE CITED

[1] G. V. Kurdyumov, Modern Metallurgical Problems [in Russian] (Izd. AN SSSR, 1958) p. 546.

[2] G. V. Kurdyumov, The Effects of Hardening and Tempering Steel [in Russian] (Moscow, 1960).

[3] B. Ya. Lyubov and A. L. Roitburd, Doklady Akad. Nauk SSSR 120, 5, 1011 (1958).*

[4] O. P. Maksimova and É. I. Éstrin, Fiz. Metal. i Metalloved. 9, 3, 426 (1960).

[5] A. P. Gulyaev and E. V. Petunina, The Metallographic Study of the Transformation of Austenite to Martensite [in Russian] (Moscow, 1952).

[6] A. N. Alfimov and A. P. Gulyaev, Izvest. Akad. Nauk SSSR, Otdel. Tekh. Nauk 4, 93 (1954).

[7] E. S. Machlin and M. Cohen, J. Metals 3, 9, 746 (1951).

[8] E. S. Machlin and M. Cohen, Trans. Am. Inst. Metallurg. Eng. 194, 489 (1952).

[9] C. H. Shih, B. L. Averbach, and M. Cohen, J. Metals 7, 2, 183 (1955).

[10] J. C. Fisher and D. Turnbull, Acta Metallurg. Sin. 1, 310 (1953).

[11] C. Crussard and J. Philibert, Rev. metallurgie 53, 12, 973 (1956).

[12] S. G. Glover and T. B. Smith, The Mechanism of Phase Transformations in Metals (London, 1956) p. 265.

[13] C. H. Shih, Acta Metallurgica 1, 3, 289 (1956).

[14] Sakamoto Kashiro and Sugeno Takesi, Mem. Inst. Scient. and Industr. Res. Osakava Univ. 16, 119 (1959).

[15] S. C. Das Gupta and B. S. Lement, Trans. Am. Inst. Metallurg. Eng. 191, 727 (1951).

* Original Russian pagination. See C. B. Translation.

[16] G. V. Kurdyumov, Zhur. Tekh. Fiz. 18, 8, 999 (1948).

[17] G. V. Kurdyumov, Problems in Metallography and Metal Physics Collection [in Russian] (1952) No. 3, p. 9.

[18] S. S. Shteinberg, Trudy Ural'sk. Fil. Akad. Nauk SSSR 9, 8 (1937).

[19] M. E. Blanter and P. V. Novichkov, Metalloved. i Obrabotka Metallov, 6, 11 (1957).

[20] O. P. Maksimova and É. I. Éstrin, Doklady Akad. Nauk SSSR 132, No. 6 (1960).*

[21] G. V. Kurdyumov, O. P. Maksimova, and A. I. Nikonorova, Doklady Akad. Nauk 114, 4, 768 (1957).*

[22] R. E. Cech and D. Turnbull, J. Metals, 8, 2, 124 (1956).

[23] A. P. Gulyaev and A. P. Akshentseva, Zhur. Tekh. Fiz. 25, 2, 299 (1955).

[24] O. P. Maksimova and E. G. Ponyatovskii, Problems in Metallography and Metal Physics, Collection [in Russian] (1955) Vol. 4, p. 180.

* See C. B. Translation.

THE TEMPERATURE DEPENDENCE OF THE SEPARATION COEFFICIENT FOR THE $C^{13}O$–$C^{12}O$ SYSTEM

N. N. Sevryugova and N. M. Zhavoronkov, Corresponding Member, Acad. Sci. USSR

L. Ya. Karpov Physicochemical Institute

Translated from Doklady Akademii Nauk SSSR, Vol. 134, No. 4, pp. 875-878, October, 1960
Original article submitted July 15, 1960

Rayleigh distillation and the differential pressure method are the most commonly employed, and at the same time, most exact procedures for determining the coefficient of separation of isotopic compounds in the liquid – vapor equilibrium. The second of these procedures involves the direct measurement of the difference in the vapor pressures of two specimens of different isotopic composition. Unfortunately, this calls for a product which is highly enriched in the rare isotope and for especially high purity in the specimens as well, since the presence of contaminants of higher volatility can lead to a considerable error in the values of the separation coefficient.

The $C^{13}O$–$C^{12}O$ system selected for study is one for which separation coefficients have been determined by a number of authors working over the interval of temperatures from the melting point up to the boiling point [1-4]. Our own measurements were carried out over a still wider temperature interval, using pressures in excess of one atmosphere.

Measurement was made of the difference in the vapor pressures of two specimens of carbon monoxide, one containing the natural percentages of the C^{13} and O^{18} isotopes and the other, 23 or 32% C^{13}.

Carbon monoxide of natural isotopic content was obtained by the reaction of chemically pure sulfuric and formic acids at 100°C. The reaction product was run through a trap immersed in liquid oxygen in order to freeze out traces of moisture and then passed through a tubular furnace filled with cupric oxide at 300°C, where it was converted to CO_2 according to the reaction

$$CO + CuO = CO_2 + Cu. \quad (1)$$

The carbon dioxide was collected in a trap immersed in liquid oxygen and the uncondensed gases (N_2, O_2, A, etc.) pumped off at a pressure of $5 \cdot 10^{-5}$ mm. The pure CO_2 was then passed into a tubular furnace filled with asbestos spheres upon which zinc dust had been deposited. This furnace had been evacuated earlier for an extended period of time at a temperature of 300-320°C and a pressure of $5 \cdot 10^{-5}$ mm. Here reaction occurred between the CO_2 and the heated zinc:

$$CO_2 + Zn = ZnO + CO. \quad (2)$$

The purity of the resulting carbon monoxide was checked from a spectrograph obtained with a MS-4 mass-spectrometer and from the freezing point.

Specimens of CO enriched in C^{13} and O^{18} were available from the Karpov Laboratories for Adsorption Processes of the Karpov Physicochemical Institute. It was necessary to separate these isotopes so as to obtain

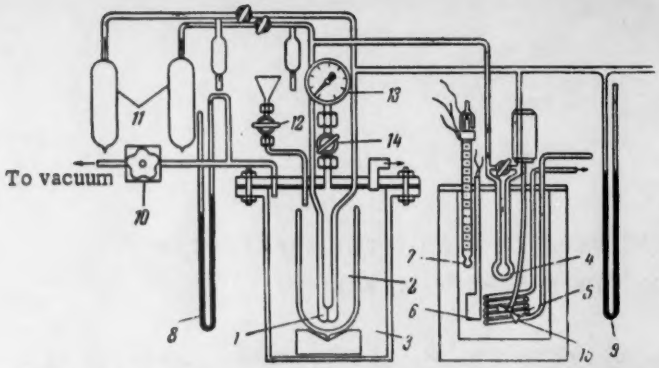

Fig. 1. Apparatus for measuring the difference in vapor pressures of two isotopic forms.

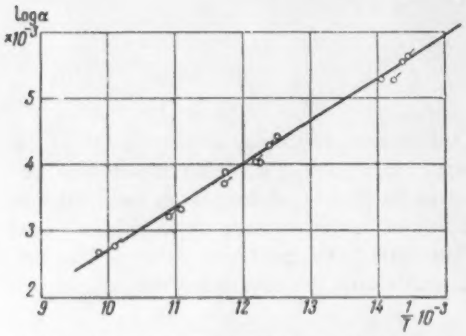

Fig. 2. Temperature dependence of the separation coefficient in the $C^{13}O-C^{12}O$ system.

specimens which would contain the natural percentage of O^{18} and an enhanced percentage of C^{13}. Such a separation was carried out through the reactions:

$$C^{13}O^{18} + CuO^{16} = Cu + C^{13}O^{16}O^{18}; \quad (3)$$

$$C^{13}O^{16}O^{18} + 4H_2 = C^{13}H_4 + H_2O^{16} + H_2O^{18} \quad (4)$$

$$C^{13}H_4 + 4CuO^{16} = 4Cu + 2H_2O^{16} + C^{13}O_2^{16}; \quad (5)$$

$$C^{13}O_2^{16} + Zn = ZnO + C^{13}H^{16}. \quad (6)$$

The resulting specimens of CO were purified, and their purity checked, in the same manner as the standard specimens.

Measurements of the difference in vapor pressures (ΔP) were carried out in the apparatus of Fig. 1. Here, the principal component is the vessel (1) which is separated into two cells, one filled with the standard specimen and the other with the C^{13}-enriched specimen. Each of these cells was connected to one side of the differential manometer (4). The cell filled with the standard was also connected to the mercury manometer (9) which was used in measuring the absolute value of the CO pressure.

This vessel was set in a cryostat consisting of a Dewar flask (2) in a hermetically sealed container (3), the latter being equipped with a window through which the liquid level could be observed.

The Dewar flask was filled with either liquid nitrogen or liquid oxygen and the desired pressure and temperature then established in the cryostat by use of a pump and control valve (10) system. The pressure in the cryostat could be read on either the manometer (8) or the vacuum gauge (13). The temperature was varied over the interval from -170 to -205°C, by altering the CO pressure in the cell from 100 mm of Hg to 5 atm. The differential manometer was filled with mercury and placed in a 25° thermostat whose temperature was held constant to within ± 0.1°C. The pressure difference was read from this manometer with a cathetometer, the accuracy of determination being ± 0.02 mm.

The apparatus was calibrated prior to measurement. Both cells were filled with the standard specimen and the reading of the differential manometer observed over the entire temperature interval. This procedure was repeated with other standards, the resulting calibration curves being in good agreement with one another.

One of the cells was then filled with the standard CO and the other with CO containing 23 or 32% C^{13} and readings made on the differential manometer (ΔP). Separation coefficients were calculated from the equation:

$$(\alpha - 1) = \frac{\Delta P}{P(N_1 - N_2)}, \quad (1')$$

TABLE 1

Results of Measurements of the Temperature Dependence of α for the $C^{13}O-C^{12}O$ System

Temp., °K	$\frac{1}{T}\cdot 10^3$	P_{CO}, mm with 23%	P_{CO} with 23%	P_{CO} with 23%	P_{CO} with 100%	α	Error	log α·10³
69,0	14,492	132,0	0,38	—	1,73	1,0131	±0,0004	5,65
69,4	14,409	144,0	—	0,57	1,84	1,0128	±0,0004	5,52
70,1	14,265	155,0	—	0,59	1,90	1,01226	±0,0004	5,29
71,0	14,084	174,0	0,48	—	2,18	1,0125	±0,0003	5,39
79,8	12,531	513,7	—	1,88	6,06	1,0102	±0,0003	4,41
80,7	12,391	656,0	1,43	—	6,50	1,00991	±0,0002	4,28
81,6	12,254	760;0	—	2,2	7,10	1,00934	±0,0002	4,04
81,9	12,210	800,0	1,65	—	7,50	1,00938	±0,0002	4,05
85,0	11,764	1026	—	2,8	9,03	1,00903	±0,0002	3,90
85,2	11,737	1064	2,03	—	9,23	1,00867	±0,0002	3,75
90,2	11,086	1634	—	3,91	12,61	1,00772	±0,0001	3,34
91,7	10,905	1824	3,00	—	13,64	1,00748	±0,0001	3,23
99,2	10,080	3116	4,43	—	20,14	1,00646	±0,0001	2,79
101,2	9,881	3752	—	7,21	23,26	1,00620	±0,0001	2,68

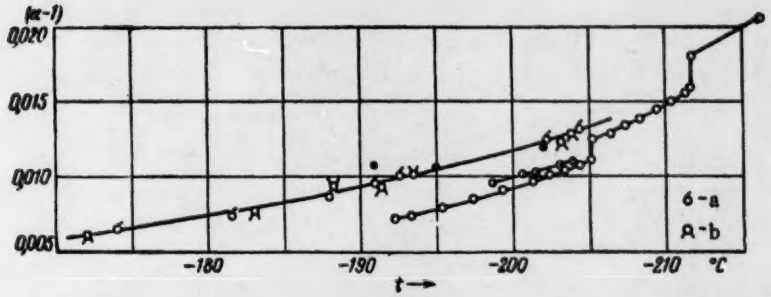

Fig. 3. Comparison of the values of the separation coefficients obtained by various investigators: 1) according to [4]; 2) according to [2]; 3) according to [3]; 4) experimental data for specimens containing: a) 23% $C^{13}O$; b) 32% $C^{13}O$.

in which ΔP is the measured pressure difference, P is the pressure in the cells, and N_1 and N_2 are the respective mole fractions of C^{13} in the cell contents.

The results of these measurements are presented in Table 1 and in Fig. 2. It is to be seen from the table that α diminishes with rising temperature. The temperature dependence of the separation coefficient can be represented by the equation:

$$\alpha = Ae^{B/T}. \tag{2'}$$

This is the equation of a straight line in the coordinates log α, 1/T. The values of the constants A and B can be obtained from Fig. 2.

$$A = 0{,}9954 \text{ and } B = 1{,}477.$$

The coefficient B is equal to the ratio between the difference in the heats of vaporization of the two isotopic forms of carbon monoxide and the molar gas constant:

$$B = \frac{\lambda_{C^{13}O} - \lambda_{C^{12}O}}{R} = \frac{\Delta\lambda}{R}. \tag{3'}$$

$$R = 1{,}987 \text{ cal/deg} \qquad \Delta\lambda = 2{,}93 \text{ cal/mole}$$

The results of our measurements on the separation coefficient in the $C^{13}O-C^{12}O$ system over the extended temperature interval from −205 to −170°C are in good agreement with those of Devyatykh et al., [3], but deviate somewhat from the values obtained by Groth et al., [2], Kronberger [1], and Johns [4].

Figure 3 shows the temperature dependence of the α values reported by various investigators.

LITERATURE CITED

[1] H. Kronberger, Birmingham Univers. (1948).

[2] W. Groth, H. Ihle, and A. Murrenhoff, Z. Naturforsch. 9A, 805 (1954).

[3] G. G. Devyatykh, A. D. Zorin, and N. N. Nikolaev, Zhur. Priklad. Khim. 3 (1958).*

[4] T. F. Johns, Proceedings of the International Symposium on Isotope Separation (North-Holland, Amsterdam, 1958).

*Original Russian pagination. See C. B. Translation.

ANODIC PROCESSES IN THE ELECTROLYSIS OF SALTS OF CARBOXYLIC ACIDS

M. Ya. Fioshin and Yu. B. Vasil'ev

Institute of Electrochemistry of the Academy of Sciences of the USSR
(Presented by Academician A. N. Frumkin, May 6, 1960)
Translated from Doklady Akademii Nauk SSSR, Vol. 134, No. 4, pp. 879-882, October, 1960
Original article submitted April 28, 1960

It has more than once been noted in the literature [1-9] that the Kolbe reaction, $2CH_3COO^- - 2e \rightarrow C_2H_6 + 2CO_2$, takes place at the anode at potentials higher than the potential corresponding to oxygen evolution. It is only possible for such processes to take place in aqueous solutions under conditions under which the evolution of oxygen is impeded.

A number of authors [10-20] have observed during studies of the anodic evolution of oxygen under high potentials at a platinum electrode that retardation of this reaction occurs, and that waves appear whose maximum current diminishes with increase in the concentration of the solution. In certain cases [13], the investigators consider that the retardation is due to a change in the composition of the surface caused by the formation of higher oxides of platinum, or compounds of platinum with the radicals formed by ion-discharge. It is supposed by other authors that the phenomenon is due to the adsorption of anions [11, 12, 15].

We have investigated the anode process taking place during the electrolysis of sodium acetate, using a rotating platinum disc anode. The investigation has taken the form both of recording the polarization curves by the compensation method, and of obtaining polarograms on PÉ-312 and Heyrovsky polarographs. As the result of preliminary alternating cathode-anode polarization (by the method described in [21]), and high purity of solution, excellent reproduction was attained, amounting to 1% for the current, and 5 mv for the potential.

Figure 1 gives the anodic curves for sodium acetate in a base solution of 0.575 N sodium bicarbonate. It can be seen from this that the curve obtained in the absence of sodium acetate rises smoothly, but that the curves acquire maxima as soon as sodium acetate is present in the solution. The first portion of the curves corresponding to the presence of sodium acetate always reproduce the base-solution curve, while the second part lies beneath the base-solution curve. The higher the acetate concentration, the lower the height of the maximum, and the lower the positive potential at which the braking process occurs. All this evidence points to the retardation process being associated with the concentration of acetate in the solution and not with the formation of higher oxides – which cannot be reconciled with the absence of retardation in the pure base solution. We have studied the effect of various factors on the retardation process. The fact that the current at the maximum is independent of the rate of rotation of the electrode suggests that the cause of the maximum is of a kinetic nature.

Figure 2 gives the curves of potential against log I for pure solutions of sodium acetate of various concentrations. The curves possess two linear portions. The first, 1.8–2.1 v, of slope 0.220, corresponds to evolution of oxygen, as analysis of the anode gases has proved. The negligible increase in the overpotential in this region for high concentrations of sodium acetate is probably connected with the reduction in the activity of the water in concentrated solutions. The anode gases at the second part of the curves contain carbon dioxide, ethane, and other products of the Kolbe synthesis, which therefore indicates that discharge of acetate ions is taking place. Changing the acetate activity by a factor of 10 causes a parallel shift of the second portion of the curve by

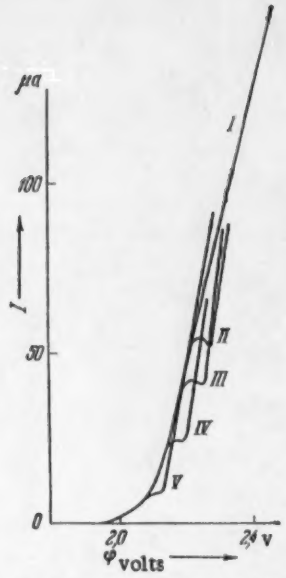

Fig. 1. Polarograms of sodium acetate on a platinum electrode I) Base solution of 0.575 N sodium bicarbonate; II) base solution + 0.1 N sodium acetate; III) base solution + 0.2 N sodium acetate; IV) base solution + 0.3 N sodium acetate; V) base solution + 1 N sodium acetate. Temperature = 25°C.

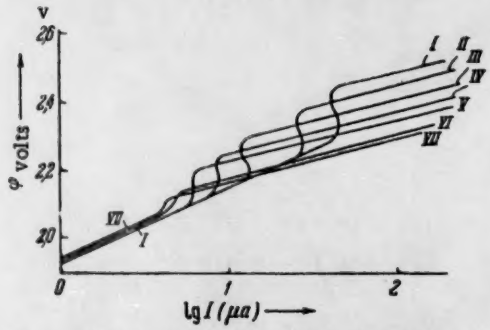

Fig. 2. Polarization curves for solutions of sodium acetate of various concentrations: I) 0.1 N; II) 0.2 N; III) 0.6 N; IV) 1 N; V) 1.6 N; VI) 3.0 N; VII) 4.0 N. Temperature = 25°C.

0.120 volt in the direction of less positive values. At constant potential, the relationship between the current and the acetate activity on the second part of the polarization curve is linear, and the line passes through the origin: that is, the discharge of acetate ions is a first-order reaction. This second part of the polarization curve, corresponding to the discharge of acetate ions, may be described by the following equation, which we have derived from the experimental data:

$$\varphi' = 2{,}43 - 0{,}120 \lg a_{CH_3COO^-} + 0{,}120 \lg I. \quad (1)$$

(where a is the activity of the acetate ions).

The transition to the Kolbe electrochemical synthesis is only possible because of the retardation of the oxygen evolution process, and the maximum on the curve at a potential of 2.1 to 2.2 volts is a consequence of this phenomenon.

The current at this maximum diminishes with increase in the acetate activity, and the relationship of log I at the maximum to the logarithm of the activity corresponds to a straight line (see Fig. 3), from which it follows that:

$$I_{max} = \frac{A}{a^n_{CH_3COO^-}}, \quad (2)$$

where A is a constant, and n = 0.56 for sodium acetate. As has been said, a tenfold increase in the acetate activity causes the potential Φ, at which retardation arises, to shift by 120 mv towards a lower positive potential, and thus,

$$\Phi = \Phi^0 - \frac{RT}{\alpha_2 F} \ln [CH_3COO^-] = 2{,}134 - 0{,}120 \lg a_{CH_3COO^-}. \quad (3)$$

The relationship of the potential at the commencement of retardation and of the maximum value of the current to the activity of the acetate shows that the retardation is observed because of the adsorption of acetate ions, which leads to a reduction in the surface concentration of water molecules (or hydroxyl ions) and therefore, to a drop in the current. This drop in current will occur for as long as the potential has not reached the discharge potential of the acetate ions, after which a new rise in the polarization curve will be observed, corresponding to the occurrence of the Kolbe synthesis. When the potential change is reversed, the maximum is not

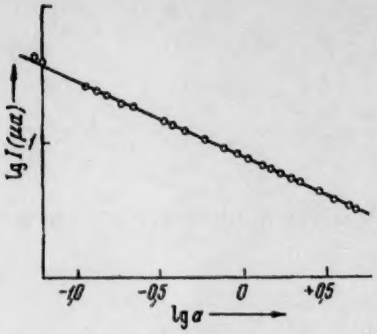

Fig. 3. Relationship of the logarithm of the maximum current to the logarithm of the activity of the sodium acetate at 25°C.

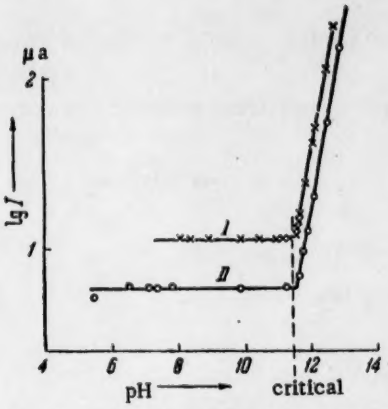

Fig. 4. Effect of the pH of the solution on the maximum current: I) 0.6 N sodium acetate; II) 2.0 N sodium acetate. Temperature = 25°C.

reproduced, and hysteresis occurs. Variation in the rate of potential change causes variation in the height of the maximum current, and also in the depth of the drop.

Change in the pH of the solution up to pH = 11.5 has no effect on the polarization curve or on the maximum current. When the pH is greater than 11.5 the first part of the curve, which corresponds to the evolution of oxygen, is shifted by an amount of 220 mv towards lower potentials for unit pH increase. The position of the second part of the polarization curve, corresponding to the discharge of acetate ions, is not altered. This phenomenon is presumably connected with the the fact that in acid, neutral and weakly alkaline solutions of sodium acetate, the oxygen is evolved because of the discharge of molecules of water: $H_2O - e \rightarrow OH^- + H^+$, so that the position of this part of the curve does not depend on the pH. When pH is greater than 11.5, the evolution of oxygen occurs through the discharge of hydroxyl ions:

$$OH^- - e \rightarrow OH.$$

It follows that in sodium acetate solutions the transition from the evolution of oxygen by discharge of water molecules to its formation by the discharge of hydroxyl ions only occurs when the pH has reached 11.5.

It is very clear from Fig. 4 that the maximum current is independent of the pH right up to the value of 11.5, while further rise in pH causes a rapid increase in the current. That is:

$$\lg I_{max} = \text{const} + \text{pH}. \quad (4)$$

The potential at retardation Φ is not changed at all over the whole range of pH changes. It is known from earlier publications [8, 22] that when pH exceeds 11 the Kolbe reaction is suppressed, and once again oxygen becomes the major product at the anode.

Temperature change has a profound influence on the composition of the products in the Kolbe electrochemical synthesis. Our investigations have shown that the height of the current maximum, which corresponds to the retardation of the oxygen evolution process, increases rapidly. The relationship of the logarithm of the maximum current to the reciprocal of the temperature is a straight line, or,

$$\lg I_{max} = A + \frac{B}{T}. \quad (5)$$

As the temperature rises the retardation potential, in accordance with Eq. (3), is only slightly shifted in the direction of smaller values.

We have thus been able to establish laws for the transition from the anodic evolution of oxygen to the Kolbe electrolytic synthesis which show that it is due to the retarding effect on the former process caused by adsorption of acetate ions. The effect of various conditions on the inhibition of oxygen evolution has been studied.

LITERATURE CITED

[1] E. Bose, Z. Elektrochem. 5, 169 (1898-1899).

[2] F. Foerster and F. Piguet, Ann. 323, 304 (1902).

[3] B. Hofer and M. Moest, Z. Elektrochem. 10, 833 (1904).

[4] G. Preuner, Z. Phys. Chem. 59, 670 (1907).

[5] G. Preuner and E. B. Ludlam, Z. Phys. Chem. 59, 682 (1907).

[6] O. J. Walker, J. Chem. Soc. 2040 (1928).

[7] S. Glasstone and A. Hickling, Trans. Electrochem. Soc. 25, 333 (1939); A. Hickling, Trans. Farad. Soc. 133, 1540 (1937).

[8] N. I. Dedusenko, Dissertation [in Russian] (Alma-Ata, 1950).

[9] K. Sugino and S. Aoyagi, Nikhon kagaku dzassi 79, 1202 (1958).

[10] R. I. Kaganovich, M. A. Gerovich, and É. Kh. Enikeev, Doklady Akad. Nauk SSSR 108, 107 (1956).*

[11] M. A. Gerovich, R. I. Kaganovich, V. A. Vergelesov, and A. N. Gorokhov, Doklady Akad. Nauk SSSR 114, 1049 (1957).*

[12] A. N. Frumkin, R. I. Kaganovich, M. A. Gerovich, and V. N. Vasil'ev, Doklady Akad. Nauk SSSR 102, 981 (1955).

[13] V. I. Veselovskii, Papers presented to the Fourth Conference on Electrochemistry [in Russian] (Moscow, 1959) p. 241.

[14] A. A. Rakov, É. V. Kasatkin, and K. I. Nosova, Papers presented to the Fourth Conference on Electrochemistry [in Russian] (Moscow, 1959) p. 834.

[15] G. Érdei-Gruz and I. Shafarik, Papers presented to the Fourth Conference on Electrochemistry [in Russian] (Moscow, 1959) p. 263.

[16] Chu Yung-chao, Hsü Chen-yen, Huang Ch'u-pao, Ling Chao-ch'in, Sci. Res. 2, 373 (1958).

[17] Ts'u Yung-ts'ao and Mi T'ieng-ying, Doklady Akad. Nauk SSSR 125, 1069 (1959).*

[18] I. I. Appenin, Zhur. Fiz. Khim. 33, 367 (1959).

[19] K. Sugino and S. Aoyagi, J. Electrochem. Soc. 103, 166 (1956).

[20] R. I. Kaganovich and M. A. Gerovich, Papers presented to the Fourth Conference on Electrochemistry [in Russian] (Moscow, 1959) p. 277.

[21] G. A. Tedoradze, Dissertation [in Russian] (Moscow, 1957).

[22] I. Petersen, Z. Phys. Chem. 33, 99 (1900).

* Original Russian pagination. See C. B. Translation.

THE STATISTICAL THEORY OF RADIATION-CHEMICAL REACTIONS IN CONDENSED MATERIALS

Yu. L. Khait

The Institute of Petrochemical Synthesis of the Academy of Sciences of the USSR
(Presented by Academician A. V. Topchiev, May 10, 1960)
Translated from Doklady Akademii Nauk SSSR, Vol. 134, No. 4, pp. 883-886, October, 1960
Original article submitted May 10, 1960

It is known that radiochemical reactions consist of a series of successive stages (the formation of ions, free radicals, etc.). Some of the stages of these reactions constitute the elementary acts of activation processes, in each of which a work E' is performed, where E' is a value exceeding certain threshold values $E \gg kT$ (where k is the Boltzmann constant and T the mean absolute temperature of the system). Under the influence of irradiation, the rates of the reactions increase, and it is not possible to explain this by any increase in the mean temperature T which the irradiation may bring about [1-3]. Attempts to explain this fact on the basis of the theory of absolute rates, without taking into account the collective character of the movement of particles in a condensed phase, have encountered serious difficulties. In [4] a method is proposed for calculating the rate of activation processes in condensed bodies, accounting statistically for the collective character of the movement of their particles, without reference to mechanisms.

This method is generalized below, with a view to taking into consideration also the effect of ionizing radiation. We consider initially a homogeneous equilibrium system with volume V and energy E_0. We divide this up into $N = V/l^3$ elements of volume μ_p, with mean volume l^3 ($p = 1,2,\ldots N$) under conditions such that $V^{1/3} \gg l \gg h\nu/kT = \varkappa$ [10], where ν is the mean rate of transfer of energy to the system of particles (quasiparticles) involved in the process under consideration. The multiplicity M of possible values of the energy U_p of each element μ_p is unlimited. Chance variations in U (and the internal parameters f_p) we describe by local probability functions $U_p(t, \beta)$ and $f_p(t, \beta)$, where t is the time, β is the realization number $U^{(\beta)}(t)$ of the process $U_p(t, \beta)$ [5, 6]. It is usually accepted that the states of equilibrium of the system form a homogeneous Markovskii process, possessing ergodic properties, while the fluctuations are described by a gaussian distribution [7]. In accordance with this, we shall assume that N processes $U_p(t,\beta)$ [or $f_p(t, \beta)$] form an N-fold stationary normal Markovskii probability function $U(t,\beta)$ [or $f(t, \beta)$] [6], which may be differentiated throughout with the exclusion of the final multiplicity of points. With stationary processes the distribution for $U_p(t,\beta)$ and $\dot{U}_p(t)$ are independent [8, 9]. Therefore $\sigma^2 = \overline{[U_p(t)]^2}$ does not depend on the values of $U_p(t,\beta)$ and is equal to $\sigma = \omega_0\alpha$ [8, 9], where $\alpha^2 = \overline{(U(t, \beta) - \bar{U})^2}$; ω_0 is a quantity with the dimensions of a frequency depending on l, and the line denotes averaging. The mean change $\overline{\Delta U(\tau)}$ in the energy U for a time τ is equal to $\overline{\Delta U(\tau)} \approx \sigma\tau = \omega_0\alpha\tau$ [6, 8]. We select l in such a way as to fulfill the conditions:

$$\overline{\Delta U(\tau)} < E \ll \bar{U}_0, \tag{1}$$

where $U_0 = nkT$; $n = \gamma l^3/d^3$; γ is the number of degrees of freedom in the volume d^3 entering into a single particle. The relationship $\omega_0(l)$ is, in general, of unknown form. We shall therefore avail ourselves of the indeterminacy relationship:

$$l^2 \ll d^2 \frac{E}{kT}\frac{d}{\lambda_T}; \quad l^3 \gg \frac{E}{kT\gamma} d^3; \quad \left(\frac{E}{\gamma kT}\right)^{1/2} \gg \left(\frac{\lambda}{d}\right)^{1/2}, \quad \lambda = \frac{\hbar v}{kT}. \tag{2}$$

The regions μ_p, limited by the conditions (1) and (2) in the time interval τ are, with a sufficient degree of accuracy, closed.

We divide the time of observation into nonoverlapping intervals $\tau_s = \tau$ (s = 1,2,...). To each value of τ_s we compare N infinite differentiated functions $\{\delta_p(\tau_s, t)\}$, , equal to zero outside the intervals τ_s, and the normalized conditions $\int_{-\infty}^{\infty} \delta_p(\tau_s, t)\, dt = 1$. By means of these we construct generalized probability processes [11]: $U_p(\tau_s, \beta) = \int_{-\infty}^{\infty} \delta(\tau_s, t) U_p(t, \beta)\, dt = \hat{\delta}_p(\tau_s) U_p(t, \beta)$, which we consider as real operators $\hat{\delta}_p(\tau_s)$ with argument t. We introduce the operator R acting on the variable β, which we determine by means of the formula $\hat{R}U_p(t, \beta) = \overline{U}_p^{(\beta)}(t)$, for which $\hat{R}\hat{\delta}_p(\tau_s) - \hat{\delta}(\tau_s)\hat{R} = 0$, since the two operators operate in different areas. We divide the multiplicity M by the nonoverlapping integrals $\Delta_r \approx \overline{\Delta U(\tau)}$ $(r = 1,2,\ldots)$. During each interval τ_s the values $U = U_\tau$ are on the average in some interval Δ_r and are equal to $U_\tau \approx U_p^{(\beta)}(\tau_s) = \hat{\delta}_p(\tau_s)\hat{R}U_p(t, \beta)$. If we make use of the concept of the generalized vector function [12] and the quasienclosed regions μ_p, we may write the law of conservation of energy in the form $\hat{\delta}(\tau_s)\hat{R}\,\mathbf{U}(t, \beta) = \sum_p U_p^{(\beta)}(\tau_s) = E_0$ where $\hat{\vec{\delta}}(\tau_s)$ is a vector operator with components $\hat{\delta}_p(\tau_s)$. The state of the system in the time interval τ_s may be determined by means of completing numbers b_r of intervals Δ_r, the mean value of which $\overline{b}_r$ may be found (taking no account of the mutual correlation of the regions μ_p) by the methods set out in [13]. On the other hand, the state of the system constitutes a homogeneous probability gaussian field [6], set by the threefold summation of the regions μ_p, which corresponds to the treatment of the fluctuations as a function of the coordinates [7], while U(t, β) describes the evolution of these states with time.

We consider a nonequilibrium system in which the thermal activation process is possible but other process forms do not occur. Appreciable changes in the mean values $\overline{U_p(t, \beta)}$ are brought about in the interval $\Delta t > 1/w$, where $\underline{w}$ is the probability of the elementary act in the region μ_p reduced to unit time. Hence, during a small interval of time, the quantity $\overline{U}(t)$ is a linear function of the time, and such a system may be described by means of a probability process with stationary increment [6, 11] which, during an interval of the order of 1/w may be regarded as stationary and have applied to it the description given above. The energy U_τ is distributed in a probability manner between $\underline{n}$ degrees of freedom of the region μ_p, to which some distribution and entropy function $S(U_\tau)$ will apply. There exists a conditional probability $w(E/U_\tau)\tau_s$ such that in the time interval τ_s the energy $E' \geq E$ is found to be focussed in different degrees of freedom [the entropy is $S(U_\tau - E)$], on account of the considerable change in state of the residual degrees of freedom of the region μ_p (the act of destruction of the casual process [5]).* This probability is determined by means of the statistical weight of the corresponding states [4]:

$$w\left(\frac{E}{U_\tau}\right) \approx \frac{kT(U_\tau - E)}{\hbar} \exp\left\{\frac{S(U_\tau - E) - S(U_-)}{k}\right\}. \tag{3}$$

A similar result may be obtained for each τ_s and U_τ, while $\underline{w}$ is found by neutralizing $w(E/U_\tau)$ with time, which, because of the ergodic processes $U_p(t, \beta)$, can be changed to neutralizing with respect to the probability W(U) dU (normal distribution). This method permits one to find the rates of the processes occurring on

*We note that (2) gives rise to the inequality $\tau \ll t_0 \ll 1/w$, making it possible to describe the process $U_p(t, \beta)$ by means of a discrete multiplicity of values [17], and also to neglect the correlation between the unit acts in one region and in the other regions μ_p (t_0 = "radius" of the autocorrelation).

thermal excitation of the regions μ_p [4, 15].* We are here neglecting the influence of ionizing radiation. If we suppose that a particle enters the system having an energy $\epsilon_0 \gg E$, and a velocity v_0, we may suppose that its interaction with the body leads to the generation of energy E in a volume Q, and that the occurrence of any elementary acts with threshold energy E within the volume Q is determined by the statistical weight of the state of this volume as expressed in its entropy. This assumption would be a good approximation if the volume Q possessed many degrees of freedom, and the equilibrium set up within it exists in exchange interaction with the remaining particles of the system.** If we limit the volume Q by conditions similar to (1), but taking into account the effect of irradiation, we have:

$$\overline{\Delta U_f(\tau_f)} < E < U_0 + \Delta E; \quad \frac{U_0 + \Delta E}{m} = aE, \; 0 < a \lesssim 1, \tag{4}$$

where $m = \gamma Q/d^3$. We consider the thermal excitation in the regions Q as being the same as in the subsystems μ_p. It then follows from the inequality (4) that the concentration of the products of the activation process in the volume Q may be regarded as quasistationary, while the energy of movement of the different degrees of freedom is less than the threshold energy E. If, however, the equilibrium is not completely established, then we should expect that the statistical description would give an upper limit of the number of completed elementary acts.

We consider the multiplicity of the volumes Q which simultaneously undergo excitation by means of ionizing particles, and deal with the state of statistical equilibrium between the forward and reverse acts. By means of the principle of detailed equilibrium similar to that described in [4], in relationship to the thermal excitation of the regions μ_p we obtain the formula:

$$w\left(\frac{E}{U_f}\right) = q\,\frac{kT\,(U_f - E)}{\hbar}\exp\left\{\frac{S\,(U_f - E) - S\,(U_f)}{k}\right\}, \tag{5}$$

similar to (3) for the conditional probability $w(E/U_f)$ converted to unit time, for the formation in volume Q_f of excitation $E' \geq E$, which leads to the occurrence of the reaction with which we are concerned. In formula (5), in distinction to (3), the magnitude $U_f = U_\tau + \Delta E$ is the total energy of the degrees of freedom considered in the volume Q_f; and U is their energy at the instant of impact of the ionizing particle in the volume Q_f. The mean probability w_r, which is being searched for, (in relation to unit time) of the occurrence of a single act in the region Q is found by means of the neutralization of the quantity $w(E/U_f)$ for all possible values of U_f according to the formula:

$$w_r = \frac{1}{b}\iint w\,(U_f)\,w\left(\frac{E}{U_f}\right)\tau_f dU\,d\,(\Delta E), \tag{6}$$

where $w\,(U_f)\,dU\,d\,(\Delta E) = w\,(U)p\,(\Delta E)\,dU\,d\,(\Delta E)$ is the probability (in unit time) of the occurrence of two independent events: first, that at the moment of impact of the ionizing particle in the volume Q its energy is equal to U; and, second, that the ionizing particle releases the energy ΔE in the volume Q. The probability of the latter event is given by:

$$p(\Delta E) = \int \varphi\,(\varepsilon_0)\,p\,(\varepsilon_0,\,\Delta E)\,d\varepsilon_0 = j\int \varphi\,(\varepsilon_0)\,\Sigma\,(\varepsilon_0,\;\Delta E)\,d\varepsilon_0 = \overline{j\Sigma\,(\Delta E)}, \tag{7}$$

where $\underline{j}$ is the density of the current of ionizing particles making impact on the volume Q_f; $\varphi\,(\epsilon_0)$ is the distribution function for the energy in this current; $p(\epsilon_0, \Delta E)$ is the probability (in unit time) that a particle with energy ϵ_0 will liberate to the volume Q_f the energy ΔE; and $\Sigma\,(\varepsilon_0,\;\Delta E) = p\,(\varepsilon_0,\;\Delta E)/j$ is the cross section of this process. Taking into account that w(U) is the normal distribution, and utilizing the method which

* If in each elementary act a contribution is made to the degrees of freedom of various types, these contributions must be considered as local chance events, taking account of their partial entropies, etc. With change of temperature and other conditions the part played by these contributions can also be changed.

** There is here assumed a situation in some sense analogous to the statistical theory of the multiplicity of the origin of mesons [18].

was also used in [15], we may carry out the division of $S(U_f - E)$ according to the stages E, and integrate with respect to dU, obtaining by means of (5) and (6), the relationship:

$$w_r \approx \frac{jq^k\tau_j}{b\hbar}\int \overline{\Sigma(\Delta E)}\, T(U_f)\exp\left\{\frac{E^2}{2\alpha^2}\right\}\exp\left\{-\frac{E}{kT_{ef}}\right\} d(\Delta E), \qquad (8)$$

where c is the heat capacity of the degrees of freedom considered for the volume Q, while $T_{ef} \approx T + \Delta E/c$. It follows from (8) that the probabilities of the elementary acts are determined, not by the mean temperature T, but by the local time-dependent temperature $T_{ef} > T$ of the region Q. For values of ΔE which are not too low, and small values of c, the "addition" $T = \Delta E/c$ may be seen to be large. In particular, a considerable reduction in T leads to a retardation of the radiation-chemical reaction which is not specially great, since in this case c is small, and $\Delta T \approx \Delta E/c$, and therefore T_{ef} will not be small. If $(\Delta E/cT)^2 \ll 1$, then Eq. (8) may be rewritten in the form:

$$w_r = \frac{j\tau_f q^k}{b\hbar}\int \overline{\Sigma(\Delta E)}\, T(U_f)\exp\left\{\frac{E^2}{2\alpha^2}\right\}\exp\left\{\frac{E\Delta E}{kT^2c}\right\}\exp\left\{-\frac{E}{kT}\right\} d(\Delta E). \qquad (9)$$

It follows from Eqs. (8) and (9) that increase in E may cause an increase in the rates of the radiation-chemical processes or, at all events, only a relatively small reduction in these. In the calculation it is assumed that $\Delta E \ll \bar{U}$ and $\Sigma(e_0, \Delta E)\tau_i j \ll 1$. To obtain the complete number of elementary acts, it is necessary to carry out a summation of the magnitudes w_r for all the volumes Q which are simultaneously submitted to radiation excitation, and then to sum the result with respect to time. The values of the quantities ΔE, l, Q should be determined from the experiment.*

Finally, we would express our deep gratitude to L. S. Polak, and also to Yu. S. Lazurkin for discussion of the results and critical comments, and to A. Ya. Temkin and M. A. Mokul'skii for helpful discussions.

LITERATURE CITED

[1] M. A. Makul'skii, Yu. S. Lazurkin, et al., Doklady Akad. Nauk SSSR 125, 1007 (1959).**

[2] N. M. Tikhomirova, Yu. M. Malenskii and V. L. Karpov, Doklady Akad. Nauk SSSR 130, 5, 1081 (1960).**

[3] M. A. Makul'skii, Vysokomolekulyarnye soedineniya 1 (1960).

[4] Yu. L. Khait, Izvest. Akad. Nauk SSSR, Ser. Fiz. 24, 202 (1960).

[5] B. V. Gnedenko, Course in the Theory of Probability [in Russian] (1954).

[6] A. M. Yaglom, Usp. Maten. Nauk, 7, No. 5 (1952).

[7] M. A. Leontovich, Statistical Physics [in Russian] (1944).

[8] Bartlett, Introduction to the Theory of Chance Processes [Russian translation] (IL, 1958).

[9] B. R. Levich, The Theory of Chance Processes and Their Application in Radiotechnique [in Russian] (1937).

[10] L. É. Gurevich, The Bases of Physical Kinetics [in Russian] (1940).

[11] I. M. Gel'fand, Doklady Akad. Nauk SSSR 100, 853 (1955).

[12] I. M. Gel'fand and G. E. Shilov, Generalized Functions [in Russian] (1958) Vol. 1.

[13] E. Schrodinger, Statistical Thermodynamics [in Russian] (1948).

[14] L. D. Landau and E. M. Livshits, Statistical Physics [in Russian] (1951).

* We note that in the expression for the distance r from the trajectory of a charged particle in the spectrum of the field, the fundamental frequency occurs: $\nu \approx v_0/r$ [16]. It follows that a considerable contribution to the distances $r \lesssim v_0 h/E$ is given by frequencies $\nu > E/h$, which are able to bring about excitation $E' \gtrsim E$.

** Original Russian pagination. See C. B. Translation.

[15] S. Z. Roginskii and Yu. L. Khait, Doklady Akad. Nauk SSSR 130, No. 2 (1960).*

[16] L. D. Landau and E. M. Livshits, Electrodynamics of Continuous Media [in Russian] (1957).

[17] Yu. K. Belyaev, The Theory of Probability and Its Applications [in Russian] (1959) Vol. 4, p. 437.

[18] E. Fermi, Elementary Particles [Russian translation] (IL, 1953); L. D. Landau, Izvest. Akad. Nauk SSSR, Ser. Fiz. 17, 51 (1953).

*See C. B. Translation.

THE VOLUMES OF GASEOUS SOLUTIONS OF WATER IN ETHYLENE AT HIGH PRESSURES AND TEMPERATURES

D. S. Tsiklis, A. I. Kulikova, and L. I. Shenderei*

State Scientific and Research and Planning Institute for the Nitrogen Industry and the Products of Organic Synthesis
(Presented by Academician A. N. Frumkin, May 18, 1960)
Translated from Doklady Akademii Nauk SSSR, Vol. 134, No. 4, pp. 887-890, October, 1960
Original article submitted May 18, 1960

The volumes of gaseous solutions of water in compressed ethylene at temperatures between 200° and 300° and pressures between 100 and 150 atm have been measured by a method employing a constant capacity piezometer. The plant is described in Fig. 1. Into apparatus 1 of known capacity a definite quantity of water and of ethylene was introduced through valve 3. The composition of the solution was chosen in accordance with data concerning the phase equilibria in this system which has been obtained earlier [1]. The apparatus was heated, the gaseous solution was stirred by means of the electromagnetic stirrer 2. The pressure was measured and, by means of the membrane valve 4, part of the solution was transferred to the evacuated, calibrated flask 13, and then condensed by means of water in the ampoule 11. After the removal of the sample the solution was stirred again, the pressure measured, and a portion of the solution again removed. The procedure was repeated until the whole of the mixture charged into the apparatus had been exhausted. When a balance was set up, the mean composition of the mixture was determined, and, knowing the relationship between the molar volume of a solution of this composition and the pressure, the molar volume was found from the saturation curve.

The membrane valve 6 mounted in the column 5 served to connect the pressure-measuring apparatus 7 with the system. The measuring system consisted of membranes, which acted as a null point,** and electron tubes 8, which were activated by the closing of an electrical circuit by the membranes. The oil pressure created by the compressor 9 in the space above the membrane was so arranged that the tube 8 was activated or extinguished by pressure changes of the order of an atmosphere. At this point the pressure of oil (which is equal to the pressure in the apparatus) is measured by means of the standard manometer 10 of type 0.35. On removal of a test specimen the water in the ethylene is condensed into ampoule 11 at the temperature of liquid nitrogen. The ampoule is then heated to the temperature maintained by a mixture of solid carbon dioxide and acetone, and the evaporated ethylene is pumped out by means of the mercury pump 12 into an evacuated flask of 15 liters capacity.

The volume of the column is determined by calibration by means of a gas having a known compressibility. The change in volume of the column with temperature is estimated from the equation for the cubical expansion of stainless steel [3]. The experimental results are given in Table 1.

Figure 2 gives the values found for the extrapolated volumes of solutions of water in ethylene along the saturation curve.

---

* V. I. Alisova helped in the carrying out of the experiments.

** The apparatus was constructed by us on the principle of fully supported membranes which had been used earlier in the membrane valve [2].

EXPERIMENTAL

The thermodynamic properties of a substance are most conveniently expressed in terms of p, v and T data, if these are presented in the form of an equation of state. We have made attempts to express the behavior of the solutions studied by the equation of state in the virial form [4]:*

$$pv = RT\,(1 + B\,(T)/v + C\,(T)/v^2), \tag{1}$$

Equation (1), in which p is the pressure, v the molar volume, R the gas constant, and B(T) and C(T) the second and third virial coefficients, is the form employed. For the determination of the coefficients B and C the equation is converted into the straight-line form,

$$\left(\frac{pv}{RT} - 1\right) v = B + C/v. \tag{2}$$

If the experimental data are inserted in Eq. (1), the values of the left-hand side of Eq. (2), calculated from the experimental data and against 1/v, should lie on a straight line intersecting the axis at a value B_p, and having a slope against the axis of abscissas equal to C_p (where B_p and C_p are the second and third virial coefficients of a gaseous solution of the given concentration).

The calculations we have made show that the values given for the left-hand side of Eq. (2) – Δ fit well on to a straight line, and therefore we have been able to calculate the values of B_p and C_p for the solutions which we have studied.

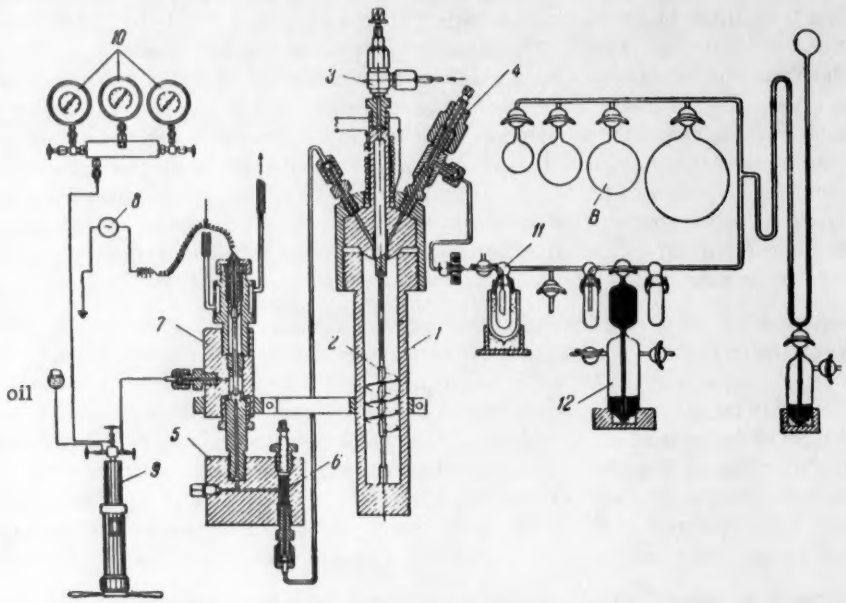

Fig. 1. Apparatus for the determination of the volumes of gaseous solutions.

In order to be able to calculate the volumes of solutions of any composition, in addition to those which have been investigated, it is necessary to know the dependence of the second and third coefficients on the concentration. This is given by Eqs. (3) and (4):

$$B_p = B_{11}N_1^2 + 2B_{12}N_1N_2 + B_{22}N_2^2; \tag{3}$$

$$C_p = C_{111}N_1^3 + 3C_{112}N_1^2N_2 + 3C_{122}N_1N_2^2 + C_{222}N_2^3. \tag{4}$$

* This idea and the method of calculation were proposed by I. R. Krichevskii.

TABLE 1

Molar Volumes (liters/mole) of Solutions of Water in Ethylene. N_2 = Molar Fraction of Ethylene in the Solution

P, atm	v	P, atm	v	P, atm	v	P, atm	v
			200°				
$N_2 = 0,287$		$N_2 = ,500$		$N_2 = 0,773$		$N_2 = 0,90$	
1,97	17,85	1,77	29,3	3,70	10,26	8,8	4,32
4,70	7,86	5,16	7,39	14,45	2,55	32,6	1,112
8,16	4,43	9,13	4,05	27,1	1,38	58,6	0,594
11,7	2,94	14,07	2,45	39,85	0,914	84,3	0,403
15,9	2,14	23,75	1,45	53,80	0,662	98,3	0,340
			250°				
$N_2 = 0,237$		$N_2 = 0,546$		$N_2 = 0,760$		$N_2 = 0,925$	
2,3	18,45	6,3	6,63	51,0	0,823	7,8	5,247
10,1	3,81	24,6	1,684	67,8	0,616	43,6	0,925
19,3	2,04	42,6	0,974	83,8	0,489	74,1	0,549
30,2	1,27	59,6	0,674	101,2	0,398	100,2	0,399
42,2	0,889	76,0	0,508	115,7	0,345	126,8	0,314
				128,8	0,306		
			300°				
$N_2 = 0,212$		$N_2 = 0,385$		$N_2 = 0,551$			
6,4	7,152	4,7	9,63	5,8	7,59		
20,4	2,224	21,8	2,023	25,2	1,801		
40,9	1,055	35,5	1,242	50,4	0,879		
70,4	0,592	52,2	0,827	74,4	0,578		
88,1	0,451	68,0	0,621	107,5	0,394		
		83,7	0,496	128,3	0,325		
		90,5	0,457				
		98,8	0,419				

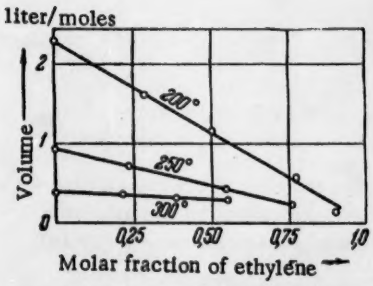

Fig. 2. Volumes of gaseous solutions of water in ethylene along the saturation lines.

where B_{11}, B_{22}, C_{111} and C_{222} are the second and third virial coefficients of pure water and pure ethylene, while B_{12}, C_{112} and C_{122} are the second and third virial coefficients, taking account of binary and ternary interactions. Knowing the values of B_{12}, C_{112} and C_{122}, it is possible to calculate B and C, and therefore also the molar volumes of solutions of water in ethylene of any composition.

For the calculation of B_{12} a graph was constructed of the values of the right-hand side of Eq. (5) against N_1N_2, using the direct method of least squares. The slope of this straight line was then obtained.

$$[2B_{12}N_1N_2 = (B_p - B_{11}N_1^2 - B_{22}N_2^2). \qquad (5)$$

Equation (3) was then used again for the calculation of the values of B_p. These were in satisfactory agreement with those calculated from Eq. (2). The method of least squares was then employed again to calculate the slope of the straight lines obtained by plotting the left-hand side of Eq. (2) against 1/v, using the values of B_p calculated from Eq. (3) and the experimental values of Δ. The slope of these straight lines is equal to C_p.

TABLE 2

Values of the Second (cm^3/mole) and Third (cm^6/$mole^2$) Virial Coefficients in Equations (3) and (4)

Temp., °C	B_{11}	B_{12}	B_{22}	$C_{111} \cdot 10^3$	$C_{112} \cdot 10^3$	$C_{122} \cdot 10^3$	$C_{222} \cdot 10^3$
200	—213	—488	—71	+0,50	+263	—43	+60
250	—154	— 61	—18	—0,18	—123	+72	—18
300	—117	— 58	—39	+0,82	+ 24	+2,2	+7,4

TABLE 3

Values of the Pressure in the Ethylene-Water System at 300° Calculated from Eq. (1) and Read Off from the Manometer

v, liter/mole	P, atm		v, liter/mole	P, atm		v, liter/mole	P, atm	
	exp.	calc.		exp.	calc.		exp.	calc.
$N_2 = 0,212$			$N_2 = 0,385$			$N_2 = 0,551$		
2,224	20,4	20,3	9,63	4,7	4,8	7,49	5,8	6,23
1,055	40,9	41,1	2,023	21,8	22,41	1,801	25,2	25,27
0,592	70,4	69,7	1,242	35,5	35,75	0,879	50,4	50,37
0,451	88,1	89,1	0,827	52,5	52,39	0,578	74,4	75,10
			0,621	68,0	68,26	0,394	107,5	108,7
			0,496	83,7	83,90	0,325	128,3	132,1
			0,457	90,5	90,48			
			0,419	98,8	98,00			

The values of C_p obtained are then used to calculate C_{122} and C_{112}. Transforming Eq. (4) into a straight line form:

$$(C_p - C_{111}N_1^3 - C_{222}N_2^3) / N_1^2 N_2 = 3C_{112} + 3C_{122}N_2 / N_1, \quad (6)$$

the method of least squares is used to obtain the straight line in coordinates of $\frac{C_p - C_{111}N_1^3 - C_{222}N_2^3}{N_1^2 N_2}$ against N_2/N_1. The intercept on the axis of ordinates gives the value of $3C_{112}$, and the slope gives the value of $3C_{122}$. Table 2 gives the values of all the virial coefficients needed for the calculation on the basis of Eq. (1).*

The cubic Eq. (1) was solved relative to the pressure, and to confirm the accuracy of our calculations we did not calculate the volumes, which would have been very complicated, but the pressures for experimental values of the volumes, and compared the results obtained for the values of the pressures with those which had been fixed in the experiments. The comparison data are given in Table 3.

It is seen from Table 3 that the difference between the experimental and calculated values of the pressure is, as a rule, small. Such a good correspondence shows that Eq. (1) describes the volume behavior of solutions of water in ethylene satisfactorily for pressures up to 150 atm and at temperatures between 200° and 300°.

The authors would express their gratitude to I. R. Krichevskii for his interest in the work and his valuable advice.

LITERATURE CITED

[1] D. S. Tsiklis, E. V. Mushkina and L. I. Shenderei, Inzh.-Fiz. Zhur. 1, 8, 3 (1958).

* The coefficients for pure water and pure ethylene are calculated according to the data given in [5, 6].

[2] D. S. Tsiklis, The Technique of Physicochemical Investigations at High Pressures [in Russian] (1958); Compare also D. White, Rev. Scient. Instrum. 29, 648 (1958).

[3] H. Landolt and R. Börnstein, Physikalisch-Chemische Tabellen (1936).

[4] I. P. Krichevskii, Phase Equilibrium in Solution Under High Pressures [in Russian] (1952).

[5] R. Iork and E. White, Am. Inst. Chem. Eng. J. A40, 2, 227 (1944).

[6] M. P. Vukalovich and I. I. Novikov, Thermodynamic Properties of Water and Water Vapor [in Russian] (Moscow, 1955).

RADIATION REDUCTION OF FERRIC IONS IN SOLUTIONS SATURATED WITH HYDROGEN UNDER PRESSURE

V. N. Shubin and P. I. Dolin

Institute of Electrochemistry, Academy of Sciences of the USSR
(Presented by Academician A. N. Frumkin, May 20, 1960)
Translated from Doklady Akademii Nauk SSSR, Vol. 134, No. 4, pp. 891-894, October, 1960
Original article submitted May 20, 1960

In degassed sulfuric acid solutions, Fe^{3+} ions do not undergo conversions when irradiated, as the sum of the oxidizing components $G_{OH} + 2G_{H_2O_2}$ is greater than that of the reducing ones, G_H; the H_2 formed during radiolysis enters the gas phase and does not participate in reactions. Therefore, the kinetic characteristics of Fe^{3+} ions are studied in systems containing various additives [1-4]. The kinetic processing of the data for such systems is difficult due to their complexity and the large number of competing reactions.

Experiments in sulfuric acid solutions indicated that the reduction yield depended on the acidity of the solution. No unequivocal explanation has been given for this relation. Apparently, when molecular hydrogen is present in the solution, part of the OH radicals are converted to H atoms by the reaction $H_2 + OH \rightarrow H_2O + H$, and as a result, the number of reduction components increases at the expense of the oxidation components. In addition, a fall in the OH radical concentration hinders the recombination of the radicals to form water.

In the present work we measured the yields from the reduction of trivalent iron in an acid solution under the action of Co^{60} γ-radiation at various concentrations of H_2, Fe^{3+}, and acid.

Procedure. The solution of Fe^{3+} being investigated was saturated with hydrogen in a glass cell [5] at atmospheric temperature, after which the cell was sealed and placed in a steel bomb, where the solution was saturated with H_2 at a given pressure.

Chemically pure reagents were used. The starting solutions were prepared with doubly distilled water. The dose strength was $\sim 3 \cdot 10^{15}$ ev/cc·sec. The Fe^{2+} ion concentration was determined by the o-phenanthroline method. The extinction coefficient was 10,700 liter/mole·cm.

Results and discussion. The relation of reduction yield of H_2 pressure over the solution was determined for a $2 \cdot 10^{-3}$ M solution of Fe^{3+} in 0.8 N H_2SO_4. The initial sections of the reduction curve were plotted for each H_2 concentration. The initial reduction yields calculated from these data are given in Fig. 1 in relation to the hydrogen pressure above the solution. As Fig. 1 shows, the reduction yields increased with a rise in pressure. This characteristic of the relation is explained by the competition for OH radicals in the two following reactions:

$$H_2 + OH \xrightarrow{k_1} H_2O + H; \quad (1)$$

$$H + OH \xrightarrow{k_2} H_2O. \quad (2)$$

Atomic hydrogen, formed during radiolysis and by reaction (1), participates in the reduction of Fe^{3+} by the reaction

$$Fe^{3+} + H \xrightarrow{k_3} Fe^{2+} + H^+. \quad (3)$$

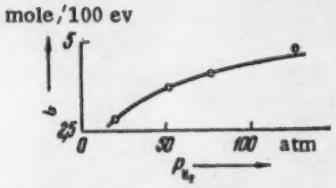

Fig. 1. Relation of Fe^{3+} reduction yields to hydrogen pressure above the solution.

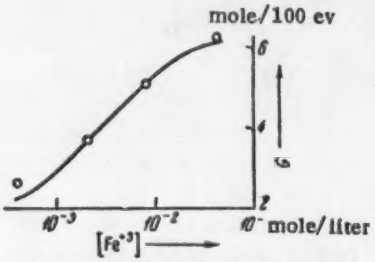

Fig. 2. Relation of reduction yield to Fe^{3+} concentration.

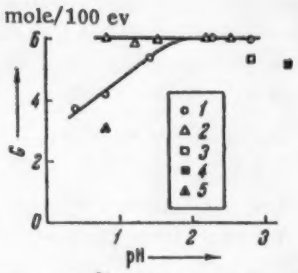

Fig. 3. Fe^{3+} reduction in solutions with different concentrations of H_2SO_4 and $HClO_4$ in solutions containing Na_2SO_4 and $NaHSO_4$. 1) H_2SO_4 solution; 2) $HClO_4$ solution; 3) solution of $HClO_4$ + 0,1 M Na_2SO_4; 4) solution of $HClO_4$ + + 1 M Na_2SO_4; 5) solution of $HClO_4$ + 0,3 M $NaHSO_4$.

Reaction (3) competes with reaction (2). Apparently, the reduction yield should increase with an increase in Fe^{3+} concentration.

The relation of yield to Fe^{3+} concentration was determined in a 0,8 N solution of H_2SO_4, saturated with H_2 at 50 atm. The reduction yields calculated from the initial sections of the reduction curves are given in Fig. 2 in relation to log $[Fe^{3+}]$.

Assuming that the initial yield is determined by the above three reactions, from the kinetic equations we can derive the following expression for the ratio of the constants:

$$\frac{k_2}{k_1 \cdot k_3} = \frac{[G_H + G_{OH} - G(Fe^{2+})][H_2][Fe^{3+}]}{[G(Fe^{3+}) + G_{OH} - G_H]\, G(Fe^{2+}) \cdot M}. \qquad (I)$$

In the derivation of a formula on the basis of Dainton and Sutton's data [6], it is assumed that the H_2O_2 formed during radiolysis did not have enough time to react appreciably during irradiation with the Fe^{2+} ions obtained by reduction. However, even if all the peroxide reacted during the irradiation, Eq. (I) would change little and instead of the term in the square brackets in the denominator, the term $[G(Fe^{2+}) + G_{OH} - G_H + 2G_{H_2O_2}]$ would appear. However, the Fe^{2+} concentration was several units times 10^{-5} after irradiation. With such a concentration, only a very small part of the peroxide could have reacted during the irradiation time (3-9 min).

The irradiated solution was kept under pressure for an hour after irradiation. Whereupon, according to reaction Fe^{2+} + + $H_2O_2 \rightarrow Fe^{3+} + OH^- + OH$, a certain amount of the Fe^{2+} formed disappeared but the OH radicals formed by reaction (1) were converted to H atoms, which reduced an equivalent amount of Fe^{3+} ions. Thus, reduction yield remained the same.

From the radiolysis scheme suggested above it follows that the reduction yield should not depend on the acid concentration of the solution. Such a relation was observed experimentally in sulfuric acid solutions. However, trivalent iron is known to form complex ions in sulfuric acid solutions. Evidently, the rate constant of the reaction of such an ion with an H atom is different from the rate constant of a free ion. The ratio between the amount of free Fe^{3+} ion and the complex ion may change with a change in H_2SO_4 concentration and this would, in its turn, affect the yield. On the other hand, the Fe^{3+} ion is known to exist as a free ion in $HClO_4$ solutions. This makes it possible to compare the behavior of a free and a complex ion.

The relations of reduction yields to H_2SO_4 and $HClO_4$ concentrations are given in Fig. 3. As Fig. 3 shows, in sulfuric acid solution the yield increased with a fall in H_2SO_4 concentration while in $HClO_4$ the yield remained the same for the whole range of acid concentrations investigated. The results obtained in $HClO_4$ solutions thus confirm the accuracy of the radiolysis scheme proposed above and of Eq. (I) derived from it.

We carried out experiments with Na_2SO_4 and $NaHSO_4$ added to perchloric acid solutions to establish which of the anions forms a complex with the ion. Experiments with Na_2SO_4 added were carried out at a high pH so that only a small portion of the SO_4 was converted to HSO_4^-.

In this case only a small fall in the reduction yield was observed (Fig. 3) even at SO_4^{2-} concentrations of ~ 1 M. On the other hand, the presence of 0.3 M* of HSO_4^- decreased the yield sharply (see Fig. 3). The experiments were carried out in 0.2 M $HClO_4$ in which HSO_4^- dissociation was suppressed. These results indicate that the complex-forming ion was HSO_4^-. Then, from data on the relation of the yield to H_2SO_4 concentration, we may calculate the equilibrium constant of the reaction

$$Fe^{3+} + HSO_4^- \overset{K_a}{\rightleftarrows} FeHSO_4^{2+}. \qquad (I)$$

From equation (I) we calculated the value $[k_2/(k_1 \cdot k_3)] \cdot \alpha$, where $\alpha = [Fe^{3+}]_{tot}/[Fe^{3+}]_{free}$. Then, if we denote the values of α for sulfuric acid solutions with pH's of 0.4, 0.8, and 1.4 as α_1, α_2, and α_3, respectively, we can determine the ratio $\alpha_1 : \alpha_2 : \alpha_3$.

To determine the amount of trivalent iron in the form of free ion and complex ion we can write the equation:

$$[Fe^{3+}]_{free} + K_a \frac{f_{HSO_4^-} \cdot f_{Fe^{3+}}}{f_{FeHSO_4^{2+}}} [HSO_4^-][Fe^{3+}]_{free} = [Fe^{3+}]_{tot}. \qquad (II)$$

Using this equation and the ratio $\alpha_1 : \alpha_2 : \alpha_3$, we calculated the value K_a = 91 liter/mole.

Then, using the experimental data on the relation of the reduction yield to the H_2, Fe^{3+}, and H_2SO_4 concentrations and Eq. (I), we can determine the ratio of the constants $k_2/(k_1 \cdot k_3) = 71 \pm 5$. The concentration of free Fe^{3+} ions needed for substituting in (I) was calculated from Eq. (II).

To determine the absolute value k_3 we evaluated the absolute constants k_1 and k_2 as follows.

Reaction (2) proceeds without activation energy. The steric factor equals 0.5. In this case the rate constant of the reaction, equal to the number of impacts multiplied by the steric factor, will be:

$$k_2 = 2{,}8 \cdot 10^{11} \cdot 0{,}5 = 1{,}4 \cdot 10^{11} \text{ liter/mole} \cdot \text{sec}.$$

The value for k_1 we took from the paper by Avraamenko and Lorentso [7], $k_1 = 2{,}5 \cdot 10^3$ liter/mole · sec, as we considered that its value would not change much with a change from the gas to the aqueous phase.

The value of k_3 calculated from these data was $k_3 = (8 \pm 0{,}56) \times 10^5$ liter/mole · sec.

LITERATURE CITED

[1] T. Rigg, G. Stein, and J. Weisse, Proc. Roy. Soc. 211, 375 (1952).

[2] E. J. Hart, J. Am. Chem. Soc. 77, 5786 (1955).

[3] D. M. Donaldson and N. Miller, Radiation Res. 9, 487 (1958).

[4] J. Bednar, Collect. Czechoslovak. Chem. Communication 25, 1104 (1960).

[5] V. N. Shubin and P. I. Dolin, Doklady Akad. Nauk SSSR 125, 1298 (1959).**

[6] F. Dainton and H. Sutton, Trans. Farad. Soc. 49, 1011 (1953).

[7] L. I. Avraamenko and R. V. Lorentso, Zhur. Fiz. Khim. 24, 207 (1950).

* The HSO_4^- ion concentration is ~ 0.3 M in 0.8 N H_2SO_4 solutions.

** Original Russian pagination. See C. B. Translation.

THE ELECTRICAL CONDUCTIVITIES OF POLYMERS WITH CONJUGATED DOUBLE BONDS

E. I. Balabanov, A. A. Berlin, V. P. Parini, V. L. Tal'roze,

E. L. Frankevich, and M. I. Cherkashin

Chemical Physics Institute, Academy of Sciences of the USSR
(Presented by Academician V. N. Kondrat'ev, June 14, 1960)
Translated from Doklady Akademii Nauk SSSR, Vol. 134, No. 5, pp. 1123-1126, October, 1960
Original article submitted June 11, 1960

The synthesis of organic polymers with various electrical and physical properties, as well as the problem of organic semiconductors, have created the need for a broad investigation of the electrical properties of various kinds of polymers containing conjugated double-bond systems and atoms other than carbon in the principal chain [1]. The authors of this paper synthesized the types of polymers listed below, then studied their electrical conductivities σ and the temperature dependence of σ.

1. Polymers containing conjugated acyclic chains [2, 3]; polyphenylacetylene (1), polyphenylacetylene–hexyne copolymers (2), and polyphenylacetylene–paradiethynyl benzene copolymers (3).

2. Polymers containing benzene rings in the conjugated chain: polyphenylene,

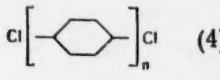
(4),

and polyphenylene azo derivatives [4-6] of the type

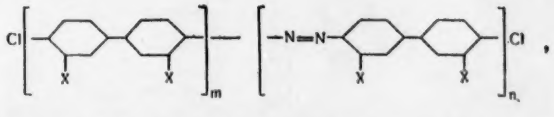

where X = H (5), CH_3 (6), COOH (7), aromatic and mixed aliphatic–aromatic polymers containing quinoid and amino groups [7, 8]: polyphenylene aminoquinones of the type

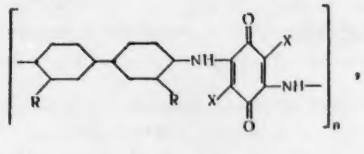

where X = H (8) or Cl (9) when R = H, and X = H (10) when R = COOH; poly-n-phenylenediaminoquinone (11) and polyhexamethylenediaminoquinone (12):

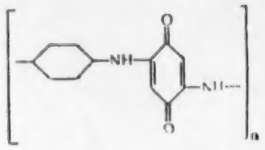
(11)

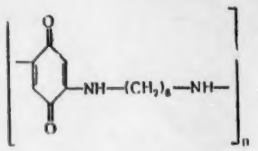
(12)

polyphenyleneazoquinones of the type:

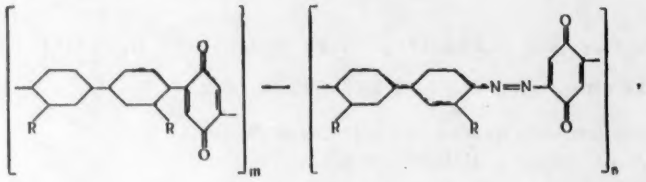

where R = H (13) and COOH (14); polymeric triazine (15) and polymers containing quinimine groups (16):

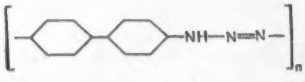
(15);

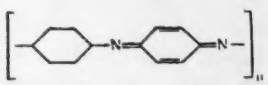
(16);

polymeric chelates [9] such as the copper complex of polydiphenylaminoquinone (17):

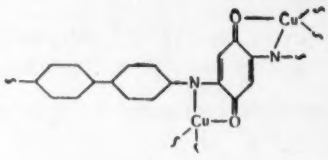

We also synthesized molecular π-complexes of acenaphthene with chloranil (18) and with the pyridone derivative of polyphenyleneaminoquinone (19).

3. Compounds containing nonbenzenoid rings in the conjugated chain: tetrasalicyl ferrocene (20) and its polymeric chelates [10] with Fe^{++} and Be^{++} (21, 22):

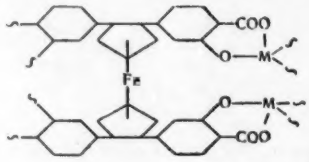

Polymeric percyanoethylene chelates of Cu^{++} (23) and Fe^{++} [11, 12] were also prepared.

The synthesis and properties of some of the enumerated compounds (for example, 8, 10, 11, 13, and 14) have not been previously described in the literature. These will soon be described by us in a series of papers.

We were particularly interested in polymers containing quinoid rings (10, 14) in the conjugated chain and primarily compounds in which the quinoid system was conjugated through a nitrogen atom (16). The excitation energy of such compounds would be expected to sharply decline into a triplet state and in certain cases ion-radical structures might arise.

TABLE 1

Sample No.	σ_0, ohm^{-1}·cm^{-1}	E, kcal/mole	$\sigma_{300°K}$	Remarks
1a	$4 \cdot 10^{18}$	49,5	10^{-17}	Polymeric film prepared at 150°C
1b	$5 \cdot 10^{17}$	47,6	$2 \cdot 10^{-17}$	Polymerized at 400°C
1c	$2 \cdot 10^{11}$	37	$3 \cdot 10^{-16}$	Films of mixed polymers 1a and 1b
1d	$3 \cdot 10^{8}$	32,2	10^{-15}	
1e	*10^{2}	22	10^{-14}	Benzene-soluble fraction of polymer 1b
1f	$2 \cdot 10^{-2}$	8,5	10^{-8}	Pyridine-soluble fraction of polymer 1b
1g	$2 \cdot 10^{-4}$	15,4	$2 \cdot 10^{-15}$	Polymerized at 150°C, pellet compressed at 200°C
2′	10^{20}	49	10^{-15}	Between 20 and 50°*
2″	$5 \cdot 10^{7}$	29	—	Between 50 and 100°C
3	$6,4 \cdot 10^{-4}$	17,5	10^{-16}	
4	10^{-12}	5,1	$2 \cdot 10^{-16}$	
5a	40	25	$4 \cdot 10^{-17}$	Sample heated at 200°C
5b	1	21	10^{-15}	Unheated
6	1—0,1	20—22	10^{-14}—10^{-16}	
7	1	18,4	$4 \cdot 10^{-14}$	
8	30	24	10^{-16}	
9	$2 \cdot 10^{2}$	23,7	10^{-15}	
10a	10^{8}	29	10^{-13}	Prepared according to the same directions
10b	10^{-3}	9,2	$2 \cdot 10^{-10}$	Prepared according to the same directions
11	10	20,2	$2 \cdot 10^{-14}$	
12	10^{-4}	15,6	$5 \cdot 10^{-16}$	
13a	10^{-7}	13	$2 \cdot 10^{-16}$	Prepared according to the same directions
13b	10^{-8}	39	10^{-20}	Prepared according to the same directions
14	$5 \cdot 10^{4}$	20,2	10^{-10}	
15a	50	23	10^{-15}	
15b	$6 \cdot 10^{6}$	30,2	10^{-15}	
16′	10^{2}	10,3	$3 \cdot 10^{-6}$	Between 20 and 40°C
16″	30	4,6	—	Between 40 and 80°C
17	10^{4}	25,4	$4 \cdot 10^{-15}$	
18a′	$3 \cdot 10^{34}$	67,5	$3 \cdot 10^{-15}$	Acenaphthene: chloranil ratio 1:1, between 20 and 50°C
18a″	$5 \cdot 10^{20}$	48,5	—	Between 50 and 80°C
18b	$6,4 \cdot 10^{51}$	92	$2 \cdot 10^{-15}$	Acenaphthene: chloranil ratio 1:2, between 20 and 45°C
19	$3 \cdot 10^{5}$	24,8	$3 \cdot 10^{-13}$	
20a	10^{-1}	12,6	10^{-10}	
20b	$5 \cdot 10^{-3}$	12	10^{-11}	Compound 20a heated at 200°C
21	1	10,6	10^{-8}	
22	5	11,7	10^{-8}	
23	2	15,3	10^{-11}	

*Samples in which the line log σ vs 1/T had a break. Prime and double-prime numbers refer to the same samples before and after the break.

Most of the samples were studied in the form of pellets 10-12 mm in diameter.

In this communication we will limit ourselves to a general description of the observed relationships. In all of the cases the electrical conductivities increase with temperature according to the law $\sigma = \sigma_0 \cdot e^{-E/kT}$, where σ_0 and E are constant for a given sample.

Deviations from this law were only observed near temperatures at which these compounds decompose. The value of E usually ranged from 4.6 kcal/mole (0.2 ev) for compound (16) to 49.5 kcal/mole (2.1 ev) for polyphenylacetylene and was as large as 92 kcal/mole in the acenaphthene–chloranil complex. At the same time σ_0 ranged from 10^{-12} ohm^{-1} cm^{-1} in polyphenylene to $6 \cdot 10^{51}$ ohm^{-1} cm^{-1} in the acenaphthene–chloranil complex.

The type of treatment used in preparing the samples has a very pronounced effect on the value of these parameters. Thus, for example, the preexponential coefficient of polyphenylacetylene decreased by 22 orders of magnitude when we changed from a film prepared in a solvent to a pellet compressed at 200°C.

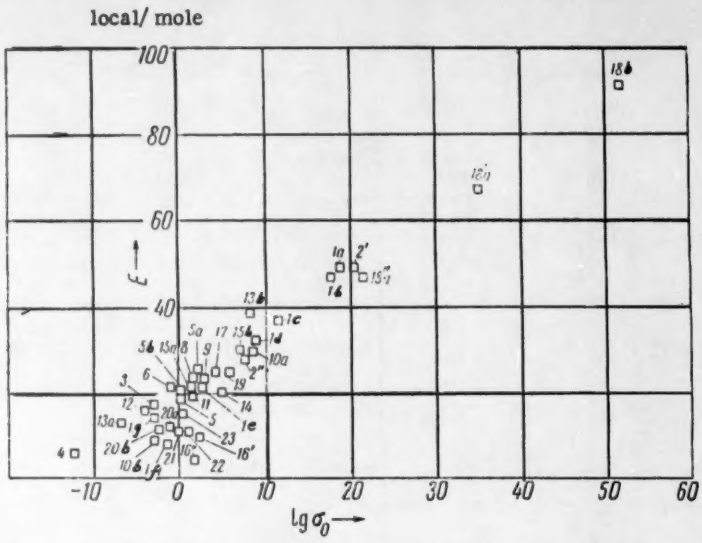

Fig. 1. Relationship between the preexponential coefficient and the electrical conductivity activation energy.

However, the "activation energy" E declines correspondingly so that at room temperature the electrical conductivities of both samples turn out about the same. Such a parallel change in the coefficient and the activation energy is frequently called a compensation effect (c.e.) and has several anologies in chemical kinetics and catalysis; this effect has also been observed in the electrical conductivities of metal oxides [13]. The nature of this c.e. is not yet understood; recently a theoretical approach has been attempt to this problem [14].

It turned out that in our case the c.e. was a general property exhibited by all, or almost all the synthesized compounds. This is particularly evident in Fig. 1 where the data from Table 1 are plotted as log σ_0 vs E. We are dealing here with an entirely unique form of c.e., where compounds of different structures have preexponential coefficients differing by sixty (!) orders of magnitude and the activation energies by a factor of twenty.

Several of our compounds had electrical conductivities exceeding by several orders of magnitude those of ordinary organic dielectrics. This applies primarily to samples 16, 21, and 22 which approach in their electrical conductivities certain known organic semiconductors [15-17].

It is interesting to note that in the case of polyphenylacetylenes σ changes very sharply with T, which indicates that E is very large (at room temperature these compounds behave like ordinary insulators). Since σ_0 is quite large to begin with, as the temperature is raised the σ of polyphenylacetylene "catches up" with the σ of several polymers which have high electrical conductivities at room temperature.

One might expect that further investigation will make it possible to establish relationship between the electrophysical properties and the structures of individual polymeric molecules and the materials made of these.

LITERATURE CITED

[1] A. A. Berlin and V. P. Parini, Izvest. Vyssh. Ucheb. Zav. Ser. Khim. and Khim. Tekh. 4, 122 (1958).

[2] A. A. Berlin, M. I. Cherkashin, O. G. Sel'skaya, and V. E. Limanov, Vysokomolek. Soed. 1, 12, 1817 (1959).

[3] A. A. Berlin, L. A. Blyumenfel'd, M. I. Cherkashin, A. E. Kalmanson, and O. G. Sel'skaya, Vysokomolek. Soed. 1, 9, 1362 (1959).

[4] V. P. Parini and A. A. Berlin, Izvest. Akad. Nauk SSSR, Ser. Khim. 12 (1958).

[5] A. A. Berlin and V. P. Parini, Izvest. Akad. Nauk SSSR, Ser. Khim. 9, 1674 (1959).

[6] A. A. Berlin, B. I. Liogon'skii, and V. P. Parini, Vysokomolek. Soed. 2, 5, 689 (1960).

[7] A. A. Berlin and N. G. Matveeva, Vysokomolek. Soed. 2, 1643 (1959).

[8] L. A. Blyumenfel'd, A. A. Berlin, N. G. Matveeva, and A. É. Kalmanson, Vysokomolek. Soed. 1, 11, 1647 (1959).

[9] A. A. Berlin, V. P. Parini, and N. G. Matveeva, Authors Certificate, 128,606, May 11, 1959, kl. 39c, 3.

[10] A. A. Berlin, and T. V. Kostroma, Authors Certificate, 129,018, April 25, 1959, kl. 39c, 30.

[11] A. A. Berlin, N. G. Matveeva, and A. I. Sherle, Izvest. Akad. Nauk SSSR, Ser. Khim. 12, 2261 (1959).

[12] A. A. Berlin, N. G. Matveeva, and A. I. Sherle, Author's Certificate, 126,612, April 7, 1959, kl. 39c, 30.

[13] W. Meyer and H. Neldel, Phys. Z. 38, 1014 (1937).

[14] S. Z. Roginskii, Yu. L. Khait, Doklady Akad. Nauk SSSR 130, 2, 366 (1960).*

[15] A. V. Topchiev, M. A. Geiderikh, et al., Doklady Akad. Nauk SSSR 128, 2, 312 (1959).*

[16] H. A. Pohl, Electronic News (Feb. 8, 1960).

[17] A. Epstein and B. S. Wildi, J. Chem. Phys. 32, 324 (1960).

* Original Russian pagination. See C. B. Translation.

THE INTENSITY OF THE INFRARED ABSORPTION OF THE CARBONYL GROUP IN SYDNONES AND TROPONE AND THE POLARITY OF THE C= O BOND

Yu. G. Borod'ko and Corresponding Member Acad. Sci. USSR Ya. K. Syrkin

M. V. Lomonosov Moscow Institute of Fine Chemical Technology
Translated from Doklady Akademii Nauk SSSR, Vol. 134, No. 5, pp. 1127-1130, October, 1960
Original article submitted July 1, 1960

One frequently encounters the statement that a decrease in the carbonyl vibrational frequency indicates increased bond polarity and a decreased bond order. Thus, by comparing the vibrational frequencies of the C=O bonds of various molecules with the corresponding frequency for acetone (dipole moment 2.7 D, frequency 1710 cm^{-1}) it has been concluded that conjugation increases the polarity and reduces the bond order ($\rangle \overset{+}{C}-\overset{-}{O}$) which results in the observed frequency lowering and increased dipole moment. This conclusion was based on the experimentally observed $\rangle C=O$ bond frequencies in various organic molecules.

Increased frequencies have been frequently attributed to increased bond orders by assuming that the oxygen acquires some oxonium character and that in acetyl chloride (CH_3COCl) for example, an electron is partially displaced towards the halogen. However, in our opinion, there is no adequate basis for such a conclusion. In any case, there are no grounds for the reverse argument that if the vibrational frequency of a carbonyl bond exceeds that in acetone, then the bond order is also greater. Moreover, one can not use arguments based on the known frequency sequence from a single, to a double, and a triple bond $\rangle C-C\langle$, $\rangle C=C\langle$, $-C\equiv C-$, since in such a case we would be dealing with bonds involving one, two, and three electron pairs, respectively. It is more appropriate to try and deduce the bond polarities from the IR intensities of the carbonyl vibrations. It is a known fact that in the case of several diatomic molecules (HCl, HBr, and HI) the IR adsorption intensities, which are a function of the matrix elements of the dipole moments, increase with increasing dipole moment μ. There is a correspondence between the known values of $d\mu/dr$ and μ_{exp}/r_0 (where r_0 is the equilibrium distance), which is a measure of the bond polarity. It is also known that, as a rule, the infrared absorption of ionic bonds is more intense than that of covalent bonds.

One has to be particularly cautious in estimating the bond orders and polarities of carbonyl bonds in cases where one deals with a new class of molecules having a unique structure as, for example, in five-membered sydnone rings (1), in seven-membered tropone rings (2), or three-membered rings such as diphenyl-cyclopropenone (3).

(1) 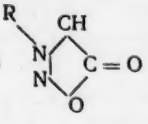

(2) 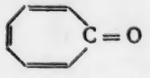

(3) 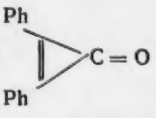

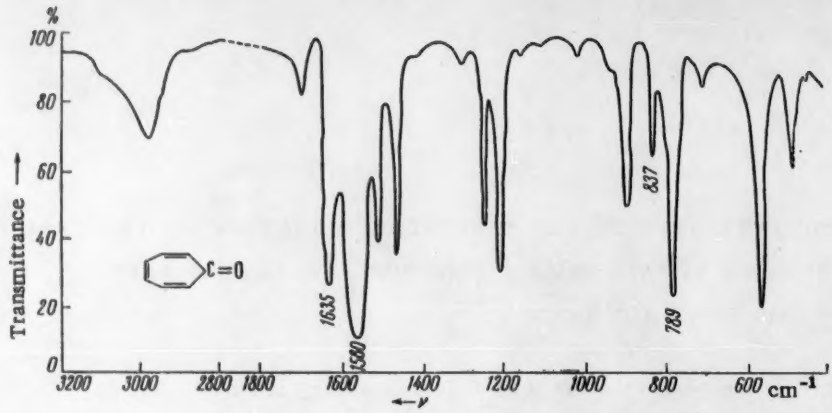

Fig. 1.

TABLE 1

Compound	μ, D	In CCl_4, [C] ≈ 10^{-3} moles/liter	
		$\nu_{C=O}$, cm^{-1}	$I_{C=O}$, $1.2 \cdot 10^4$ liter/mole · cm^2
Acetone	2,7	1710	1,6
Benzophenone	2,9	1692	2,1
Acetophenone	3,0	1668	2,2
Tropone	4,3 [3]	1590	2,6
Diphenylcyclopropenone	5,08 *	1845	6,4
3-Phenylsydnone	6,48 [4]	1760	10
3-Ethylsydnone	~6	1745	11

* Measured by A. N. Shidlovskaya and Ya. K. Syrkin.

The compounds shown have dipole moments greatly exceeding the moment of acetone, and their vibrational frequencies are also higher: for diphenylcyclopropenone $\nu_{C-O} = 1845\ cm^{-1}$ and for sydnones $\nu_{C-O} = 1760\ cm^{-1}$. This indicates that the relationship between the vibrational frequencies and the dipole moments, which are a measure of the polarity, is not consistent for all the molecules. The vibrational frequency of a carbonyl group could hardly be an indication of the bond polarity in as it is not directly connected with the dipole moment but is a complex function of a great number of variables.

To measure the polarity of the carbonyl bond, or for that matter, of any other bond, it would be more appropriate to use the IR intensity of the corresponding vibrational frequency. The intensity depends on the transition from a vibrational quantum state v_1 to a state v_2 and is given by the square of the matrix element $Mv_1v_2(Q)$, which is equal to

$$\int \psi^*_{v_1}(Q)\, M(Q)\, \psi_{v_2}(Q)\, dQ,$$

where M(Q) is the dipole moment operator for a molecule of the configuration Q [1]. Hence any increase in the integral intensity of the carbonyl IR absorption band is an indication of an increased bond polarity. In Table 1 we have listed some measured frequencies and integral intensities of the carbonyl IR bands of several compounds (measurements were carried out on an UR-10 double-beam spectrometer). A technique described by Ramsay [2] was used for the determination of intensities. Table 1 shows very clearly that the intensity increases sharply with increasing dipole moment but that there is no direct relationship between the frequency and the dipole moment. In our table we used the intensity of the 1590 cm^{-1} band of tropone instead of the 1635 cm^{-1} band which has previously been assigned to the carbonyl stretch [5]. Our choice followed an investigation of the frequency and intensity changes in the 1590 cm^{-1} and the 1635 cm^{-1} bands in various solvents and at different temperatures (in Fig. 2 we have reproduced the IR spectrum of tropone [2].) The intensity of the 1635 cm^{-1} band of tropone is $1.2 \cdot 10^4$ liters/mole · cm^2 in CCl_4 solution, or in other words it is smaller than in the case of acetone. In our opinion this is incompatible with the high dipole moment of tropone (4.3 D). When a chloroform solution is used the intensity of this band declines to $0.9 \cdot 10^4$ liters/mole · cm^2 with no detectable frequency shift; this would be in direct conflict with the great amount of available experimental data which have

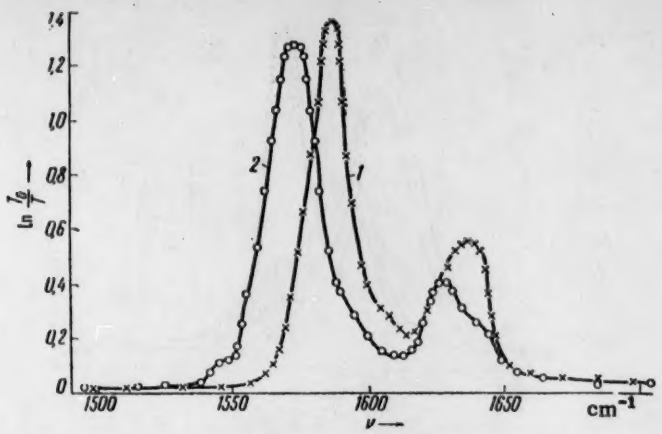

Fig. 2. The observed (at 30°) shapes of the 1590 cm^{-1} and 1635 cm^{-1} bands of tropone dissolved in: 1) CCl_4 (conc. = $12.3 \cdot 10^{-2}$ moles/liter, d = 0.1 mm); 2) $CHCl_3$ (conc. = $11.2 \cdot 10^{-2}$ moles/liter, d = 0.1 mm).

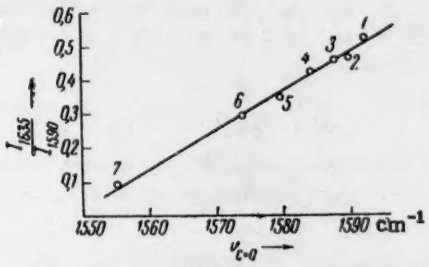

Fig. 3. The ratio of integral intensities I_{1635}/I_{1590} for the adsorption bands of tropone in various solvents: 1) cyclohexane; 2) tetrachloroethylene; 3) carbon tetrachloride; 4) benzene; 5) pyridine; 6) chloroform; 7) acetic acid.

shown that hydrogen bonding to chloroform increases the intensity and lowers the frequency of the carbonyl group vibration [6]. At the same time the intensity of the 1590 cm^{-1} band increases from $2.6 \cdot 10^4$ liters/mole · cm^2 in CCl_4 to $3.4 \cdot 10^4$ liters/mole · cm^2 in $CHCl_3$, while the frequency decreases from 1590 cm^{-1} to 1574 cm^{-1} (Fig. 2). Measurements at temperatures between 20 and 60° yielded similar results.

Figure 3 shows that the ratio of absorption-band intensities I_{1635}/I_{1590} declines as the 1590 cm^{-1} band shifts towards lower frequencies. One can select a solvent in which the intensity of the 1635 cm^{-1} band will correspond to a second-order line. This result seems to indicate that the 1635 cm^{-1} band constitutes a combination tone (837 cm^{-1} + 789 cm^{-1}) which is intensified by Fermi resonance with the carbonyl band. As the carbonyl band shifts towards lower frequencies (due to an interaction with the solvent) and away from the combination tone the conditions for the resonance become much less favorable and consequently the intensity of the combination tone declines sharply [7].

We must therefore conclude that it is the most intense absorption band in the IR spectrum at 1590 cm^{-1} which represents the carbonyl vibrational frequency.

It should also be pointed out that the carbonyl bands in 3-phenylsydnone and 3-ethylsydnone are split. In Fig. 4 we have shown the effects of temperature and solvent on the frequencies and intensities of the two

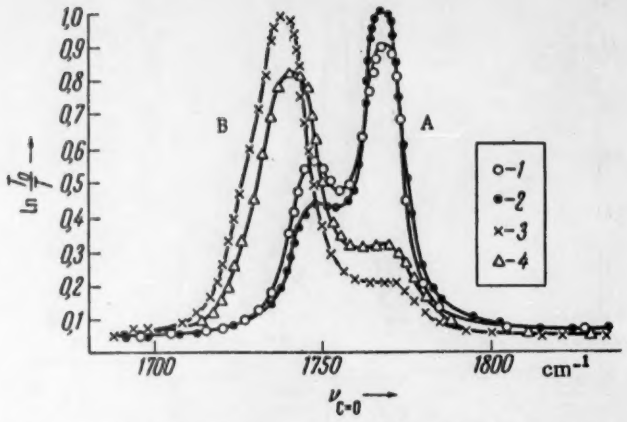

Fig. 4. The observed shape of the carbonyl band of 3-phenylsydnone. A) In CCl_4 (conc. = $7.2 \cdot 10^{-4}$ moles/liter): 1) at 12°; 2) at 50°. B) In $CHCl_3$ (conc. = $7.24 \cdot 10^{-4}$ moles/liter); 3) at 9°; 4) at 50°.

components of the 3-phenylsydnone carbonyl band. We are currently studying the nature of this splitting in the bands of various sydnones. In concluding we would like to thank M. E. Vol'pin and V. S. Yashunskii for kindly supplying us with the necessary compounds.

LITERATURE CITED

[1] G. Herzberg, The Vibration and Rotation Spectra of Polyatomic Molecules [Russian translation] (Moscow, 1949); S. Bogavantam, Group Theory and Its Application to Physical Problems [Russian translation] (Moscow, 1959).

[2] D. A. Ramsay, J. Am. Chem. Soc. 74, 1, 72 (1952).

[3] A. Giacomo and C. P. Smyth, J. Am. Chem. Soc. 74, 17, 4411 (1952).

[4] R. A. W. Hill and L. E. Sutton, J. Chem. Soc. 746 (1949).

[5] K. Kuratani, Bull. Chem. Soc. Japan, 25, 250 (1952); P. L. Pauson, Chem. Rev. 55, 1, 9 (1955).

[6] H. W. Thompson and D. J. Jewelle, Sp. Acta 13, 3, 254 (1958); G. Borrow, J. Chem. Phys. 21, 11, 2008 (1953); Ya. K. Syrkin and Yu. G. Borod'ko, Doklady Akad. Nauk SSSR 131, 4, 868 (1960).

[7] L. J. Bellamy and R. L. Williams, Trans. Farad. Soc. 55, 1, 16 (1959).

*Original Russian pagination. See C. B. Translation.

EVIDENCE OF HYDROGEN BONDING OF THE TYPE OH...O= C IN THE CARBONYL INFRARED BAND OF KETONES

G. S. Denisov

A. A. Zhdanov Leningrad State University
(Presented by Academician A. P. Terenin, May 19, 1960)
Translated from Doklady Akademii Nauk SSSR, Vol. 134, No. 5, pp. 1131-1134, October, 1960
Original article submitted May 10, 1960

By learning to detect hydrogen bonding in the bands of proton-acceptor groups one can obtain a great amount of information about the distortion produced in the electron cloud around the acceptor molecule by such bond formation. The purpose of this work was to establish a correlation between the spectroscopic manifestations of hydrogen bonding, such as OH...O=C, in the vibrational band of carbonyls and the properties of the molecules involved in hydrogen bonding.

The molecular properties responsible for the strength of interaction such as XH...V are: the extent to which the proton in the molecule XH remains unshielded by the molecular electron cloud [1] and the magnitude of the atomic dipole of the free electron pair on atom V [2]. Since in molecules of a given general type these functions vary due to the fact that different substituents have different inductive effects, it is possible to utilize the known relative inductive effects of various radicals [3] to arrange these molecules in the order of increasing strength as proton donors or electron donors. The extent to which the proton on the OH group remains unshielded by electrons determines the acidic properties of compounds containing hydroxyl groups and hence the dissociation constants of corresponding acids (in a suitable solvent) can be used as a measure of such shielding.

It seems that the first ionization potential of ketones, which gives the energy required to strip the free electron pair from the oxygen, can provide a quantitative measure of the electron-donor strength of ketones [4]. The manner in which this function changes within our series of compounds is entirely consistent with Ingold's data [3].

The following compounds containing hydroxyl groups (arranged in the order of increasing strength as proton donors) were investigated by us in this work: CH_3OH, C_6H_5OH, $CH_2ClCOOH$, CCl_3COOH, and CF_3COOH; the following ketones (arranged here in the order of increasing strength as electron donors) were also studied: 1,3-dichloroacetone (10.12), chloroacetone (9.90), acetone (9.71), cyclohexanone (9.14), camphor (8.76), and pivalone (2,2,4,4-tetramethyl-3-pentanone) (8.65); the numbers in parentheses give the ionization potentials in electron volts as determined by F. I. Vilesov [5]. We studied acid–ketone mixtures without a solvent as well as in a solution of CCl_4. The work was done using an IKS-6 spectrometer with NaCl prisms and an OAP-1 recorder; the calculated slit width was 3.2-4.6 cm^{-1}. We used fixed-size fluorite cells (the size was determined interferometrically) as well as adjustable-size cells with a ring and a gasket. The frequencies were precisely determined to within 1-3 cm^{-1}, depending on the band width.

Since the frequency and intensity of the carbonyl band is very sensitive to the dielectric properties of the solvent (for example, it has been found [6] that the value of $\nu_{C=O}$ can differ by as much as 12 cm^{-1} from one solvent to another), we found it desirable to reduce this effect to a minimum in order to be able to record strictly the changes induced by hydrogen bonding. This was achieved by diluting the double system of acid–ketone with an inert solvent (CCl_4), the dielectric properties of which would essentially control the interfering effect of the medium. We can therefore assume that this effect remained constant in our experiments.

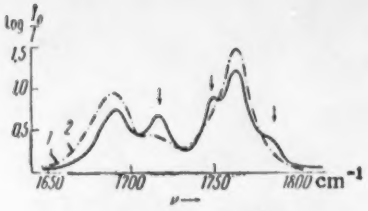

Fig. 1. The absorption spectra of CCl_4 solutions containing equimolar amounts of cyclohexanone and trichloroacetic acid; the concentration of each component was: 1) 0.194 mole/liter; 2) 0.0155 mole/liter.

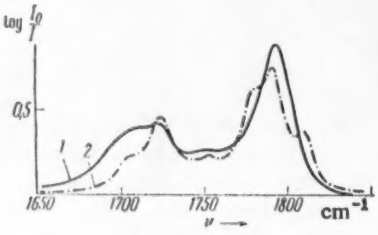

Fig. 2. The absorption spectra of CCl_4 solutions containing equimolar amounts of chloroacetone and trifluoroacetic acid; the concentration of each component was: 1) 2.15 moles/liter; 2) 0.028 moles/liter.

While studying the spectra of the ketone – acid systems we found that over a certain concentration range all of them revealed two bands in the 1700 cm^{-1} region; one of these bands was located at the same frequency as the $\nu_{C=O}$ of the ketone itself (in CCl_4) while the other one was shifted towards lower frequencies. When the solution concentration was changed the intensities redistributed themselves between these two bands, and we have therefore attributed the former to free ketone molecules and the latter to ketones hydrogen-bonded to the acid, OH...O=C. We correlated the shift of the $\nu_{C=O}$ band with the proton-donating and electron-donating properties of the molecules involved in complex formation.

The difference between the electronic structures of an aliphatic ketone carbonyl group and the carbonyl in a halosubstituted carboxylic acid is responsible for the fact that these acids may be used as proton donors despite their tendency to dimerize. Due to the strong negative inductive effect of the halogen the atomic dipole of the free electron pair on the carbonyl group of the acid should be much smaller than the corresponding dipole in a ketone, and hence one would expect that in an equimolar mixture of acid and ketone the energetically more favorable association between unlike components would greatly predominate over a simple dimerization (it is hard to work with solutions containing excess acid due to the fact that the acids themselves absorb in the vicinity of $\nu_{C=O}$).

As a matter of fact, the spectra of equimolar mixtures of ketones with either trichloroacetic or trifluoroacetic acids exhibit two bands in the carbonyl vibration region which are usually absent in the spectrum of either individual component (in CCl_4). When such mixtures are diluted with carbon tetrachloride these bands decline in intensity and new bands appear which are characteristic of the individual ketones and acids in CCl_4. This is illustrated in Fig. 1, where we have plotted two absorption spectra of the $CCl_3COOH-(CH_2)_5CO$ system in CCl_4. One can see that as the solution concentration is decreased the $\nu_{C=O}$ bands of cyclohexanone at 1717 cm^{-1} and of the acid at 1751 cm^{-1} (dimer) and at 1787 cm^{-1} (monomer) increase in intensity (these bands are indicated by arrows). The 1691 cm^{-1} band is assigned to the cyclohexanone carbonyl group hydrogen-bonded to trichloroacetic acid, while at 1764 cm^{-1} we have the C=O band of the acid molecule which is bonded to the ketone through its hydroxyl group. It is apparent that at moderately low concentrations the hydrogen bonding in this system is predominantly between unlike molecules. The mixtures of ketones with trifluoroacetic acid have very similar spectra, but in the spectrum of monochloroacetic acid mixed with cyclohexanone the intensities of bands representing the mixed species are comparable in magnitude to that of the ketone or the acid itself and they rapidly decline when the mixture is diluted with CCl_4. Mixtures of CF_3COOH with chloroacetone or dichloroacetone give somewhat more complicated spectra. These ketones have several rotational bands in the $\nu_{C=O}$ region, and at the same time both the relative intensities as well as the positions of these bands are very sensitive to external conditions, particularly to the type of solvent used [7]. Hydrogen bonding gives rise to new bands, and in interpreting these it is important to consider the possibility of a shift in the equilibrium between the rotational isomers. In Fig. 2 we have reproduced the absorption spectra of chloroacetone – CF_3COOH mixtures in solution. The 1724 and the 1752 cm^{-1} bands belong to the skew and the cis configurations of chloroacetone, while the broad bandcentered at 1709 cm^{-1} belongs to the hydrogen-bonded chloroacetone carbonyl group. If the last band were to belong to bound molecules having the skew configuration (shifted by 15 cm^{-1} from the monomer band) then at 1737 cm^{-1} we would expect a band representing hydrogen-bond molecules in the cis configuration. No distinct maximum could be detected

TABLE 1

The cyclohexanone–acid system		The CF_3COOH–ketone system		
acid	shift in the $\nu_{C=O}$ of the ketone,* cm^{-1}	ketone	shift in the $\nu_{C=O}$ of the ketone,* cm^{-1}	relative shift
CH_3OH	12	$(CH_2Cl)_2CO$	$6\leqslant$	$3{,}5\cdot10^{3}\leqslant$
C_6H_5OH	15	$CH_2ClCOCH_3$	15	$8{,}7\cdot10^{3}$
$CH_2ClCOOH$	19	CH_3COCH_3	25	$14{,}5\cdot10^{3}$
CCl_3COOH	26	$(CH_3)_2CO$	29	$16{,}9\cdot10^{3}$
CF_3COOH	29	Camphor	33	$18{,}9\cdot10^{3}$
		Pivalone	21,5	$12{,}7\cdot10^{3}$

in that region apparently due to the large width and overlapping of adjacent bands, and we can only deduce that some absorption takes place in the 1737 cm^{-1} region from the slightly elevated background. If on the other hand the 1709 cm^{-1} band should represent bound molecules in the cis configuration (shifted by 43 cm^{-1} from the monomer peak) then due to the absence of a shifted band at 1681 cm^{-1} belonging to the skew configuration we would have to assume that hydrogen bonding is not possible in the skew configurations, and yet if Bellamy's and Williams' interpretations are correct the reverse assumption would be more reasonable for steric reasons [7]. Hence it is natural to assume that the $\nu_{C=O}$ band of chloroacetone shifts by only 15 cm^{-1} when the compound is mixed with CH_3COOH. In the case of 1,3-dichloroacetone hydrogen bonding to CF_3COOH (OH...O=C) does not shift $\nu_{C=O}$ by more than 6 cm^{-1}.

Our results are summarized in Table 1. In cases where an associated band had some structure the shift was measured from the center of the complex band. One can see that in the cyclohexanone–acid series the shift in the ketone carbonyl band increases with increasing acid strength (proton-donor strength) while in the trifluoroacetic acid–ketone series the same pattern is observed with increasing electron-donor strength of ketones.

Pivalone does not fit into the sequence. This we are inclined to attribute to the fact that the molecule has a unique structure with the carbonyl group shielded by the methyl radicals. The same factor is apparently responsible for the unreactive nature of pivalone, which fails to enter into some typical reactions of ketones [8]. For stable hydrogen bonding (O...HO) the molecules have to approach quite closely, and this can only be achieved in the absence of steric hindrance. It is quite probable that this requirement can not be fulfilled in the case of hydrogen bonding between pivalone and trifluoroacetic acid. In the spectrum of the pivalone–phenol–CCl_4 system (which was recorded for the sake of comparison) the $\nu_{C=O}$ band of pivalone is shifted by 15.5 cm^{-1}; this shift is equal to that detected in the spectra of cyclohexanone or dipropyl ketone mixed with phenol in CCl_4 solutions. Consequently one can assume that steric hindrance interferes much less with hydrogen bonding between phenol and pivalone due to a greater equilibrium O...HO distance.

In concluding we would like to point out that hydrogen bonding increases considerably the integral absorption coefficient of the $\nu_{C=O}$ band (up to 200%).

The author wishes to express his deep gratitude to Prof. V. M. Chulanovskii for directing the work and valuable comments.

LITERATURE CITED

[1] V. M. Chulanovskii, Izvest. Akad. Nauk SSSR, Ser. Fiz. 22, 9, 1103 (1958).

[2] W. G. Schneider, J. Chem. Phys. 23, 1, 26 (1955).

[3] H. K. Ingold, Reaction Mechanisms and the Structure of Organic Compounds [Russian translation] (IL, 1959) p. 60.

[4] D. Cook, J. Am. Chem. Soc. 80, 1, 49 (1958).

* Shifts are measured relative to the corresponding band for a solution of the ketone in CCl_4.

[5] F. L. Vilesov, Doklady Akad. Nauk SSSR 138, 6 (1960).*

[6] L. B. Archibald and A. D. E. Pullin, Spectrochim. Acta 12, 1, 34 (1958).

[7] L. J. Bellamy and R. L. Williams, J. Chem. Soc. 4294 (1957).

[8] A Dictionary of Organic Compounds [Russian translation] (IL, 1949) Vol. 3, p. 506.

*See C. B. Translation.

REDUCTION OF COMPLEX COBALTAMMINES CONTAINING NEGATIVE SUBSTITUENTS IN THE INNER RING AT THE DROPPING-MERCURY ELECTRODE

N. V. Nikolaeva-Fedorovich and Academician A. N. Frumkin

M. V. Lomonosov Moscow State University
Translated from Doklady Akademii Nauk SSSR, Vol. 134, No. 5, pp. 1135-1137, October, 1960
Original article submitted July 19, 1960

There exists at the present time a large amount of experimental material to show that the reduction of bi- and multivalent anions at negative-charged surfaces proceeds (as revealed by the current-potential curves) under inhibition which is due to the repulsion of anions from such negative surfaces, and their consequent reduction in concentration in the surface layer [1]. When indifferent electrolytes are added to the solution, the drop in current may be eliminated in the case of the reduction of certain anions, which is explained by supposing that increased concentration of cations of the base material in the neighborhood of the electrode weakens the electrical field due to the negative charges on the surface of the electrode.

This inhibition of the electrolytic reduction is not only observed for the case of complex anions, but also for that of neutral molecules. Kivalo and Laitinen [2] observed a reduction of the current for the current–potential curves of the reduction of cis-$Pt(NH_3)_2Cl_2$; and inhibition of the reduction of the neutral complex $Pt(OH)_2(NH_3)_2Cl_2$ has also been observed in the neighborhood of the potential corresponding to zero charge on a mercury electrode by the authors of the current communication [3].

The reductions in the current during the reduction of neutral particles may be explained if we suppose that at the positively charged mercury surface a bond is formed through the chlorine atoms of these complexes which will be negatively charged; it then follows that increase in the negative charge at this surface will make the adsorption of the complexes increasingly difficult [3, 4]. This suggestion as to the reason for the inhibition of the reaction when the surface is negatively charged has been put to use in explaining the drop in current during the deposition of indium from solutions of its halides [5]. The reduction in the current in the neighborhood of the point of zero charge (P.Z.C.) during the deposition of indium on a dropping-mercury electrode has been observed by a number of authors, and a variety of explanations of the phenomenon have been proposed [5-7]. In [7] the existence of a minimum on the polarization curves for the deposition of indium is explained as due to "the anionic character of the complex indium ions." It is shown in the work of Kh. Z. Brainina, that 0.1 to 3 N potassium chloride in the indium solutions gives rise to the presence of neutral and positively charged complexes of indium, and the shape of the current-potential curve which is obtained is due to the reduction of these complexes. Thus, at the present time there are no unequivocal data concerning the sign of the charge of the complex indium ion which is reduced at the mercury electrode.

During their investigation of the reduction of the compound $[Co(NH_3)_6]Cl_3$, Laitinen, Frank and Kivalo [8] have observed a fall in current on the polarographic curve, and explained this by the formation of a film of cobalt hydroxide on the electrode surface. This film is believed to be formed as the result of a local alkalization of the solution through the decomposition of the cobalt complex which takes place when it is deposited on the electrode surface. We have shown [9] that acidification of the $[Co(NH_3)_6]Cl_3$ solution leads to the elimination of the minimum on the current-potential curve, for the reduction of this complex, but that further

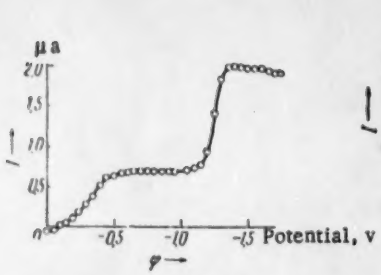

Fig. 1.

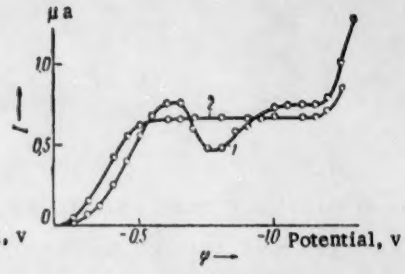

Fig. 2.

Fig. 1. Polarization curve for the reduction of 10^{-3} N $[Co(NH_3)_4CO_3]Cl$ in the presence of 0.1 N KCl.

Fig. 2. Polarization curves for the reduction of 10^{-3} N $[Co(NH_3)_4CO_3]Cl$: I) without base solution; 2) in a base solution of N KCl.

acidification leads to the reappearance of the minimum at other potentials. This phenomenon was accounted for by the formation in the solution of chlorine-substituted complex cobaltammines, which would be adsorbed on the electrode through the negatively charged chlorine atoms. In order to provide proof of this suggestion, polarograms of the complex cation $[Co(NH_3)_5Cl]^{2+}$ were recorded. In the reduction of this cation, just as in that of the anion, the current-potential curve revealed inhibition of the reaction in the neighborhood of the point of zero charge. It was found, however, that the polarization curves for the reduction of $[Co(NH_3)_5Cl]^{2+}$ altered with time, which may possibly be due to the slow reaction of the inner-ring substituents in the body of the solution [10].

In order to elucidate the possibility of the inhibition of the reaction during the reduction of positively charged complexes, we have carried out an investigation of the reduction at the dropping-mercury electrode of the cation $[Co(NH_3)_4CO_3]^+$, which appears to be stable in solution. We have not been able to find information about the polarographic reduction of the complex $[Co(NH_3)_4CO_3]Cl$ in the published literature.

Figure 1 shows that the reduction of 10^{-3} N $[Co(NH_3)_4CO_3]Cl$ in a base solution of 0.1 N potassium chloride gives an ordinary current-potential curve made up of two waves. The height of the second wave is twice as great as that of the first, showing that the first process consists of the reduction of Co^{3+} to Co^{2+}, and the second, of the reduction of Co^{2+} to metallic cobalt. If the reduction is carried out from more dilute solutions (with respect to the base salt), the magnitude of the current in the first part of the curve, in the neighborhood of the point of zero charge, is reduced; a minimum value is reached, and then the value increases again to the limiting diffusion value (Fig. 2). The inhibition of the reaction is not, as it was for the reduction of $[Co(NH_3)_6]Cl_3$, connected with the formation of a film of cobalt hydroxide on the surface of the electrode, since the introduction of 10^{-3} N hydrochloric acid into the solution does not alter the shape of the curve. The use of 0.1 N or 1 N potassium chloride as base solution completely eliminated the inhibition of the reaction. The limiting current in the presence of N potassium chloride is smaller than in the pure solution of 10^{-3} N complex salt, because of the reduction of the migration effect. Increase in the charge on the base-solution catalyst increases the effectiveness of the substance. Figure 3 shows that the addition of only 10^{-3} N barium chloride to a solution of $[Co(NH_3)_4CO_3]Cl$ is sufficient to remove the inhibition, while this is not effected by potassium chloride at lower concentrations than 0.1 N. Within the limits of experimental error, it does not appear that change in the radius of the base solution cation has any influence on the rate of reaction. Thus, the polarization curves for the reduction of $[Co(NH_3)_4CO_3]Cl$, obtained in 10^{-3} N solutions of the alkali metal chlorides are practically coincident. The addition of the organic cation $[(C_2H_5)_4N]^+$ leads to increase in the reaction rate, and then complete elimination of the inhibition, in the same way as inorganic cations (Fig. 4). If the cations used have longer organic chains, an abrupt inhibition of the reaction is found. Thus, the introduction of the salt $[(C_5H_{11})_4N]Br$ into the solution reduces the rate of reaction; but increasing the value of the negative potential to that corresponding to the desorption of the tetraamylammonium cations from the electrode surface causes an increase in the reaction rate.

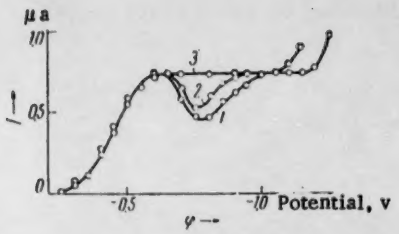

Fig. 3.

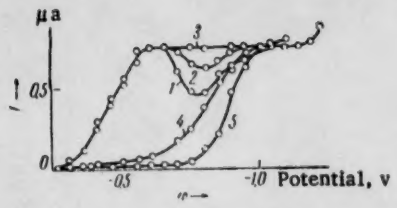

Fig. 4.

Fig. 3. Polarization curves for the reduction of 10^{-3} N $[Co(NH_3)_4CO_3]Cl$ in the presence of barium chloride. Concentration of the latter: 1) 0; 2) 10^{-4} N; 3) 10^{-3} N.

Fig. 4. Polarization curves for the reduction of 10^{-3} N $[Co(NH_3)_4CO_3]Cl$: 1) without base salt; 2) in the presence of 10^{-3} N $[(C_2H_5)_4N]_2SO_4$; 3) in presence of 10^{-2} N $[(C_2H_5)_4N]_2SO_4$; 4) in the presence of 10^{-4} N $[(C_5H_{11})_4N]Br$; 5) in the presence of $5 \cdot 10^{-4}$ N $[(C_5H_{11})_4N]Br$.

It is thus seen that, for the reduction of the cation $[Co(NH_3)_4CO_3]^+$, inhibition of the reaction is found in moving from a positively to a negatively charged surface, in the same way as for the reduction of anions. The rate of the reaction depends on the nature, the charge and the concentration of the base solution cations.

The inhibition of the reaction of $[Co(NH_3)_4CO_3]^+$ ions may be explained as due to change in the adsorption conditions when the sign of the surface charge on the mercury is latered [3-5]. The positively charged complex cation of the ammine is, when the surface is also positively charged, adsorbed through the negatively charged CO_3^{2-} group. When the surface acquires a negative charge, such a bond with the electrode surface would be weakened, and the rate of reduction of the complex cation would be reduced. If the negative charge on the surface is screened by the cations of the base salt the rate of reaction will increase. Cations which are strongly adsorbed and so cover the electrode surface, such as the tetraamylammonium ion, may displace the complex cation from the electrode surface, and so produce a sudden inhibition of the reaction.

The inhibition of the reaction with change in sign of the surface charge, which is characteristic for the reduction of a number of anions, has thus been found by us to apply to the cationic complex ion $[Co(NH_3)_4CO_3]^+$. We have also found that it applies to certain other cations, such as trans-$[Co(NH_3)_4Cl_2]^+$, $[Co(NH_3)_5NO_2]^+$.

LITERATURE CITED

[1] T. A. Kryukova, Doklady Akad. Nauk SSSR 65, 517 (1949); A. N. Frumkin and G. M. Florianovich, Doklady Akad. Nauk SSSR 80, 907 (1951); Zhur. Fiz. Khim. 29, 1827 (1955); A. N. Frumkin and N. V. Nikolaeva-Fedorovich, Vestn. MGU, Ser. Fiz. Khim. 4, 169 (1957).

[2] P. Kivalo and H. Laitinen, J. Am. Chem. Soc. 77, 5205 (1955).

[3] A. N. Frumkin and N. V. Nikolaeva, J. Chem. Physics 26, 1552 (1957); N. V. Nikolaeva-Fedorovich and Yu. M. Povarov, Zhur. Anal. Khim. 14, 663 (1959).*

[4] A. N. Frumkin, Discussion: Proceedings of the Fourth Conference on Electrochemistry [in Russian] (Izd. AN SSSR, 1959).

[5] Kh. E. Brainina, Doklady Akad. Nauk SSSR 130, 797 (1960).*

[6] M. Bulovova, Coll. Czech. Chem. Com. 19, 1123 (1954).

[7] P. I. Zabotin, S. P. Bukhman, and G. Z. Kir'yakov, Proceedings of the Fourth Conference on Electrochemistry [in Russian] (Izd. AN SSSR, 1959) p. 179.

[8] H. Laitinen, A. Frank, and P. Kivalo, J. Am. Chem. Soc. 75, 2865 (1953).

* Original Russian pagination. See English translation.

[9] N. V. Nikolaeva-Fedorovich and B. B. Damaskin, Thesis: Communication on Polarographic Analysis in October, 1959 [in Russian] (Kishinev, 1959).

[10] N. V. Nikolaeva and V. N. Presnyakova, Doklady Akad. Nauk SSSR 87, 61 (1952).

TRANSITION OF ELECTRONIC CONDUCTION INTO IONIC CONDUCTION AS RELATED TO THE COMPOSITION OF SOLID OXIDE SOLUTIONS

S. F. Pal'guev, S. V. Karpachev, A. D. Neuimin, and Z. S. Volchenkova

Institute of Electrochemistry, Ural Branch of the Academy of Sciences of the USSR
(Presented by Academician A. N. Frumkin, June 6, 1960)
Translated from Doklady Akademii Nauk SSSR, Vol. 134, No. 5, pp. 1138-1141, October, 1960
Original article submitted June 6, 1960

At 1000°C solid CeO_2-ZrO_2 solutions are practically electronic conducters [1]. On the other hand, solid solutions of the oxides ZrO_2-CaO have a purely ionic conduction in which only the oxygen ions are mobile [2-4]. To evaluate the influence which introduction of calcium oxide into $(Ce, Zr)O_2$ oxide mixtures has upon the electric conductivity we made measurements and determined the character of the conductivity for a series of samples having the composition $(0.75\ CeO_2 \cdot 0.25\ ZrO_2)$ + CaO. The composition $0.75\ CeO_2 \cdot 0.25\ ZrO_2$ was taken as one of the components, since in the system CeO_2-ZrO_2 maximum conductivity is found at the said composition [1].

The samples were prepared from CeO_2 (pure), ZrO_2 (p.a.) and calcium carbonate (p.a.). The method of preparing the samples and measuring their electric conductivity was analogous to that described in the study [1]. For each sample the temperature dependence of the electric conductivity was determined in the range 500-1000° and from this the activation energy was calculated. The character of the conductivity was determined by measuring emf's. The method is based on the following principle. It is known [5, 6] that the emf of a cell in which the electrolyte, besides ionic, also has electronic conductivity (whether p- or n-type) is given by the relation $E = [1 - (\bar{t}e + \bar{t}_0)]E_0$, where E is the measured electromotive force of the cell; $\bar{t}e$ and $\bar{t}_0$ are the mean transference numbers of the electrons and the holes, respectively, in the electrolyte; E_0 is the thermodynamic value of the electromotive force of the cell investigated (that is, the value it should have, when the solid electrolyte did not show electron or hole conduction). To evaluate the value of $(\bar{t}e + \bar{t}_0)$, that is, the fraction of electronic conductivity in the electrolyte, it is sufficient to measure the emf of the cell containing the electrolyte investigated and compare it with the value calculated thermodynamically. For this, of course, the electrochemical cell must be composed in such a way that it is indeed possible to calculate the thermodynamic value of its emf. We used two types of cells:

$$(Pt),\ O_2,\ p_1 \mid \text{solid electrolyte} \mid O_2,\ p_2,\ (Pt) \qquad \text{(I)}$$

$$Me', Me'(O) \mid \text{solid electrolyte} \mid Me''(O),\ Me'' \qquad \text{(II)}$$

In the cells indicated the emf is determined by the oxygen pressures at the electrodes. Its thermodynamic value can be calculated from the relation: $E_0 = (RT/4F)\ln(p_2/p_1)$. Here p_1 and p_2 represent the oxygen pressures at the right and left side, respectively, of the cell. Because when working with cell (I) the electrolyte is in contact with oxygen and in case (II) it is in vacuum, the way in which the electronic (hole) conduction of the electrolyte

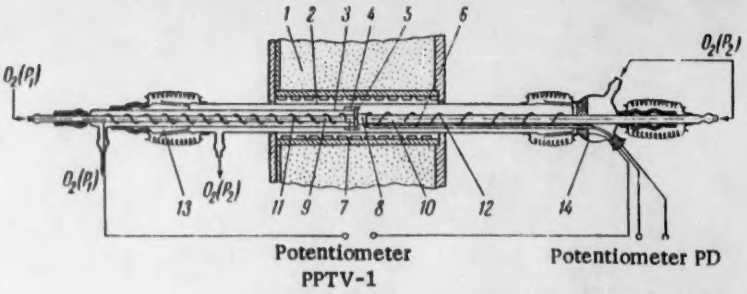

Fig. 1.

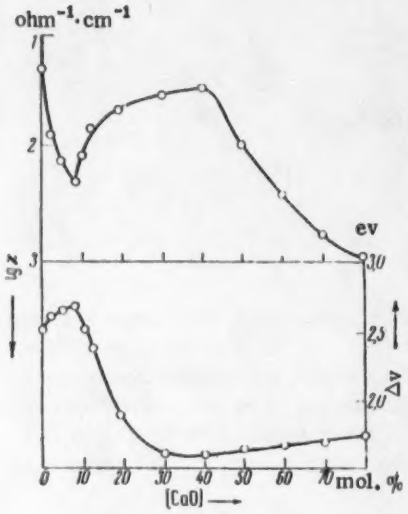

Fig. 2.

depends upon the partial pressure of oxygen in the gas phase may be evaluated by comparing the results obtained with both types of cells; in many cases this is of great interest.

The construction of the type (I) cell is shown in Fig. 1. The solid electrolyte (5) with both faces coated with platinum electrodes is fixed between two quartz tubes (9 and 10) by which gas is fed to the electrodes. The electrodes make contact with platinum nipples (7 and 8) to which platinum current leads (11 and 12) are welded. The slab of solid electrolyte is carefully ground to fit in the quartz tube (3) by means of which the electrode spaces are separated. The quartz tubes (9 and 10) are clamped to the molybdenum glass caps (13 and 14). By means of ground joints these caps fix the whole system inside the quartz tube (2), which is placed in the furnace (1). The thermocouple (6) is very close to the sample. It is indicated by arrows how gases with oxygen partial pressures varying generally 5-10 times are fed. Measurements with the cell (I) enable the fraction of ionic conductivity to be evaluated with an accuracy of 2-3%.

The construction of the type (II) cell is analogous. In it the electrode spaces are not separated, since it does not contain the system to feed gases to the electrodes. The partial oxygen pressures at the electrodes are here determined by the dissociation pressures of the corresponding oxides. For this purpose we used Fe, FeO and Cu, Cu_2O mixtures [2]. The accuracy of measurements with this type of cell decreases with increasing fraction of electronic conductivity.

In Fig. 2 the results of the conductivity measurements at 1000° are given. However, the change of the activation energy with varied composition is not shown here. The results obtained when investigating the character of electric conduction for the ternary system studied by us and for the separate oxides are given in Table 1.

As follows from Table 1 and Fig. 2, the total conductivity in the system drops at small additions of calcium oxide, although the ionic conductivity increases. Meanwhile, as the experiment [3] shows, addition of calcium oxide to zirconium oxide and also to cerium oxide itself results in an increasing conductivity, while the thus formed solid solutions also have a higher fraction of ionic conductivity the higher their CaO content [7]. An explanation of these experimental results may be given by starting from the following considerations.

It is known [8, 9] that a relatively small but noticeable decrease in weight is observed, when CeO_2-ZrO_2 solid solutions are heated. Obviously, this is caused by a loss of oxygen from the side of cerium. Therefore, it may be assumed that part of the cerium in the CeO_2-ZrO_2 solid solution is in the trivalent state. The occurrence of noticeable quantities of trivalent cerium ions side by side with tetravalent ones may give rise to a considerable electronic conductivity. In this connection, the decrease in electronic conduction, found at

TABLE 1

Temp., °C	Fraction of ionic conductivity (in percents) in samples with compositions:									
	CeO_2*	ZrO_2*	CaO **	0.75 CeO_2·0.25 ZrO_2 + CaO (mol. %)						
				0.0	5.0	8.0	12.5	19.0	40.0	60.0	80.0
600	3.4	89,8	—	2,1	—	86,4	91,8	96,9	99,0	90,0	93,3
650	5.2	88,8	—	2,9	—	89,4	95,2	98,1	99,7	94,1	96,8
700	9,5	87,8	—	2,1	51,7	90,3	96,3	99,1	99,1	96,4	98,7
750	16,0	87,7	—	2,3	60,6	91,0	97,1	100,0	100,0	98,0	98,7
800	21,4	89,3	63,3	3,1	57,2	88,6	97,2	98,9	100,0	98,3	99,3
850	21,2	91,0	69,7	2,4	48,5	84,4	96,3	98,4	99,5	98,4	99,3
900	18,0	89,2	66,9	2,5	45,9	79,2	94,7	97,5	98,7	98,4	98,7
950	13,7	89,7	61,8	2,9	41,5	74,4	92,4	97,6	98,3	98,6	98,3
1000	10,3	79,8	60.3	2.1	36,8	69,9	89,9	96,0	99,1	98,3	98,2

* The samples were prepared from specially pure cerium dioxide with an impurity content not higher than 0.01%.

** The measurements were done in a type (II) cell. In the course of time these values decrease.

increasing calcium oxide content, may be explained by a lowered degree of reduction of the tetravalent cerium, which is caused by the presence of calcium oxide in the solid solution. In ternary CeO_2-ZrO_2-CaO solutions oxygen ions will be the carriers effecting ionic conduction, since this is the case in the system ZrO_2-CaO [3, 4].

In general, conductivity based on oxygen ions may be expected in solid oxide solutions of metals with variable valence of the substitutional type and having a cubical crystal lattice (usually of the fluorite type). Owing to the variable valence of the cations there are vacancies in the anodic part of the crystal lattice of the solid solution and they enable the migration of oxygen ions to take place. As x-ray studies have revealed, we have such a case: in the ternary CeO_2-ZrO_2-CaO system. In the range of CaO contents between 0 and 40 mol.% CaO there is a continuous series of solid solutions. Meanwhile the crystal lattice (fluorite type) of the solid solution 0.75 CeO_2 · 0.25 ZrO_2 is conserved.

From this point of view it is easy to explain the changing character of the conductivity in our samples, observed when varying the CaO content. Solid solutions of ZrO_2 in CeO_2, which do not contain calcium oxide, have practically no ionic conductivity, since the number of oxygen ion vacancies in their crystal lattice is very small. On the other hand, for the reason mentioned above, the electronic conductivity is high. Upon raising the CaO content in the solid solution the fraction of ionic conductivity also increases continuously and attains practically 100% in the samples with 20-40 mol.% CaO, where the number of defects in the anodic part of the lattice is high.

Since in this range the total conductivity remains nearly the same, we have the interesting case of a gradual transition from electronic to ionic conduction and not of a relatively increasing ionic conduction with an unchanged electronic contribution.

Probably, the presence of a minimum conductivity is connected here with the following aspect. By the introduction of calcium oxide into the lattice of the solid solution of cerium and zirconium dioxide the oxygen ion deficiency is raised. The latter is accompanied by some distortion; that is, energy is consumed. The presence of trivalent cerium in the solid solution has the same effect and at increasing CaO content the trivalent cerium ions will tend to go back to the tetravalent state (in an oxidizing atmosphere). This lowers the electron-donor (Ce^{3+}) concentration and the fraction of electronic conductivity drops sharply. Although meanwhile the fraction of ionic conductivity rises, the number of oxygen ion vacancies, obviously, is still too small to provide a considerable conduction. Therefore, in the samples with a CaO content up to 8 mol.% the total conductivity drops. Only at higher values of the calcium content in the solid solutions does the ionic conductivity increases so much that it overcompensates the continued decrease (already relatively small) of the electronic contribution and, consequently, the total conductivity begins to rise.

The supposition that the electronic conductivity of the solid CeO_2-ZrO_2 solutions has its origin in a partial reduction of Ce^{4+} to Ce^{3+} is also confirmed by the fact that CeO_2 and ZrO_2 itself have a considerably higher

fraction of ionic conductivity than their solid solutions. At the formation of solid solutions the ionic conductivity existent in pure CeO_2 and ZrO_2 remains present, but is not noticed, because the electric conductivity of the solid solutions is several orders of magnitude higher than that of the pure oxides [1].

The data, given in Table 1, have been obtained by measurements in the type (I) cell, that is, under conditions where the solid electrolyte was in contact with gases having a relatively high (1.0-0.2 atm) oxygen partial pressure. Under these conditions the ionic conductivity in the solid solution is near to 100% at a CaO content of 20-40 mol.%. In the case that the measurements were done at very small oxygen pressures: $10^{-7} - 10^{-25}$ atm [in the type (II) cell], electronic conductivity also completely dominates in these solid solutions. It should be remarked that in the latter measurements the samples changed their color and after the experiment actually collapsed, which points out that cerium had been reduced to a very considerable extent.

The fraction of ionic conductivity in the oxide system investigated is markedly dependent upon temperature and has a maximum at 750°. The increase in ionic conductivity at higher temperatures originates from the raised mobility of the ions and its decrease at still higher temperatures is a result of the thermal decomposition of cerium dioxide into Ce_2O_3. As follows from Table 1, the latter is diminished, for reasons considered above, when the calcium oxide content in the solid solution increases.

The change in activation energy of electric conductivity found in the experiment (Fig. 1) is in agreement with the mechanism described above.

In the system investigated the electric conductivity rises until the highest calcium oxide content (40 mol.%) allowed in solid solution is reached. From this it may be concluded that, in contrast with ZrO_2-CaO solid solutions [3], here the interaction between lattice defects (oxygen vacancies), if any is present, has no noticeable influence upon the electric conductivity and that the latter is mainly determined by the number of these defects.

The drop in electric conductivity, found when increasing the CaO content above 40 mol.%, obviously is connected with the presence of free calcium oxide.

LITERATURE CITED

[1] S. F. Pal'guev and S. Z. Volchenkova, Zhur. Fiz. Khim. 34, No. 2 (1960).

[2] K. Kiukkola and C. Wagner, J. Electrochem. Soc. 104, 379 (1958).

[3] Z. S. Volchenkova and S. F. Pal'guev, Trudy Inst. Elektrokhim. Ural Fil. Akad. Nauk SSSR, 1 (1960).

[4] W. D. Kingery, J. Pappis, M. E. Doty, and D. C. Hill, J. Am. Ceram. Soc. 42, 393 (1959).

[5] C. Wagner, Z. Phys. Chem. 21, 25 (1933).

[6] S. V. Karpachev and S. F. Pal'guev, Trudy Inst. Elektrokhim. Ural Fil. Akad. Nauk SSSR, 1 (1960).

[7] S. F. Pal'guev and A. D. Neuimin, Trudy Inst. Elektrokhim. Ural Fil. Akad. Nauk SSSR, 1 (1960).

[8] H. Vartenberg and W. Gurr, J. Am. Ceram. Soc. 196, 374 (1931).

[9] S. F. Pal'guev, S. I. Alyamovskii, and Z. S. Volchenkova, Zhur. Neorg. Khim. 4, 2571 (1959).

THE INTERACTION OF HYDROGEN WITH URANIUM TRIOXIDE

V. G. Vlasov and V. N. Strekalovskii

S. M. Kirov Ural Polytechnic Institute
(Presented by Academician V. I. Spitsyn, July 11, 1960)
Translated from Doklady Akad. Nauk SSSR, Vol. 134, No. 6, pp. 1384-1386, October, 1960
Original article submitted July 8, 1960

The present communication is a report of the results obtained in a study of the kinetics of reduction of uranium trioxide by gaseous hydrogen at temperatures over the interval from 350 to 500°C and at pressures ranging from 50 to 400 mm of Hg. These experiments were carried out in a high-vacuum system in which spring balances were employed to give a continuous indication of the loss of mass in the charge.

Experimentally developed curves are presented in Figs. 1 and 2. Treatment of the experimental data led to the rate relations which are graphed in Figs. 3 and 4.

A 100% reduction was considered as involving complete conversion of the trioxide into the dioxide, since, on thermodynamic grounds, reduction of the higher oxides of uranium by hydrogen can proceed no further.

Figures 3 and 4 show the initial step in the reduction to proceed at a constant rate under all temperatures and gas pressures. The length of the plateau corresponding to this step increases with rising temperature at fixed pressure, and with rising pressure at fixed temperature.

In this stage, the relation between the reaction rate and the hydrogen pressure at constant temperature is described well by the equation

$$V = kP_{H_2}^{1/2}. \quad (1)$$

The apparent energy of the activation of the reaction is 20.8 kcal/mole.

The rate of reaction diminishes sharply when the degree of reduction reaches a definite value which is fixed by the working temperature and pressure. This fall in the reaction rate is accompanied by a relatively small alteration in the degree of reduction.

The experimental conditions employed here were such that the final stage of the reduction is also characterized by constancy of the reaction rate. The experiment performed at 500° and P_{H_2} = 200 mm of Hg is exceptional in this respect. In this instance, the second plateau on the curve (Fig. 3) is followed by a segment along which the reaction rate diminishes with increasing reduction. The apparent energy of activation for 70% reduction is 30 kcal/mole. In this stage of the reduction, the relation between the reaction rate and the hydrogen pressure at constant temperature and with P_{H_2} = 50-200 mm of Hg is described satisfactorily by the equation:

$$V = k_1 P_{H_2}. \quad (2)$$

The compositions of the products obtained at the various temperatures are given in Table 1; the reduction never proceeded as far as UO_2, and went beyond U_4O_9 only at 500°. Work carried out in this laboratory [1] has proven that vacuum dissociation of uranium trioxide occurs only at temperatures in excess of 430°. Our

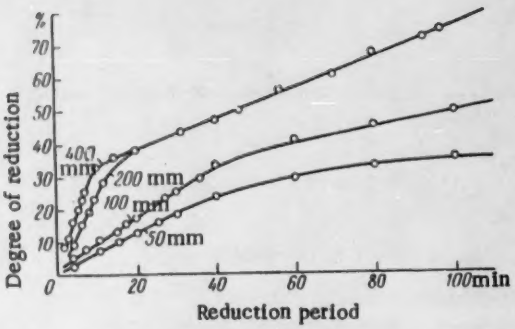

Fig. 1. Degree of reduction as a function of time at various temperatures with P_{H_2} = 200 mm.

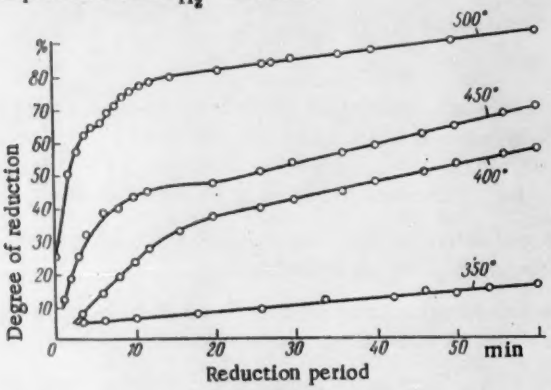

Fig. 2. Degree of reduction as a function of time under various hydrogen pressures and at a temperature of 400°.

TABLE 1

Composition of Final Reduction Products (P_{H_2} = 200 mm; reduction period, two hours)

Temperature, °C	O: U ratio in final product
500	2.09
450	2.30
400	2.43
350	2.83

observations show the reduction of UO_3 by hydrogen to begin at 350°. Thus the possibility of dissociation prior to reduction of the trioxide can be ruled out.

Certain conclusions concerning the limiting steps in the various stages of reduction can be based on these kinetic data. The interpretation will make use of the U–O phase diagram from [2].

The first plateau on the curves of Figs. 3 and 4 corresponds to the reduction of UO_3 to U_3O_8. The limiting step in this stage of the reduction is the surface reaction between the oxygen of the oxide and the hydrogen which is adsorbed on it. The fact that Eq. (1) is applicable here justifies the assumption that the hydrogen is rather rapidly adsorbed on the uranium trioxide surface in this intermediate step and an equilibrium is set up so that the adsorption isotherm would have the form: $a = k'P_{H_2}^{1/2}$. The ½ exponent in this last equation can be explained by supposing the hydrogen molecules to dissociate into atoms. Thus, according to F. F. Vol'kenshtein [3]: "The adsorption of hydrogen does not usually occur in the molecular state, but in the atomic condition."

The concentration of the oxygen in the oxide can be considered as constant, so that the rate of the surface reaction with hydrogen should be directly proportional to the concentration of the latter on the adsorbent surface.

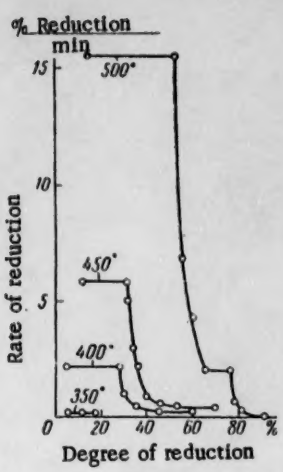

Fig. 3.

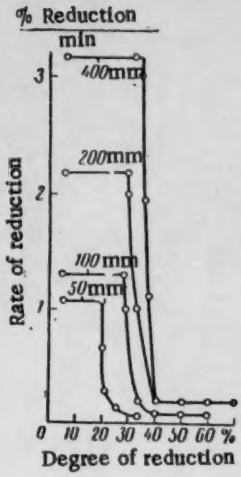

Fig. 4.

Fig. 3. Rate of reaction as a function of degree of reduction at various temperatures.

Fig. 4. Rate of reaction as a function of degree of reduction at various hydrogen pressures.

Thus the over-all rate of reduction would be proportional to the one-half power of the hydrogen pressure if this is actually the limiting step, just as our experiments show the case to be.

It should be noted that similar relations have been established for the hydrogen reduction of oxides of lead, cadmium, and tin [4]. The curve segments along which the rate diminishes with increasing degree of reduction correspond to a gradual transition from U_3O_8 to a $UO_{2.6} \pm x$ phase in which the oxygen content is at a minimum for the temperature in question. No new phase is formed during this time, the diminution of the rate being due to the reduction of the oxygen concentration in the solid state.

The second plateau on the curves of Figs. 3 and 4 corresponds to the reduction of the $UO_{2.6} \pm x$ phase of minimal oxygen content into a tetragonal phase.

The adsorption of hydrogen on the oxide surface is the limiting step in this stage of the reduction. This is indicated by the fact that the over-all rate of reduction is proportional to the hydrogen pressure.

LITERATURE CITED

[1] V. G. Vlasov and A. G. Lebedev, Izvest. Vyssh. Uch. Zav., Chernaya Metallurgiya 7, 5 (1960).

[2] Atomnaya Énergiya 4, 2, 215 (1958).*

[3] F. F. Vol'kenshtein, Usp. Fiz. Nauk 50, 2, 257 (1956).

[4] G. Björling, Svensk kem. tidskr. 67, 6-7, 319 (1955).

*Original Russian pagination. See C. B. Translation.

THE SURFACE STATE OF ANODICALLY POLARIZED GERMANIUM IN ALKALINE SOLUTIONS

E. A. Efimov and I. G. Erusalimchik

(Presented by Academician A. N. Frumkin, June 8, 1960)
Translated from Doklady Akad. Nauk SSSR, Vol. 134, No. 6, pp. 1387-1389, October, 1960
Original article submitted June 8, 1960

In recent times alkaline solutions have been extensively used in electrochemical etching of germanium for the production of semiconductor devices. In spite of this, there are in literature very few data on the state of a germanium electrode during electrochemical etching.

Turner, Bardeleben and other investigators, when studying the surface state of anodically polarized germanium, did experiments in acid solutions.

After having investigated the behavior of a germanium anode in NaOH and NH_4OH solutions Jirsa [1] came to the conclusion that during the corrosion of germanium a monoxide layer is formed on its surface. Beck and Gerisher [2] when discussing the mechanism of anodic corrosion on germanium, prove that this process certainly proceeds via the formation of oxidic germanium compounds on the surface.

In the present study we used the method of charge curves to investigate the state of anodically polarized germanium in alkaline solutions. All experiments were done with a polycrystalline degenerate germanium electrode in a 0.1 N KOH solution at 20°C.

The impurity concentration in the degenerate germanium, which had no semiconducting properties, was close to 0.01%, so, from a chemical point of view, it was very pure. We used degenerate germanium in order to avoid in the electrode processes all complications connected with the passing of a current through a semiconducting electrode. Preliminary experiments showed that the kinetics of anodic corrosion for degenerate germanium and p-germanium are identical. For both types of germanium, for instance, the φ versus log I curves practically coincide, which is in complete accordance with established rules, since the anodic corrosion of p-germanium is not retarded by a deficiency of holes in the semiconductor-electrolyte boundary.

The germanium electrode was exposed to anodic polarization at various current densities during a fixed time, and after that the charge curve at a cathodic current density of 10^{-3} amp/cm, was recorded by means of the oscillograph ÉNO-1. Before each experiment the germanium electrode was etched in CP-4 and thereafter brought to a constant potential (~ -0.55 v) by a cautious cathodic polarization.

Cathodic charge curves, obtained after a previous anodic polarization during 10, 20, 60 or 120 sec at the potential -0.350 or -0.330 v, are shown in Fig. 1. In all cases at a potential of nearly -0.75 v there is observed a retarded rise of the potential, which is connected with the removal of oxygen from the germanium surface. At the anodic polarization potential $\varphi = -0.35$ v the amount of electricity, required for this purpose, is $\sim 4.5 \cdot 10^{-4}$ coul/cm^2 and does not depend upon the duration of the polarization. Charge curves, obtained after a polarization at a more negative anode potential, in their appearance remind one of curves 1 of Fig. 1. However, here the amount of electricity, consumed by the removal of adsorbed oxygen will be smaller. For instance at $\varphi = -0.420$ v it is $2 \cdot 10^{-4}$ coul/cm^2.

The potential of ~ -1.4 v corresponds with the potential of hydrogen evolution on a clean germanium surface in 0.1 N KOH at $I = 10^{-3}$ amp/cm^2.

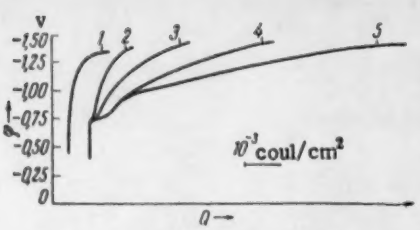

Fig. 1.

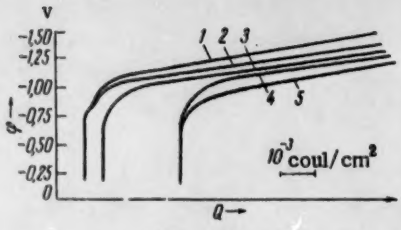

Fig. 2.

Fig. 1. Charge curves, obtained after a previous anodic polarization at $\varphi = -0.35$ v and $\varphi = -0.33$ v. 1) $\varphi = -0.35$ v, 10-120 sec; 2) $\varphi = -0.33$ v, 10 sec; 3) $\varphi = -0.33$ v, 20 sec; 4) $\varphi = -0.33$ v, 60 sec; 5) $\varphi = -0.33$ v, 120 sec.

Fig. 2. Charge curves, obtained after a previous anodic polarization at $\varphi = -0.18$ v and $\varphi = -0.15$ v. 1) $\varphi = -0.18$ v, 10 sec; 2) $\varphi = -0.18$ v, 20 sec; 3) $\varphi = -0.18$ v, 10 sec; 4) $\varphi = -0.15$ v, 10 sec; 5) $\varphi = -0.15$ v, 60 sec.

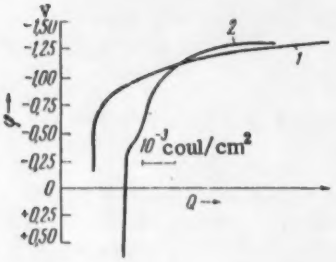

Fig. 3. Charge curves, obtained after a previous anodic polarization at $I = 2.5 \cdot 10^{-2}$ amp/cm². 1) 10-60 sec; 2) 120 sec.

The shape of curve 1 in Fig. 1 indicates that all oxygen adsorbed on the germanium surface is removed during cathodic polarization and that the amount of oxygen deposited depends upon the potential of anodic polarization. The character of curve 1 in Fig. 1 allows us to suppose that at $\varphi \leq -0.35$ v ($I \leq 10^{-4}$ amp/cm²) an electrochemical adsorption of oxygen takes place. It can easily be calculated [3] that 1 oxygen atom occupies 1 germanium atom.

When the potential of the previous anodic polarization is raised to -0.33 v, ($I = 2.5 \cdot 10^{-4}$ amp/cm²), at $\varphi \approx -0.75$ v, a horizontal platform makes its appearance in the charge curves (curves 2, 3, 4, 5 of Fig. 1) and the amount of electricity required to remove the oxygen from the electrode increases by about an order of magnitude. Moreover, it increases symbatically with the duration of the anodic polarization (from 10^{-3} coul/cm² at $\tau = 10$ sec to $7 \cdot 10^{-3}$ coul/cm² at $\tau = 120$ sec). When the potential of the anodic polarization is further raised to $\varphi \approx -0.20$ v, the character of the cathodic charge curves does not change, although the amount of electricity consumed during the levelling off increased to $1.2 \cdot 10^{-2}$ coul/cm².

The appearance of a horizontal level in curves 2, 3, 4, 5 of Fig. 1 allows to suppose that at anodic potentials less negative than -0.33 v part of the electrochemically adsorbed oxygen is bound more strongly to the surface. The amount of electricity consumed on the horizontal level does not exceed $4.4 \cdot 10^{-4}$ coul/cm². This points out that a monolayer of an oxidic surface compound, containing 1 oxygen atom per germanium atom [3], is formed on the germanium electrode.

The horizontal level at $\varphi = -0.75$ v is observed in the cathodic charge curves obtained at anodic polarization with a potential not exceeding $\varphi = -0.180$ v (Fig. 2). When the duration of anodic polarization is prolonged or the potential is raised to $\varphi = -0.15$ v, $I = 10^{-2}$ amp/cm², the shoulder disappears (curves 3, 4, 5 of Fig. 2), although the amount of oxygen deposited approximately is conserved.

Charge curves, obtained after an anodic polarization at $I = 2.5 \cdot 10^{-2}$ amp/cm² ($\varphi = -0.03$ v), are shown in Fig. 3. If the duration of anodic polarization is prolonged to 120 sec, then, owing to concentration effects connected with the slow diffusion of OH^- ions to the electrode surface [2], the electrode potential rises to $\sim +0.6$ v and a new shoulder at $\varphi = -0.25$ v appears in the charge curve connected with a considerable change (due to the prolonged anodic polarization) in the pH of the solution in the layer adjacent to the electrode (Fig. 3, 2).

From the experimental data obtained it is clear that the total amount of oxygen adsorbed on germanium may attain 10 or more monolayers. So it is reasonable to assume that during the anodic corrosion of germanium a layer of an oxide phase, which starts to be reduced cathodically at $\varphi = -0.75$ v, is formed on its surface.

LITERATURE CITED

[1] F. Jirsa, Z. anorg. Chem. 268, 84 (1952).

[2] F. Beck and H. Gerisher, Z. Electrochem. 63, 500 (1959).

[3] I. Law and P. Meigs, Semicond. Surface Physics (1957) p. 383.

THE PROBLEM OF THE SOLVATION OF IONS

N. A. Izmailov and Yu. A. Kruglyak

The A. M. Gor'kii Khar'kov State University

(Presented by Academician M. I. Kabachnik, May 23, 1960)
Translated from Doklady Akademii Nauk SSSR, Vol. 134, No. 6, pp. 1390-1393, October, 1960
Original article submitted May 12, 1960

According to current theories [1], the thermodynamic functions of the hydration of ions – the isobaric-isothermal potential ΔZ_h^i, the enthalpy ΔH_h^i, and the entropy ΔS_h^i – are evaluated on purely electrostatic premises. There has, however, not been produced up to the present evidence which validates the electrostatic nature of the interaction between ions and the molecules of the solvent. Calculation shows [1] that, because of the compensation of certain energy factors, the main contribution to the total energy of hydration is provided by the energy of ion-dipole interaction, which is usually written in the form:

$$A = -nze\mu/r^2, \tag{1}$$

where n is the hydration number, z the charge on the ion, and μ the dipole moment of the water molecule.

It may be noted that this formula is accurate if $r \gg d$, where d is the length of the dipole, which is definitely not the case in the solutions. Hence, according to the assumptions of the theory, the thermodynamic functions of cobalt would be expected to depend strongly on the dimensions which are selected for the dimensions of the molecules and ions, and for the dipole moments and the dielectric constant D. In the calculations which have been made, investigators have used various values for the quantities n, μ and r, and have obtained agreement within limits of 10 to 15% with the experimental data.

Table 1 gives the values of u, D, the molecular volume V_M and $-\Delta Z_s^i$ for a series of solvents calculated by one of us [2] by extrapolation of the sum and difference of the chemical energies of solvation of one given ion with those of a series of other ions of steadily increasing radius (as determined by $1/r_{cryst}$ for these ions) to zero. We see that the data in Table 1 reveal the practical independence of ΔZ_s^i of the properties of the solvent which have been mentioned. It is probable that this is due to the fact that the magnitudes of ΔZ_s^i depend on more general causes than those taken into account in the calculations based on an electrostatic model.

N. A. Izmailov, together with E. F. Ivanova [3] has attempted the calculation of ΔH_s^i in alcohols by the method of K. P. Mishchenko and A. M. Sukhotin. It was only possible to get agreement with the experimental data (within limits of 30%) when the radius of the alcohol was taken in the form: $r_{alc} = r_{H_2O} \times$ (M. W. of alcohol)/(M. W. of water). This itself bears witness to the very limited applicability of the electrostatic model – in effect, to aqueous solutions only.

A. F. Kapustinskii and K. B. Yatsimirskii have shown that there is a unique relationship between $\Delta H_h^i/z^2$ and the radius of the ion, independently of its charge, while according to the electrostatic theory we should expect a linear relationship between A and Z, as in Eq. (1).

According to the view developed by A. F. Kapustinskii, the correction b (which is ± 0.28 A), which must be applied to the crystal radius r_{cryst} in order to obtain a single relationship between ΔH_h^i and r_{aq}, is easily explained if the formation of hydrates is omitted from the electrostatic scheme, and instead it is assumed that the formation of hydrates causes the cation to be surrounded by a "layer" of four electron pairs provided by

TABLE 1

Solvent	D (25°C)	$\mu \cdot 10^{18}$	V_M	$-\Delta Z_s^i$[2], kcal/g·ion at 25°C							
				Li^+	Na^+	K^+	Rb^+	Cs^+	Cl^-	Br^-	I^-
H_2O	78,25	1,84	18,07	117,0	96,0	78,0	74,4	64,0	74,0	68,0	59,4
H_2O[3]	78,25	1,84	18,07	121	97	79	74	66	79	72	64
CH_3OH	32,63	1,66	40,71	116,0	93,0	76,0	—	60,4	71,0	67,0	59,6
C_2H_5OH	24,30	1,68	58,71	115,0	90,0	73,2	—	—	71,3	66,2	58,5
HCOOH	58,5 (16°)	1,19	37,93	116,0	99,5	73,9	73,2	65,0	78,3	—	—
NH_3	16	1,46	20,84	124,0	99,0	79,4	73,3	65,6	65,6	62,8	57,0

TABLE 2

Ion	Vacant orbits	Type of hybridization	Structure of hydrate	n from our data	n according to K. P. Mishchenko	n according to A. F. Kapustinskii	$-\Delta H_h^i$, kcal/g·ion
Li^+	2s, 2p	sp^3	Tetrahedral	4	4	4	124
Na^+	3s, 3p	sp^3	Tetrahedral	4	6	4	100
F^-	3s, 3p	sp^3	Tetrahedral	4	6	4	109
K^+	4s, 3d	sd^5	Mixed	6	8	4	80
Cl^-	4s, 3d	sd^5	Mixed	6	8	4	79
Rb^+	5s, 4d	sd^5	Mixed	6	8	4	75
Br^-	5s, 4d	sd^5	Mixed	6	8	4	72
Cs^+	6s, 4f	sf^7	—	8	8	4	65
I^-	6s, 4f	sf^7	—	8	8	4	62

four water molecules. On the basis of the spherical model of the atom worked out by this author, it has been shown that the mean thickness of the eight electrons amounts to 0.26 A.

The data which have been produced show clearly that the electrostatic model of solvation, and the method for calculating the energy of solvation based on this model, are inadequate. In view of this it seemed to us appropriate to consider the possibility of other explanations, and to attempt the explanation of solvation on the assumption that complex formation occurs. Until recently, the calculation of the energy of complex formation, like that of solvates, was based on the assumption of an electrostatic process for the interaction, but within the last few years the method of molecular orbitals has been employed instead [5]. This has the advantage that it can take into account every type of bond from the purely covalent to the purely ionic. In particular, for the purpose of explaining the nature of the bonds formed in solvates, it can take account of donor-acceptor bond types.

It may be assumed that the electron donors in the formation of hydrates are the oxygen atoms present in the water molecules, which possess free, unshared electron pairs in the state n = 2, while the electron acceptors are the elementary ions, which offer empty orbits. As the vacant orbits we have taken those free orbits whose energy is nearest to the correspondingly placed filled electronic levels in the atoms. Starting from the equivalence in energy of the bonds in the solvates, it is necessary to consider the hybridization of the vacant orbits in the ions. Hence the choice of orbits is at once seen to depend on the solvation number, and the geometrical arrangements of the addends in the solvates. Table 2 gives the probable vacant orbits for the ions produced by the alkali metals and the halogens, together with the type of hybridization [6], the geometrical location of the water molecules in the hydrates, the hydration number and the value of H_h^i as calculated from the data given by N. A. Izmailov [3]. For comparison the values of the hydration number taken by K. P. Mishchenko and A. F. Kapustinskii are also given. Isoelectronic ions are linked in the table by brackets in the last column. The data in this table show that the arrangement of the water molecules in hydrates of lithium, sodium and fluoride ions should be tetrahedral, which is in harmony with the current view that these ions exercise little influence on the structure of water, so that their hydration may really be simply considered as the substitution of molecules by ions in the tetrahedral water unit. For the remaining ions it must be supposed that hybridization of the sd^5 and sf^7

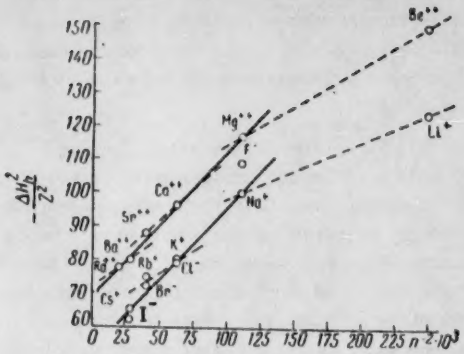

Fig. 1.

types will occur, giving solvation numbers of 6 and 8, respectively. This will result in a larger derangement of the water structure, which accounts for the difference between the hydration of potassium and chloride, rubidium and bromide, cesium and iodide ions, and that of lithium, sodium and fluoride.

In solvates, as well as in complex compounds, the covalent character of the bonds is diminished with increase in the atomic radius, so that the solvation of most ions may to a first approximation be considered as an ion-dipole interaction.

According to the electrostatic theory, all the terms in the equation for ΔZ_h^i depend on the value of $1/r$. For these reasons the functional relationship between them has repeatedly been determined. In the course of this, the different nature of the relationship for cations and anions has been discovered. But if we start from the assumptions now under review, it is more appropriate to look for the relationship between ΔZ_h^i (or ΔH_h^i) and the energy characteristics of the vacant orbits of the ions, expressed by the principal quantum number n. On the simplest assumption it might be expected that the energy of the chemical interaction of the ions with the solvent would be inversely proportional to n^2. Increase in n should cause the energy of hydration to diminish. The difference between the solvation energies of neighboring members of a group should also diminish with increase in n, which is a consequence of the fact that with increase in the value of n, the terms for successive ions approach constantly closer to each other. This suggested regularity is confirmed by the data in Table 2.

Calculation by Mishchenko and Sukhotin [1] has shown that the total energy of hydration, ΔZ_h^i differs from the energy of primary hydration, ΔZ_{prim}^i, by the presence of terms nl, B and g. Here l is the "internal" heat of evaporation of water, B is the energy of polarization of water by the ion field according to Born, and g is the energy of interaction between molecules of the hydrated complex and the water surrounding it. But it appears from the data given by Mishchenko and Sukhotin that these terms are mutually compensating (that is, $nl + B + g \cong 0$), so that in practice the value of ΔZ_h^i is nearly the same as that of ΔZ_{prim}^i. Further, part of the energy released on hydration is expended in orientating the molecules of water around the ion, in harmony with which $\Delta S_h^i < 0$. The magnitude of ΔS_h^i defines the change in the state of the water in the field of the ion. We have therefore, in characterizing the relationship between ΔZ_{prim}^i and n, made use of the values of ΔH_h^i given by the relationship: $\Delta H_h^i = \Delta Z_h^i + T\Delta S_h^i$. Figure 1 gives a graphical presentation of the relationship between $-\Delta H_h^i/z^2$ and n^{-2} for the principal subgroups of groups I, II and VII of the periodic table. It follows from Table 2 and Fig. 1 that the magnitude of ΔH_h^i for the ions of the alkali metals and the halogens with the same vacant levels should, within the limits of the experimental accuracy in determining ΔH_h^i, be in agreement among themselves. It can be seen that the ions from cesium, rubidium, potassium, sodium, iodine, bromine and chlorine have one relationship amongst themselves, while the ions of lithium and fluorine deviate from this straight line. The relationship between $-\Delta H_h^i/z^2$ and n^{-2} has a similar character for the ions of the alkaline earth metals. Strictly speaking, the relationship shown should be divided into three linear sections (dotted lines), which is explained by the change in the hydration number (see Table 2). The fact that the singly charged cations and anions correspond to a single relationship points to the existence of a single mechanism for their hydration (or solvation). Similar relationships for nonaqueous solvents point to the same conclusions.

In agreement with the point of view developed here, the values of ΔH_h^i for the isoelectronic ions SH^-, Cl^- and K^+ (82, 84 and 81 kcal/g·ion, respectively), whose vacant orbits can be regarded as approximately the same, lie very close to each other. The same is true for such isoelectronic ions as OH^-, H_3O^+, F^- and Na^+ [3].

The views put forward provide a ready means of substantiating the method used by many investigators, in which the total energy of hydration of a salt can be divided among the ion constituents, such as the pairs Cs^+ and I^-, or K^+ and Cl^-.

It is also possible from this standpoint to explain the practical independence shown by ΔZ_s^i, and especially ΔH_s^i, of the nature of the solvent if this contains oxygen (water, alcohols and carboxylic acids) or nitrogen

(ammonia and amines). In the former group, the electron donors are the oxygen atoms, and in the latter the nitrogen atoms, each of which has available for the formation of molecular orbitals electrons from the same principal quantum group, for which n = 2. It may be expected that values of ΔH_s^i for all the solvents would lie very close to each other, when these contain electron donors whose free electrons are in the same energy level (such as oxygen, nitrogen and fluorine).

It follows from Table 1 that the difference in the values of ΔZ_s^i for the ions considered amounts to between 5 and 10 kcal/g·ion. It can be supposed that these differences arise through changes in the energy of secondary solvation, which depends strongly on the properties of the solvent (such as its dielectric constant, dipole moment and molecular volume. Thus, the total hydration energy of ions in solvents whose molecules contain atoms with free electrons in similar levels, consist of the energy of primary solvation, ΔZ_{prim}^i, which is large in value and depends only slightly on the properties of the solvent, and a much smaller energy of secondary solution, ΔZ_{sec}^i, which depends considerably on the properties of the solvent. The principles given here indicate that the values of ΔZ_{prim}^i for different isoelectronic ions, possessing the same vacant orbits, and giving the same molecular electronic orbitals at identical levels, will be very close to one another.

LITERATURE CITED

[1] K. P. Mishchenko and A. M. Sukhotin, Zhur. Fiz. Khim. 27, 1, 26 (1953).

[2] N. A. Izmailov, Doklady Akad. Nauk SSSR 126, 1033 (1959).*

[3] N. A. Izmailov, Electrochemistry of Solutions [in Russian] (Khar'kov, 1959] pp. 304, 343.

[4] Program of Work at the Scientific and Technical Conference, D. I. Mendeleev Moscow Scientific and Technical Institute [in Russian] (Moscow, 1960).

[5] Ya. K. Syrkin, Usp. Khim. 8, 903 (1959).

[6] G. Eyring, J. Walter, and J. Kimball, Quantum Chemistry [Russian translation] (IL, 1948) p. 306.

* Original Russian pagination. See C. B. translation.

EFFECT OF OXYGEN AND WATER ON THE ELECTRICAL CONDUCTIVITY OF ZINC OXIDE DYED WITH ERYTHROSINE

G. A. Korsunovskii

(Presented by Academician A. N. Terenin, May 23, 1960)
Translated from Doklady Akademii Nauk SSSR, Vol. 134, No. 6, pp. 1394-1396, October, 1960
Original article submitted May 10, 1960

In previous communications [1] we examined the possible mechanism of the electron exchange occurring on the surface of a number of oxide semiconductors with electron conductivity during their irradiation in the region of natural absorption in the presence of oxygen and water vapor. It was shown that the suppression of the electrical conductivity of these semiconductors by water vapor is caused by the reaction of the latter with chemisorbed oxygen, as a result of which it is oxidized to hydroxyl. The action of light evidently consists of desorption of the radicals formed.

The work of E. K. Putseiko and A. N. Terenin [2, 3] showed that the photoconductivity of zinc oxide may be sensitized to visible light by dyeing itwith organic dyes. We undertook a comparative investigation of the change in electrical conductivity of polycrystalline samples of zinc oxide under the action of irradiation in the natural absorption region of the semiconductor and in the sensitization region and also the effect of oxygen and water on these processes. Photoresistors of zinc oxide were made by the method described previously [1]. For the preparation of sensitized samples, zinc oxide powder was mixed in an alcohol solution of erythrosine with a concentration of $\sim 10^{-5}$ M.

The advantage of erythrosine in comparison with other sensitizing dyes lies in its low absorption in the region of photoelectric sensitivity of zinc oxide, due to which the same dyed sample may be investigated both in this region (mercury line at 366 mμ) and in the sensitization region (mercury line at 546 mμ).

The electrical conductivity was measured with a dc amplifier, which made it possible to measure currents of $3 \cdot 10^{-13}$ to $3 \cdot 10^{-5}$ a. The samples were irradiated with an SVDSh-250 mercury lamp through a narrow-band light filter. The irradiation of the sample was 2.5-3 $\mu w/cm^2$ or $4.5\text{-}5.5 \cdot 10^{12}$ quanta/$cm^2 \cdot$ sec for λ 366 mμ and 3-4 $\mu w/cm^2$ or $8\text{-}11 \cdot 10^{12}$ quanta/$cm^2 \cdot$ sec for λ 546 mμ. Considering that the dyed sample absorbed about 35-40% of the radiation with λ 546 mμ, which was checked by measuring the spectrum of diffuse reflection of the samples, the number of quanta absorbed for this wave length was $2.5\text{-}4.5 \cdot 10^{12}$ per cm^2 per sec.

Figure 1 shows the change in electrical conductivity of dyed zinc oxide during irradiation in an atmosphere of undried air. In this case the stationary current during irradiation in the sensitization region (curve 1) was greater than during irradiation in the region of natural sensitivity of zinc oxide (curve 2), despite the fact that the number of quanta absorbed was less in the first case. The inertia of the process, especially in the fall, was much greater in the first case. During irradiation in dry air (curves 3 and 4), the inertia of the processes was practically the same, while the stationary current was greater for irradiation in the region of natural sensitivity of ZnO.

Irradiation in high vacuum (Fig. 2, curves 1 and 2) was characterized by a considerable increase in the electrical conductivity, which was somewhat greater during irradiation in the region of natural absorption of

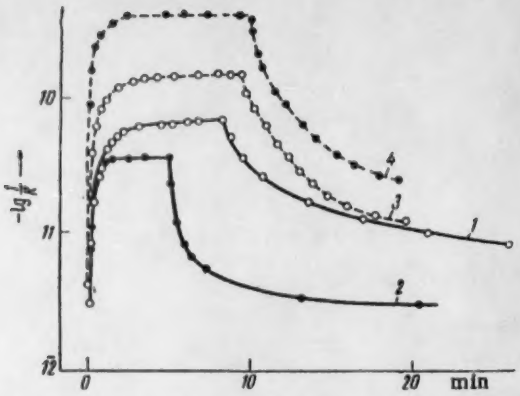

Fig. 1. Increase in electrical conductivity of sample during irradiation and fall in dark in air at atmospheric pressure. 1) Undried air, λ 546 mμ; 2) the same at λ 366 mμ; 3) dry air, λ 546 mμ; 4) the same at λ 366 mμ.

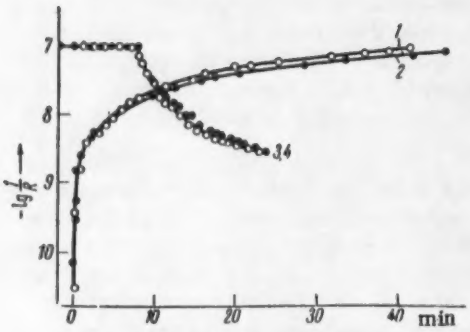

Fig. 2. Increase in electrical conductivity of sample during irradiation in vacuum and fall in the dark with the admission of dry air: 1) irradiation with light at λ 546 mμ; 2) the same at λ 366 mμ; 3) fall with admission of dry air after irradiation at λ 546 mμ; 4) the same at λ 366 mμ. The radiation intensities at λ 546 and 366 mμ were chosen so that the stationary currents were the same in the two cases.

ZnO_2 and an extremely slow fall in the dark. This fall could be accelerated considerably if dry air or oxygen were admitted and the rate of fall from identical electrical conductivity values, reached by irradiation at λ = 546 or 366 mμ, was also the same.

A substantial difference in the behavior of zinc oxide irradiated in the region of natural absorption and in the sensitization region appeared during the action of water vapor in the dark. The admission of water vapor at a pressure of 20 mm Hg to a sample in vacuum that had previously been irradiated in the region of natural absorption produced a rapid and deep fall in electrical conductivity to values equal to those before irradiation. The effect of water vapor on the same sample irradiated in the sensitization band was much weaker (Fig. 3).

The observed characteristics of the increase in electrical conductivity during irradiation in the sensitization region and the fall in the dark may be explained by the mechanism of sensitized photoconductivity (proposed by E. K. Putseiko and A. N. Terenin), which consists of the transfer of light energy by oxygen traps. These traps may be surface compounds $Zn^+O_2^-$ [4], the levels of which lie at a distance of ~1 ev from the bottom of the conductivity zone. Irradiation with visible light with quantum energies >1 ev (in our case, 2.3 ev) produces decomposition of this compound and desorption of oxygen:

$$Zn^+ O_2^- \overset{h\nu}{\rightleftarrows} Zn^+ + e + O_2. \qquad (1)$$

During irradiation in the region of natural absorption, it was observed that in addition there was desorption of hydroxyl radicals, occurring as a result of the decay of an exciton at their chemisorption levels, which lie below the oxygen levels due to the high electron affinity of hydroxyl:

$$Zn^+ OH^- \overset{h\nu'}{\rightleftarrows} Zn^+ + e + O: \qquad (2)$$

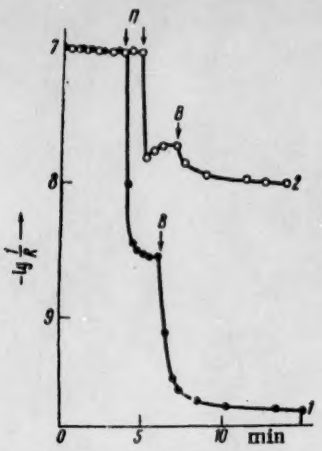

Fig. 3. Fall in electrical conductivity of sample on admission of water vapor in the dark after irradiation in high vacuum with light at λ 366 mμ (1) and at λ 546 mμ (2).

The desorption of hydroxyls did not occur during irradiation in the sensitization region as the energy of visible light quanta was found to be insufficient for decomposition of the surface compound Zn^+OH^-. The chemisorption levels of hydroxyls remained occupied and therefore when water vapor was admitted there was no decomposition of molecules of the latter and the chemisorption of new hydroxyls. The slight decrease in electrical conductivity in this case, which is shown in Fig. 3 (curve 2), may be produced by chemisorption of water molecules without their decomposition, but this hypothesis requires further experimental confirmation. The admission of dry oxygen produced an identical fall in the electroconductivity (Fig. 2), regardless of the nature of the radiation with which the semiconductor was irradiated previously, as in both cases the freed oxygen levels were filled.

The absence of chemisorption of hydroxyls after irradiation in the sensitization region determined the characteristics of the increase in electrical conductivity during irradiation in moist air and the fall in the dark. During irradiation in the region of natural absorption in the presence of water vapor, the reverse reaction according to Eq. (2) proceeded rapidly and the equilibrium was displaced to the left, as a result of which the stationary (equilibrium) electrical conductivity was lower than during irradiation in the sensitization region when reaction (2) did not occur and the reverse reaction (1) proceeded slowly, as is shown by a comparison of the rates of fall in the electrical conductivity under the action of water and oxygen.

The considerations presented explain the absence of photochemical oxidation of water during the irradiation of aqueous suspensions of dyed zinc oxide with visible light [5]. Despite the formation of a large number of conductivity electrons, the decomposition of water molecules does not occur and photooxidation products, namely, hydrogen peroxide and hydroxyls, are not formed.

In conclusion, we would like to thank Academician A. N. Terenin, under whose direction this work was carried out.

LITERATURE CITED

[1] G. A. Korsunovkii, Zhur. Fiz. Khim. 34, 510 (1960); Problems in Kinetics and Catalysis [in Russian] (1960) Vol. 10, p. 83.

[2] E. K. Putseiko and A. N. Terenin, Zhur. Fiz. Khim. 23, 676 (1949); Doklady Akad. Nauk SSSR 90, 1005 (1953).

[3] E. K. Putseiko, Doklady Akad. Nauk SSSR 91, 1071 (1953).

[4] L. A. Myasnikov, Izvest. Akad. Nauk SSSR, Ser. Fiz. 21, 192 (1957).

[5] G. A. Korsunovskii, Author's Abstract of Dissertation [in Russian] (GOI, 1960).

REVEALING OF DISLOCATIONS AND SOME ETCH PATTERNS IN SILICON SINGLE CRYSTALS

Academician N. N. Sirota (Acad. Sci. Belorussian SSR)

and A. A. Tonoyan

Branch of Physics of the Solid State and Semiconductors, Academy of Sciences of the Belorussian SSR

Translated from Doklady Akademii Nauk SSSR, Vol. 134, No. 6, pp. 1397-1398, October, 1960
Original article submitted June 17, 1960

In the study [1] it has been shown that, when etching polished silicon cuts, the (111) plain, on which faults are observed preferably in the form of etch pits, is developed most clearly. These etch pits are ascribed to dislocations chiefly because of their surface structure. In the paper [2] a method to develop etch pits in germanium and silicon is described; however, it does not reveal their structure.

The purpose of the present study was to investigate in more detail the etch patterns originating from dislocations and other faults and to reveal the nature of the etch pits.

The samples for this study were cut in the form of slabs from single crystals along fixed crystallographic directions, mainly along planes close to (111). The accurate orientation was effected by means of an optical equipment, constructed by I. E. Voitsekhovich and described in his thesis (1959). After having been cut the slabs were polished with abrasive powders of various sizes (Nos. 14, 10, 7). Then the slabs underwent chemical polishing and practically at the same time were etched in order to reveal the dislocations and the faults. The chemical polishing was carried out at a temperature of 30-35° during 2-3 min in a reagent consisting of 10 cc hydrofluoric acid (37-38%), 10 cc concentrated nitric acid, 10 cc glacial acetic acid. After this 15 cc of double-distilled water was added to the reagent and the etching and development of the faults was carried out at the same temperature during 1.5-2 min. In contradiction to the recommendations of paper [3] the polishing and etching was done under heating.

In the etch patterns, which are developed on the (111) plain inside the pits and originate from the presence of dislocations, faults and growth structure, several characteristic types may be distinguished.

Etch patterns having a helical shape are often found. In Fig. 1 typical helical etch patterns are shown: a) a left-hand helix; b) a right-hand one. Analogous etch patterns with a helical shape on silicon single crystals have been revealed in the papers [4, 5].

In several cases, for instance in Fig. 1c, etch patterns are found having in the center a helix which in the outer part degenerates into a terrace structure in the form of irregular triangles placed one above the other. Occasionally an array of etch figures, consisting of helices and an intermediate form of terraces, is found (Fig. 1d). The occurrence of etch patterns consisting of helices, which at their start and termination again have helices lying in a perpendicular plain, deserves much attention (Fig. 1e).

The occurrence of etch patterns, consisting merely of nonintersecting terraces in the form of irregular polygons situated one above the other, is also characteristic for the (111) plain of silicon single crystals and for plains deviating little from this direction. An etch pattern with clearly developed terraces, which are inclined and merge in one direction, is shown in Fig. 2a.

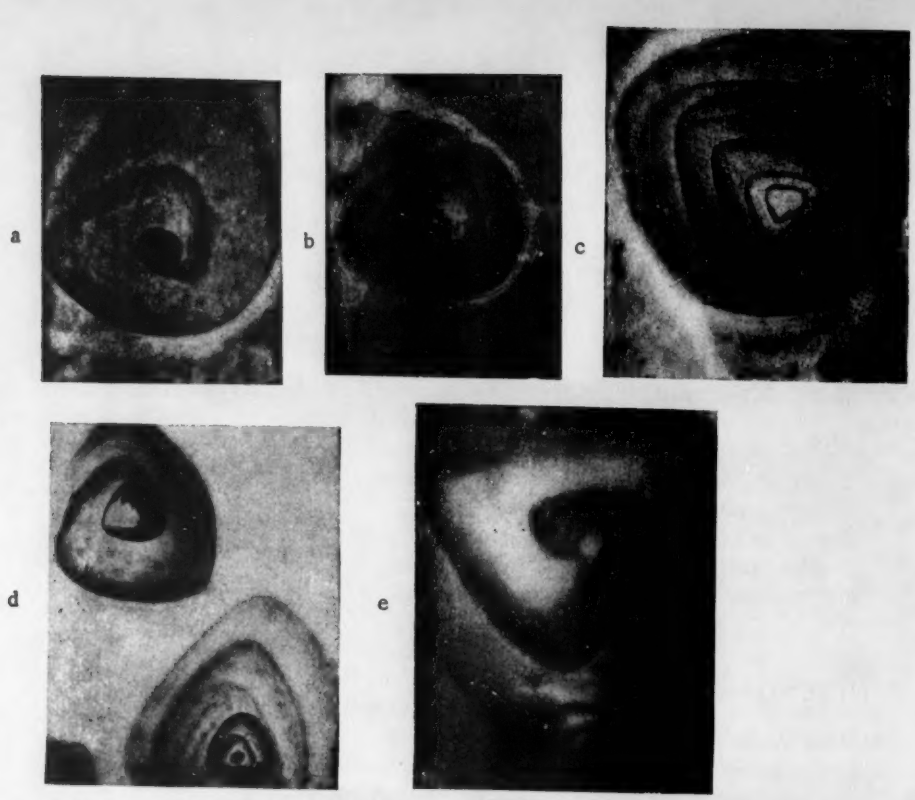

Fig. 1. a) 4666 ×; b) 1833 ×; c) 1333 ×; d) 1333 ×; e) 3125 ×.

Fig. 2. a) 1500 ×; b) 170 ×; c) 362 ×.

TABLE 1

H_μ, kg/mm^2	1218,9	1430,5	1130,3	1130,3	857,4	601,8	541,7	857,4	329,61
r, mm	0,25	0,22	0,19	0,16	0,13	0,1	0,7	0,04	0,01

Upon etching single crystals of low-ohmic (ρ = 0.1 ohm · cm) silicon during 10 min in a boiling 20% KOH solution, etch patterns consisting of sharply outlined closed polygons, situated one above the other with their sides practically parallel, are visible at a relatively small magnification (Fig. 2b). Meanwhile, in some cases besides such isolated patterns, an array of analogous ones, which intersect each other, is observed (Fig. 2c).

In the etch patterns described the step height of the helices is of the order of 100-1000 A: the distance between the nonintersecting terraces is usually of the order of 1000-10000 A. Meanwhile the helices as well as the nonintersecting terraces, which are connected with dislocations and growth structures, lie preferentially in (111) plains. Measurements of microhardness which we have performed showed in particular that in several cases the microhardness H_μ considerably decreases, as one approaches an etch pit or a dislocation exit (Table 1).

A further investigation of the change in physical and mechanical properties as a function of dislocation density and shape of the etch pattern is of considerable interest.

The new data obtained show that etch pits in principle are connected with dislocations and faults, which originate from the growth structure.

LITERATURE CITED

[1] N. N. Sirota and A. V. Shibaeva, Inzh.-Fiz. Zhur. 1, 2, No. 10, 57 (1959).

[2] A. D. Trakhtenberg and S. M. Fainshtein, Fiz. Tverd. Tela 1, No. 3 (1959).

[3] C. A. F. T. Spray, Proc. Phys. Soc. 69, 438, 689 (1956).

[4] F. L. Vogel and L. C. Lovell, J. Appl. Phys. 27, No. 12 (1956).

[5] J. Matsukura and T. Suzuki, J. Phys. Soc. Japan 12, 8, 976 (1957).

THE PART PLAYED BY PHYSICOCHEMICAL PROCESSES IN THE SURFACE LAYERS OF STEEL DURING CYCLIC DEFORMATION IN MELTS OF READILY FUSIBLE METALS

M. I. Chaevskii

Machine Control and Automation Institute, Academy of Sciences
of the Ukrainian SSR
(Presented by P. A. Rebinder, May 25, 1960)
Translated from Doklady Akademii Nauk SSSR, Vol. 134, No. 6, pp. 1399-1402,
October, 1960
Original article submitted May 4, 1960

It is known that the fatigue strength of steel may be reduced considerably by the influence of surface-active media [1, 2]. These results confirm Academician P. A. Rebinder's theory that adsorption facilitates the deformation and decreases the strength of solids [3].

If, however, a surface-active medium does not influence the strength of solids, or if it increases the strength [4-6], then the reason for this phenomenon must be sought in supplementary or secondary surface phenomena, which mask the adsorption effects, although they may be related to these effects. In particular, the production of compressive stresses in the surface layers of a metal by means of rolling [7, 8] prevents the harmful effect of the surface-active medium during cyclic deformation of the metal. This is due to the fact that the rolling process closes the surface defects so that the surface-active medium cannot penetrate into the metal.

It has been found [4-6] that there is a considerable increase in the fatigue strength of steel specimens with stress concentrators when the specimens are under the influence of a melt of tin or Pb–Sn eutectic. It has been assumed [6], that this phenomenon is produced by plastification of the bottom of the concentrator by the liquid molten metal, as a result of which the concentration of stresses is decreased.

In connection with this positive effect of molten Sn or Pb–Sn on steel undergoing cyclic deformation, it is also of interest to examine whether other melts have an analogous effect. The experiments which were carried out showed that this is not the case. Figure 1 shows that the action of molten Pb–Bi eutectic* leads to a sharp decrease in the fatigue strength of specimens with stress concentrators.** Analogous results were also obtained when specimens of 1 Kh18N9T steel were tested. Consequently, the effect of increase in the fatigue strength under the action of a melt of tin or Pb–Sn eutectic results not only from plastification, but also from diffusion and chemical processes which take place while the steel undergoing deformation is in contact with tin.

To confirm this assumption, the fatigue strength tests in the molten Pb–Sn eutectic were carried out by a slightly different method than that used earlier [4-6].

The specimens were tinned with Pb–Sn eutectic and tested in air at the same temperature as that at which they had already been tested for fatigue strength in a bath of molten Pb–Sn eutectic. Figure 1 shows that the

* To ensure efficient wetting of the steel specimens by the molten Pb–Bi eutectic, the specimens were first tinned with a melt of Pb–Sn eutectic and then dipped in a bath of molten Pb–Bi eutectic. During the fatigue strength testing, the specimens were kept in the bath of molten Pb–Bi eutectic.

** The specimens had the same stress concentrators as in [5], but with an angle of 45° at the apex.

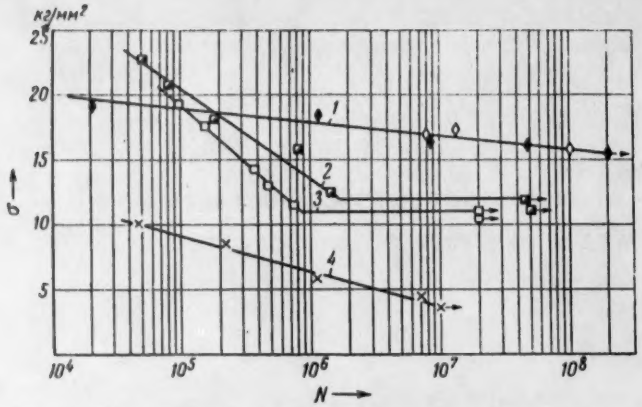

Fig. 1. Fatigue strength curves for specimens with stress concentrators; specimens made of normalized 50 steel. Frequency of stress changes 50 cps. 1) Specimens tinned with Pb–Sn eutectic in air at 400°. The white diamonds denote control points obtained when the tinned specimens were tested in molten Pb–Sn eutectic; 2) specimens in air at 400°; 3) specimens in air at 20°; 4) tinned specimens in molten Pb–Bi eutectic at 400°.

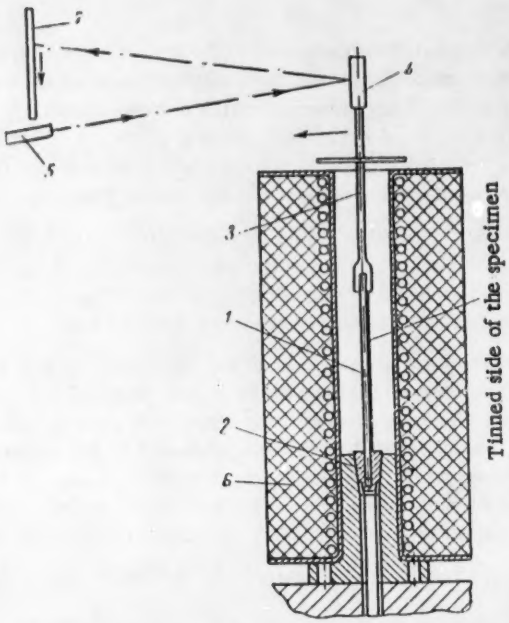

Fig. 2. Diagram of the apparatus used to study the stresses produced in the surface layer of steel as a result of diffusion of the melt.

life of the specimens still had increased values. A significant feature of these experiments is that during the testing, the surface film of the melt was oxidized, so that the plastification effect disappeared. Nevertheless, the specimen still stands up to an increased cyclic load.

It might therefore have been thought that the plastification of the steel by the melt has no effect on the production of increased fatigue strength, and that the effect is produced entirely by the physicochemical processes which take place while the steel is being tinned. This conclusion was not confirmed by experiment, however, since tinned specimens tested at room temperature have a fatigue strength which is 30-35% less than that of specimens which have not been tinned.

Experiments have also been carried out which show directly the important part played by the plastification of the steel by the melt in the initial moment of the cyclic deformation. It is known [9] that when fatigue strength tests are carried out in a Pb–Sn melt on specimens which have not been previously tinned, the fatigue strength may be considerably reduced. Consequently, the fatigue strength of steel can only be increased by the combined effect of plastification and the other physicochemical processes in the initial moment of cyclic deformation.

It is known that the plastification effect is the most general and universal effect of the action of a surface-active medium, and always arises during the deformation of a metal in any surface-active medium [10]. The plastification effect is related to the fact that the movement of the dislocations out on to the surface of the metal undergoing deformation is facilitated [11]. In addition, an important part in the plastification effect may be played by subsurface sources of dislocations (with one point of attachment) for which the stresses at the start of working are much lower than those for sources for two attached points. Decrease in the surface energy should lead to an increase in the activity of the subsurface sources and to a decrease in the yield point of the metal [10].

Consequently, an essential feature of the positive effect of plastification of the surface layer of the metal in the initial moment of cyclic deformation is the removal of local, internal, normal stresses produced at the head of the accumulation of dislocations in the surface layer of the metal, which in the usual state may be a considerable obstacle to the movement of the dislocations [12].

It must be remembered, however, that the plastification effect leads to an increase in the fatigue strength only if the surface-active melt is for some reason unable to penetrate into the metal along the defects which are developing. There is no such reason when the Pb–Bi eutectic is used, so that a considerable decrease in the fatigue strength is observed. In this case we have only the effect of the adsorptive decrease in the cyclic strength, since neither lead nor bismuth react chemically with steel at the temperatures used [13].

A different process takes place during the cyclic deformation of steel in molten tin or Pb–Sn eutectic.

The molten tin diffuses into the interior of the metal along the defects which are developing, and reacts chemically with the steel to form an intermetallic compound of the $FeSn_2$ type. Since the dimensions of the cell of the $FeSn_2$ lattice are greater than those of the Fe atomic lattice [13], compressive stresses arise in the surface layer of the metal and prevent the penetration of the molten tin to the interior of the metal.

The tin from the melt will naturally penetrate by diffusion through the intermetallic layer into the interior of the metal. When it meets the Fe, however, chemical reaction again takes place with the formation of new compressed volumes of metal.

The dissolution of the surface layer of steel, which takes place when the tests are carried out in a bath of molten tin or Pb–Sn eutectic, therefore does not lead to removal of the compressive stresses.

It has been shown [14] that the compressive stresses which are produced are stable over a fairly wide temperature range.

The production of compressive stresses in the surface layer of steel as a result of the diffusion of tin and the formation of an intermetallic compound of the $FeSn_2$ type can be observed qualitatively on the following simple apparatus (Fig. 2). One end of the planar specimen 1 is pressed into the holder 2. The free end of the specimen is attached to an extension piece 3 fitted with a mirror 4, which reflects the beam from the light source 5. The specimen is tinned on one side. The electric heater 6 is used to raise the temperature of the specimen to the required value (400°). The movement of the beam over the scale 7 can then be used to follow the gradual bending of the specimen in the direction indicated by the arrow. This bending can result only from compressive stresses in the surface layer.

Thus during prolonged fatigue testing, a phase film of the intermetallic compound $FeSn_2$ is formed in the microscopic cracks produced, and this film leads to the production of compressive stresses in the surface layer of the specimen and thus prevents the further development of the microscopic cracks. As a result, the fatigue strength of the steel is increased. In the case where side reactions of this type do not take place (for example, in the fatigue testing of steel in Pb–Bi melts), the effect of the sharp decrease in the fatigue strength of the steel is complete, as should be the case in highly surface-active media. The Rebinder effect is a universal effect, which always takes place during the deformation of metals in surface-active media, but in some cases it may be masked by secondary phenomena associated with the formation of new phases.

LITERATURE CITED

[1] V. I. Likhtman, P. A. Rebinder, and G. V. Karpenko, The Influence of a Surface-Active Medium on the Deformation of Metals [in Russian] (Izd. AN SSSR, 1954).

[2] G. V. Karpenko, The Effect of Active Liquid Media on the Strength of Steel [in Russian] (1955).

[3] P. A. Rebinder, Jubilee Collection Dedicated to the 30th Anniversary of the Great October Socialist Revolution [in Russian] (Izd. AN SSSR, 1947) Vol. 1, p. 123.

[4] M. I. Chaevskii, Collection: Some Problems in the Physical Chemistry and Mechanical Properties of Metals [in Ukrainian] (Kiev, 1958).

[5] M. I. Chaevskii, Doklady Akad. Nauk SSSR 124, No. 5 (1959).*

[6] M. I. Chaevskii, Doklady Akad. Nauk SSSR 125, 2 (1959).*

[7] G. V. Karpenko and I. I. Ishchenko, Collection: Problems of Machine Control and Strength in Mechanical Engineering [in Russian] (Acad. Sci. Izd. AN UkrSSR, 1953) Vol. 1.

[8] G. V. Karpenko, Priklad. Mekh. 3, No. 1 (1957).

[9] M. I. Chaevskii, Metalloved. i Termich. Obr. Metallov, 8 (1959).

[10] V. A. Labzin and V. I. Likhtman, Doklady Akad. Nauk SSSR 129, No. 3 (1959).*

[11] V. I. Likhtman and E. D. Shchukin, Usp. Fiz. Nauk 66, 213 (1958).

[12] C. S. Barrett, Acta Metall. 1, 2 (1953).

[13] M. Hansen, Constitution of Binary Alloys (1958).

[14] M. I. Chaevskii, Fiz. Metal. i Metalloved. 8, No. 5 (1959).

* Original Russian pagination. See C. B. Translation.